WATER INJECTION SYSTEM FOR POWER AUGMENTATION AND EMISSION CONTROL FOR HYDROGEN-FUELLED COMPRESSION IGNITION ENGINE

ADNAN BIN ROSELI

THESIS SUBMITTED IN FULFILLMENT OF THE REQUIREMENTS FOR THE DEGREE OF DOCTOR OF PHILOSOPHY

FACULTY OF ENGINEERING
UNIVERSITY OF MALAYA
KUALA LUMPUR

2012

ABSTRACT

The increase in demand and depletion of fossil fuels has led the search for alternative fuels become mandatory. Hydrogen is one of the promising alternative fuels for combustion engines and it can be used in compression ignition engine with the help from pilot ignition of diesel. Hydrogen-fuelled dual fuel compression ignition engine produces a reasonable increase in power output and thermal efficiency but suffers from higher concentrations of HC, CO and NO_x. In this research, experimental investigations have been conducted on performance and emission characteristics of a compression ignition engine running on hydrogen gaseous fuel. The experimental works have been carried out on a single cylinder, 4-stroke direct injection YANMAR L100AE compression ignition engine. Timed port injection for hydrogen and timed manifold water injection systems were developed in order to control its injection timing and duration. Electronic control unit (ECU) was used to fix injection timing of hydrogen fuel from 0°CA to 20°CA at constant flow rate of 3 LPH. Injection timings of water were in the range of 20°BTDC to 20°ATDC with variable injection duration of 20°CA and 40°CA.

Experimental results pertaining to performance and emission characteristics of HFCI engine with variable water injection timings are presented in detail. It is then compared with diesel alone and diesel-hydrogen operations. Numerical simulations based on the developed mathematical models are performed to study the emissions of diesel combustion with hydrogen and water addition. Numerical results are analyzed in order to validate experimental emissions characteristics of HFCI engine with and without water injection.

In this study, the results indicate that water injection timing of 20°ATDC and duration of 20°CA has shown better engine performance due to increased gross indicated work, indicated thermal efficiency and it also has shown lower indicated specific energy consumption especially at 2000 RPM. Water injection timing of 20°BTDC and duration of 40°CA has shown the highest heat release rate and the longest ignition delay.

In emission analysis, water injection timing of 0°CA and duration of 40°CA indicated the lowest CO_2 concentration throughout entire speed range. Water injection timing of 20°BTDC and duration of 20°CA has shown the lowest SO_2 emission. Water injection timing of 0°CA and duration of 20°CA has shown the lowest CO emission for higher speed range. Water injection timing of 20°ATDC and duration of 20°CA indicated the lowest HC emission and EGT throughout all engine speeds. All water injection timings indicated lower NO_x concentration for entire speed range. Experimental emission characteristics have been validated and it is in good agreement with numerical simulation.

It is concluded that water injection timing of 20°ATDC and duration of 20°CA is the optimum timing for power augmentation and better control of emissions. Generally, water injection system with optimum injection timing appears to be a promising method to enhance the performance and emissions quality of HFCI engine effectively.

ABSTRAK

Peningkatan permintaan dan kekurangan bahanapi fosil menjadikan pencarian bahanapi alternatif sebagai mandatori. Hidrogen merupakan salah satu bahanapi alternatif yang baik dan ia boleh digunakan di dalam enjin cucuhan mampatan dengan bantuan daripada cucuhan perintis diesel. Enjin cucuhan mampatan menggunakan hidrogen menghasilkan kenaikan kuasa keluaran dan kecekapan terma akan tetapi ianya menyebabkan penambahan emisi HC, CO dan NO_x. Di dalam penyelidikan ini, kajian eksperimen dijalankan ke atas prestasi dan ciri-ciri emisi enjin cucuhan mampatan menggunakan gas hidrogen. Kerja-kerja eksperimen dijalankan ke atas enjin satu silinder, 4-lejang suntikan terus YANMAR L100AE. Sistem suntikan berkala hidrogen dan air dibangunkan bagi mengawal pemasaan dan tempoh suntikan. Unit kawal elektronik (ECU) digunakan bagi menetapkan masa suntikan hydrogen dari 0°CA sehingga 20°CA pada kadar aliran malar sebanyak 3 LPH. Masa suntikan air adalah di dalam julat 20°BTDC hingga 20°ATDC dengan tempoh suntikan 20°CA dan 40°CA.

Keputusan eksperimen yang berkaitan dengan prestasi dan ciri-ciri emisi enjin HFCI dengan perubahan masa suntikan air dibentangkan secara terperinci. Ia kemudiannya diperbandingkan dengan keputusan operasi diesel sahaja dan operasi diesel-hidrogen. Simulasi berangka berasaskan model matematik dilaksanakan untuk mengkaji emisi pembakaran diesel dengan penambahan hidrogen dan air. Keputusan simulasi berangka dianalisis bagi mengesahkan ciri-ciri emisi dari kajian eksperimen untuk enjin HFCI dengan dan tanpa suntikan air.

Di dalam kajian ini, keputusan menunjukkan bahawa masa suntikan air 20°ATDC dengan tempoh 20°CA memberikan prestasi enjin yang lebih baik dengan

penambahan kerja tertunjuk kasar, kecekapan terma tertunjuk dan ianya juga menyebabkan pengurangan penggunaan tenaga tentu tertunjuk terutamanya pada 2000RPM. Masa suntikan air 20°BTDC dengan tempoh 40°CA menunjukkan kadar pembebasan haba yang tertinggi dan kelewatan cucuhan yang paling lama.

Di dalam analisa emisi, masa suntikan air 0°CA dengan tempoh 40°CA menunjukkan konsentrasi emisi CO_2 terendah pada semua kelajuan enjin. Masa suntikan 20°BTDC dengan tempoh 20°CA menunjukkan konsentrasi emisi SO_2 terendah. Masa suntikan 0°CA dengan tempoh 20°CA menunjukkan konsentrasi emisi CO terendah bagi kelajuan enjin yang tinggi. Masa suntikan air 20°ATDC dengan tempoh 20°CA menunjukkan konsentrasi emisi HC dan juga menunjukkan penurunan suhu ekzos gas bagi semua julat kelajuan enjin. Emisi NO_x adalah rendah bagi kesemua masa suntikan dan julat kelajuan enjin. Ciri-ciri konsentrasi emisi yang diperolehi secara eksperimen disahkan dan ianya menunjukkan keserasian yang baik dengan simulasi berangka.

Dengan ini dapat dirumuskan bahawa masa suntikan air 20°ATDC dengan tempoh 20°CA adalah optimum bagi penambahan kuasa dan pembaikan emisi. Secara umumnya, sistem suntikan air dengan suntikan optimum merupakan kaedah yang berkesan untuk peningkatan prestasi dan kualiti emisi enjin HFCI.

ACKNOWLEDGEMENT

I wish to express my sincere appreciation and thanks to Prof. Dr. Masjuki Bin Hj. Hassan and Prof. Dr. T.M. Indra Mahlia for their supervision, encouragement, understanding and cooperation during the course of this research. I wish to thank University of Malaya for providing the fund to support this research work.

I would like to acknowledge Associate Professor Dr. Mohd. Azree Bin Idris and Mr. Mohd. Zaki Bin Mohd. Ali, Department of Mechanical Engineering, Universiti Tenaga Nasional, and Mr. Syed Sulaiman Bin Kaja Mohideen, Department of Electrical Communication, Universiti Tenaga Nasional for their technical guidance in completing this research.

I wish to thank Mr. Sulaiman Bin Ariffin, Laboratory Technician, Department of Mechanical Engineering, University of Malaya for his cooperation in conducting experiments for this research.

Finally, my special thanks to my mother and my wife for their patience and encouragement, and to my family for their support.

TABLE OF CONTENTS

DECLARATION…….. ii

ABSTRAC T…… iii

ABSTRAK……... v

ACKNOWLEDGEMENT……... vii

LIST OF FIGURES…….. xii

LIST OF TABLES……... xiv

NOMENCLATURES……... xv

Chapter 1 INTRODUCTION……... 1

1.1 Research Background……... 1

1.2 Research Objective……... 4

1.3 Limitations of Research……... 5

1.4 Research Contributions ……... 7

Chapter 2 LITERATURE REVIEW…… 9

2.1 Introduction…….…… 9

2.2 Recent Research on Hydrogen Engine…… 10

2.3 Recent Research on Hydrogen Engine (Simulation)…..……... 12

2.4 Research on Hydrogen Engine with Water Injection Techniques… 14

Chapter 3 RESEARCH METHODOLOGY…… 17

3.1 Introduction…….. 17

3.2 Theoretical Background……... 17

3.2.1 Compression Ignition (CI) Engine…… 17

3.2.2 Operating Parameters of Internal Combustion Engines… 18

3.2.3 Engine Parameters……. 19

3.2.4 Work…….. 22

3.2.5 Mean Effective Pressure…… 24

3.2.6 Torque and Power…….. 25

3.2.7 Air to Fuel Ratio…… 27

3.2.8 Stoichiometric Air to Fuel Ratio…… 28

3.2.9 Actual Air to Fuel Ratio……. 28

3.2.10 Equivalence Ratio…….. 29

3.2.11 Specific Fuel Consumption……... 29

3.2.12 Engine Efficiencies…… 30

3.2.13 Water Addition in Internal Combustion Engine…… 32

3.2.14 General Chemical Equilibrium…….. 33

3.2.15 Equilibrium Constant……. 33

3.2.15.1 Basic Equations…….. 34

3.2.16 Equilibrium Constant Method……... 36

3.2.17 Governing Equations……. 36

3.3 Experimental Investigation…….. 41

3.3.1 Engine Modification and Instrumentation…… 41

3.3.2 Hydrogen Fuel Management System……... 45

3.3.3 Water Injection System……. 49

3.3.4 Development of Electronic Control Unit……. 51

3.3.5 Experimental Procedures…….. 57

3.4 Error Analysis 59

3.5 Numerical Investigation Using Newton-Raphson Method…….. 60

3.5.1 MATLAB Inputs……... 62

Chapter 4 RESULTS AND DISCUSSION…….. 64

4.1 Introduction…….. 64

4.2 Experimental Investigation…….. 64

4.2.1 Performance Analysis……... 64

4.2.1.1 In-Cylinder Pressure…… 65
4.2.1.2 Peak Pressure……... 67
4.2.1.3 Heat Release Rate…… 69
4.2.1.4 Ignition Delay…….. 71
4.2.1.5 Gross Indicated Work……... 72
4.2.1.6 Indicated Thermal Efficiency……... 74
4.2.1.7 Indicated Specific Energy Consumption…….. 76
4.2.2 Emissions Analysis……... 77
4.2.2.1 Nitric Oxides…… 78
4.2.2.2 Carbon Monoxide…… 79
4.2.2.3 Carbon Dioxide…… 81
4.2.2.4 Sulfur Dioxide…….. 83
4.2.2.5 Hydrocarbon……. 84
4.2.2.6 Exhaust Gas Temperature…… 86
4.3 Numerical Investigation……... 90
4.3.1 Effect of Equivalence Ratio on Emissions…….. 90
4.3.2 Effect of Temperature on Emissions……... 100
4.4 Experimental Validation……... 108
4.4.1 Oxides of Nitrogen……... 109
4.4.2 Carbon Monoxide……. 111
4.4.3 Carbon Dioxide…… 112
4.4.4 Hydrocarbon……. 114
Chapter 5 CONCLUSIONS AND SUGGESTIONS FOR FUTURE WORK……. 117
5.1 Conclusions…….. 117
5.2 Suggestions for Future Work……...…… 119

References……..…….. 123

Appendix A: Coefficients of Equilibrium Constant Method……..…. 130

Appendix B: Photographic Views of Experimental Apparatus……..……. 133

Appendix C: Mikroelectronika C Language Compiler for ECU development…..... 142

Appendix D: The Elements of Jacobian Matrix……..……. 146

Appendix E: MATLAB Program for HFCI Combustion…….……... 151

Appendix F: Performance Characteristics of HFCI Engine…….…… 162

Appendix G: Emissions Characteristics of HFCI Engine……..……. 184

Appendix H: Details of Publication…….…… 199

LIST OF FIGURES

Figure 3.1	Piston and cylinder geometry of reciprocating engine	19
Figure 3.2	P-*v* diagram for 4-stroke cycle engine	23
Figure 3.3	Configuration for sampling interval	45
Figure 3.4	Hydrogen fuel management setup	48
Figure 3.5	Schematic diagram of experimental apparatus	49
Figure 3.6	Schematic diagram of water and hydrogen injection system	50
Figure 3.7	Main flowchart for ECU operation	53
Figure 3.8	TRI flowchart for ECU operation	54
Figure 3.9	CAM flowchart for ECU operation	55
Figure 3.10	Circuit diagram of the developed ECU	56
Figure 3.11	Terminal program for hydrogen and water injection system	58
Figure 3.12	Flowchart of overall MATLAB program	63
Figure 4.1	Variation of in-cylinder pressure with crank angle at 2000 RPM	65
Figure 4.2(a)	Variation of peak pressure with engine speed (injection duration of 20°CA)	67
Figure 4.2(b)	Variation of peak pressure with engine speed (injection duration of 40°CA)	67
Figure 4.3(a)	Variation of heat release rate with crank angle at 2000 RPM	70
Figure 4.3(b)	Peak heat release rate with different SOI and duration at 3000 RPM	70
Figure 4.4	Variation of ignition delay with different type of experiment	72
Figure 4.5(a)	P-*V* diagram at 2500 RPM and 2 kW load	73
Figure 4.5(b)	Gross indicated work at 1500RPM and 5 kW load	73
Figure 4.6	Variation of ITE with different injection timing at 2500 RPM and 2 kW load	76
Figure 4.7	Variation of ISEC with injection timing at 2000 RPM	77
Figure 4.8	Variation of NO_x emission with engine speed at 2 kW load	79
Figure 4.9	Variation of CO emission with engine speed at 3 kW load	80
Figure 4.10	Variation of CO_2 emission with engine speed at 3 kW load	83
Figure 4.11	Variation of sulfur dioxide emission with engine speed	84
Figure 4.12	Variation of hydrocarbon emission with engine speed	86
Figure 4.13	Variation of exhaust gas temperature with engine speed at 1kW load	87
Figure 4.14	Variation of exhaust gas temperature with engine speed at 3kW load	89
Figure 4.15	Mole fractions of CO_2 with equivalence ratio	91
Figure 4.16	Mole fractions of H_2O with equivalence ratio	92
Figure 4.17	Mole fractions of O_2 with equivalence ratio	93

Figure 4.18	Mole fractions of N_2 with equivalence ratio	94
Figure 4.19	Mole fractions of CO with equivalence ratio	95
Figure 4.20	Mole fractions of CH_4 with equivalence ratio	96
Figure 4.21	Mole fractions of HCN with equivalence ratio	97
Figure 4.22	Mole fractions of NO with equivalence ratio	98
Figure 4.23	Mole fractions of NO_2 with equivalence ratio	99
Figure 4.24	Mole fractions of CO_2 with temperature	100
Figure 4.25	Mole fractions of H_2O with temperature	101
Figure 4.26	Mole fractions of O_2 with temperature	102
Figure 4.27	Mole fractions of N_2 with temperature	103
Figure 4.28	Mole fractions of CO with temperature	104
Figure 4.29	Mole fractions of CH_4 with temperature	105
Figure 4.30	Mole fractions of HCN with temperature	106
Figure 4.31	Mole fractions of NO with temperature	107
Figure 4.32	Mole fractions of NO_2 with temperature	108
Figure 4.33	Simulated and experimental values of NO_x emission in DA operation	109
Figure 4.34	Simulated and experimental values of NO_x emission in DH operation	110
Figure 4.35	Simulated and experimental values of NO_x emission in DHW operation	110
Figure 4.36	Simulated and experimental values of CO emission in DA operation	111
Figure 4.37	Simulated and experimental values of CO emission in DH operation	111
Figure 4.38	Simulated and experimental values of CO emission in DHW operation	112
Figure 4.39	Simulated and experimental values of CO_2 emission in DA operation	113
Figure 4.40	Simulated and experimental values of CO_2 emission in DH operation	113
Figure 4.41	Simulated and experimental values of CO_2 emission in DHW operation	114
Figure 4.42	Simulated and experimental values of HC emission in DA operation	115
Figure 4.43	Simulated and experimental values of HC emission in DH operation	115
Figure 4.44	Simulated and experimental values of HC emission in DHW operation	116

LIST OF TABLES

Table 3.1	Engine specifications of YANMAR L100AE-D2YC	41
Table 3.2	Valve timing of YANMAR L100AE-D2YC	42
Table 3.3	Technical specifications of generator	42
Table 3.4	Properties of hydrogen and diesel fuels	43
Table 3.5	Specifications of OMEGA digital mass flow meter	46
Table 3.6	Diesel energy replacement by hydrogen	47
Table 3.7	NAMUR hydrogen fuel injector technical specifications	48
Table 3.8	Technical specifications of Microchip PIC18F452 microcontroller	53
Table 3.9	Start of injection timings and injection durations for DHW operation	57
Table 3.10	Water injection flow rate	57
Table 3.11	Error analysis of measured and derived quantities	60

NOMENCLATURES

a	Crank Radius
A	Surface Area of Combustion Chamber
A_{ch}	Surface Area of Cylinder Head
ADM	Adomian's Method
AF	Air to Fuel Ratio
AF_{actual}	Actual Air to Fuel Ratio
AF_s	Stoichiometric Air to Fuel Ratio
Amp	Ampere
A_p	Cross-sectional Area of a Cylinder
a_s	Stoichiometric Molar Air-Fuel Ratio
ATDC	After Top Dead Center
B	Bore
bmep	Brake Mean Effective Pressure
bsfc	Brake Specific Fuel Consumption
BTDC	Before Top Dead Center
C	Atom Carbon
CA	Crank Angle
CAM	Crank Angle Measurement
CFD	Computational Fluid Dynamics
CH_4	Methane Gas
CI	Compression Ignition Engine
CO	Carbon Monoxide
CO_2	Carbon Dioxide
DA	Diesel Alone
DAS	Data Acquisition System
DH	Diesel with Hydrogen Fuel
DHW	Diesel with Hydrogen Fuel and Water Injection
ECM	Equilibrium Constant Method
ECU	Electronic Control Unit
EGR	Exhaust Gas Recirculation
EGT	Exhaust Gas Temperature
EOI	End of Injection
fsfc	Friction Specific Fuel Consumption

G_F	Gibbs Function
G_i	Gibbs Molar Function
H	Atomic Hydrogen
H_2	Hydrogen
H_2O	Water
HC	Hydrocarbon
HCCI	Homogeneous Charge Compression Ignition
HCN	Hydrogen Cyanide
HFCI	Hydrogen-fuelled Compression Ignition Engine
HHO	Hydroxy
HNO_3	Nitric Acid
HPM	Homotopy Perturbation Method
HRR	Heat Release Rate
I/O	Input Output
igsfc	Indicated Gross Specific Fuel Consumption
IMC	Integrated Measurement and Control
imep	Indicated Mean Effective Pressure
insfc	Indicated Net Specific Fuel Consumption
ISEC	Indicated Specific Energy Consumption
isfc	Indicated Specific Fuel Consumption
ITE	Indicated Thermal Efficiency
K	Equilibrium Constant
k_f	Rate Coefficient for Forward Reaction
K_n	Equilibrium Constant
k_r	Rate Coefficient for Reverse Reaction
kW	Kilowatt
LPH	Liter per Hour
LTCM	Low Temperature Combustion Model Method
MEP	Mean Effective Pressure
MOSFET	Metal Oxide Semiconductor Field Effect Transistor
N	Atomic Nitrogen
N_2	Nitrogen
N_c	Number of Engine Cylinders
n_i	Number of Moles for species *i*
NO	Nitrogen Oxide

NO_2	Nitrogen Dioxide
NO_x	Oxides of Nitrogen
NR	Newton–Raphson method
n_T	Total Number of Mole
O	Atomic Oxygen
O_2	Oxygen
O_3	Tri-Oxygen
OH	Hydroxide
P	Pressure
PHRR	Peak Heat Release Rate
psfc	Pumping Specific Fuel Consumption
r	Connecting Rod Length
r_c	Compression Ratio
RPM	Revolutions per Minute
s	Instantaneous Stroke
S	Stroke
sfc	Specific Fuel Consumption
SI	Spark Ignition
SIM	Simulated Values
SOI	Start of Injection
TDC	Top Dead Center
TRI	Trigger
UHC	Unburned Hydrocarbon
V	Voltage
V	Volume
v	Specific Volume
V_c	Clearance Volume
V_d	Displacement Volume
W	Work
W_b	Brake Power
w_f	Specific Work Lost Due to Friction and Parasitic Loads
w_i	Indicated Work
θ	Instantaneous Crank Angle
$\overline{U}_p$	Average Piston Speed

η_m	Mechanical Efficiency
η_f	Fuel Conversion Efficiency
η_c	Combustion Efficiency
P_e	Total Pressure of the System
ϕ	Equivalence Ratio
μ-MUSYCS	Multi Synchronous Channel Data Acquisition System
20CA	Injection Duration of 20°CA
40CA	Injection Duration of 40°CA

Chapter 1

INTRODUCTION

1.1 Research Background

The world fossil fuels resources are depleting very fast and it is reported that it will last only for about 50 more years (Boretti et al. 2011). The predicted period is even shorter for some Asian countries with high development rate such as Malaysia. Therefore, researches on alternative and renewable source of energy are being extensively carried out (Masjuki et al. 2001). Another motive for the search of alternative fuels particularly in the transportation sector is that fossil fuels are causing serious environmental problems such as air pollution and global warming. In this case, the increasing use of natural gas in the transportation sector especially in Malaysia is a major breakthrough because it is cleaner to handle and more environmental friendly than other fossil fuels. However, since it contains hydrocarbon, natural gas can still contaminate the environment. In fact, natural gas can be considered a suitable bridge for the ultimate fuel such as hydrogen that may help to resolve the world energy crisis.

It has been reported recently that a vast reservoir of hydrogen is trapped beneath the earth crust (Papagiannakis et al. 2004). Although hydrogen can be obtained from natural gas but natural gas is not renewable. Hydrogen can also be obtained from biomass using various techniques, but the most environmental-friendly method is to generate hydrogen from water electrolysis.

In 1800's Francois Isaac de Rivaz invented the world's first hydrogen powered internal combustion engine. During that time, hydrogen engine did not receive much of attention due to abundant diesel and petrol supplies to power the engine. The usage of

hydrogen in transportation specifically for petrol engine was vastly introduced in the market since early year 2000. Car manufacturers such as BMW, Mitsubishi, Toyota and Nissan have monopolies mid-range market segment for hydrogen powered petrol engine. Hydrogen usage in diesel engine is very rare as compared to its application on petrol engine (Verhelst et al. 2001).

The higher efficiency and lower fuel costs makes diesel engines a clear choice in applications requiring relatively large amounts of power such as in large ships, heavy trucks and power generation units. Generally, diesel engines have higher thermal efficiencies due to higher compression ratios. However, high compression ratio also leads to higher combustion temperature and encourages the formation of nitrogen oxides (NO_x) emissions. High compression ratio is particularly suitable for some alternative fuels such as hydrogen. It is widely accepted as the ultimate fuel of the future because of its wide flammability limit and high flame speeds which lends itself readily to ultra lean combustion that allows the use of higher compression ratios (Overend, 1999). Although the use of hydrogen as fuel for internal combustion engines eliminates the emissions of sulphur oxides (SO_x), oxides of carbon (CO and CO_2), unburned hydrocarbons (UHC) and soot, some studies have shown that the NO_x emissions increased as the compression ratio increased and even exceeded that of conventional fossil fuels (DeBoer, 1976).

Hydrogen is seen to have very wide ignition limits and its self-ignition temperature is in the range of 800K to 900K (Ikegami et al. 1982). Due to that, it is very difficult to ignite hydrogen by compression ignition process and consequently it is unsuitable fuel for conventional diesel engine. At the same time, it would be highly desirable to develop methods to utilize hydrogen in diesel engines since they form a sizable portion of the engines used in transportation industry and power generation. In the initial research stage, attempts have been made to inject hydrogen under pressure

into compressed air as in the normal diesel engine (Gopal et al. 1982). The aid of glow plugs and modifying the engine for higher compression ratios has been found to be necessary to initiate compression ignition. Injection of hydrogen into the engine cylinder and modifying geometric parameter of the engine in order to achieve higher compression ratio are inherently difficult tasks. In this case, a considerable modification of the engine is necessary to convert the existing conventional diesel engines to run on hydrogen. The most applicable method for hydrogen-fuelled diesel engine is to induct hydrogen along with air into the cylinder by installing hydrogen injector near to the intake port (Das, 1990).

Hydrogen addition leads to higher local temperature at the earlier stage in the expansion process, resulting in rapid NO_x formation rate. The issue of high NO_x formation in hydrogen-fuelled engine is well known and the solution is taken periodically by many researchers. The method of introducing water injection system would be the best solution to reduce NO_x formation. The dissociation process of water to form hydroxide and hydrogen at high temperature absorbs the heat during combustion. The capability of water to absorb heat of combustion specifically at high temperature range reduces the temperature of combustion products and leads to lower NOx emissions.

In tropical regions, naturally aspirated internal combustion engines suffer from engine performance deterioration due to the effects of high ambient temperature. High temperature reduces the air density and mass flow rate of air into the engine cylinder. This, in turn, reduces both engine power and thermal efficiency. The proposed research project addresses these problems and provides solution by introducing water injection for both power augmentation and control of emissions.

Fundamentally, water injection in the engine helps to control combustion temperature and pressure. Hence, it is beneficial in controlling unwanted emissions. It

can also improve the volumetric efficiency of the engine and consequently augment its power. Water injection system has been used for this purpose in gas turbines cycle for which the technology is well established (Deboln et al. 1998). Its usage in internal combustion engines fuelled with conventional petroleum-based fuels or natural gas is rare. However, water injection system is considered as a cheaper solution and more relevant in hydrogen-fuelled internal combustion engines for power augmentation and emissions control.

1.2 Research Objective

The primary objective of this dissertation is to investigate the performance and emissions of hydrogen-fuelled compression ignition (HFCI) engine with water injection system. The objectives of this dissertation are as given below:

a) To modify the compression ignition (CI) engine.

- To develop and install timed port injection system for hydrogen gaseous fuel on CI engine.
- To develop and install timed manifold water injection system on CI engine

b) To study the effect of water injection system on HFCI engine.

- To investigate the performance and emissions of CI engine using conventional diesel, hydrogen gaseous fuel with and without water injection system.
- To analyze the experimental results of HFCI with water injection system.
- To compare the performance and emissions of HFCI with and without water injection system.

c) To validate the experimental results on emission characteristics of HFCI.

- To develop mathematical model on emission characteristics of HFCI with and without water injection.
- To validate the experimental results on emission characteristics of HFCI engine using the developed mathematical model.

d) To determine the optimum water injection timing for better performance and emission control.

1.3 Limitations of Research

This research includes the study of performance and emissions control of HFCI with water injection system. Experimental validation on emission characteristics will be carried out based on the developed mathematical model. This research is performed in the following sequences:

(a) Preliminary investigation:

This phase is aimed to develop HFCI engine with water injection system experimental setup. Hydrogen flash back arrestor, single-flow valve and water-flame trap are installed to prevent backfire in the fuel management system. Timed port injection system of hydrogen gaseous fuel and timed manifold water injection system are used in order to introduce hydrogen and water droplets into the combustion chamber at a specific crank angle (CA). This study is limited to a constant 3 liter per hour (LPH) hydrogen supply at injection timing of 0°CA to 20°ATDC. Water is at room temperature and it is injected at intake manifold of the engine with constant injection

pressure of 1 bar. Water injection duration is limited to 20°CA and 40°CA and its start of injection (SOI) is in the range between 20°BTDC to 20°ATDC. Due to limitation of experimental apparatus, the performance analysis is limited to indicated properties of the engine with applied loads in the range of 1kW to 5kW and speed in the range of 1500RPM to 3000RPM. At higher speeds, operations are restricted only for lower loads. The incremental values for loads and speeds are 1kW and 500RPM, respectively.

(b) Detailed investigation of HFCI engine with water injection system.

The effect of water injection in HFCI on performance and emissions are investigated. Experimental work will be performed in order to find the optimum timing of water injection for power augmentation and emissions control. The mathematical model based on nine (9) combustion products of HFCI engine will be developed. Input data especially pressure and temperature will be determined from heat release analysis at respective crank angle towards the end of combustion phase. Newton-Raphson Method is selected to solve equilibrium constants combustion equations of hydrogen-diesel dual fuels with water addition. In this research, only experimental emission characteristics will be validated with the developed mathematical model. Experimental validation on emissions characteristics will be performed based on four (4) types of measured emissions namely oxides of nitrogen (NO_x), carbon monoxide (CO), carbon dioxide (CO_2) and hydrocarbon (HC). Diesel used for this model is assumed as Malaysian diesel with chemical formula of $C_{12}H_{23}$ without any sulfate contents meaning that emissions of sulfur dioxide cannot be validated.

(c) Evaluating the experimental and numerical results.

The results obtained from the investigations are analyzed and conclusions drawn on the performance and emissions of HFCI engine. The optimum injection timing for better power performance and emissions will be identified.

1.4 Research Contribution

The development of experimental setup with extreme safety measures in order to prevent backfire of hydrogen gaseous fuel provides room for improvement especially for other Malaysian researchers and industry that are going to utilize hydrogen as a source of combustion energy.

The development of timed port injection system of hydrogen fuel provides better fuel economy and safety as compared to continuous port injection system. Continuous injection of hydrogen at the intake port or manifold promotes the occurrence of backfire which worsens the performance and emission of HFCI. The developed system is able to detect and respond on crank angle signals based on the desired SOI and EOI effectively. Furthermore, the detection technique of the system is able to distinguish between compression and power strokes.

The development of timed manifold water injection system contributes towards better emissions control and power augmentation as compared to continuous water injection system. Continuous water injection at the intake manifold causes water to dribble and mix with engine lubricant resulting in deterioration of engine performance. The developed system is able to operate based on the desired injection timing. In this case, water will only be injected during intake stroke and provides better premixing with intake air and hydrogen gaseous fuel. The developed system is very responsive

towards signals from crank angle encoder and it provides better control of injection timing and duration.

The developed mathematical model based on Equilibrium Constant Method and solved using Newton-Raphson Method helps to predict the effect of hydrogen and water addition in diesel fuel combustion. This model is a powerful tool in simulating emission characteristics of HFCI engine. It is also very useful in experimental validation.

Results from the research may help to reduce hazardous emission of CI engine especially NO_x and hence reduces environmental pollution which contributes towards sustainability. Power augmentation of HFCI engine with water injection system leads to better fuel consumption and energy saving.

Power producing company especially in Malaysia will benefit from this research in such a way that, with proper injection timing of hydrogen fuel it will provide better fuel economy for diesel power generation unit. Water injection system is also useful in power generation unit since it is environmental-friendly and lower operational cost.

This research generated a proper guidance for researchers and engineers to further research water injection technique in combustion engine. This is essential for substantial environmental benefits and energy efficiency.

Chapter 2

LITERATURE REVIEW

2.1 Introduction

Diesel engine is known as dominant in power-train solution in the world especially in transportation sector. The challenges that diesel engine is facing now are due to its poor pollutant emissions quality and brake engine efficiency (Hountalas et al. 2005). More stringent emission regulation forces rapid impact to transportation sector. On the other hand, increasing price of crude oil and poor emissions of diesel engines have motivated researchers to investigate the application of alternative fuels such as hydrogen in diesel cycles (Nabi et al. 2010). Its application in combustion engine especially in spark ignition (SI) engine has been investigated for decades and extensive reviews are provided by researchers (Verhelst et al. 2006).

Hydrogen, as an energy medium, has some distinct benefits for its high efficiency and convenience in storage, transportation and conversion. Hydrogen has found vast applications in fields such as electricity generation, vehicle engines and aerospace. The space program has used hydrogen for years in its electrical power system (EPS). Hydrogen fuel cell provides electrical power to the shuttle and the by-product which is water and consumed by the crew (Brenda et al. 2005). The most important advantage of hydrogen engine is that it emits fewer pollutants than other engine. Experiments have been done decades before to investigate the effectiveness of using hydrogen as a fuel. Hydrogen offers a possible solution to such problems as energy security resource availability and environmental concerns (Wallner et al. 2008).

Many researchers have used hydrogen as a fuel in spark ignition (SI) engine. A significant reduction in power output was observed while using hydrogen in SI engine

and in addition pre-ignition, backfire, and knocking problems were observed at high load. These problems have resulted in using hydrogen in SI engine within a limited operation range (Caton, 2001). However, hydrogen cannot be used as a sole fuel in a diesel engine, since the compression temperature is not enough to initiate the combustion due to its higher self-ignition temperature (Saravanan et al. 2008). Hence, an ignition source is required while using it in a diesel engine. The applicable method of using hydrogen in a diesel engine is to run in the dual fuel mode with diesel as the main fuel that acts as an ignition source for hydrogen (Wimmer et al. 2005). In a hydrogen-diesel dual fuel engine, the main fuel is either inducted or injected into the intake air stream with combustion initiated by the diesel. The major energy is obtained from diesel while the rest of the energy is supplied by hydrogen (Xing-hua et al. 2008).

2.2 Recent Research on Hydrogen Engine

Most research in hydrogen-diesel dual fuel diesel engine has concentrated on experimental study on performance and emissions. Saravanan et al. reported several investigations on hydrogen fuelled single cylinder diesel engine and concluded dramatic decrease in NO_x at full load operation with optimum injection duration of 90°CA and SOI at 5°ATDC for the best results on performance and emissions. Saravanan et al. concluded hydrogen with diethyl ether showed significant reduction in smoke and NO_x emissions. The optimum hydrogen flow rate of 7.5 liter per minute (LPM) was determined for better performance and emissions. Timed port injection technique showed better specific energy consumption and smoke level as compared to carburetion technique. Increase in 15% of NO_x emissions with improved engine efficiency was observed at injection timing of gas exchange top dead center. In subsequent work, Saravanan et al. also investigated on exhaust gas recirculation (EGR) in hydrogen diesel fuel mode and concluded that reduction in NO_x concentration with

EGR system. Start of injection (SOI) at 5°CA before gas exchange top dead center and duration of 30°CA showed the optimum performance and emissions hydrogen dual fuel diesel engine system (Saravanan et al.2007-2010).

Sentil et al. studied the application of small quantity of hydrogen along with Jatropha oil in diesel engine. Results showed increased power output and brake thermal efficiency to a maximum of 30% (Sentil et al. 2003). Szwaja et al. investigated combustion of hydrogen under homogeneous charge compression ignition (HCCI) conditions in a CI engine. They concluded that a small amount of hydrogen shorten the ignition lag of diesel and decreases the rate of pressure rise (Szwaja et al. 2009).

Singhyadav et al. researched on direct injection CI engine in dual fuel mode (hydrogen-diesel) with EGR system. In their work, specific energy consumption, brake specific fuel consumption, brake thermal efficiency, NO_x, HC, CO, CO_2, O_2 and exhaust gas temperature were measured. EGR system resulted in lowered emissions and improved performance as compared to conventional diesel operation (Singhyadav et al. 2011).

Roy et al conducted a series of experiments on direct injection SI engine to study the flame characteristics. They reported that ignition timing influences combustion characteristics in hydrogen direct-injection combustion and tail ignition resulted in minimum IMEP (Roy et al. 2011). In subsequent work, they investigated the effect of hydrogen content in the producer gas on the performance and emissions of a supercharged dual fuel diesel engine fueled at constant injection pressure and injection quantity (Roy et al. 2009).

Gomez et al. developed an experimental setup for direct injection hydrogen-fuelled diesel engine. They concluded that hydrogen direct injection in diesel engine produces higher power to weight ratio and 14% increase in peak pressure as compared to diesel alone operation (Gomez et al. 2009).

Liew et al. investigated on the effect of small amount of hydrogen on a heavy-duty diesel engine. The addition of small amount of hydrogen has shown mild increase on cylinder pressure and elongated diffusion combustion phase (Liew et al. 2010).

Miyamoto et al. experimentally researched cyclic variation of combustion characteristics of hydrogen-diesel fuel mode with blow-by gas addition at the intake air. Preflame reaction that ignited hydrogen and then diesel fuel was observed when blow-by gas was injected at the intake port (Miyamoto et al. 2011).

Karim concluded that at low loads, much of the primary gaseous fuel remains unburned leading to high hydrocarbon (HC) and CO emissions especially for hydrogen gaseous fuel. At high loads, a large amount of gaseous fuel admission resulted in uncontrolled reaction rates near to pilot spray causing rough engine operation and consequently deteriorated the engine performance (Karim, 2003).

2.3 Recent Research on Hydrogen Engine (Simulation)

Computer simulation was conducted by Masood et al. using Low Temperature Combustion Model Method (LTCM) with ten (10) combustion product species under hydrogen-diesel dual fuel mode and concluded significant reduction in CO_2 and NO_x (Masood et al. 2008). In other investigation, Masood et al. validated hydrogen combustion in diesel engine using Computational Fluid Dynamics (CFD) software FLUENT. The standard combustion models were used for the analysis and concluded that hydrogen-diesel co-fuelling help in lean combustion of diesel. Good agreement was obtained between simulated and experimental results (Masood et al. 2007). Ma et al. (2003) developed computer simulation to predict the performance of a hydrogen vehicle engine.

Boretti et al. have performed series of simulations on two-stroke compression ignition engine with direct injection of hydrogen, oxygen and water by using STAR-

CCM and DARS. They reported that water injection reduces metal temperature of the cylinder block that resulted in a reduction in heat loss. They also concluded that direct water injection is capable of increasing fuel conversion efficiency and BMEP in hydrogen-oxygen compression ignition engine (Boretti et al. 2011).

Waller et al. analyzed three-dimensional CFD model of direct injection hydrogen SI engine and validated with series of experiments. A decrease in engine efficiency was reported at lower speed due to higher heat wall release. NO_x formation was the highest at the peak indicated efficiency (Waller et al. 2011).

Perini et al. investigated two zone quasi-dimensional models for the simulation of combustion process in spark ignition engines fueled with hydrogen, methane, or hydrogen-methane blends (Perini et al. 2010).

The mathematical models to predict pressure, net heat release rate, mean gas temperature, and brake thermal efficiency for dual fuel diesel engine operated on hydrogen, LPG and mixture of LPG and hydrogen as secondary fuels were developed by Lata et al. (Lata et al. 2010).

Lilik et al. developed numerical NO_x models emissions using finite volume method and then validated experimentally. Numerical results concluded that temperature alone is not enough to explain increase in NO_x emissions (Lilik et al. 2010). Verhelst et al. have developed a quasi-dimensional two-zone combustion model framework to calculate the pressure and temperature development in hydrogen engines (Verhelst et al. 2007). Wang et al. have developed a multidimensional model based on CFD and coupled with detail reaction kinetics to study the combustion process in H_2/CNG engine (Wang et al. 2010).

2.4 Research on Hydrogen Engine with Water Injection Techniques

Tesfa et al. investigated on the effects of water injection system in biodiesel engine. Experimental works were conducted to measure in-cylinder pressure, specific fuel consumption, water injection flow rate, fuel flow rate and exhaust characteristics. It showed that water injection of 3 kg/h resulted in NO_x reduction by 50% without deteriorate engine performance (Tesfa et al. 2012).

Tauzia et al. researched on the effects of water injection on ignition delay, rate of heat release and emissions of an automotive direct injection diesel engine. They concluded that higher water flow rate contributes towards longer ignition delay, higher peak heat release, lowered NO_x emissions but deteriorated production of CO and HC (Tauzia et al. 2010).

Comparison of water-diesel emulsion and timed intake manifold water injection on diesel engine was investigated by Subramanian. He concluded that both methods could reduce NO_x emission drastically in a diesel engine. However, CO and HC levels were higher with emulsion than that of water injection. Peak pressure, ignition delay and maximum rate of pressure rise were lesser with water injection as compared to emulsion method (Subramaniam, 2011)

Prabhukumar et al. investigated on the effects of continuous water induction in hydrogen-diesel dual fuel diesel engine. They concluded that power output of a hydrogen-diesel dual-fuel engine is limited by the onset of knock especially when hydrogen exceeds about 60% of input energy at a pilot diesel quantity of 30% of full load diesel amount. At higher rates of hydrogen induction, the richer hydrogen-air mixture is more prone to knocking. Water induction serves as coolant in decreasing the unburned mixture temperature to improve knocking in diesel engine (Prabhukumar et al. 1987).

Hountalas et al. developed multi-zone simulation model to investigate the effect of water emulsion and water injection on NO_x for heavy-duty diesel engines. It was concluded that with optimum water to fuel ratio during the intake provides maximum NO_x reduction without affecting engine power output. In subsequent work, the same researcher performed extensive research on advanced injection strategies, increased injection pressure of water as solution for NO_x reductions (Hountalas et al. 2002-2006).

Nande et al studied the influence of water injection on performance and emissions direct injection hydrogen spark ignition (SI) engine. They concluded that water injection is more effective technique to reduce NO_x as compared to retarding spark timing of SI engine. At high load, water injection retarded the combustion phase which requires advanced spark timing in order to maintain its power output (Nande et al. 2008). Almost the same study was conducted by Gadallah et al. on hydrogen fuelled direct injection SI engine with water injection system. They reported that with optimum injection timing especially during the later stage of compression stroke improves indicated thermal efficiency and maximum NO_x reduction (Gadallah et al. 2009).

Water injection technique is the cheapest available method to reduce local combustion temperature and consequently NO_x emissions in the engine (Conklin et al. 2010). In combustion chamber, water droplet is classified as inert with powerful heat absorption causes decrease in local adiabatic flame temperature (Lin et al. 2006). Reduced flame temperature contributes towards lowered NO_x emissions, HC and soot as reported by (Kadota et al. 2002). The optimum water injection system is water direct injection technique which requires high pressure of injection into combustion chamber. This technique provides better control of fuel to water ratio in the combustion chamber (Stanglmaier et al. 2008). The same system was developed by Southwest Research Institute and Delphi Diesel Systems for heavy-duty diesel engines. It is integrated with electronic control unit and common-rail fuel pumps that deliver water and diesel at

injector tip. This method has reported to reduce NO_x emissions by 42% and with EGR combination this technique is capable to reduce NO_x until 82% (Chadwell et al. 2008).

Mathur et al. investigated the effects of continuous water induction on performance and emission characteristics of hydrogen-fuelled diesel engine. In their work, hydrogen in gaseous form has been continuously injected at the intake manifold before it is premixed with intake air. The system was run in dual-fuel mode with hydrogen induction rates ranging from zero to 60 LPM. They concluded that continuous water induction in hydrogen-fuelled diesel engine causes decreased thermal efficiency in the range of 5% to 15% at 60 LPM of hydrogen supply and 75% loads. However, with an increased amount of water induction, thermal efficiency has shown some increment in the range of 4% to 6% as compared to that of diesel alone operation. The greater the amount of water induced better control on emission parameters. Smoke levels are almost negligible, while NO_x emissions are reduced to the minimum (Mathur et al. 1992-1993].

In the present research, experimental investigations will be carried out to analyze the effect of timed manifold water injection on performance and emissions of HFCI engine. Numerical investigation will be performed to research the effect of water injection on exhaust gas emissions characteristics of HFCI engine. An effort is made to simulate the exhaust emissions of HFCI with and without water injection system. Based on Equilibrium Constant Method (ECM), a computer program using MATLAB has been developed for the blended fuels to calculate mole fractions of the emission gases. Equilibrium constant is based on thermodynamic measurements and empirical calculations are used in solving chemical kinetics of HFCI combustions. Experimental validations will be carried out on exhaust gas emissions characteristics of HFCI engine.

Chapter 3

RESEARCH METHODOLOGY

3.1 Introduction

This chapter addresses experimental and numerical methods. The properties of fuel used, apparatus setup, experimental and numerical procedures are also presented. Experimental investigation will be carried out to research the performance and emissions of HFCI engine. The essential components for the experimental setup were selected with a clear understanding of their capabilities and limitations. A fully functional electronic control unit (ECU) was designed for timed port hydrogen and water injection systems. Numerical investigation will be carried out to study the emissions characteristics of HFCI combustion. Heading towards this, mathematical model will be developed based on Equilibrium Constant Method (ECM) to investigate emissions characteristics and then utilized for experimental validation.

3.2 Theoretical Background

3.2.1 Compression Ignition (CI) Engines

CI engine use fuels of lower volatility with compression ratios from 15 to 25 and compression pressures between approximately 4 MPa and 6 MPa. Advantages of CI engine over SI engine include a lower specific fuel consumption, slightly higher thermal efficiency, relatively cheaper fuel costs, lower CO and hydrocarbon emissions at low and medium loads, lower capital costs and higher durability. Disadvantages include higher noise of operation, higher engine weight required to withstand the higher pressures and higher emission of NO_x. Based on processes involved in compression

stroke, diesel fuel is pre-mixed with the cylinder charge just before the combustion begins. However, there is a constraint in diesel engine emission which is the formation of smoke due to inadequate mixing of fuel and air.

CI engines can be characterized by the injection type namely direct injection (DI) or indirect ignition (IDI). YANMAR L100AE experimental diesel engine is DI type, implying that diesel fuel is sprayed through a multi-hole injector nozzle directly into the combustion cylinder to mix with the cylinder charge. IDI type diesel engine mixes diesel fuel and air in the antechamber prior to entering the main combustion chamber in an attempt to improve mixing and therefore better combustion especially during lower ambient temperature. Diesel fuel is sprayed from an essentially single-hole injector nozzle into a divided type of combustion chamber (antechamber). This antechamber is formed partly in the cylinder head and partly by a saucer shaped depression on the piston head (Nunney, 1982).

3.2.2 Operating Parameters of Internal Combustion Engines

This section discusses the operation parameters of reciprocating internal combustion engines. The purpose of presenting the operating characteristics is to be familiar with the parameters which will be encountered in the analysis of data obtained from series of experiments and simulations conducted pertaining to performance and emissions of HFCI engine.

3.2.3 Engine Parameters

Referring to Figure 3.1, the parameters shown are piston and cylinder geometry of an engine. The parameters are:-

- B = bore
- S = stroke
- r = connecting rod length
- a = crank radius
- s = instantaneous stroke
- θ = instantaneous crank angle
- V_c = clearance volume
- V_d = displacement volume

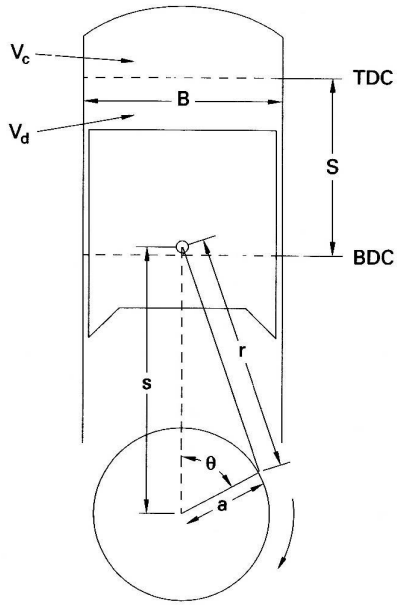

Figure 3.1 Piston and cylinder geometry of reciprocating engine

For an engine with bore, B, crank offset, a, stroke length, S, revolving at an engine speed of N yields:

$$S = 2a \tag{3.1}$$

Average piston speed is given as:

$$\overline{U}_p = 2SN \tag{3.2}$$

As for all engines, average piston speed will be normally in the range of 5 to 15 ms^{-1}. This range is limited with the concern of safety factor for the material strength of

the engine components. In CI engines, piston speed determines the instantaneous flow rate of air into the combustion chamber during intake stroke and flow rate of exhaust gases out from combustion chamber during exhaust stroke.

The range of sizes for engine bore is from 0.5 m down to 0.5 cm. For small engines, the ratio of bore to stroke, *B/S* is usually from 0.8 to 1.2. An engine with $B = S$ is often called a square engine. If bore diameter is less than stroke length, the engine is under square. Whereas, the engine is over square when bore diameter is larger than stroke length. Large engines are always classified as under square with stroke lengths up to four (4) times more than its bore size (Ganesan, 2004).

The distance *s* between crank axis and wrist pin axis can be calculated from the expression below:

$$s = a\cos\theta + \sqrt{r^2 - a^2 \sin^2\theta} \tag{3.3}$$

When *s* is differentiated with respect to time and the instantaneous piston speed U_p is obtained as shown below:

$$U_p / \overline{U}_p = (\pi/2)\sin\theta[1 + (\cos\theta / \sqrt{R^2 - \sin^2\theta})] \tag{3.4}$$

where: $R = r/a$ (3.5)

R is the ratio of connecting rod length to crank offset. Usually, for small engines the values are in the range of 3 to 4 whereas larger engines have values in between 5 to 10.

Stroke or displacement volume, V_d, refers to the volume displaced by the piston as it moves from BDC to TDC:

$$V_d = V_{BDC} - V_{TDC} \tag{3.6}$$

Displacement volume can be represented in terms of the volume per cylinder or the entire engine. For one cylinder:

$$V_d = (\pi / 4) B^2 S \tag{3.7}$$

For an engine with N_c number of cylinders:

$$V_d = N_c (\pi / 4) B^2 S \tag{3.8}$$

where: N_c = number of engine cylinders

The unit of engine displacement is in cubic meter (m^3), cubic centimeter (cm^3), cubic inches (in^3) and most commonly is in liters (L).

When piston is at TDC, the cylinder volume would be at minimum, which is called the clearance volume, V_c

$$V_c = V_{TDC} \tag{3.9}$$

$$V_{BDC} = V_c + V_d \tag{3.10}$$

The compression ratio of an engine is defined as:

$$r_c = V_{BDC} / V_{TDC} = (V_c + V_d) / V_c \tag{3.11}$$

For modern SI engines, the compression ratios are in between 8 to 11, while for CI engines the compression ratios are in the range of 12 to 24 (Pulkrabek, 2004). At any respective crank angle, the instantaneous cylinder volume would be:

$$V(\theta) = V_c + (\pi B^2 / 4)(r + a - s) \tag{3.12}$$

Such an expression can also be represented in non-dimensional form by dividing with clearance volume, V_c and is shown below:

$$V / V_c = 1 + \frac{1}{2}(r_c - 1)[R + 1 - \cos\theta - \sqrt{R^2 - \sin^2\theta}] \tag{3.13}$$

Where: r_c = compression ratio and R = r/a

The cross-sectional area of a cylinder is given as A_p:

$$A_p = (\pi / 4) B^2 \tag{3.14}$$

The surface area of combustion chamber is given as:

$$A = A_{ch} + A_p + \pi B(r + a - s) \tag{3.15}$$

where A_{ch} is the surface area of cylinder head which is larger that A_p.

Equation 3.15 can be written as:

$$A = A_{ch} + A_p + (\pi BS/2)[R + 1 - \cos\theta - \sqrt{R^2 - \sin^2\theta}] \tag{3.16}$$

3.2.4 Work

In a reciprocating engine, work is generated by the gases in combustion chamber. As commonly known, work is the result of force acting through a distance. The gas pressure acting on the piston as force on moving piston generates work in an engine cycle.

$$W = \int F dx = \int P A_p dx \tag{3.17}$$

where: P = pressure in combustion chamber

A_p = area against which the pressure acts (i.e., the piston head)

x = distance the piston moves

and: $$A_p dx = dV \tag{3.18}$$

dV represents the differential volume displaced by the piston, so work done can also be expressed as:

$$W = \int P dV \tag{3.19}$$

where: $$w = W/m \quad \text{and} \quad v = V/m \tag{3.20}$$

and yields: $$w = \int P dv \tag{3.21}$$

Figure 3.2 shows the P-*v* diagram of a 4-stroke engine. The indicated work can be determined from the enclosed area under the curves. The pressure inside the combustion chamber is represented as, P in the respective figure. From Equation 3.21 and the computation of areas shown in Figure 3.2, work inside the combustion chamber is obtained as indicated work. In fact, there is some mechanical friction and parasitic loads of the engine which cause the work delivered by crankshaft to be less than indicated work. The components like oil pump, supercharger, air conditioner compressor and alternator contributes to parasitic load.

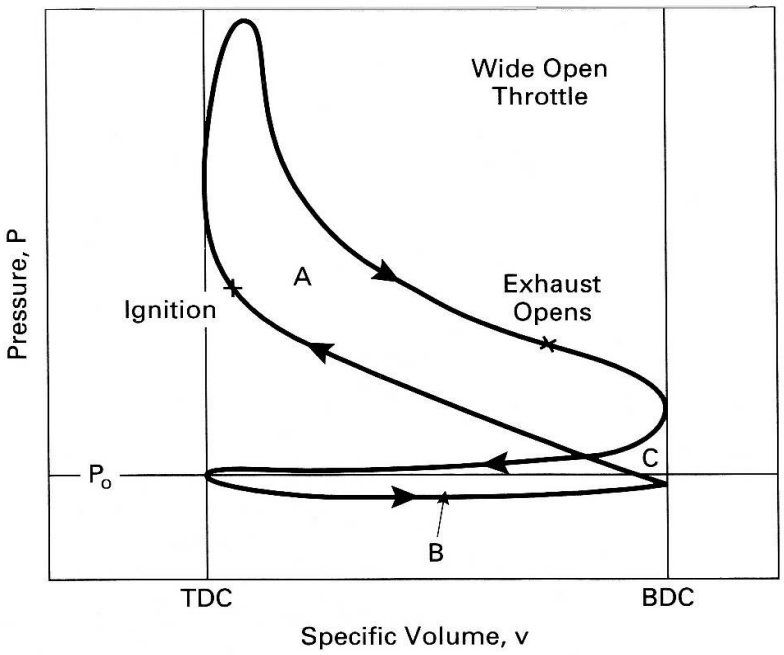

Figure 3.2 P-*v* diagram for 4-stroke cycle engine.

Hence, the actual work available at the crankshaft is called brake work, w_b:

$$w_b = w_i - w_f \tag{3.22}$$

where: w_i = indicated work

w_f = specific work lost due to friction and parasitic loads

In Figure 3.2, the upper curves A and B of engine cycle are known as compression and power strokes. The enclosed area under these curves produces output

work known as gross indicated work. The lower curves B and C comprises of intake and exhaust strokes. The enclosed area under these curves produces pump work. The total of gross indicated work and pump work gives net indicated work and represented as:

$$w_{net} = w_{gross} + w_{pump} \tag{3.23}$$

Mechanical efficiency of an engine can be obtained from the ratio of brake work at the crankshaft to indicated work in the combustion chamber:

$$\eta_m = w_b / w_i = W_b / W_i \tag{3.24}$$

3.2.5 Mean Effective Pressure

Mean effective pressure (*mep*) is the work done per unit displacement volume (Saravanan et al. 2010). Based on the Figure 3.2 as shown in preceding section, the P-v diagram shows that in-cylinder pressure continuously changes with the change in instantaneous volume. Thus, an average or mean effective pressure (*mep*) can be defined as:

$$w = (mep)\Delta v \tag{3.25}$$

or:

$$mep = w / \Delta v = W / V_d \tag{3.26}$$

and: $$\Delta v = v_{BDC} - v_{TDC} \tag{3.27}$$

Mean effective pressure is independent of engine size and speed, such parameter provides an ideal way in comparing engine performance. Since a larger engine would often produce more torque while speed greatly influences the generated power.

Various mean effective pressures can be defined by using different work terms in Equation 3.27 (Nunney, 1982). When brake work term is used to define mean

effective pressure, such parameter refers to external shaft work per unit volume done by the engine, which is given by:

$$bmep = w_b / \Delta v \tag{3.28}$$

Indicated work gives indicated mean effective pressure as given below:

$$imep = w_i / \Delta v \tag{3.29}$$

Indicated mean effective pressure (*imep*) is the net work per unit displacement volume done by the gas during compression and expansion. Moreover, *imep* can further be divided into gross indicated mean effective pressure and net indicated mean effective pressure:

$$(imep)_{gross} = (w_i)_{gross} / \Delta v \tag{3.30}$$

$$(imep)_{net} = (w_i)_{net} / \Delta v \tag{3.31}$$

If mean effective pressure is defined in terms of pump work, this yield the following expression in negative values:

$$pmep = w_{pump} / \Delta v \tag{3.32}$$

Friction mean effective pressure:

$$fmep = w_f / \Delta v \tag{3.33}$$

For CI engines, these engines often have maximum values of bmep in the range of 700 to 900 kPa (100 to 130 psi).

3.2.6 Torque and Power

Torque indicates an engine's ability to do work and is defined as force acting at a moment distance. The unit of torque is in Newton-meter (Nm) or lb_f-ft. Torque, τ can be related to work as:

$$2\pi\tau = W_b = (bmep)V_d / n \tag{3.34}$$

where: W_b = brake work of one revolution

V_d = displacement volume

n = number of revolutions per cycle

For 4-stroke engine with two revolutions of piston to complete a cycle hence, torque is defined as:

$$\tau = (bmep)V_d / 4\pi \tag{3.35}$$

For any type of engine, maximum torque is achieved at certain engine speed and the point of maximum torque is called maximum brake torque speed (MBT). In the design of modern engines, the major goal is to flatten the torque versus speed curve in order to have high torque at high and low speed range. Large engines often have high torque values with MBT at relatively low speed (Pulkrabek, 2004).

Power refers to the rate of work of an engine. If n and N represents number of revolution per cycle and engine speed, respectively then:

$$\dot{W} = WN / n \tag{3.36}$$

$$\dot{W} = 2\pi N\tau \tag{3.37}$$

$$\dot{W} = (1/2n)(mep)A_p\overline{U}_p \tag{3.38}$$

$$\dot{W} = (mep)A_p\overline{U}_p / 4 \tag{3.39}$$

From Equation 3.38 to Equation 3.42, these equations are defined in terms of work and *mep*. Power can be defined as brake power, net indicated power, gross indicated power, pumping power, and even friction power. Also:

$$\dot{W}_b = \eta_m\dot{W}_i \tag{3.40}$$

$$(\dot{W}_i)_{net} = (\dot{W}_i)_{gross} - (\dot{W}_i)_{pump} \tag{3.41}$$

$$\dot{W}_b = \dot{W}_i - \dot{W}_f \tag{3.42}$$

where η_m is the mechanical efficiency of the engine.

Both torque and power are dependent variables to engine speed. As usual, the torque of an engine increases as engine speed increases. However, there is a point where the torque of the engine reaches maximum as engine speed is being increased and decreases thereafter. This is because the engine is unable to ingest a full charge of air at higher speeds.

3.2.7 Air to Fuel Ratio

Combustion is a chemical reaction where large quantity of energy is released from oxidation process of fuels. Such chemical reaction involves reactants that are comprised of air and fuel. In fact, it is actually the oxygen in the air that is required for the combustion of fuel to occur. Hence, oxygen is sourced from air as it is free and readily available from surroundings.

In order to quantify the amount of fuel and air being utilized in any combustion process, there is a corresponding parameter known as air to fuel ratio, *AF*. It is usually expressed on a mass basis and is defined as the ratio of the mass of air to the mass of fuel in a combustion process and it is shown in Equation 3.43 (Cengel, 2011):

$$AF = \frac{m_{air}}{m_{fuel}} \tag{3.43}$$

Or the above parameter can also be expressed as follows:

$$AF = \frac{\dot{m}_{air}}{\dot{m}_{fuel}} \tag{3.44}$$

Where: $\dot{m}_{air}$ = mass flow rate of air

$\dot{m}_{fuel}$ = mass flow rate of fuel

The air to fuel ratio can also be expressed in terms of mole i.e., ratio of the mole numbers of air to the mole numbers of fuel.

3.2.8 Stoichiometric Air to Fuel Ratio

Stoichiometric or theoretical combustion is defined when fuel is burned completely with theoretical air. The theoretical air here refers to chemically correct amount of air required for stoichiometric combustion of fuel to occur. Hence, the amount of air supplied for this combustion of fuel must neither be deficient nor in excess in order to quantify as theoretical air. Such combustion is deemed as ideal combustion process which can be represented as stoichiometric combustion reaction. The general stoichiometric combustion equation is given as:

$$C_\alpha H_\beta O_\gamma N_\delta + a_s\left(O_2 + 3.76N_2\right) \rightarrow n_1 CO_2 + n_2 H_2 O + n_3 N_2 \tag{3.45}$$

From the above equation, only carbon dioxide and water are present as combustion products. The stoichiometric air to fuel ratio, AF_s, for type of fuel used can be obtained from the formula below:

$$AF_s = \frac{28.85\left(4.76a_s\right)}{\left(12.01\alpha + 1.008\beta + 16.00\gamma + 14.01\delta\right)} \tag{3.46}$$

In this research, the fuel used is diesel with chemical formula of $C_{12}H_{23}$. The stoichiometric air to fuel ratio, AF_s for this diesel is determined as 14.6.

3.2.9 Actual Air to Fuel Ratio

Actual air to fuel ratio, AF_{actual} refers to the ratio of amount of air to amount of fuel being consumed in combustion process of an engine. These quantities are often described in terms of time rate of mass change due to the ease of measurements taken during engine operation. In this research, air flow meter is used to determine the mass flow rate of air. Similarly, the mass flow rate of fuels which are diesel and hydrogen are obtained by measuring the time taken to consume a determined amount of fuel. These measured mass flow rate of air and hydrogen yields actual air to fuel ratio, AF_{actual} and

it is summarized below:

$$AF_{actual} = \frac{\dot{m}_{air}}{\dot{m}_{fuel}} \tag{3.47}$$

3.2.10 Equivalence Ratio

For actual combustion in an engine, the equivalence ratio, ϕ, is defined as the stoichiometric air to fuel ratio, AF_s, divided by the actual air to fuel ratio, AF_{actual}, or equivalently, the actual fuel to air ratio, FA_{actual}, divided by the stoichiometric fuel to air ratio, FA_s as shown below:

$$\phi = \frac{AF_s}{AF_{actual}} = \frac{FA_{actual}}{FA_s} \tag{3.48}$$

The equivalence ratio has the same value on a mole or mass basis.

For $\phi < 1$: Mixture is lean.

$\phi > 1$: Mixture is rich.

$\phi = 1$: Mixture is stoichiometric.

3.2.11 Specific Fuel Consumption

Specific fuel consumption is defined as amount of fuel consumed to produce 1kW of power within one hour and it is equivalent to:

$$sfc = \dot{m}_f / \dot{W} \tag{3.49}$$

where: $\dot{m}_f$ = rate of fuel flow into engine

$\dot{W}$ = engine power

Brake power gives brake specific fuel consumption:

$$bsfc = \dot{m}_f / \dot{W}_b \tag{3.50}$$

Indicated power gives indicated specific fuel consumption:

$$isfc = \dot{m}_f / \dot{W}_i \tag{3.51}$$

Apart from these expressions, specific fuel consumption can be defined using the following terms:

fsfc = friction specific fuel consumption

igsfc = indicated gross specific fuel consumption

insfc = indicated net specific fuel consumption

psfc = pumping specific fuel consumption

It also follows that:

$$\eta_m = \dot{W}_b / \dot{W}_i = \left(\dot{m}_f / \dot{W}_i\right) / \left(\dot{m}_f / \dot{W}_b\right) = \left(isfc\right) / \left(bsfc\right) \tag{3.52}$$

In addition, *bsfc* also depends on compression ratio and fuel equivalence ratio. As for the effect of fuel equivalence ratio, the engine consumes the least fuel when combustion occurs in a mixture with fuel equivalence ratio at around one, (ϕ = 1). Higher fuel consumption would be resulted if engine is operated further from stoichiometric combustion, either rich or lean.

Indicated specific fuel consumption is not suitable to be used in hydrogen-fuelled diesel dual fuel operation since amount of hydrogen gaseous fuel is too minimal as compared to diesel fuel though hydrogen augments the power of the engine. The most practical way is to define energy content for each fuel which yields indicated specific energy consumption (ISEC) derived from Equation 3.51 and gives:

$$ISEC = \frac{\left(m_f Q_{HV} \eta_c\right)_{diesel} + \left(m_f Q_{HV} \eta_c\right)_{hydrogen}}{\dot{W}} \tag{3.53}$$

3.2.12 Engine Efficiencies

Considering the cycle occurring in engines, the time available for the combustion process is very short whereby not all fuel molecules are able to react with oxygen

molecules. Perhaps, this could also be due to the local temperature which does not favor combustion reactions to occur. Thus, there will be a small fraction of unburned fuel expelled together with exhaust gases in the form of unburned hydrocarbon (UHC). To account for the fraction of fuel burned in combustion process, a parameter is defined known as combustion efficiency, η_c. The common values for combustion efficiency fall in the range 0.95 to 0.98 when an engine is operated properly. For engine cycle in single cylinder, the heat addition is given as:

$$Q_{in} = m_f Q_{HV} \eta_c \qquad \text{or} \qquad \dot{Q}_{in} = \dot{m}_f Q_{HV} \eta_c \tag{3.54}$$

and thermal efficiency is defined as:

$$\eta_t = W / Q_{in} = \dot{W} / \dot{Q}_{in} = \dot{W} / \dot{m}_f Q_{HV} \eta_c = \eta_f / \eta_c \tag{3.55}$$

where: m_f = mass of fuel for one cycle

$\dot{m}_f$ = mass flow rate of fuel

Q_{HV} = heating value of fuel

η_f = fuel conversion efficiency

Indicated power or brake power can be used to obtain thermal efficiency and represented accordingly to respective term used. This allows the engine mechanical efficiency to be defined as:

$$\eta_m = (\eta_t)_b / (\eta_t)_i \tag{3.56}$$

For fuel conversion efficiency, this parameter is defined as:

$$\eta_f = W / m_f Q_{HV} = \dot{W} / \dot{m}_f Q_{HV} \tag{3.57}$$

or: $$\eta_f = 1/(sfc) Q_{HV} \tag{3.58}$$

3.2.13 Water Addition in Internal Combustion Engine

During World War II, water injectors were installed on the intake system of high performance reciprocating engines of warplanes. It is believed that as the water evaporates it increases evaporative cooling which lowers the intake temperature and raises intake density. This increases the volumetric efficiency resulting in increase of output power (Matekunas, 1983). In recent years, the technology of adding water to the intake systems of engines is again being used. This is done in both automobile engines and in large ship and stationary engines. In addition to increasing volumetric efficiency and power, this is also done to decrease the generation of NO_x emission (Mullins, 2000). The disadvantage of water technology are corrosion problems at the intake system, storage tank and water injector, and continuous water induction causes water to accumulate at closed intake port and dribbles and mix with engine oil when it is opened which deteriorating engine performance and cause corrosion of the engine parts. Water can be added in internal combustion engine by one of these methods:

i) Emulsification of water with fuel.

ii) Water induction or continuous injection at the intake port or manifold.

iii) Timed port or manifold water injection.

iv) Direct water injection into the cylinder.

Saab Automobile Company has been experimenting water injection to improve fuel economy at high speed and fast acceleration. It is proven that high speed fuel consumption has been reduced by 20-30% (Jost, 1995).

Dissociation of water occurs when combustion temperatures are greater than 1600K that produces more oxygen and hydrogen for improving combustion in the engine (Moran et al. 2004). Water addition is also capable of promoting better mixing of in-cylinder charge since additional mass of water increases angular momentum of the charge (Pulkrabek, 2004).

3.2.14 General Chemical Equilibrium

In combustion processes, the fuel is mixed with air at variable equivalence ratio, ϕ. Chemical kinetics involves during high temperature combustion dissociates combustion products to produce minor species. It is defined as the rate of a product produce or reactant consumed per unit time as shown in Equation 3.59:

$$aA+bB \rightarrow yY+zZ \tag{3.59}$$

Increase in chemical kinetic of product Y and Z concentration causes decrease in chemical kinetic of reactant A and B. The concentration changes of reactant A and B need to be multiplied by (-1) to determine the rate. Reactions that proceed in reverse direction that dissociates products Y and Z could form back reactant A and B. Thus, the net rate of reaction, R_n is the difference between forward and reverse rates as shown in Equation 3.60.

$$R_n = forward\ rate - reverse\ rate \tag{3.60}$$

In combustion modeling, forward and reverse reactions are considered as separate reaction. Since chemical kinetics of each reaction is proportional to the reactant concentration, thus, the forward and reverse reactions can be written as below:

$$forward\ rate = k_f [A]^a [B]^b \tag{3.61}$$

$$reverse\ rate = k_r [Y]^y [Z]^z \tag{3.62}$$

$$R_n = k_f [A]^a [B]^b - k_r [Y]^y [Z]^z \tag{3.63}$$

Where, k_f and k_r are the rate coefficients for forward and reverse reactions, respectively.

3.2.15 Equilibrium Constants

In combustion flame zone, many products species are in chemical equilibrium state. Olikara et al. applied a solution for the equilibrium composition products based on

equilibrium constant of the gas phase products during combustion of hydrocarbon fuels (Olikara et al. 1975). The basic equations of chemical equilibrium are presented below.

3.2.15.1 Basic Equations

Equation 3.63 shows that when the reaction is in a state of chemical equilibrium, the reverse and forward reaction rates are in balance. In other words, the concentration of reactant and products are constant with zero net rates (R_n=0). This is shown in equation below:

$$k_f [A]_e^a [B]_e^b = k_r [Y]_e^y [Z]_e^z \tag{3.64}$$

Where, the suffix *e* denotes the equilibrium concentration. Thus, at equilibrium:

$$\frac{k_f [A]_e^a [B]_e^b}{k_r [Y]_e^y [Z]_e^z} = K_n \tag{3.65}$$

Where, K_n, the equilibrium constant that varies with temperature.

The concept of equilibrium constant is based on the minimization of the Gibbs free energy of the gas. The value of Gibbs Function (G_F) of the mixture is minimum for constant mixture temperature and pressure in order to be in equilibrium state. G_F can be written in the form of Gibbs Molar Function G_i and number of moles n_i for species *i* as shown below:

$$G_F = \sum_i n_i G_i = \sum_i n_i (H_i - TS_i) \tag{3.66}$$

Considering the mixture of the substances *A*, *B*, *Z* and *Y* may react according to the chemical Equation 3.59. Thus, at equilibrium state, G_F is given as:

$$yG_Y + zG_Z - aG_A - bG_B = 0 \tag{3.67}$$

Where, at a temperature T:

$$G_i = H_i - TS_i \tag{3.68}$$

At a constant temperature, the entropy (S_i) at a pressure (P_i) is related to the absolute entropy (S_i^0) at the standard state pressure (P_0) by the following equation:

$$S_i = S_i^0 - R\ln(P_i/P_0) \tag{3.69}$$

Combining Equations 3.69 and 3.70 yields:

$$G_i = H_i - TS_i^0 + RT\ln(P_i/P_0) = G_i^0 + RT\ln(P_i/P_0) \tag{3.70}$$

Where, G_i^0 is the value of the Gibbs molar free energy at the standard state pressure (P_0) at the pertained temperature. Combining Equations 3.67 and 3.70 yields:

$$yG_Y^0 + zG_Z^0 - aG_A^0 - bG_B^0 = -\overline{RT}\left[y\ln(P_Y/P_0) + z\ln(P_Z/P_0) - a\ln(P_A/P_0) - b\ln(P_B/P_0)\right] \tag{3.71}$$

$$\frac{(P_Y)^y(P_Z)^z}{(P_A)^a(P_B)^b}\left[\frac{1}{P_0}\right]^{y+z-a-b} = \exp\left(\frac{-\Delta G_{FT}^0}{\overline{RT}}\right) = K \tag{3.72}$$

Where, ΔG_{FT}^0 is the change in Gibbs function for the reaction given by Equation 3.72. ΔG_{FT}^0 is written as a molar quantity and always be considered in conjunction with their particular chemical equation. K is equilibrium constant analogous to that given by Equation 3.73 below:

$$\frac{(P_Y)^y(P_Z)^z}{(P_A)^a(P_B)^b}\left[\frac{1}{P_0}\right]^{y+z-a-b} = P_0^{y+z-a-b}K = K_P \tag{3.73}$$

Where, K_p has dimensions of (pressure)$^{(y+z-a-b)}$. Note that when the combustion products behave as ideal gases Equation 3.73 can be written as:

$$\frac{P_i}{P_e} = \frac{n_i}{\sum n_i} = y_i \tag{3.74}$$

Where, P_e is the total system pressure, $\sum n_i = n_T$ is the total number of moles of product and y_i is the mole fraction of species *i*. The equilibrium condition can be expressed as:

$$\frac{(y_Y)^y(y_Z)^z}{(y_A)^a(y_B)^b}\left[\frac{P_e}{P_0}\right]^{y+z-a-b} = \frac{(n_Y)^y(n_Z)^z}{(n_A)^a(n_B)^b}\left[\left[\frac{P_e}{P_0}\right]\frac{1}{\sum n_i}\right]^{y+z-a-b} = K \tag{3.75}$$

Combining Equations 3.65, 3.73 and 3.75 yields:

$$K_n = K_P \left[\frac{1}{\overline{R}T}\right]^{y+z-a-b} = K\left[\frac{P_0}{\overline{R}T}\right]^{y+z-a-b} \tag{3.76}$$

3.2.16 Equilibrium Constants Method

In combustion modeling, the value of equilibrium constant, K, needs to be determined from polynomial equations. The equilibrium constant values from JANAF Tables can be written in general form as given below (JANAF, 1971):

For the temperature range between 1600K to 4000K:

$$\begin{aligned} Log_{10}K_i = {} & A_1 + A_2(T-1600)(10^{-3}) + A_3(T-1600)(T-2000)(10^{-6}) \\ & + A_4(T-1600)(T-2000)(T-2400)(10^{-9}) \\ & + A_5(T-1600)(T-2000)(T-2400)(T-2800)(10^{-12}) \\ & + A_6(T-1600)(T-2000)(T-2400)(T-2800)(T-3200)(10^{-15}) \\ & + A_7(T-1600)(T-2000)(T-2400)(T-2800)(T-3200) \\ & (T-3600)(10^{-18}) \end{aligned} \tag{3.77}$$

For the temperature range between 4000K to 6000K:

$$\begin{aligned} Log_{10}K_i = {} & A_8 + A_9(T-4000)(10^{-3}) + A_{10}(T-4000)(T-4500)(10^{-6}) \\ & + A_{11}(T-4000)(T-4500)(T-5000)(10^{-9}) \\ & + A_{12}(T-4000)(T-4500)(T-5000)(T-5500)(10^{-12}) \end{aligned} \tag{3.78}$$

The values of the equilibrium constant, K_1 to K_{14} as well as the coefficients of $A_{1\text{to}}A_{12}$ are given in Appendix A.

3.2.17 Governing Equations

Combustion of hydrocarbon fuels at low temperature produces N_2, H_2O, CO_2 and O_2 for lean mixtures ($\phi<1$) and N_2, H_2O, CO_2, CO and H_2 for rich mixtures ($\phi>1$). At higher temperatures (usually above 1600K), these major species dissociates and react to form additional species with significant amounts (Ferguson. 2001). By considering

these phenomena and assuming 18 combustion products, the reaction combustion equations for hydrocarbon fuel with air can be written as:

$$n_f C_\alpha H_\beta + \frac{a_s}{\phi}(O_2 + 3.76N_2) \rightarrow n_T \begin{pmatrix} y_1 H_2 + y_2 H_2 O + y_3 CO_2 + y_4 N_2 + y_5 O + \\ + y_6 O_2 + y_7 O_3 + y_8 H + y_9 OH + y_{10} CO + \\ y_{11} C + y_{12} CH_4 + y_{13} NO + y_{14} NO_2 + \\ y_{15} NH_3 + y_{16} HNO_3 + y_{17} HCN + y_{18} N \end{pmatrix} \quad (3.79)$$

For diesel fuel used, the subscripts α and β are given as 12 and 23, respectively. The stoichiometric molar air-fuel ratio, $a_s = \alpha + \frac{\beta}{4}$ (3.80)

From concentration conditions at equilibrium state, summation of the mole fraction of each product species equal to unity and hence:

$$\begin{aligned} &y_1 + y_2 + y_3 + y_4 + y_5 + y_6 + y_7 + y_8 + y_9 + y_{10} + y_{11} + y_{12} \\ &+ y_{13} + y_{14} + y_{15} + y_{16} + y_{17} + y_{18} = 1 \end{aligned} \quad (3.81)$$

By balancing the atoms on both sides of reactants and products from Equation 3.79, the following four equations can be obtained:

$$n_T(y_3 + y_{10} + y_{11} + y_{12} + y_{17}) = n_f \alpha \quad (3.82)$$

$$n_T(2y_1 + 2y_2 + y_8 + y_9 + 4y_{12} + 3y_{15} + y_{16} + y_{17}) = n_f \beta \quad (3.83)$$

$$n_T(y_2 + 2y_3 + y_5 + 2y_6 + 3y_7 + y_9 + y_{10} + y_{13} + 2y_{14} + 3y_{16}) = \frac{2a_s}{\phi} \quad (3.84)$$

$$n_T(2y_4 + y_{13} + y_{14} + y_{15} + y_{16} + y_{17} + y_{18}) = \frac{7.52a_s}{\phi} \quad (3.85)$$

From chemical equilibrium equations, 14 equilibrium constant equations that relates mole fractions of each combustion product are shown as below:

$$K_1 = \left(\frac{y_{10} y_6^{0.5}}{y_3}\right)(P)^{0.5}; K_2 = \left(\frac{y_{11} y_6^{0.5}}{y_{10}}\right)(P)^{0.5}; K_3 = \left(\frac{y_{11} y_1^2}{y_{12}}\right)(P)^2;$$

$$K_4 = \left(\frac{y_{11} y_1^{0.5} y_4^{0.5}}{y_{17}}\right)(P); K_5 = \left(\frac{y_1 y_6^{0.5}}{y_2}\right)(P)^{0.5}; K_6 = \left(\frac{y_9 y_1^{0.5}}{y_2}\right)(P)^{0.5};$$

$$K_7 = \left(\frac{y_8}{y_1^{0.5}}\right)(P)^{0.5};\ K_8 = \left(\frac{y_5}{y_6^{0.5}}\right)(P)^{0.5};\ K_9 = \left(\frac{y_7}{y_6^{1.5}}\right)(P)^{-0.5};$$

$$K_{10} = \left(\frac{y_{18}}{y_4^{0.5}}\right)(P)^{0.5};\ K_{11} = \left(\frac{y_{13}}{y_4^{0.5}y_6^{0.5}}\right)(P)^{0};\ K_{12} = \left(\frac{y_{13}y_6^{0.5}}{y_{14}}\right)(P)^{0.5};$$

$$K_{13} = \left(\frac{y_4^{0.5}y_1^{1.5}}{y_{15}}\right)(P) \text{ and } K_{14} = \left(\frac{y_{14}^3 y_2}{y_{13}y_{16}^2}\right)(P). \tag{3.86}$$

The expression for the equilibrium constants can be rearranged to express mole fractions of all products species in terms of y_1, y_2, y_3, and y_4, which are namely mole fractions of H_2, H_2O, CO_2, and N_2, respectively.

$$y_5 = c_5c_8\left(\frac{y_2}{y_1}\right);\quad y_6 = c_5^2\left(\frac{y_2^2}{y_1^2}\right);\ y_7 = c_5^3c_9\left(\frac{y_2^3}{y_1^3}\right);\ y_8 = c_7y_1^{0.5};$$

$$y_9 = c_6\left(\frac{y_2}{y_1^{0.5}}\right);\ y_{10} = \left(\frac{c_1}{c_5}\right)\left(\frac{y_1y_3}{y_2}\right);\ y_{11} = \left(\frac{c_1c_2}{c_5^2}\right)\left(\frac{y_1^2y_3}{y_2^2}\right);$$

$$y_{12} = \left(\frac{c_1c_2c_3}{c_5^2}\right)\left(\frac{y_1^4y_3}{y_2^2}\right);\ y_{13} = c_5c_{11}\left(\frac{y_2y_4^{0.5}}{y_1}\right);\ y_{14} = c_5^2c_{11}c_{12}\left(\frac{y_2^2y_4^{0.5}}{y_1^2}\right);$$

$$y_{15} = c_{13}y_4^{0.5}y_1^{1.5};\ y_{16} = c_5^{2.5}c_{11}c_{12}^{1.5}c_{14}^{0.5}\left(\frac{y_2^3y_4^{0.5}}{y_1^{2.5}}\right);\ y_{17} = \left(\frac{c_1c_2c_4}{c_5^2}\right)\left(\frac{y_1^{2.5}y_3y_4^{0.5}}{y_2^2}\right)$$

$$\text{and}\quad y_{18} = c_{10}y_4^{0.5} \tag{3.87}$$

where:

$$c_1 = \frac{K_1}{P^{0.5}};\ c_2 = \frac{K_2}{P^{0.5}};\ c_3 = \frac{P^2}{K_3};\ c_4 = \frac{P}{K_4};\ c_5 = \frac{K_5}{P^{0.5}};$$

$$c_6 = \frac{K_6}{P^{0.5}};\ c_7 = \frac{K_7}{P^{0.5}};\ c_8 = \frac{K_8}{P^{0.5}};\ c_9 = K_9P^{0.5};\ c_{10} = \frac{K_{10}}{P^{0.5}};$$

$$c_{11} = K_{11};\ c_{12} = \frac{P^{0.5}}{K_{12}};\ c_{13} = \frac{P}{K_{13}} \quad \text{and } c_{14} = \frac{P}{K_{14}} \tag{3.88}$$

The total number of mole, n_T can be eliminated by dividing Equation 3.83 with Equation 3.82 and yields the following equation:

$$2y_1 + 2y_2 - \left(\frac{n_f\beta}{n_f\alpha}\right)y_3 + y_8 + y_9 - \left(\frac{n_f\beta}{n_f\alpha}\right)y_{10} - \left(\frac{n_f\beta}{n_f\alpha}\right)y_{11} + \left(4 - \left(\frac{n_f\beta}{n_f\alpha}\right)\right)y_{12} + 3y_{15} + y_{16} + \left(1 - \left(\frac{n_f\beta}{n_f\alpha}\right)\right)y_{17} = 0 \quad (3.89)$$

Likewise Equations 3.84 and 3.85 can be divided with Equation 3.82 and yields:

$$y_2 + \left[2 - \left(\frac{2a_s}{n_f\alpha\phi}\right)\right]y_3 + y_5 + 2y_6 + 3y_7 + y_9 + \left[1 - \left(\frac{2a_s}{n_f\alpha\phi}\right)\right]y_{10} - \left(\frac{2a_s}{n_f\alpha\phi}\right)y_{11} - \left(\frac{2a_s}{n_f\alpha\phi}\right)y_{12} + y_{13} + 2y_{14} + 3y_{16} - \left(\frac{2a_s}{n_f\alpha\phi}\right)y_{17} = 0 \quad (3.90)$$

$$-\left(\frac{7.52a_s}{n_f\alpha\phi}\right)y_3 + 2y_4 - \left(\frac{7.52a_s}{n_f\alpha\phi}\right)y_{10} - \left(\frac{7.52a_s}{n_f\alpha\phi}\right)y_{11} - \left(\frac{7.52a_s}{n_f\alpha\phi}\right)y_{12} + y_{13} + y_{14} + y_{15} + y_{16} + \left[1 - \left(\frac{7.52a_s}{n_f\alpha\phi}\right)\right]y_{17} + y_{18} = 0 \quad (3.91)$$

By substituting Equation 3.87 into Equations 3.81, 3.89, 3.90 and 3.91 yields four equations with four main unknowns y_1, y_2, y_3, and y_4. The resulting equations as shown below are nonlinear and can only be solved using an iterative method.

$$y_1 + y_2 + y_3 + y_4 + c_5c_8\left(\frac{y_2}{y_1}\right) + c_5^2\left(\frac{y_2^2}{y_1^2}\right) + c_5^3c_9\left(\frac{y_2^3}{y_1^3}\right) + c_7y_1^{0.5} + c_6\left(\frac{y_2}{y_1^{0.5}}\right) + \left(\frac{c_1}{c_5}\right)\left(\frac{y_1y_3}{y_2}\right) + \left(\frac{c_1c_2}{c_5^2}\right)\left(\frac{y_1^2y_3}{y_2^2}\right) + \left(\frac{c_1c_2c_3}{c_5^2}\right)\left(\frac{y_1^4y_3}{y_2^2}\right) + c_5c_{11}\left(\frac{y_2y_4^{0.5}}{y_1}\right) + c_5^2c_{11}c_{12}\left(\frac{y_2^2y_4^{0.5}}{y_1^2}\right) + c_{13}y_4^{0.5}y_1^{1.5} + c_5^{2.5}c_{11}c_{12}^{1.5}c_{14}^{0.5}\left(\frac{y_2^3y_4^{0.5}}{y_1^{2.5}}\right) + \left(\frac{c_1c_2c_4}{c_5^2}\right)\left(\frac{y_1^{2.5}y_3y_4^{0.5}}{y_2^2}\right) + c_{10}y_4^{0.5} - 1 = 0 \quad (3.92)$$

$$
\begin{aligned}
&2y_1 + 2y_2 - \left(\frac{n_f\beta + 2p}{n_f\alpha}\right)y_3 + c_7 y_1^{0.5} + c_6\left(\frac{y_2}{y_1^{0.5}}\right) \\
&- \left(\frac{n_f\beta + 2p}{n_f\alpha}\right)\left(\frac{c_1}{c_5}\right)\left(\frac{y_1 y_3}{y_2}\right) - \left(\frac{n_f\beta + 2p}{n_f\alpha}\right)\left(\frac{c_1 c_2}{c_5^2}\right)\left(\frac{y_1^2 y_3}{y_2^2}\right) \\
&+ \left[4 - \left(\frac{n_f\beta + 2p}{n_f\alpha}\right)\right]\left(\frac{c_1 c_2 c_3}{c_5^2}\right)\left(\frac{y_1^4 y_3}{y_2^2}\right) + 3c_{13} y_4^{0.5} y_1^{1.5} \\
&+ c_5^{2.5} c_{11} c_{12}^{1.5} c_{14}^{0.5}\left(\frac{y_2^3 y_4^{0.5}}{y_1^{2.5}}\right) \\
&+ \left[1 - \left(\frac{n_f\beta + 2p}{n_f\alpha}\right)\right]\left(\frac{c_1 c_2 c_4}{c_5^2}\right)\left(\frac{y_1^{2.5} y_3 y_4^{0.5}}{y_2^2}\right) = 0
\end{aligned}
\tag{3.93}
$$

$$
\begin{aligned}
&y_2 + \left[2 - \left(\frac{2a_s}{n_f\alpha\phi}\right)\right]y_3 + c_5 c_8\left(\frac{y_2}{y_1}\right) + 2c_5^2\left(\frac{y_2^2}{y_1^2}\right) + 3c_5^3 c_9\left(\frac{y_2^3}{y_1^3}\right) \\
&+ c_6\left(\frac{y_2}{y_1^{0.5}}\right) + \left(\frac{c_1}{c_5}\right)\left[1 - \left(\frac{2a_s}{n_f\alpha\phi}\right)\right]\left(\frac{y_1 y_3}{y_2}\right) \\
&- \left(\frac{2a_s}{n_f\alpha\phi}\right)\left(\frac{c_1 c_2}{c_5^2}\right)\left(\frac{y_1^2 y_3}{y_2^2}\right) - \left(\frac{2a_s}{n_f\alpha\phi}\right)\left(\frac{c_1 c_2 c_3}{c_5^2}\right)\left(\frac{y_1^4 y_3}{y_2^2}\right) \\
&+ c_5 c_{11}\left(\frac{y_2 y_4^{0.5}}{y_1}\right) + 2c_5^2 c_{11} c_{12}\left(\frac{y_2^2 y_4^{0.5}}{y_1^2}\right) + 3c_5^{2.5} c_{11} c_{12}^{1.5} c_{14}^{0.5}\left(\frac{y_2^3 y_4^{0.5}}{y_1^{2.5}}\right) \\
&- \left(\frac{2a_s}{n_f\alpha\phi}\right)\left(\frac{c_1 c_2 c_4}{c_5^2}\right)\left(\frac{y_1^{2.5} y_3 y_4^{0.5}}{y_2^2}\right) = 0
\end{aligned}
\tag{3.94}
$$

$$
\begin{aligned}
&-\left(\frac{7.52a_s}{n_f\alpha\phi}\right)y_3 + 2y_4 - \left(\frac{c_1}{c_5}\right)\left(\frac{7.52a_s}{n_f\alpha\phi}\right)\left(\frac{y_1 y_3}{y_2}\right) \\
&- \left(\frac{7.52a_s}{n_f\alpha\phi}\right)\left(\frac{c_1 c_2}{c_5^2}\right)\left(\frac{y_1^2 y_3}{y_2^2}\right) - \left(\frac{7.52a_s}{n_f\alpha\phi}\right)\left(\frac{c_1 c_2 c_3}{c_5^2}\right)\left(\frac{y_1^4 y_3}{y_2^2}\right) \\
&+ c_5 c_{11}\left(\frac{y_2 y_4^{0.5}}{y_1}\right) + c_5^2 c_{11} c_{12}\left(\frac{y_2^2 y_4^{0.5}}{y_1^2}\right) + c_{13} y_4^{0.5} y_1^{1.5} \\
&+ c_5^{2.5} c_{11} c_{12}^{1.5} c_{14}^{0.5}\left(\frac{y_2^3 y_4^{0.5}}{y_1^{2.5}}\right) \\
&+ \left[1 - \left(\frac{7.52a_s}{n_f\alpha\phi}\right)\right]\left(\frac{c_1 c_2 c_4}{c_5^2}\right)\left(\frac{y_1^{2.5} y_3 y_4^{0.5}}{y_2^2}\right) + c_{10} y_4^{0.5} = 0
\end{aligned}
\tag{3.95}
$$

3.3 Experimental Investigation

3.3.1 Engine Modification and Instrumentation

In this research, a YANMAR L100AE-D2YC compression ignition (CI) engine was selected for experimental investigation. It is a direct injection (DI) CI engine that utilizes the mechanically-actuated injection fuel delivery system and the rate of injection is dependent of engine speed. Injection pressure and start of injection (SOI) are fixed at 19.6 MPa and 13°BTDC, respectively. The main engine specifications are summarized in Table 3.1 and the photographic view of the engine setup is shown in Figure B.1.

Table 3.1 Engine specifications of YANMAR L100AE-D2YC

Parameter	Specification
Engine Type	Air-cooled, Direct Injection
Number of Cylinders	1
Displacement, cm^3	406
Bore x Stroke, mm	86 x 70
Valve Train	2 valves, pushrod
Compression Ratio	19.3:1
Continuous Power Output, kW	5.7 @ 3000RPM
Maximum Power Output, kW	7.4 @ 3600RPM
Fuel Injection Pressure, MPa	19.6
Fuel Injection Type	Hole Nozzle YANMAR YDLLA-P

The selection of start and end of injections for both water and hydrogen injection systems is based on valve timing management of the engine as shown in Table 3.2 in order to prevent the effect of valve overlap. During valve overlap, there can be some reverse flow of exhaust gas back to the intake system. This small backflow of hot exhaust gas helps to heat hydrogen and water droplet. In this study, the optimum SOI for both hydrogen and water should be later than 20°ATDC or when exhaust port

is fully closed. In addition, the phenomenon of mechanical lag of approximately two milliseconds in the injectors needs to be considered. This lag is due to slow armature and spring responses prior to start of injection. In this case, mechanical lag causes SOI of hydrogen and water extended to 20°CA at 1500RPM and to the maximum of 40°CA at 3000RPM.

Table 3.2 Valve timing of YANMAR L100AE-D2YC

Item	**Valve Timing**	
Intake Valve	Opened	20°BTDC
	Closed	53°ABDC
Exhaust Valve	Opened	53°BBDC
	Closed	20°ATDC

SINCRO alternate current synchronous generator provides electrical power to turn on 1 kW bulbs that are used as loads for the CI engine. The photographic view of the generator and load bank are shown in Figure B.2 and B.3, respectively. The technical specifications of this generator are summarized in Table 3.3.

Table 3.3 Technical specifications of generator

Parameter	**Specification**
Rated Power, kVA	5
Rated Speed, RPM	3000
Frequency, Hz	50
Voltage, V	115-240
Main Winding Resistance, Ω	0.9
Driving Power, kW	8

Load is applied until the desired speed is reached and it is measured using power meter as shown in Figure B.4. Rheostat with power rating of 1 kW and track resistance of 25 ohm (Ω) is used to round-off the value of load applied to the engine. Mass flow rate of air is measured at each engine speed by using FLUKE 922 airflow

meter as shown in Figure B.5. The measuring probe of airflow meter is inserted into the outlet fitting at the intake of the surge tank where the airflow is steady. Figure B.6 shows a pipette mounted at the load bank, which is used to measure diesel fuel flow rate. The properties of diesel and hydrogen fuels used in this research are shown in Table 3.4.

Table 3.4 Properties of hydrogen and diesel fuels (Saravanan et al. 2008).

Properties	**Hydrogen**	**Diesel**
Chemical Formula	H_2	$C_{12}H_{23}$
Density @ 16°C and 1atm (kg/m^3)	0.084	833
Flammability limits (volume %)	4-74.5	0.6-5.5
Adiabatic Flame Temperature (K)	2400	2200
Gross Heat of Combustion ASTM D2382 (MJ/kg)	124	45.8
Flash Point ASTM D93 (K)	840	371
Minimum Ignition Energy (mJ)	0.02	-
Stoichiometric Air Fuel Ratio (Mass Basis)	34.3	14.5
Cetane Number	-	40-55
Flame Velocity (cm/s)	265-325	30
Color (visual)	-	Yellow
Diffusivity in air (cm^2/s)	0.63	-
Sulfur Content WT.IP 242 (%)	-	0.10
Lower Calorific Value (MJ/kg)	120	42.5
Lower Heating Value of Stoichiometric Mixture (kJ/kg)	3399	2930

KISTLER 6052C pressure transducer is mounted in the cylinder head and exposed to in-cylinder pressure with maximum range of 250 bar. The pressure acts on the diaphragm and transmit the signal onto the quartz that yields an electrostatic charge. This charge is then amplified and converted into a voltage prior to channeling to Data Acquisition System. The installation of KISTLER 2613B1 crank angle encoder needs high precision measurement before it is attached to the engine crankshaft. It is used to

track instantaneous crank angle (CA) of the engine in the range of 180° BTDC to 180° ATDC with incremental value of one (1) ° CA.

Multi Synchronous Channel Data Acquisition System (μ-MUSYCS) is used to interpret input signals from pressure transducer and crank angle encoder then display the output using Integrated Measurement and Control (IMC) application software namely IMC-μ LIGHT for real-time visualization of P-θ diagram and engine speeds (Kistler Manual, 2002). Figure B.7 shows the photographic view of KISTLER pressure transducer, crank angle encoder and μ-MUSYCS.

The sampling interval for each data needs to be identified for better precision in measurement. The shorter time for sampling interval measures more data for instantaneous pressure and crank angle which contributes towards more accurate measurement. In this research, sampling interval was set to 500μs for 1000 samples per measurement and it is shown in Figure 3.3.

In this study, two types of gas analyzer are used to measure emission concentrations present in exhaust gas of HFCI engine and they are shown in Figure B.8. BACHARACH 300NSX gas analyzer is very reliable and it has the capability in measuring flue gas temperature, nitrogen oxides (NO_x), carbon monoxide (CO), oxygen (O_2) and sulfur dioxide (SO_2). AUTOCHECK 974/5 gas analyzer is capable of measuring amount of hydrocarbon (HC), carbon monoxide (CO), oxygen (O_2) and carbon dioxide (CO_2). The gas sampling probe of both gas analyzers are inserted into exhaust hose fittings for measuring emissions.

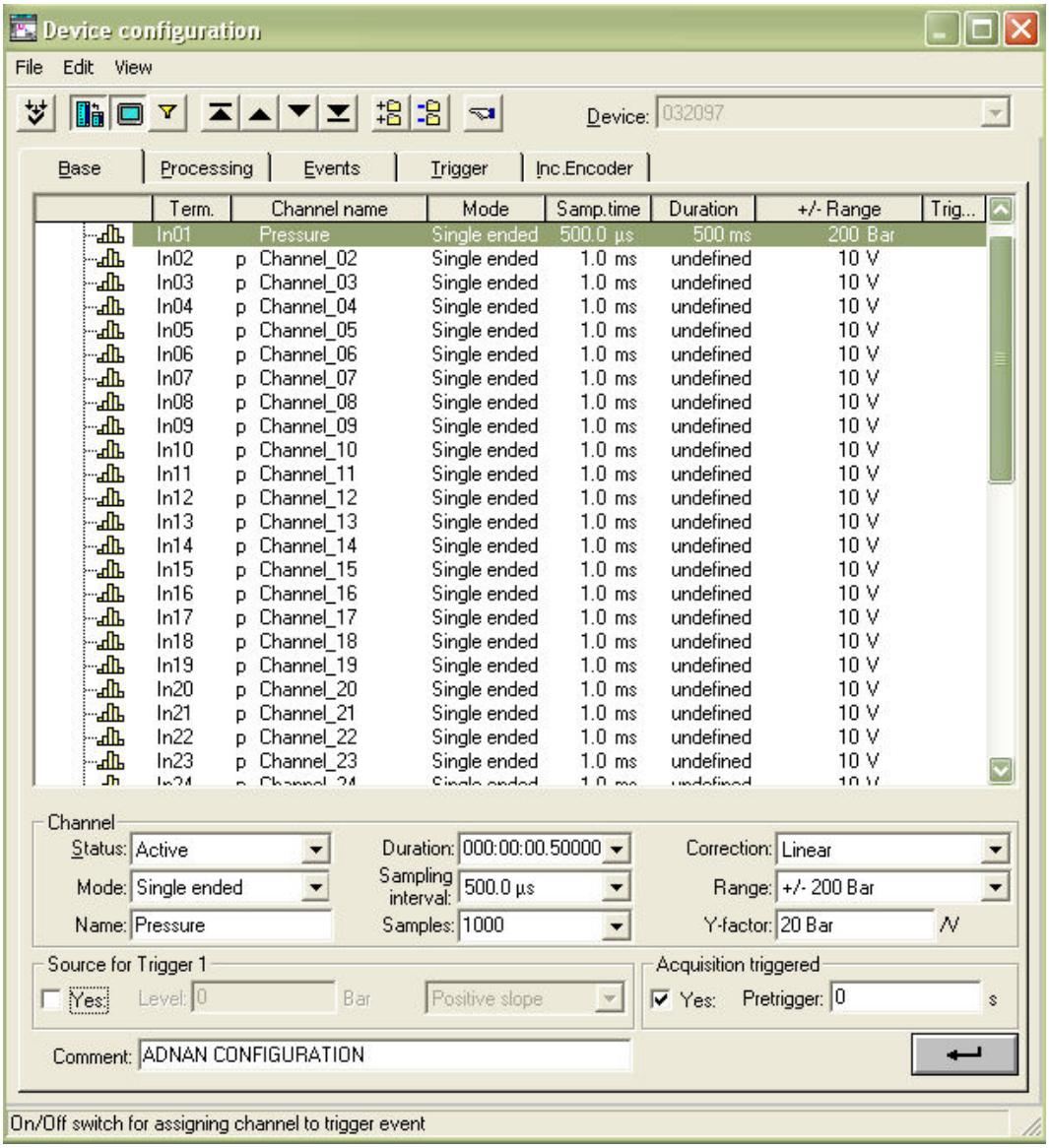

Figure 3.3 Configuration for sampling interval

3.3.2 Hydrogen Fuel Management System

In this research, timed port electronic hydrogen fuel injection system need to be developed in order to deliver hydrogen in the cylinder engine. Nowadays, timed port hydrogen gas injection is proven to be the most applicable method for supplying hydrogen into the combustion chamber due to unavailability of high-pressure hydrogen injector for direct injection purposes. At appropriate port injection timing, electronic hydrogen injection system is better than carburetion system since it can prevent

backfire, knocking and pre-ignition (Saravanan et al. 2010). Timed port hydrogen fuel injection system provides full control of injection duration and timing through the developed Electronic Control Unit. Constant voltage of 12 volt (V) is supplied to the injector whereas 2 Ampere (Amp) of current will only be supplied to the injector when the desired start of injection timing (SOI) is reached. End of hydrogen injection timing (EOI) is determined from the specified injection duration. 2 Amp of current supply to the injector will be cut-off when it reaches this crank angle (CA).

In addition to the operation of the experimental engine, an efficient safety measure for operating the engine needs to be developed. Hydrogen is filled into hydrogen storage tank from hydrogen cell until it reaches 2 bars before it is channeled to water-flame trap. It then passes through a control valve for flow rate adjustment and flows through single-flow valve, flashback arrestor and finally to hydrogen fuel injector. OMEGA digital mass flow meter is installed for measuring hydrogen flow rate with maximum range of 3 liter per hour (LPH) and it is shown in Figure B.9. Table 3.5 shows specifications of OMEGA digital mass flow meter. Figure B.10 shows the photographic view of single-flow valve and flashback arrestor.

Table 3.5 Specifications of OMEGA digital mass flow meter

Parameter	**Specification**
Maximum Flow Rate (LPH)	3
Accuracy (%)	±1.5
Response Time (ms)	800
Optimum Gas Pressure (bars)	1.4
Relative Gas Humidity (%)	70
Output Signals (VDC)	0-5
Transducer Input Power (VDC, mA)	+12, 200

Hydrogen flash back arrestor is a safety device that shuts off hydrogen flow and extinguishes the combustion flame during backfire before it reaches hydrogen storage

tank. In addition, the installation of a single-flow valve and water-flame trap in hydrogen fuel management system prevents the backfire from entering hydrogen tank that causes massive explosion (Jingding et al. 1985). Figure 3.4 shows the schematic diagram for hydrogen fuel management setup.

Hydrogen leak detector is used to sense any leakage of hydrogen gas in the pipeline. Apart from that, a frequent check for hydrogen leakage can also be done at every joint of copper hose which is insulated with white tape that links between hydrogen cell, storage tank, water-flame trap and hydrogen injector. These are considered as compulsory safety procedures before running the experiment. The schematic diagram of the experimental setup is shown in Figure 3.5.

In this research, hydrogen gaseous fuel injection is fixed from SOI of 0°CA to EOI of 20°ATDC at constant flow rate of 3 LPH. This injection timing range was selected based on a series of experiments that have been conducted on the same test engine. It was concluded that the stated hydrogen injection timing range gives optimum performance and emission characteristics in diesel-hydrogen dual fuel mode combustion. Table 3.6 indicates the percentage of diesel energy replacement with hydrogen for engine speed of 2000 RPM.

Table 3.6 Diesel energy replacement by hydrogen

Load, kW	**Diesel Energy, %**	**Hydrogen Energy, %**
1	87.27	12.73
2	88.16	11.84
3	90.12	9.88
4	93.14	6.86
5	94.61	5.39

Fuel sequence started with hydrogen gaseous fuel injection during intake stroke in order to avoid any backfire and reduction of volumetric efficiency, which in return will deteriorate engine performance and emissions. Hydrogen swirls into the cylinder

until ends of intake stroke before squishing during compression stroke. Fuel blends of hydrogen and diesel starts to occur when diesel is injected into the combustion chamber at 13°BTDC during compression stroke. Hydrogen is injected at the intake port by using NAMUR electronic fuel injector with maximum injection pressure of 3 bar. In this case, a small hole was drilled near to the intake port only to fix hydrogen injector tip in order to minimize its effect on volumetric efficiency. The technical specifications of NAMUR electronic fuel injector are summarized in Table 3.7. Figure B.11 shows the photographic view of NAMUR electronic fuel injector.

Table 3.7 NAMUR hydrogen fuel injector technical specifications

Specification	**Range**
Working Pressure (bar)	0.5-2.0
Maximum pressure (bar)	3.0
Supply voltage(V)	12±15%
Supply Current (Amp)	2±25%
Working temperature (°C)	-20 until +120

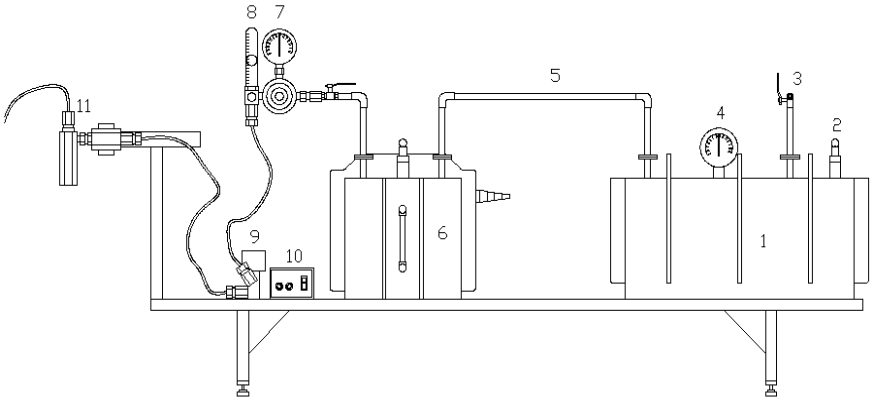

Legend:

1. Hydrogen Storage Tank
2. Safety Valve
3. Hydrogen Inlet Pipe
4. Pressure Gauge
5. Connecting Pipe
6. Water-Flame Trap
7. Pressure Gauge
8. Hydrogen Control Valve
9. Solenoid Valve
10. 12V Voltage Regulator
11. Single-Flow Valve

Figure 3.4 Hydrogen fuel management setup

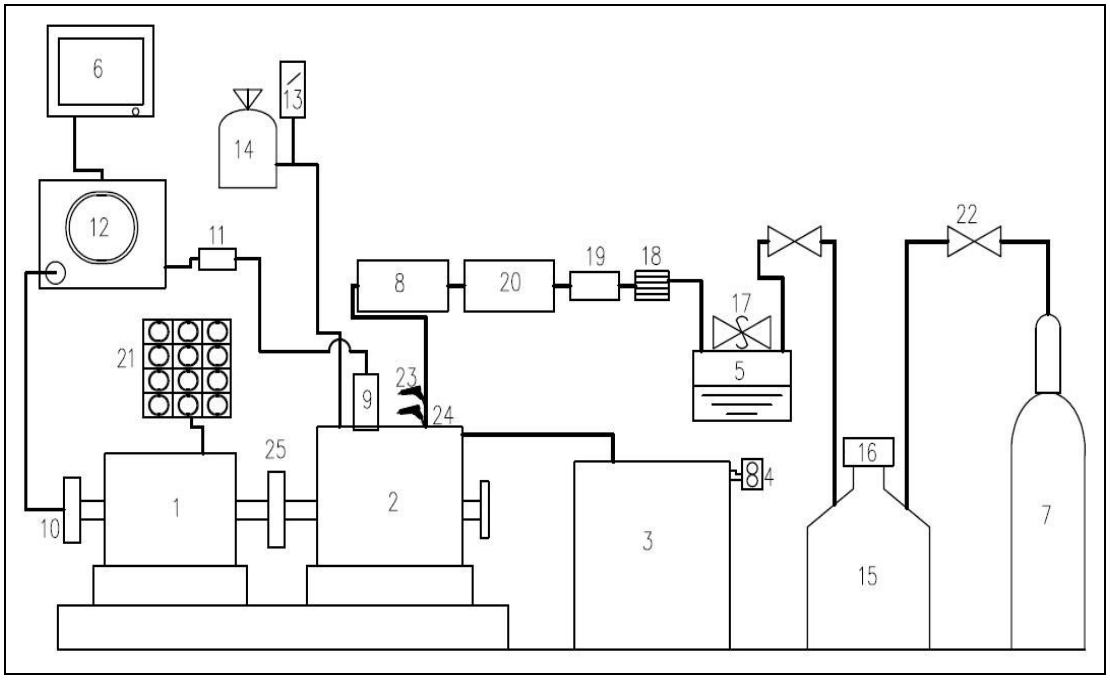

Legend:					
1	Synchronous Generator	9	Pressure Transducer	17	Safety Valves
2	Diesel Engine	10	Crank Angle Encoder	18	Flash Back Arrestor
3	Surge Tank	11	Signal Conditioner	19	Hydrogen Mass Flow Meter
4	Mass Flow Meter (Air)	12	Data Acquisition System	20	Water Tank
5	Water-Flame Trap	13	Diesel Flow Rate Pipette	21	Load Bank
6	Computer	14	Diesel Fuel Tank	22	Control Valve
7	Hydrogen Cell	15	Hydrogen Storage Tank	23	Water Injector
8	Water Pressure Regulator	16	Hydrogen Pressure Regulator	24	Hydrogen Injector

Figure 3.5 Schematic diagram of experimental apparatus

3.3.3 Water Injection System

One of the objectives of this research is to develop an efficient timed manifold water injection system. Cooling Mist Vari-Cool water injection setup is used to provide constant pressure of 1 bar from water pump through high-pressure water hose to water injector for the finest water injection droplet size. DENSO electronic injector is used to replace stock water nozzle in order to control water injection timing. Figure B.12 shows the photographic view of Cooling Mist Vari-Cool water injection system and DENSO

electronic injector. Electronic water injector is placed at a distance of approximately 175 mm upstream from the intake port for better premixing between water droplet and intake air. Water injector tip is fixed at the intake manifold in order to minimize its effect on volumetric efficiency. A schematic diagram of the water and hydrogen injection system is shown in Figure 3.6.

In this research, water is supplied at a constant pressure of 1 bar from water pump through high-pressure water hose to water injector for the finest water droplet size. Its SOI in the range of 20°BTDC to 20°ATDC and injection duration of 20°CA and 40°CA. Water injection pressure is determined from the working pressure of water injector (~3.0 bar). The earliest SOI (20°BTDC) was selected after calculating the effect of mechanical lag of two milliseconds and water injector range of 175 mm. Water droplet is expected to reach intake port exactly when exhaust port closed. Injection of water at intake manifold at these timings provides better aspiration of water into the combustion chamber especially during intake stroke. Water injection during closed intake port causes water to dribble and mix with lubricant which causes poor in performance and emissions.

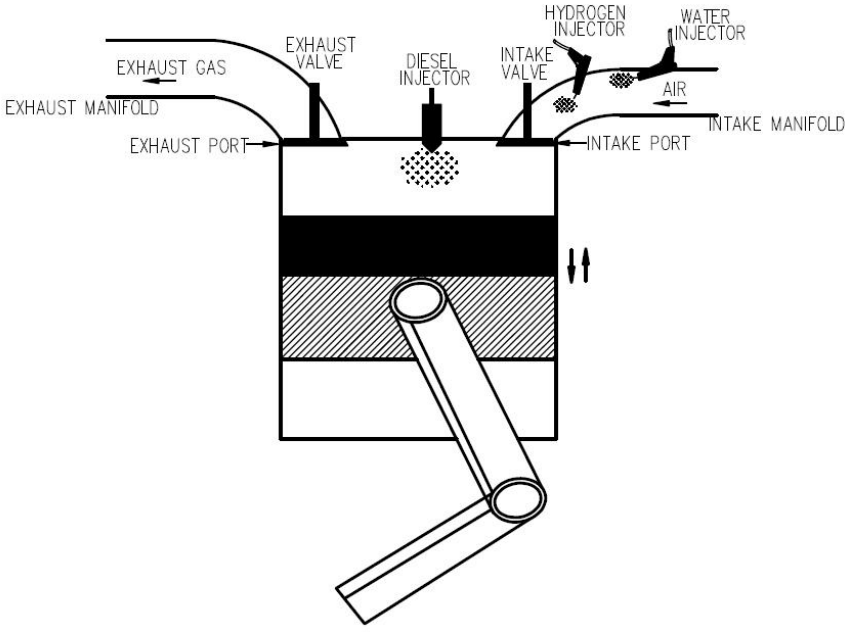

Figure 3.6: Schematic diagram of water and hydrogen injection system

3.3.4 Development of Electronic Control Unit

A fully functional electronic control unit (ECU) was designed to control hydrogen and water SOI and EOI using a Microchip PIC18F452 8-bit 40 pins Dual Inline Package (DIP) microcontroller. Table 3.8 shows specifications of this Microchip PIC18F452 microcontroller. The developed ECU is used to detect position of the piston based on crank angle value and its working principle can be described into two stages as listed below:

- *Stage 1-Determination of piston position using Trigger (TRI) signal*

  Four stroke engine requires 2 revolution of piston to complete a cycle. In this case, TRI signal is used to determine whether the piston is in the range of intake to compression strokes (0˚-360˚ CA) which is declared as PHASE 0 whereas for power to exhaust strokes (360˚-720˚ CA) which is declared as PHASE 1.

- *Stage 2-Determination of Crank Angle Measurement (CAM) signal*

  It is used to detect the exact angle within 360˚ range of intake to compression strokes or power to exhaust strokes. The incremental value of crank angle occurs at every one degree (1°CA).

Figure 3.7, 3.8 and 3.9 shows the simplified flowcharts for ECU operation. The developed ECU has four stages operation procedures as listed below:

- *Stage 1-Initialization*

  Initialization routine configures input output (I/O) of the microcontroller to receive signal from CAM and TRI as well as sending signals to injector

interface in the form of 5V and 0V voltage. The injector interface is made of semiconductor switch Metal Oxide Semiconductor Field Effect Transistor (MOSFET) BUZII amplifies signals from microcontroller to provide high voltage (12V) and current (2 Amp) to the injectors. During this stage, microcontroller will also configure its communication module that allows data to be received and sent from and to the terminal program on the computer screen.

- *Stage 2-User Input*

  Inputs in the form of SOI and EOI need to be uploaded using terminal program through computer prior to sending them to microcontroller via serial cable RS232.

- *Stage 3-Tracking Signals*

  Microcontroller tracks the current crank angle using CAM and TRI signals. The exact crank angle will be displayed in real-time basis on the computer screen.

- *Stage 4-Injection operation*

  Microcontroller will send 5V through the injector interface to amplify the voltage to 12V that will activate its solenoid for switching purposes according to the desired SOI and EOI.

The designed ECU provides precise control of water and hydrogen injection timing. Injection timing of hydrogen and water are controlled using terminal program. A circuit diagram of the developed ECU is illustrated in Figure 3.10. Mikroelectronika C Language compiler used for ECU development is shown in Appendix C. Figure B.13 shows the photographic view of the developed ECU.

Table 3.8 Technical specifications of Microchip PIC18F452 microcontroller

Specification	Range
Power Consumption (mA)	<1.6 @ 5V
Operating Frequency (MHz)	40
Data Memory (Bytes)	1536
Packages	40-pin DIP
Interrupt Sources	18
Total Power Dissipation (W)	1.0

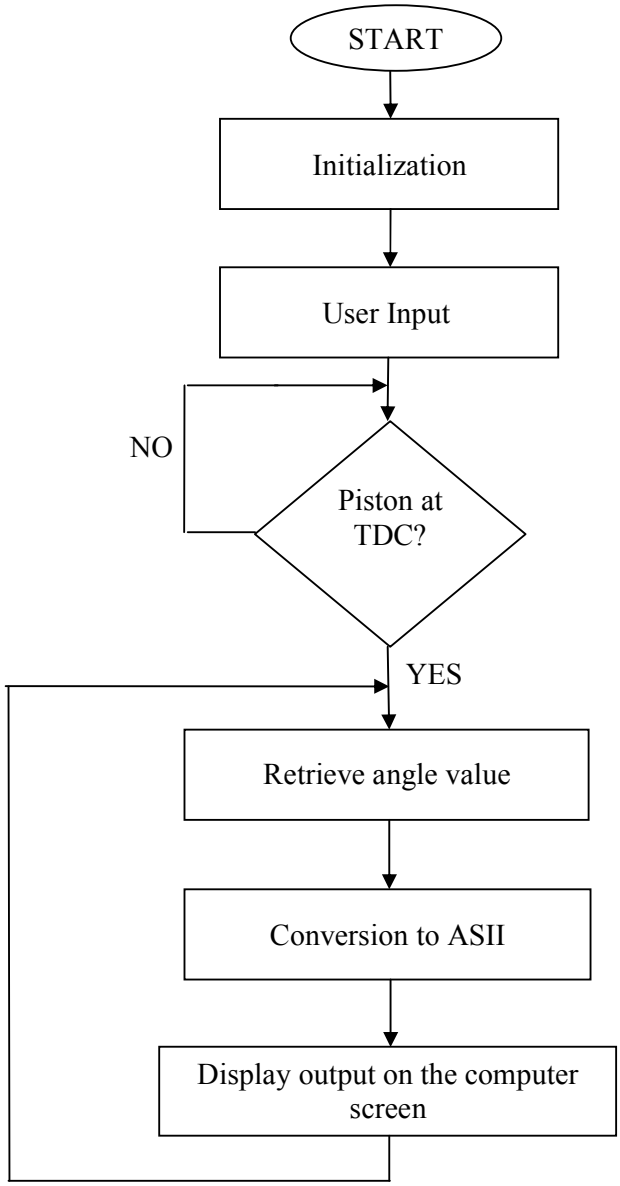

Figure 3.7 Main flowchart for ECU operation

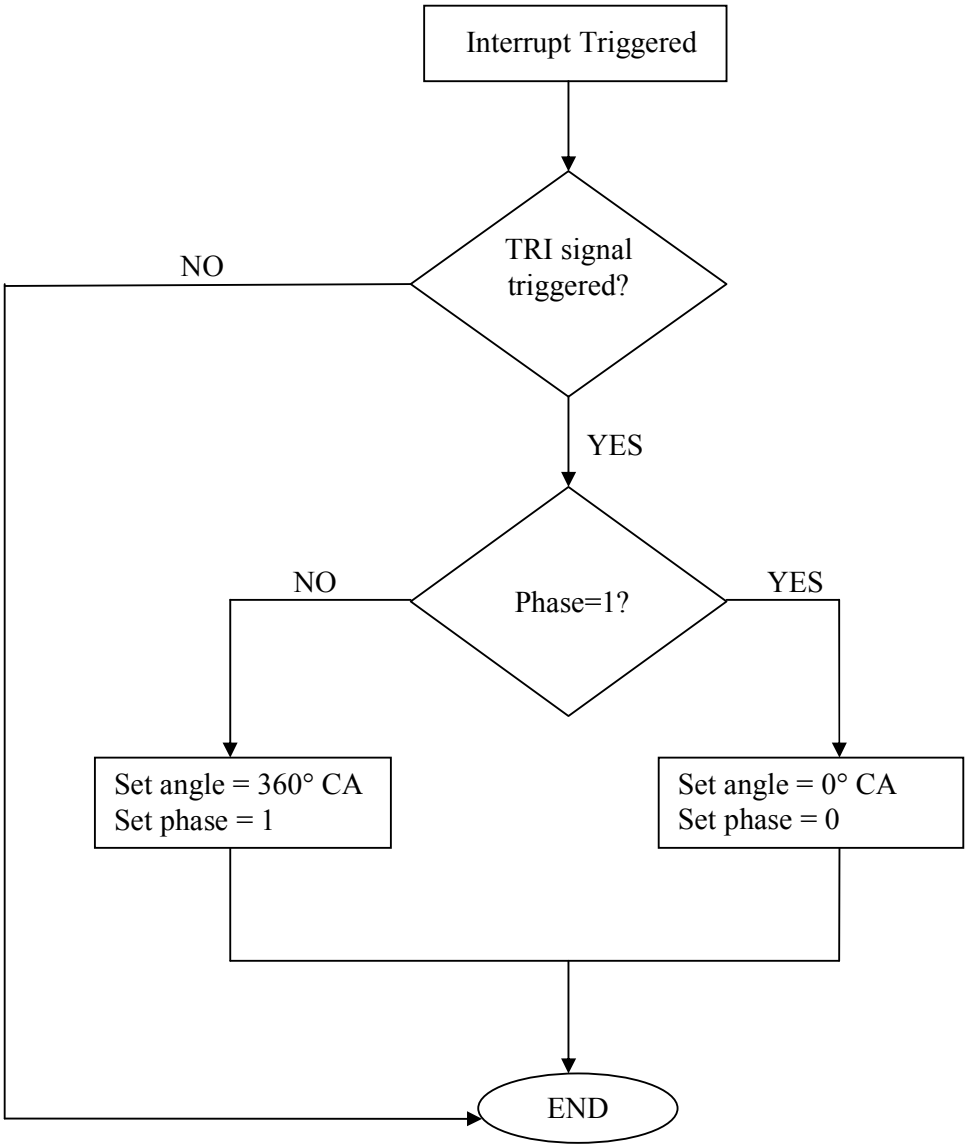

Figure 3.8 TRI flowchart for ECU operation

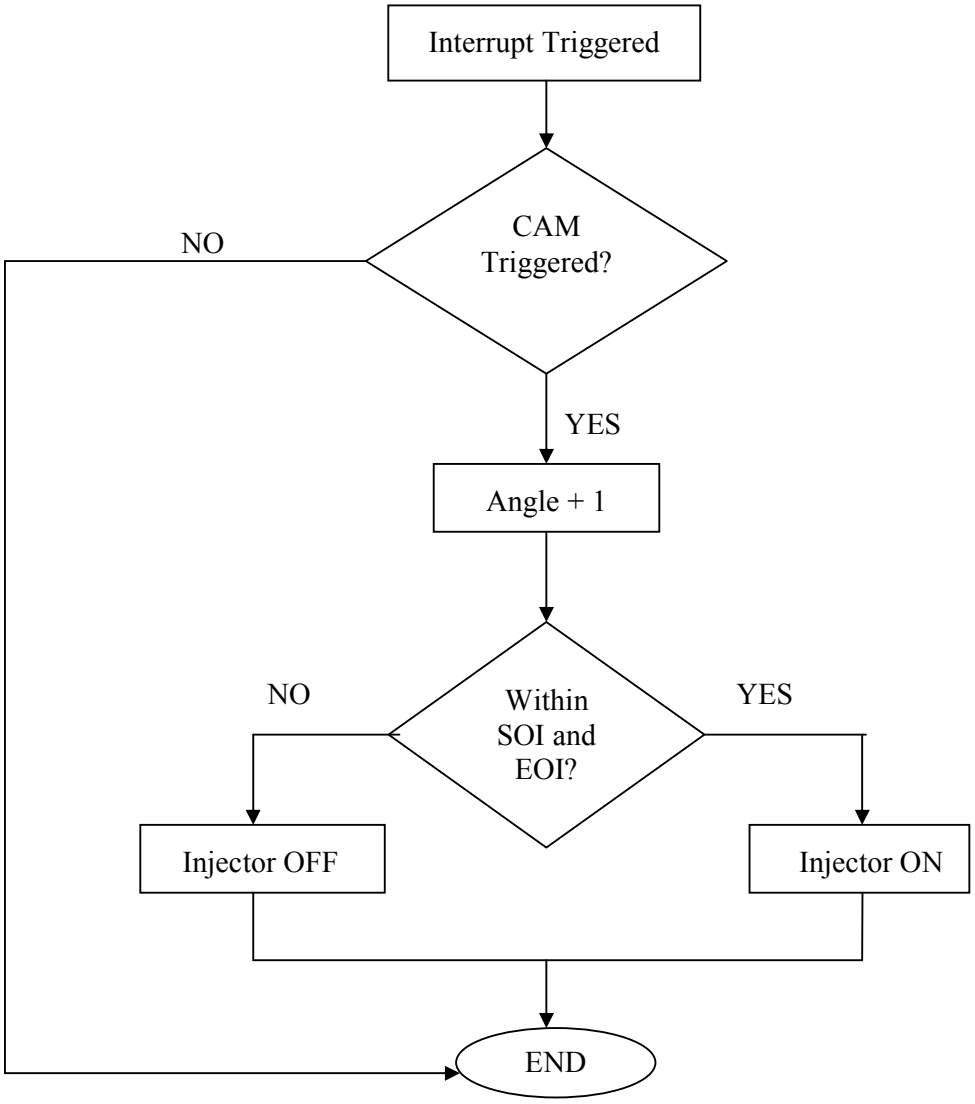

Figure 3.9 CAM flowchart for ECU operation

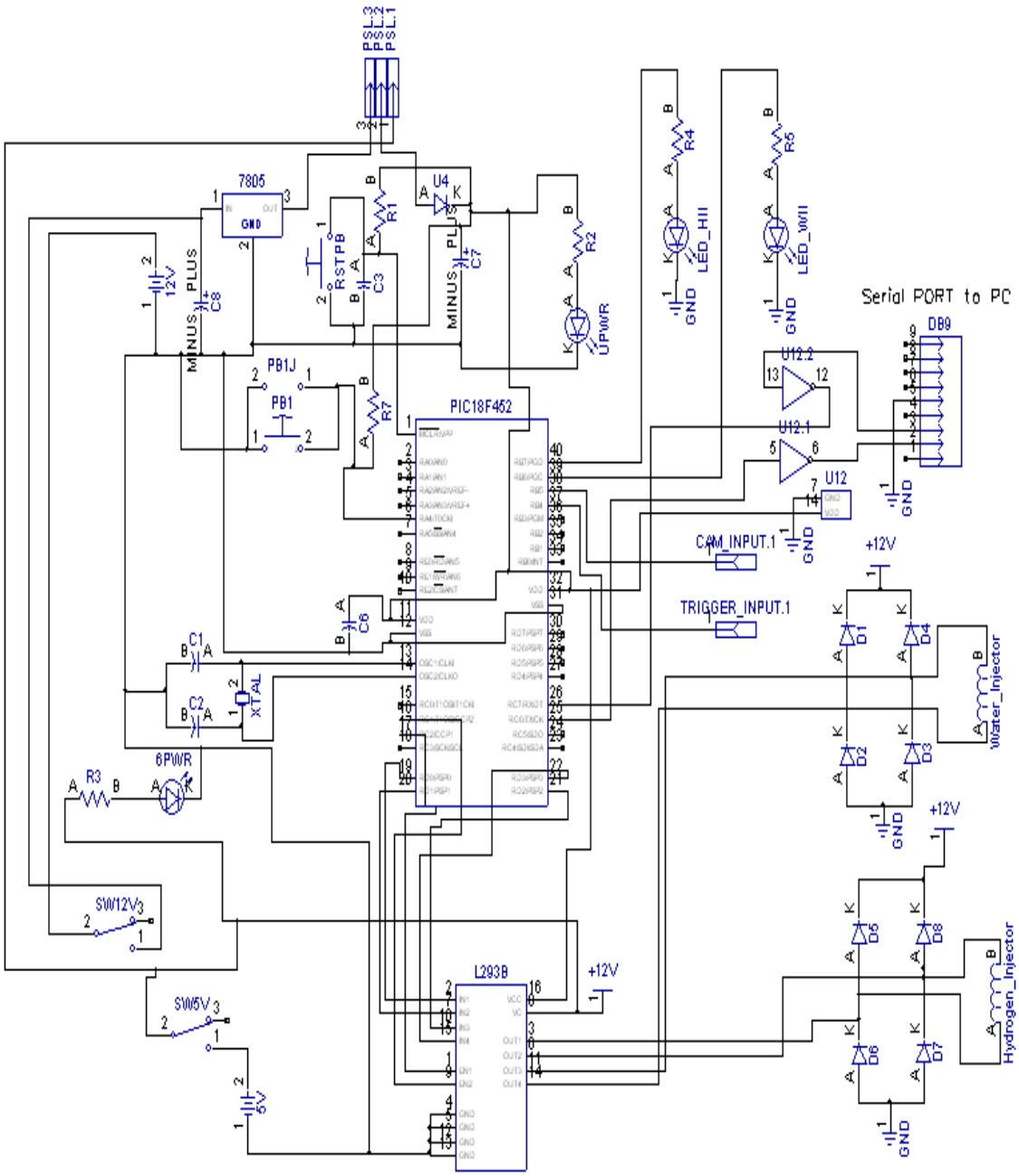

Figure 3.10 Circuit diagram of the developed ECU

3.3.5 Experimental Procedures

This section presents the detailed procedures taken in conducting series of experiments. In this research, SOI of hydrogen fuel is fixed as 0˚ CA with injection duration of 20°CA and constant flow rate of 3 LPH. The various SOI and injection duration of water are listed in Table 3.9. Water injection flow rate with respect to injection duration and engine speed are listed in Table 3.10. It also shows that the longer the injection duration, the greater flow rate of water.

Table 3.9 Start of injection timings and injection durations for DHW operation

CASE	SOI	Injection duration	CASE	SOI	Injection duration
1	20°BTDC	20°CA	6	0°CA	40°CA
2	20°BTDC	40°CA	7	10°ATDC	20°CA
3	10°BTDC	20°CA	8	10°ATDC	40°CA
4	10°BTDC	40° CA	9	20°ATDC	20°CA
5	0°CA	20°CA	10	20°ATDC	40°CA

In general, the experiments conducted in this research comprises of two main parts namely, without and with water injection. For the first part, the test engine is operated using diesel and hydrogen fuels. Initially, the engine is set to operate at speed of 1500 RPM by adjusting the accelerator until it is stabilized. The corresponding Pθ diagram is generated on the computer screen using IMC-μ LIGHT software. These data are then transferred to FAMOS command and saved in LOOK format file.

Table 3.10 Water injection flow rate

Engine Speed (RPM)	Water Flow Rate (kg/hr)	
	Injection Duration 20°CA	Injection Duration 40°CA
1500	0.6	0.69
2000	0.45	0.85
2500	0.27	0.93
3000	0.36	0.81

Diesel fuel flow rate is determined by duration taken to consume 10 ml diesel. In measuring exhaust gas emissions, the gas-sampling probe of both gas analyzers is inserted into the exhaust hose fittings. The value of each resulted exhaust gas emissions component and exhaust temperature are taken only after they are stabilized. These procedures are repeated at engine speeds of 2000, 2500 and 3000 RPM with incremental load of 1kW. As for the second part of the experiment, it was repeated accordingly to similar procedures with water injection system at the same range of engine speeds. For each series of experiment with hydrogen and water injection systems, injection timing of hydrogen and water are programmed based on cases in Table 3.3 prior to running the engine by using terminal program as shown in Figure 3.11. All the data gathered from this experiment are tabulated and then plotted the graphs. Such procedure is performed in order to facilitate the process of analysis and discussion as presented in the following chapter.

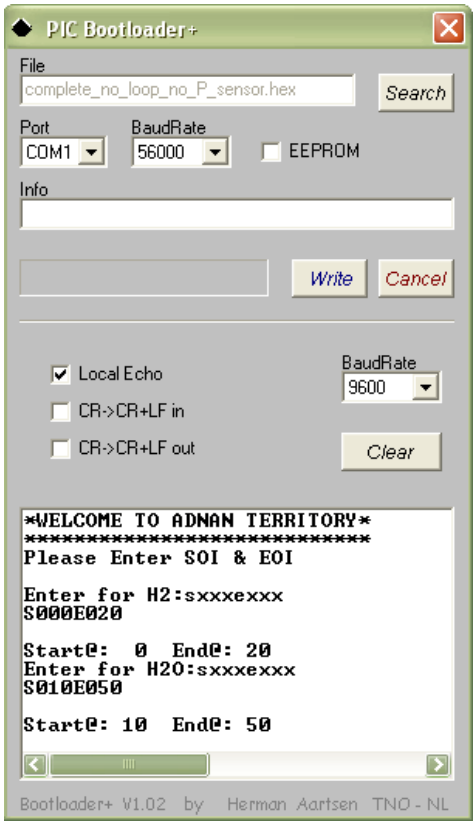

Figure 3.11 Terminal program for hydrogen and water injection system

3.4 Error Analysis

Error analysis is performed to prove measurement accuracy of the physical quantities during the conduct of experiment. Error analysis of the measured quantities can be accounted for in order to get the real measurement value. For instance, the error of crank angle was estimated by considering its encoder error, and the error of in-cylinder pressure was estimated based on the accuracy of the pressure transducer used. Error analysis of the derived quantities such as indicated work and thermal efficiency have to be analytically estimated based on rout mean square method (Sahin et al. 2008).

$$\Delta R = \sqrt{\left[\left(\frac{\partial R}{\partial x_1}\Delta x_1\right)^2 + \left(\frac{\partial R}{\partial x_2}\Delta x_2\right)^2 + \left(\frac{\partial R}{\partial x_3}\Delta x_3\right)^2 + ... + \left(\frac{\partial R}{\partial x_n}\Delta x_n\right)^2\right]} \tag{3.96}$$

Where R is the derived quantity, ΔR is the error limit, and Δx_1, Δx_2, $\Delta x_3 \ldots \Delta x_n$ are error limits of the measured values. The error of measured quantities of in-cylinder volume (ΔV) and pressure (P) based on Gaussian distribution are $\pm 0.2 \text{cm}^3$ and $\pm 0.5\%$ respectively. For in-cylinder pressure (P) of 15 bar ($15 \text{x} 10^5$ Pa), volume at 125cm^3 and indicated work of 180 Joule, a sample calculation for the error of indicated work is given as below:

$$W_i = f(\text{P,V}) = \text{PV (Joule)} \tag{3.97}$$

$$\frac{\partial W_i}{\partial P} = \text{V} \text{ and } \frac{\partial W_i}{\partial V} = \text{P} \tag{3.98}$$

$$\Delta W_i = \sqrt{\left[\left(\frac{\partial W_i}{\partial P}\Delta P\right)^2 + \left(\frac{\partial W_i}{\partial V}\Delta V\right)^2\right]} \tag{3.99}$$

$$= \sqrt{(125\times10^{-6}\times0.075\times10^5)^2 + (15\times10^5\times0.2\times10^{-6})^2} = 0.98 \text{ J}$$

$$\% \text{ Error} = \frac{180.98 - 180}{180.98}\times 100\% = 0.54\%$$

The details of the error analysis for some measured and derived quantities are given in Table 3.11. It can be observed that the error ranges from 0.2% to 5%. Hence, it

can be concluded that the error in measured and derived quantities does not significantly influence the overall uncertainty of the results.

Table 3.11 Error analysis of measured and derived quantities

Parameter	Error (%)
Crank Angle Encoder	0.2
Pressure Transducer	0.5
Hydrogen Flow Meter	1.3
Engine Speed	1.6
Temperature	1.0
Oxides of Nitrogen	5.0
Carbon Monoxide	5.0
Sulfur Dioxide	5.0
Oxygen	0.6
Indicated Work	0.54
Thermal Efficiency	1.26

3.5 Numerical Investigation Using Newton-Raphson Method

Scientists and engineers have adapted the application of iterative methods in nonlinear algebraic equations such as Newton–Raphson method (NR), Adomian's method (ADM) and Homotopy Perturbation Method (HPM) lately (Momani, 2006). It is because these methods simplify complex problems into simple solutions (Javidi, 2007). Newton–Raphson method is the most popular and powerful method in solving non-linear combustion equations. For example, Rakopoulos et al. also used this method to solve equations of chemical equilibrium combustion model in 11 species diesel alone combustion products (Rakopoulos et al. 1994). Masood et al used this method to solve equations of low-temperature combustion model with only 10 products species (Masood et al. 2008). Rashidi combined Newton–Raphson with successive substitution methods to solve combustion problem of hydrocarbon fuel with 13 products species

and concluded that the combined method gives very fast and reliable convergence during the iteration process (Rashidi, 1998).

In this research, Newton-Raphson Method was selected to solve equilibrium constants combustion equations of 9 combustion products of hydrogen-diesel dual fuels with water addition as shown below:

$$n_f C_\alpha H_\beta + m_f H_2 + p_w H_2O + \frac{a_s}{\phi}(O_2 + 3.76N_2) \rightarrow n_T \begin{pmatrix} y_1 CO_2 + y_2 O_2 + y_3 H_2O + \\ y_4 CO + y_5 CH_4 + y_6 HCN + \\ y_7 NO + y_8 NO_2 + y_9 N_2 \end{pmatrix} \quad (3.100)$$

By applying Equations 3.92, 3.93, 3.94 and 3.95 into Equation 3.100 forms a system of nonlinear equations with four unknowns as shown in Equation 3.101.

$$\begin{aligned} f_1(y_1, y_2, y_3, y_4) &= 0 \\ f_2(y_1, y_2, y_3, y_4) &= 0 \\ f_3(y_1, y_2, y_3, y_4) &= 0 \\ f_4(y_1, y_2, y_3, y_4) &= 0 \end{aligned} \quad (3.101)$$

This system can be written in more compact vector form as $F(y)=0$, where:

$$\boldsymbol{y} = [y_1, y_2, y_3, y_4] \quad (3.102)$$

$$\boldsymbol{F}(\boldsymbol{y}) = \begin{bmatrix} f_1(\boldsymbol{y}) \\ f_2(\boldsymbol{y}) \\ f_3(\boldsymbol{y}) \\ f_4(\boldsymbol{y}) \end{bmatrix} \quad \text{and} \quad \boldsymbol{0} = \begin{bmatrix} 0 \\ 0 \\ 0 \\ 0 \end{bmatrix} \quad (3.103)$$

Newton-Raphson method requires the evaluation of a matrix, known as the Jacobian of the system, which is defined as:

$$\boldsymbol{J} = \frac{\partial(f_1, f_2, f_3, f_4)}{\partial(y_1, y_2, y_3, y_4)} = \begin{bmatrix} \frac{\partial f_1}{\partial y_1} & \frac{\partial f_1}{\partial y_2} & \frac{\partial f_1}{\partial y_3} & \frac{\partial f_1}{\partial y_4} \\ \frac{\partial f_2}{\partial y_1} & \frac{\partial f_2}{\partial y_2} & \frac{\partial f_2}{\partial y_3} & \frac{\partial f_2}{\partial y_4} \\ \frac{\partial f_3}{\partial y_1} & \frac{\partial f_3}{\partial y_2} & \frac{\partial f_3}{\partial y_3} & \frac{\partial f_3}{\partial y_4} \\ \frac{\partial f_4}{\partial y_1} & \frac{\partial f_4}{\partial y_2} & \frac{\partial f_4}{\partial y_3} & \frac{\partial f_4}{\partial y_4} \end{bmatrix} \tag{3.104}$$

From Equation 3.101, the elements of the Jacobian matrix, ***J*** for the previously derived combustion reaction equations are shown from Equation 3.105 until Equation 3.120 in Appendix D.

In this study, the initial guess for four (4) main mole fractions y_1, y_2, y_3, and y_4 are $3.173e^{-5}$, $1.117e^{-1}$, $4.332e^{-2}$ and $7.45e^{-1}$, respectively. The stated values were obtained from mole fractions of these species in atmospheric air at room temperature. The solution was unique as long as mole fractions of all 9 combustion products species showed positive values. By using the stated initial guess, most of the results indicated almost constant values after tenth iterations, which shows that there were no convergence problems. Multiple solutions will be detected if the result showed negative value of mole fraction for one or more products that was due to wrong selection of initial guess. Furthermore, there was no result shown after 100 iterations, if divergence occurred.

3.5.1 MATLAB Inputs

In this study, MATLAB code for the combustion simulation has been developed. The input parameters that need to be provided into the MATLAB program are Temperature, T (K), Equivalence ratio,ϕ and Combustion Pressure, P (bar). In this study, combustion pressure and temperature are determined from instantaneous crank angle where the heat release from the combustion is about to end. The measured equivalence ratios from each series of experiments are used as input. Figure 3.12 shows

overall the flowchart of MATLAB operation for solving system of nonlinear equations using Newton-Raphson Method. Appendix E shows MATLAB program for nine combustion products simulation using Equilibrium Constant Method.

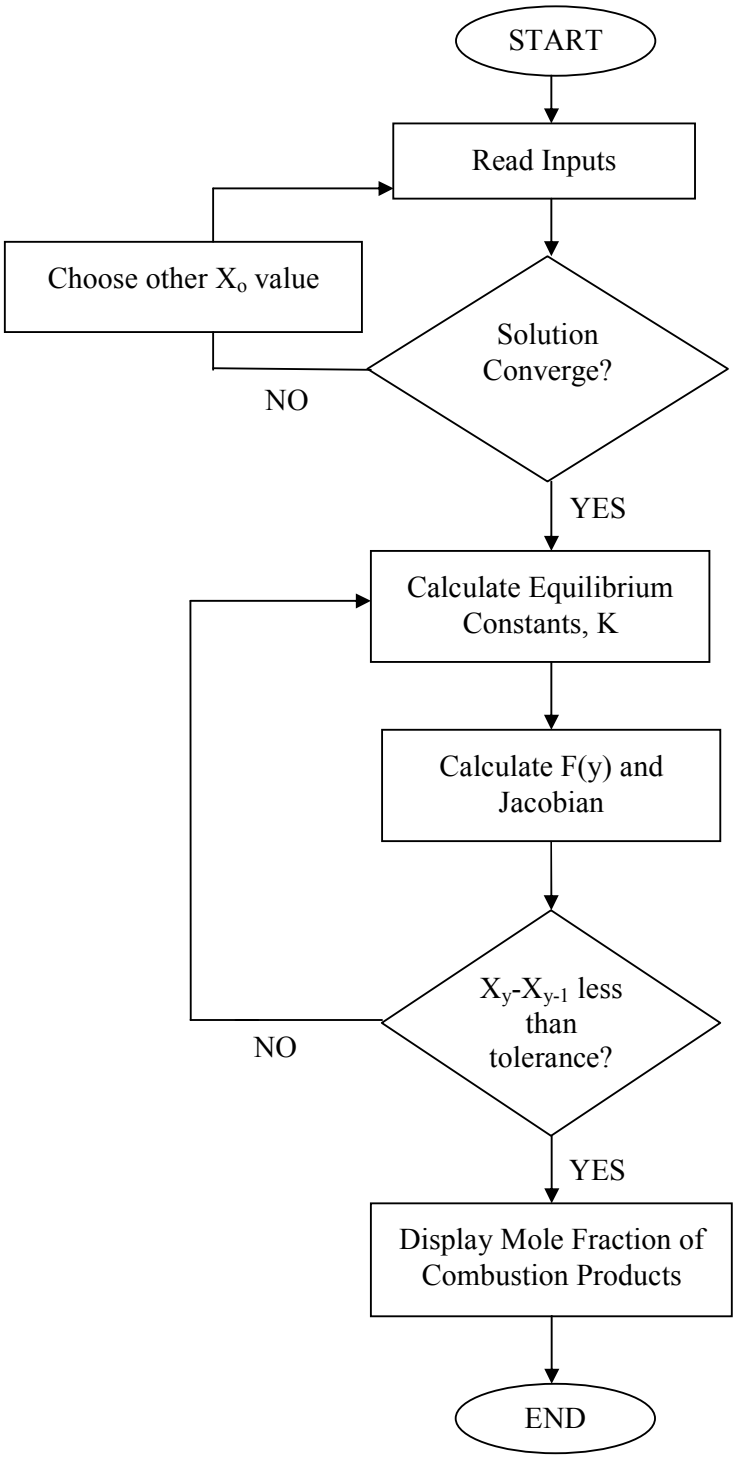

Figure 3.12 Flowchart of overall MATLAB program

Chapter 4

RESULTS AND DISCUSSION

4.1 Introduction

The results of the experimental and numerical investigations are presented, analyzed and arrived at conclusions in this chapter. Discussions are made based on the experiments and simulations carried out as discussed in the previous chapter. In this chapter, performance and emissions results of HFCI engine are discussed along with the effect of water injection system. Experimental results pertaining to performance and emission characteristics of HFCI engine with variable water injection timings are presented in detail. It is then compared with diesel alone and diesel-hydrogen operations. Brief comparisons between this study with other researchers are also presented in order to acknowledge the available research gaps even though most of the works are dissimilar. Numerical results are analyzed to evaluate emission characteristics of HFCI engine with water addition prior to experimental validation.

4.2 Experimental investigation

The experimental investigation done on HFCI with and without water injection system is discussed in this section. The major objective of this investigation is to determine the optimum water injection timing for better performance and emissions control. This section is divided into two categories namely performance and emissions analyses.

4.2.1 Performance Analysis

This section discusses experimental results on performance of HFCI engine with and without water injection. The selected chart that represents similar pattern for each

performance characteristics will be interpreted and discussed. The extensive charts on performance of HFCI engine for DA, DH and DHW operations are presented in Appendix F.

4.2.1.1 In-Cylinder Pressure

The in-cylinder pressure was measured using KISTLER pressure transducer and this input data was well-organized by DAS to visualize P-θ diagram while running the experiment. Figure 4.1 shows the variation of in-cylinder pressure with crank angle at the speed of 2000RPM and 1kW load for diesel alone (DA) operation, hydrogen with diesel (DH) operation, CASE 1 and 2. The results show that all curves move upwards with the same pattern before top dead center (TDC) which indicates normal combustion of pilot fuel without pre-ignition. The DH and diesel-hydrogen-water (DHW) pressure curves have the tendency to shift to the right where the peak pressure for DHW operation occurs in the range of 5° to 8°CA later than that of DA operation at all engine speeds.

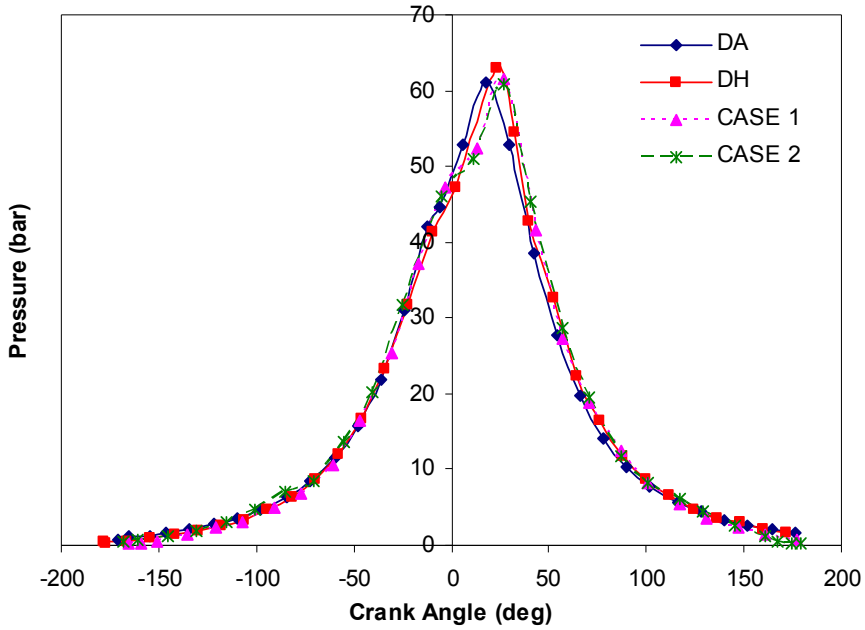

Figure 4.1 Variation of in-cylinder pressure with crank angle at 2000 RPM

The delay in peak pressure of DH and DHW operations is due to high auto-ignition temperature of hydrogen in cylinder charge causes late ignition of hydrogen after pilot ignition of diesel fuel (Shafer et al. 1995). Sudden increase in pressure after 10°ATDC indicates auto-ignition of hydrogen has been reached parallel to pilot ignition of diesel. This is due to fast combustion propagation of the cylinder charge caused by high flame speed of hydrogen (3.24 to 4.40 ms^{-1}) (Li et al. 2003).

It can also be observed that combustion of HFCI engine occurs with higher peak pressure because of higher heat of combustion (142 MJ/kg) and diffusivity (0.61cm^2/s) of hydrogen (Heywood, 1988). The high diffusivity facilitates the formation of a uniform mixture of hydrogen with other cylinder charge since this contributes greatly to ensure an equal supply of hydrogen to all regions in the cylinder (Joseph et al. 1996). Additionally, wide range flammability and minimum ignition energy (0.02MJ) of hydrogen promotes complete combustion of hydrogen throughout the cylinder even within the lean mixture regions.

The delay of peak pressure for DHW is more as compared to DH operations due to water injection reduces combustion flame temperature during premixed combustion phase of the cylinder charge. Almost similar observation has been reported by Tauzia et al. which concluded that inlet manifold water injection causes delay of peak pressure in diesel alone operation (Tauzia et al. 2010). It can be concluded that the greater the injection duration (40˚ CA), the greater water quantity induced into the cylinder charge and even lowered the combustion flame temperature which delayed the peak pressure to be reached.

4.2.1.2 Peak Pressure

The peak pressure was obtained from P-θ diagram for every speed and load during experiments. The analysis of peak pressure is significant in determining maximum force exerted on the engine piston and cylinder prior to identifying the best material for engine fabrication.

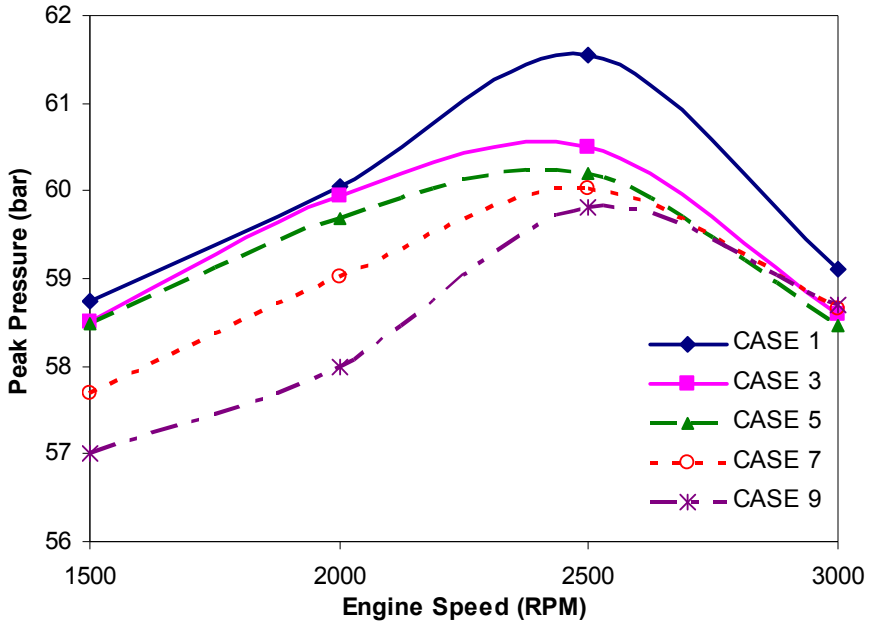

(a)

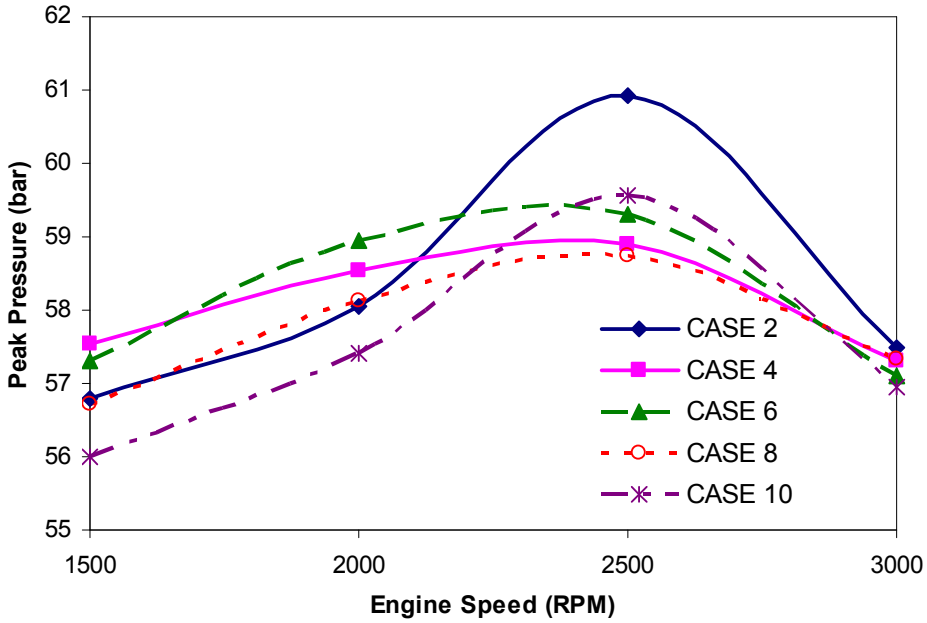

(b)

Figure 4.2 (a) Variation of peak pressure with engine speed (injection duration 20°CA) (b) Variation of peak pressure with engine speed (injection duration of 40°CA)

Figure 4.2a and 4.2b shows the variation of in-cylinder peak pressure DHW operation with speeds at different SOI and injection duration at constant load of 2 kW. They indicate that the highest peak pressure occurs in CASE 1 especially at 2500RPM and the lowest peak pressure occurs in CASE 10 at 1500RPM. The peak pressure of DHW operation is always lower than that of DH and DA operations in the range of 1 to 7 bar. This is in good agreement with research conducted on diesel engine with timed manifold water injection system by Subramanian. He reported that water injection lowered peak pressure of diesel alone operation (Subramanian, 2011).

The highest peak pressure occurs at 2500RPM for most of cases, this can be related to stronger heat release, and more complete combustion as the effects from optimum equivalence ratio of the cylinder charge with hydrogen and water droplet. Lower peak pressure for DHW operation is due to evaporative cooling of water affects the temperature during premixed combustion. Water is injected in the liquid droplet hence, heat from the cylinder charge is needed for its evaporation. The latent heat of vaporization is absorbed from the cylinder charge during evaporation of water droplet.

Lower peak pressure is shown in all the cases for lower speed range since lower engine speed provides more time for combustion to occur but explicitly causes more heat dissipation from engine cylinder to the ambient. Lower peak pressure is also shown for engine speed of 3000RPM due to increase in friction during high-speed operation, which causes more heat loss and consequently lowers in-cylinder peak pressure. Another possible reason is due to the limitation of diesel engine where the fuel hardly burned completely especially during high-speed operation (Heywood, 1988).

It can be concluded that the existence of water droplet retards the start of premixed combustion and slowly reduces combustion flame speed of the cylinder charge consequently reduces the peak pressure.

4.2.1.3 Heat Release Rate

Heat release rate (HRR) was calculated from the average pressure with respect to crank angle for 50 cycles. It is important in indentifying the rate of chemical energy released from combustion of fuels. Figure 4.3a demonstrates the heat release rate of HFCI in present investigation running on DA, DH and DHW with injection duration of 20˚CA and 40˚CA at 2000RPM. Throughout all cases, negative heat release rate have been observed before start of ignition due to diesel fuel and water droplet initiate its vaporization process resulting in heat absorption from the cylinder charge.

Figure 4.3b demonstrates PHRR for all cases at 3000RPM. It shows that injection duration of 20˚CA generates lower PHRR as compared to injection duration of 40˚CA throughout SOI 20B˚TDC to 0˚CA. CASE 7 and CASE 9 shows higher PHRR for injection duration 40˚CA as compared to 20˚CA injection duration. Different characteristics of PHRR were observed for different engine speeds and injection duration.

At engine speed of 3000RPM, CASE 10 showed the lowest PHRR with the value of 55.20 Joule per degree (J/˚deg) and this value is lower than that of DA operation. The highest PHRR is shown in CASE 1 with the value of 79.32 J/˚deg at 1500RPM. This means that water injection lowered peak heat release rate (PHRR) due to cooling effect of water during premixed combustion phase as compared to DH operation. It can also be observed that for most cases PHRR with water injection are always higher than that of DA operation and lower than DH operation. The observation on DA operation with water injection is in agreement with the previous work conducted by Tesfa et al. (Tesfa et al. 2012).

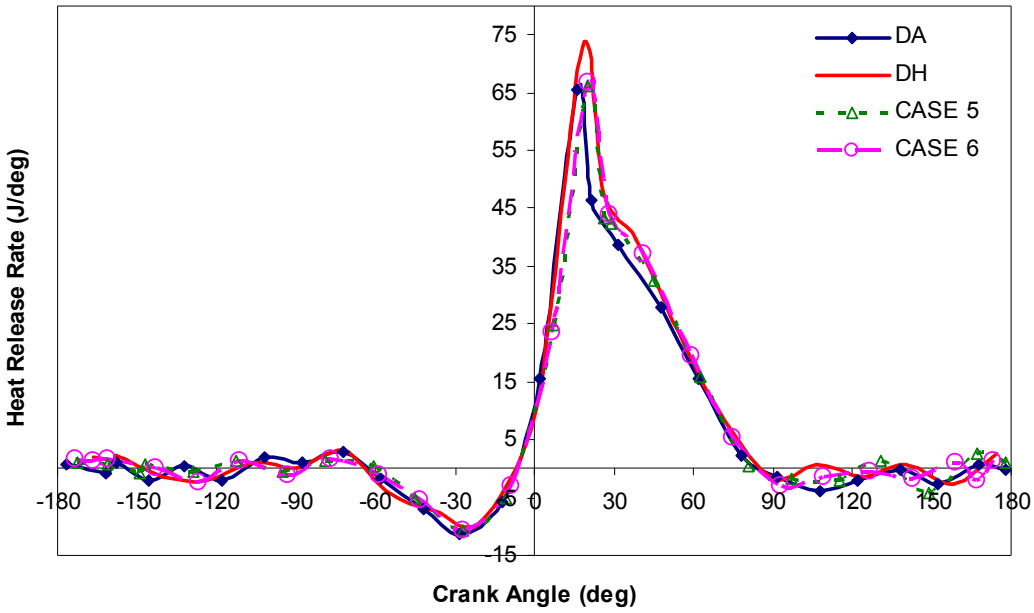

(a)

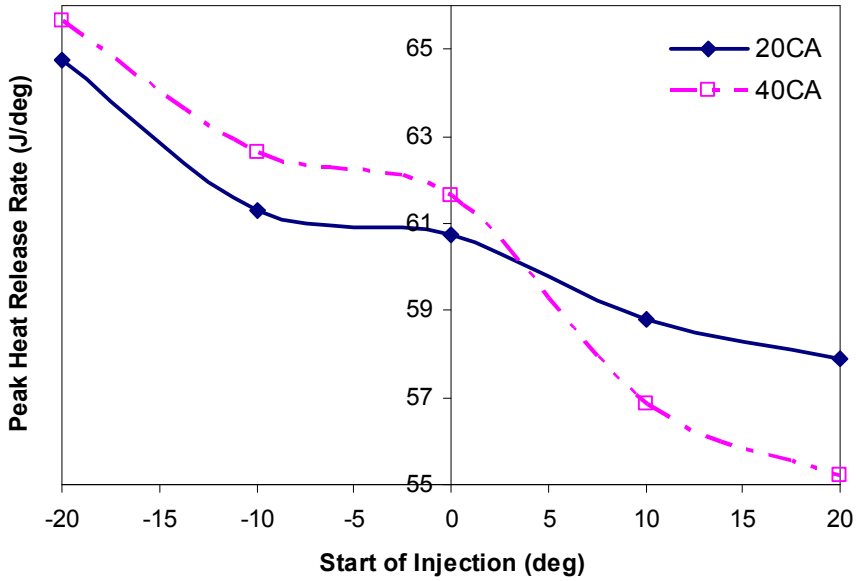

(b)

Figure 4.3 (a) Variation of heat release rate with crank angle at 2000 RPM
(b) Peak heat release rate with different SOI and duration at 3000 RPM

In DHW operation, combustion process depends on the spray quality and ignition characteristics of the pilot diesel fuel. It also depends on mixing quality of hydrogen and water droplet in the cylinder charge. Water droplet limiting the turbulent flame propagation from pilot ignition zones to cylinder charge and later affects the

concentration of heat that is being released (Karim et al. 1988). It also retard the combustion process of the charge entrained into the burning diesel and affects its turbulent mixing which contributes to lower PHRR with extended combustion duration (Liu et al. 2008).

4.2.1.4 Ignition Delay

Ignition delay was determined from the period between SOI of pilot diesel (13˚BTDC) and start of ignition using HRR analysis diagrams. Figure 4.4 illustrates the variation of ignition delay (degree) for different experimental procedures at 2000RPM. It displays trends that HFCI engine operations with or without water injection increases the delay as compared to DA operation. The delays in DHW operation are always longer than that of DH and DA operations ranging between 0.5°CA to 5°CA. The longest delay period occurred in CASE 2 with 9.5˚CA and there were no significant differences in delay periods for CASE 3, 5, 7 and 9. It also depicts that injection duration of 40˚CA extended the delay period more as compared to 20˚CA injection duration.

The trend of the graph for DHW operation shows that early water injection causes longer delay since it provides more time for water droplet to uniformly distributed and consequently absorbs more heat from the surrounding cylinder charge resulting in late self-ignition of pilot diesel fuel. It also indicates that the longer the duration, the greater is the delay since longer duration injects greater quantity of water droplet (Tauzia et al. 2010).

The longer delay period for DHW operation is due to the cooling effect of water on the intake air temperature contributes towards lower charge temperature at the time of fuel injection (Tesfa et al. 2012). This is in a good agreement with Arrhenius

function, which stated that ignition delay is strongly dependent on the intake charge temperature (Nader et al. 1998). It is concluded that the delay period increases with increasing of water injection duration for all the cases.

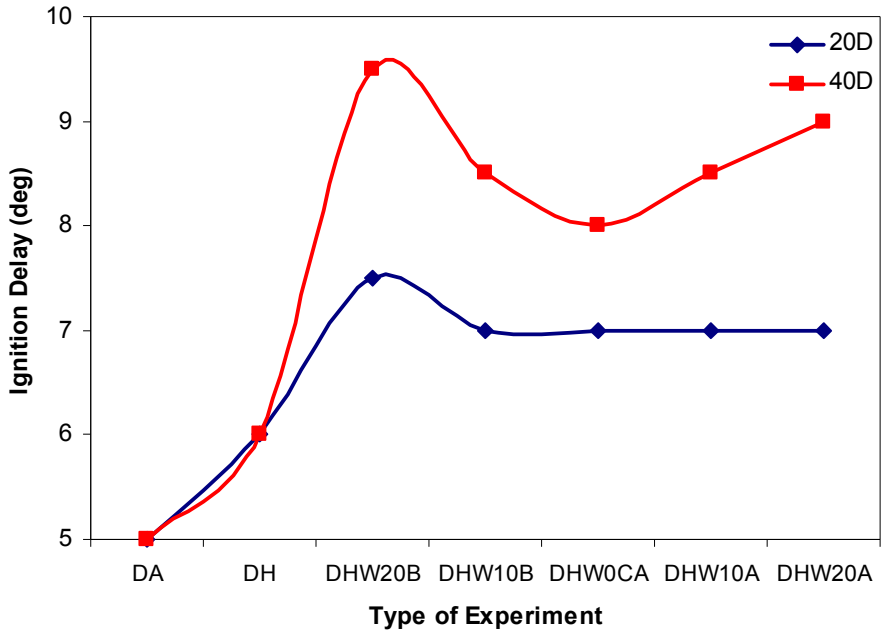

Figure 4.4 Variation of ignition delay with different type of experiment

4.2.1.5 Gross Indicated Work

Gross indicated work is known as work delivered to the piston during compression and expansion strokes namely crank angle in between 180˚BTDC and 180˚ATDC. It is also known as useful shaft work available for an engine. It is determined from enclosed area on P-*V* diagram as shown in Figure 4.5a. Figure 4.5b shows the variation of gross indicated work (in Joule) for all cases at 1500 RPM and 5 kW of load. It can be observed that increase of gross indicated work in DH operation as compared to DA operation ranges between 5% to 25%.

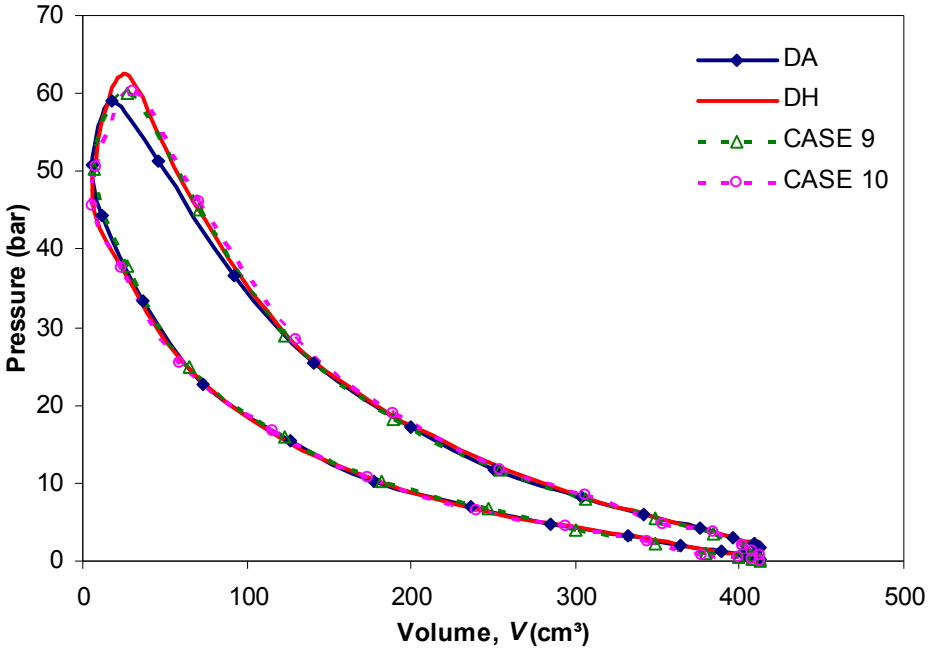

(a)

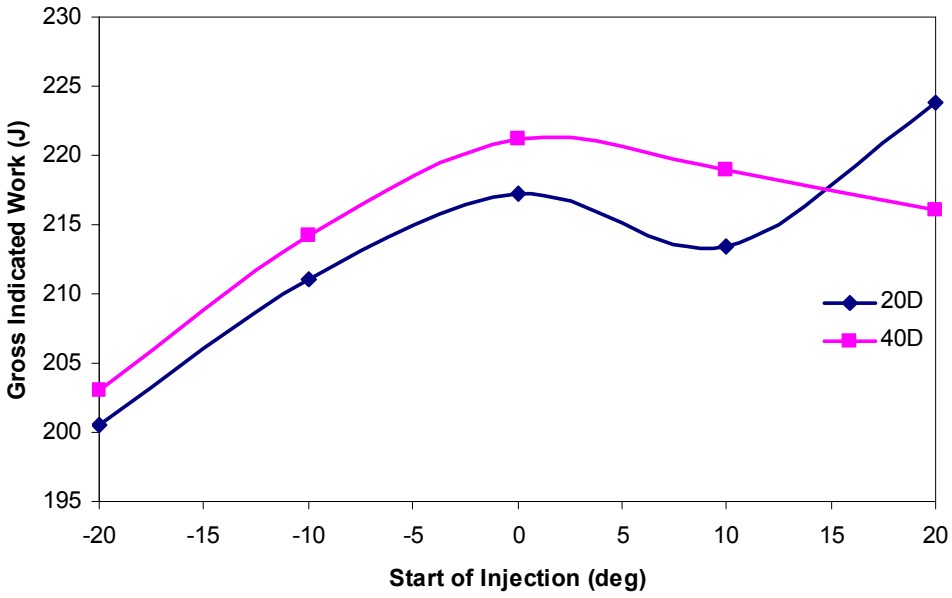

(b)

Figure 4.5 (a) P-*V* Diagram at 2500 RPM and 2 kW load
(b) Gross indicated work at 1500 RPM and 5 kW load

DHW operation produces less gross indicated work as compared to DA and DH operations especially for CASE 1 to CASE 4 in the range of 1% to 7%. DHW operation

shows increase in gross indicated work as compared to DA especially for CASE 5 until CASE 10 in the range of 3% to 32%. The optimum water injection timing occurred in CASE 9 at 1500 RPM with highest additional gross indicated work of 32%. Generally, injection duration of 40˚CA shows higher gross indicated work due to increased amount of water droplet in the cylinder charge per cycle. The optimum water injection timing for maximum gross indicated work is in CASE 9.

Higher gross indicated work shows better combustion quality and it is due to extended mixing-controlled combustion phase with the existence of water droplet. At high temperature and pressure, water autodissociates to form hydrogen and oxygen molecules. Based on dissociation mechanism, hydrogen atom becomes extremely delocalized between oxygen atoms in water molecules. During dissociation process, heat is absorbed to release the bond of delocalized hydrogen and oxygen. The extended mixing-controlled combustion provides enough time for autodissociation, which only requires a microsecond time scale (Nienhuys et al. 2000). This means that the existence of more oxygen and hydrogen molecules during mixing-controlled combustion in HFCI engine with water injection generates more gross indicated work.

4.2.1.6 Indicated Thermal efficiency

Indicated thermal efficiency (ITE) is determined from the ratio of gross indicated work and total heat generated from combustion of fuels. Figure 4.6 illustrates the variation of ITE with injection timing for all cases at 2500 RPM and 2 kW of load. It can be seen that higher ITE for SOI less than 0˚CA for injection duration of 40˚CA as compared to 20˚CA injection duration.

During late water injection, injection duration of 40˚CA shows lower ITE as compared to injection duration of 20˚CA since longer water injection duration supplies

greater amount of water. Meaning that, region that content water droplet is even larger resulting in more heat absorption that lowers ITE. On the other hand, early water injection and duration of 40˚CA shows higher ITE as compared to duration of 20˚CA since early water injection provides more time for uniform distribution of water droplet.

Longer injection duration injects more water and it is expected that more water droplet will reach cylinder wall, cylinder and piston heads and start to absorb heat from this solid materials. This will help in its dissociation process that provides more oxygen in the combustion (Heywood, 1988). Dissociation of water not only produce more oxygen, it also produce hydrogen which in the end combusted as additional fuel. Higher ITE in late water injection as compared to DH operation proves this phenomenon.

CASE 1 to CASE 4 shows decrease in ITE ranging between 2% to 7%. CASE 5 until CASE 10 indicates increase in ITE ranging between 2% to 11% as compared to DA operation. This is due to water molecule auto-dissociates to form hydrogen and oxygen molecules at high temperature. More oxygen and hydrogen molecules in extended mixing- controlled combustion phase generates more ITE. It can be concluded that indicated thermal efficiency with water injection in HFCI engine is always higher than that of DA operation especially for water injection timing greater than 20°BTDC. This observation is in agreement with Mathur et al. and Boretti et al. (Boretti et al. 2011). They concluded that optimum amount of water induction increases thermal efficiency of diesel engine (Mathur et al.1993).

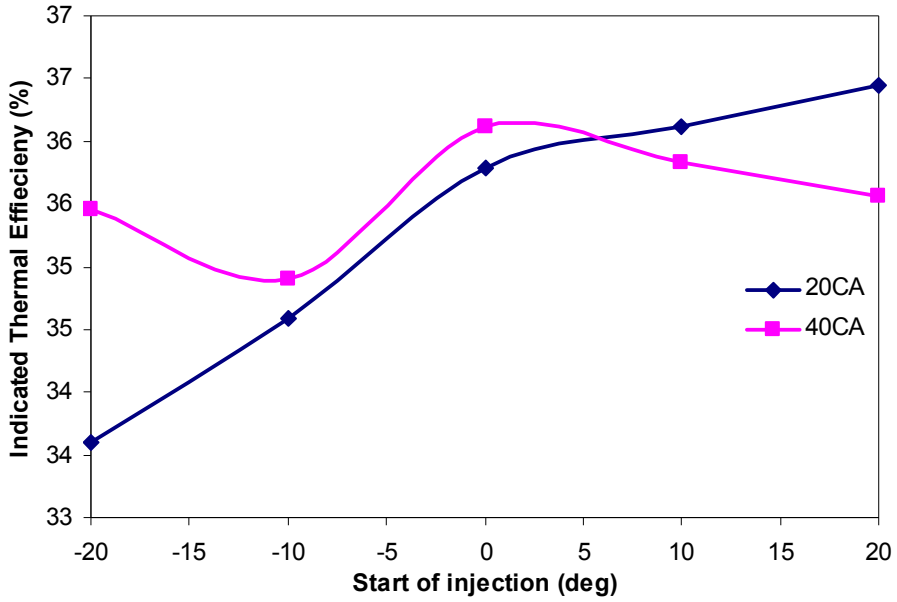

Figure 4.6 Variation of ITE with different injection timing at 2500 RPM and 2 kW load

4.2.1.7 Indicated Specific Energy Consumption

Indicated specific energy consumption (ISEC) measures how efficient an engine utilizing the chemical energy supplied from fuels in producing output work. The variation of ISEC and SOI at 2000 RPM is shown in Figure 4.7. It indicates that higher ISEC for injection duration of 20˚CA for SOI lower than 10˚ATDC in DHW operation. This trend is almost applicable throughout all speeds and cases.

Decrease in ISEC in the range of 2% to 11% in DHW operation as compared to DA operation can be associated with higher gross indicated work as discussed in the previous section. From the observation during the experiments, it was found out that the moment hydrogen gas was introduced into the combustion chamber, flow rate of diesel reduced drastically.

It can be concluded that lower indicated specific energy consumption for HFCI engine with hydrogen and water injection is due to higher peak pressure during hydrogen premixed combustion in the cylinder charge. This phenomenon causes lower

pressure gradient between diesel injection pressure and cylinder pressure which contributes towards lesser amount of diesel being injected.

Hountalas et al. have reported increase in specific fuel consumption with increasing amount of water inducted at intake manifold. This shows disagreement with the present work since the previous researcher only investigated performance and emissions of diesel alone operation without hydrogen injection. Higher peak pressure due to hydrogen combustion in the present study causes decrease in diesel fuel flow rate and it is then contributed towards lower ISEC (Hountalas et al. 2006).

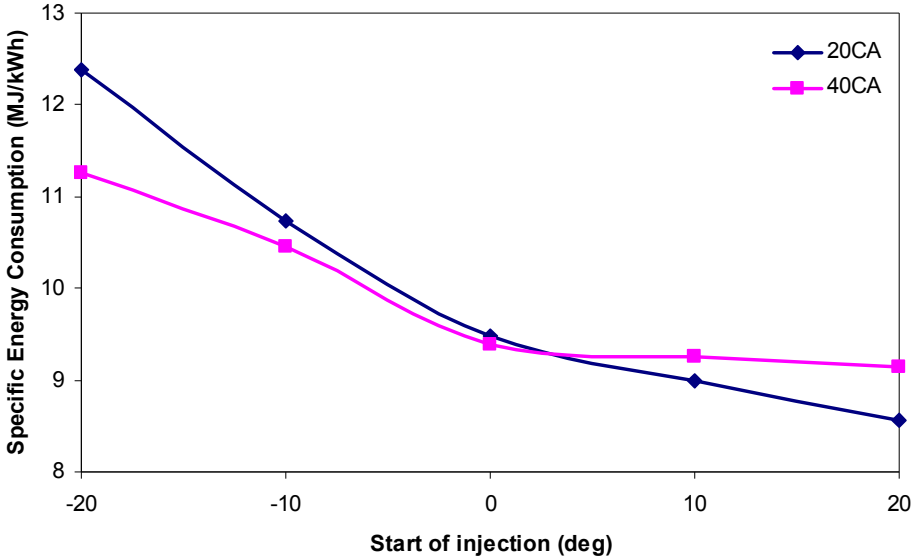

Figure 4.7 Variation of ISEC with injection timing at 2000 RPM

4.2.2 Emissions Analysis

This section discusses the results from experimental investigation on emission characteristics of HFCI engine. The selected figures that represents overall performance characteristics will be interpreted, explained and finally conclusion is drawn after each discussion. Appendix G shows figures on emission characteristics of HFCI engine with and without water injection at different speeds and loads.

4.2.2.1 Nitric Oxides

The variation of Nitric Oxides (NO_x) emission with engine speed at 2 kW load for different cases are shown in Figure 4.8. It shows that NO_x concentration decreases as speed increases until 2500 RPM, further increase in speed increases NO_x emissions. It can be seen that with timed port hydrogen injection duration of 0°CA to 20°CA reduces NO_x emission for all speed as compared to that of DA operation.

Based on Zeldovich mechanism, NO_x formation is dependent on peak combustion temperature, the effective volume of combustion zone, residence time and oxygen concentration (Lakshmanan et al. 2010). During combustion process, NO_x forms in both the flame front and the postflame charge. In diesel engine especially with DH operation, higher peak pressure combustion generates extremely thin (~ 0.1mm) flame reaction zone which shorten the residence time of combustion. This phenomena causes burned gases produced early in the combustion process are compressed to higher temperature than they reached immediately after combustion. Consequently, NO_x formations in the postflame gases are more dominant as compared to flame front NO_x. This proves that higher peak pressure cannot be associated with higher NO_x emissions (Heywood, 1988).

In DHW operation, the injection of water droplet causes lower in peak combustion temperature which contributes towards lower NO_x emissions. It can be observed that the lowest NO_x emission occurs in CASE 2 for speed range below 2500 RPM and CASE 9 for speed range greater than 2500 RPM. It can be observed that for all cases in DHW operations, NO_x emissions will always be lower than DA and DH operations in the range of 7% to 38% at all speeds.

Mathur et al., Subramanian and Hountalas et al. reported that continuous intake manifold water injection reduces NO level in diesel alone operation. This finding is

similar with the present work that shows the results obtained are in agreement with other researchers (Mathur et al. 1992, Subramanian, 2011, Hountalas et al. 2006).

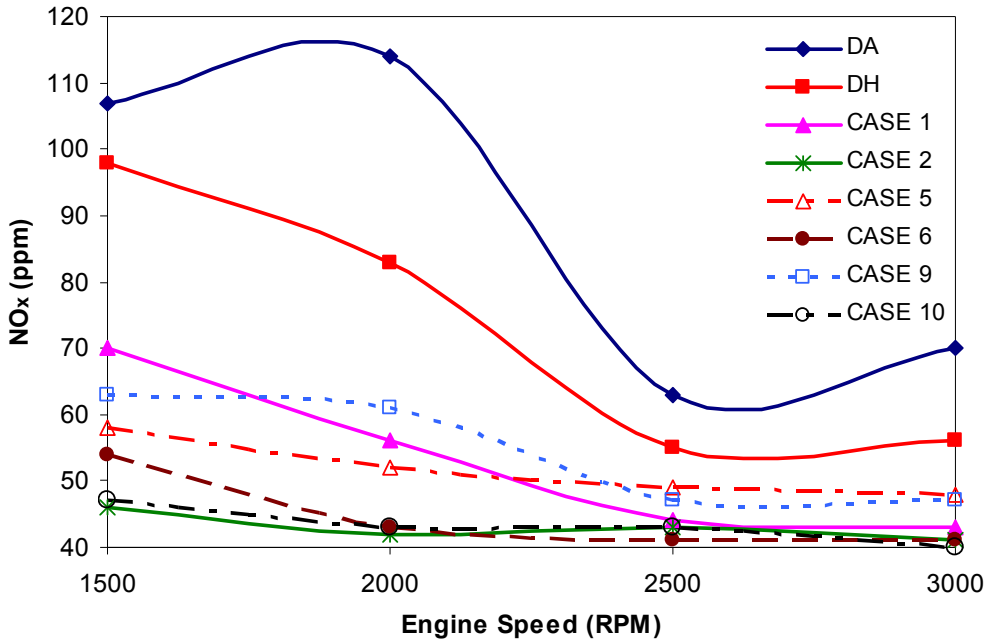

Figure 4.8 Variation of NO_x emission with engine speed at 2 kW load

Karim has stated that increasing the pilot fuel will contribute to increased NO_x formation due to the increase of combustion zone (Karim, 2003). This is also supported by Saravanan et al. and has stated that the lean mixture operation causes extended combustion process resulting in lower peak combustion temperature (Saravanan et al. 2010). In this research, lower diesel flow rate was observed as hydrogen introduced into the cylinder causes lower NO_x emission due to its lean and minimal amount of pilot diesel.

4.2.2.2 Carbon Monoxide

Figure 4.9 depicts the variation of carbon monoxide (CO) emissions with engine speed at 3 kW load for different cases. It shows that most of DHW operation has lower CO concentration at lower speed range as compared to DH and DA operations in the range of 5% to 30%. CASE 5 shows the lowest CO concentration for higher speed range.

CO emission in diesel engine is controlled by equivalence ratio of the cylinder charge. CO oxidation mechanism explains that the sequences of diesel oxidation reactions in air through hydrocarbon combustion mechanism produces higher CO concentration in the premixed flame zone. The CO formed during premixed and mixing-controlled combustion is then oxidized to carbon dioxide at slower rate depending on equivalence ratio. It is also highly dependent on the size of pilot diesel burning zones.

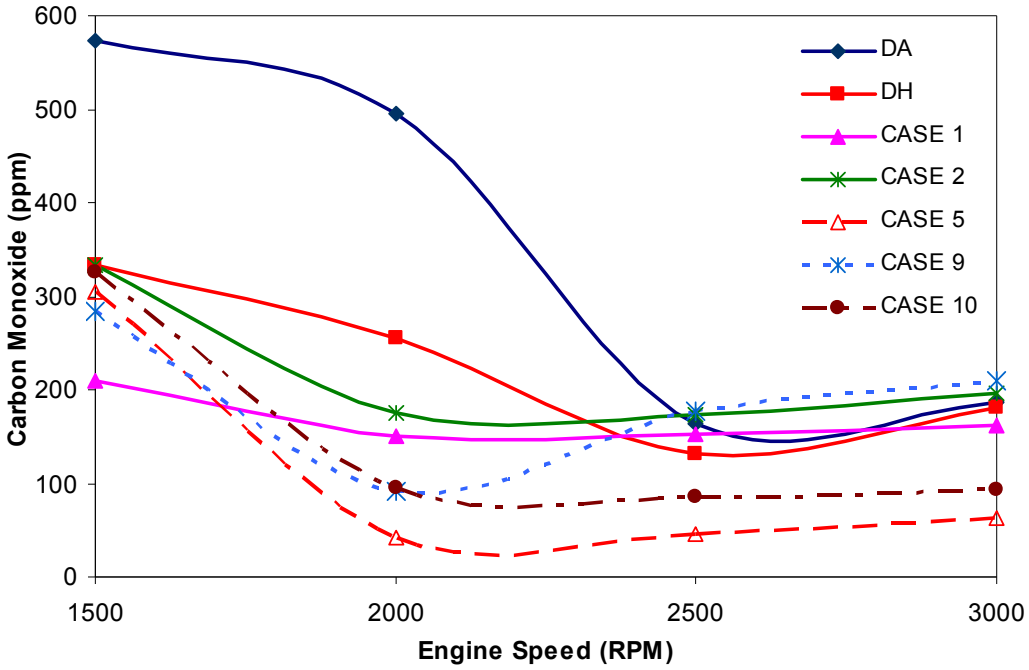

Figure 4.9 Variation of CO emission with engine speed at 3 kW load

In this research, diesel is the only source of carbon-fuel meaning that CO concentration is primarily dependent on amount of diesel fuel in the cylinder charge. Hence it is concluded that lower CO emissions in HFCI engine with water injection is due to lesser amount of pilot diesel fuel injection, since combustion of hydrogen gas resulting in lower pressure gradient between diesel injection pressure and cylinder pressure.

Tesfa et al. reported that higher water injection flow rate increases CO emissions in diesel alone operation (Tesfa et al. 2012). Their finding shows disagreement with the results from the present work. Their investigations were limited to continuous water injection on diesel alone operation but this study investigating diesel-hydrogen with timed port water injection. As discussed earlier, high pressure of hydrogen combustion limits amount of diesel injection resulting in lower CO emissions.

4.2.2.3 Carbon Dioxide

The variation of carbon dioxide (CO_2) emissions with speeds at 3kW of load is shown in Figure 4.10. It indicates that DH operation shows lower CO_2 emissions as compared to DA operation with reduction up to 2%. DHW operation shows higher CO_2 emissions as compared to DA operation in the range of 2% to 6%. CASE 5 showed the highest CO_2 emissions for all speed range. The highest CO_2 emissions can be associated with the lowest CO emission as discussed earlier. It shows a good agreement with CO oxidation mechanism where more CO oxides to form CO_2 especially for CASE 5.

Higher CO_2 emission in DHW operation is due to oxidation of CO to CO_2 since water produces more OH radical and oxygen in the cylinder charge. In addition, higher O_2 concentration also reacts with CO to form CO_2 emission. Higher OH radical concentration contributes towards higher kinetic reaction rate that also reacts with CO to form CO_2. This is proven by lower CO emission in DHW operation as discussed in the previous section (Pulkrabek, 2004).

Early water injection provides more time for O_2 formation generated from dissociation of water resulting in higher CO_2 emission. Additional O_2 concentration helps for more complete combustion of diesel to produce higher CO_2. Lower speed range provides more time for uniform distribution of water droplet which resulting in

poor mixing of diesel fuel and air. Poor mixing of diesel fuel and air causes less complete combustion resulting in lower CO_2 emission. This proves that lower speed range increases CO emission in DHW operation that was also discussed in the previous section.

Higher speed range generates more CO_2 as compared to DA operation. This is due to higher friction on the cylinder wall generates more heat dissipation to the adjacent water droplet. Dissociation of water droplet produces more oxygen concentration that will react with CO to form more CO_2 (Heywood, 1988).

Larbi et al. investigated the effect of water injection on marine diesel engine and concluded that water injection increases CO_2 emission even higher than diesel alone operation (Larbi et al. 2010). Alahmer et. al investigated the effect of emulsified diesel fuel on CO_2 and concluded that increase of CO_2 emission due to water existence which increases amount of oxygen molecule in the mixture (Alahmer et al. 2010). These investigations are in good agreement with this research.

It can be concluded that HFCI engine with water injection shows higher CO_2 concentration as compared to operations without water injection for most of the cases. One possible explanation of this phenomenon is the dissociation of CO_2 and water produces more O_2 at high temperature combustion zone and introduces more complete combustion of the charge at the beginning of expansion stroke. While piston moving down to BDC, pressure and temperature of the charge drops gradually and causes re-association of water and CO_2, which leads to increase of CO_2 emission.

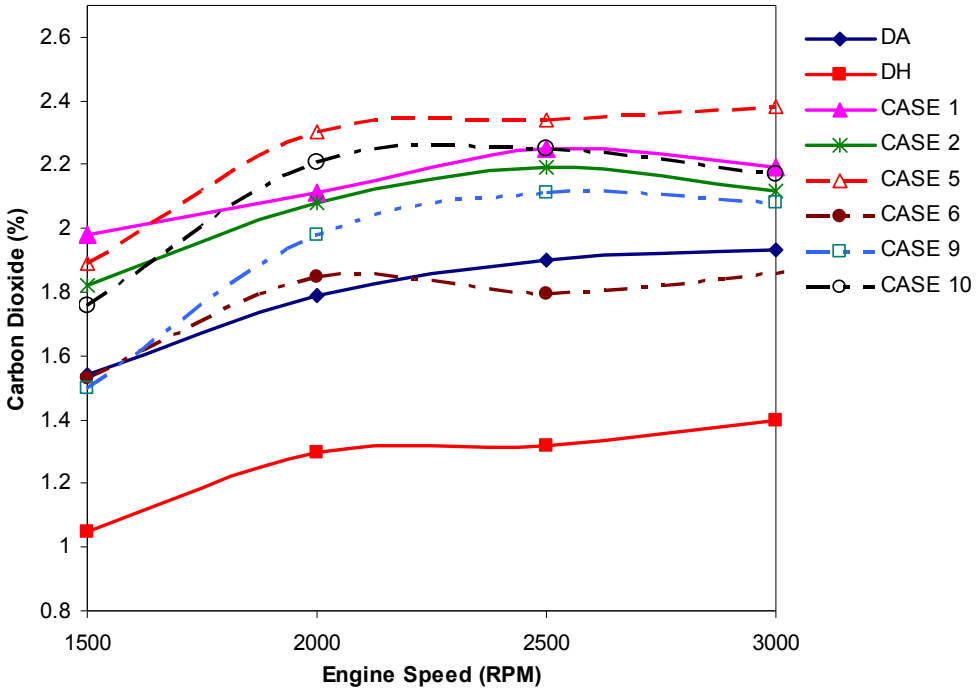

Figure 4.10 Variation of CO_2 emission with engine speed at 3 kW load

4.2.2.4 Sulfur Dioxide

Figure 4.11 presents the variation of sulfur dioxides (SO_2) emissions with speed at 1 kW load. It indicates DA operation produces highest SO_2 concentration for higher speed range and DH operation produces the lowest SO_2 concentration at low speed range. DHW operation shows decrease in SO_2 emissions in the range between 1 to 9 ppm as compared to DA operation. In DHW operation, CASE 6 produces the highest SO_2 concentration whereas, CASE 1 shows acceptable reduction of SO_2 emissions throughout the speed range.

In this research, SO_2 emissions are solely contributed from diesel pilot fuel since diesel contains sulfur element of approximately 0.1 % by weight meaning that levels of sulfate emissions depend on the amount of diesel injected into the cylinder. During combustion process, sulfur is oxidized to produce SO_2 which later combines with water to form sulfuric acid (H_2SO_4) aerosol (Heywood, 1988). Figure 4.11 also explains that SO_2 emissions can be controlled by lean mixture during DH operation and

lowering the mixing-controlled combustion temperature during DHW operations. This means that higher oxygen concentration in HFCI engine with water injection system contributes to higher SO_2 emissions as compared to operation without water injection.

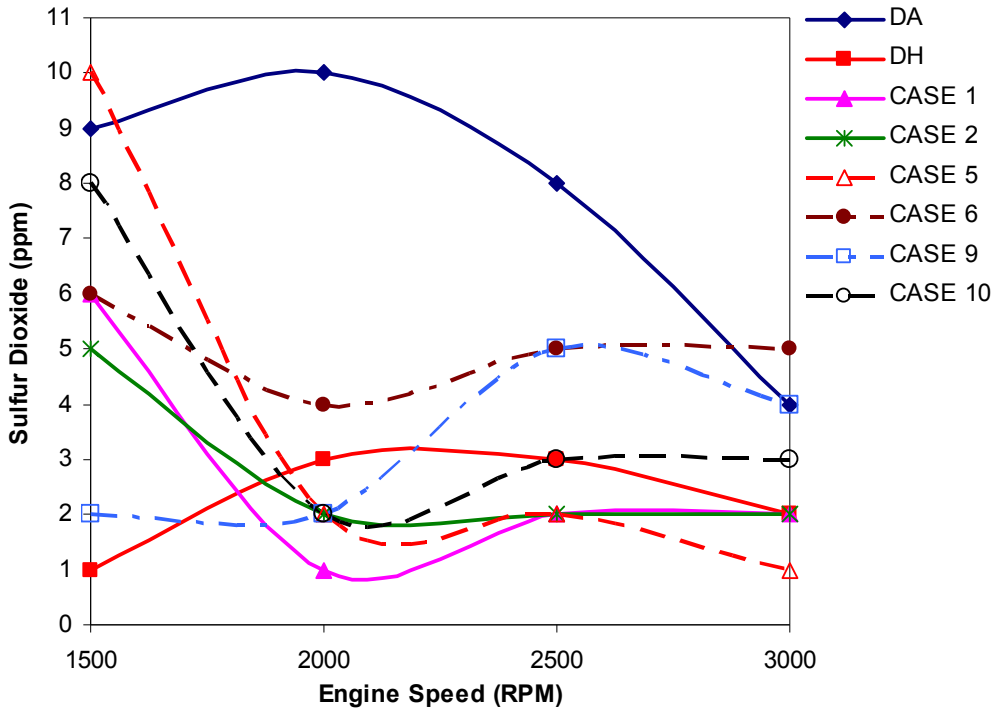

Figure 4.11 Variation of sulfur dioxides emission with engine speed

4.2.2.5 Hydrocarbon

The variation of hydrocarbon (HC) emissions with engine speed at 3 kW load is shown in Figure 4.12. DH operation has the lowest HC emissions for all speeds whereas CASE 2 is the highest. The optimum injection timing for lower HC emissions in DHW operation is CASE 9. HC emission for DA operation is always higher than that of DH operation but it is lower as compared to DHW operation in the range between 2 to 30 ppm.

One of the possible reasons of lower HC emissions for DH operation is due to hydrocarbon oxidation. High diffusivity of hydrogen reduces the flame-quenching rate in diesel engine causes wall-quench hydrocarbons apparently diffuse into the burning

charge following the quenching event. Flame quenching can be thought of as a two-stage process. The first step is the extinction of the flame at a short distance from the cylinder wall and determined by a balance between thermal conduction of heat from the hot flame zone to the wall and heat released in the reaction zone by the flame reactions. The second step is the post-quench diffusion and oxidation occurring on a time scale of one of a few milliseconds after quenching. The diffusion and oxidation process of hydrocarbon ultimately reduces the mass of wall quench hydrocarbons and leads to increase in other emissions such as CO (Westbrook et al, 1981).

In DHW operation, it is depicted that water droplet swirling and squishing within combustion chamber or piston bowl since extra volume of the combustion chamber generates lower pressure resulting in induction effect. Furthermore, bigger size and heavier water droplet limits its volatility and movement, which requires more time for uniformity of the mixture (Ferguson. 2001).

Figure 4.12 demonstrates higher HC emission from CASE 1 to CASE 5 due to early water injection timing promotes better uniformity of water droplet within cylinder charge that causes slower fuel combustion rate as a result of its cooling effect. This phenomenon also promotes poor mixing quality of fuel and air resulting in incomplete combustion and quenching of combustion reaction during mixing-controlled and late combustion phases. Higher HC emission is also due to cooling effect of water prolongs the evaporation of diesel sac volume until near to exhaust stroke. Another possible reason is that uniform water droplet generates minimal increase in pressure causes more fuel vapor being absorbed into the lubricant and pushed into the crevice volume during high-pressure combustion. It is then desorbed from the lubricant and pushed out from the crevice volume to low-pressure in-cylinder charge during exhaust stroke resulting in increase of HC emission (Pulkrabek, 2004).

It is concluded that marginal increase in HC emissions for operation of HFCI engine with water injection is due to slower mixing of fuel and pyrolysis products with the cylinder charge. This will contribute towards extremely rich mixture region and quenching of combustion reaction during mixing-controlled and late combustion phase. Odaka et al. investigated on continuous water injection with addition of EGR and reported increase in HC emission with increase of water injection and EGR (Odaka et al. 1991).

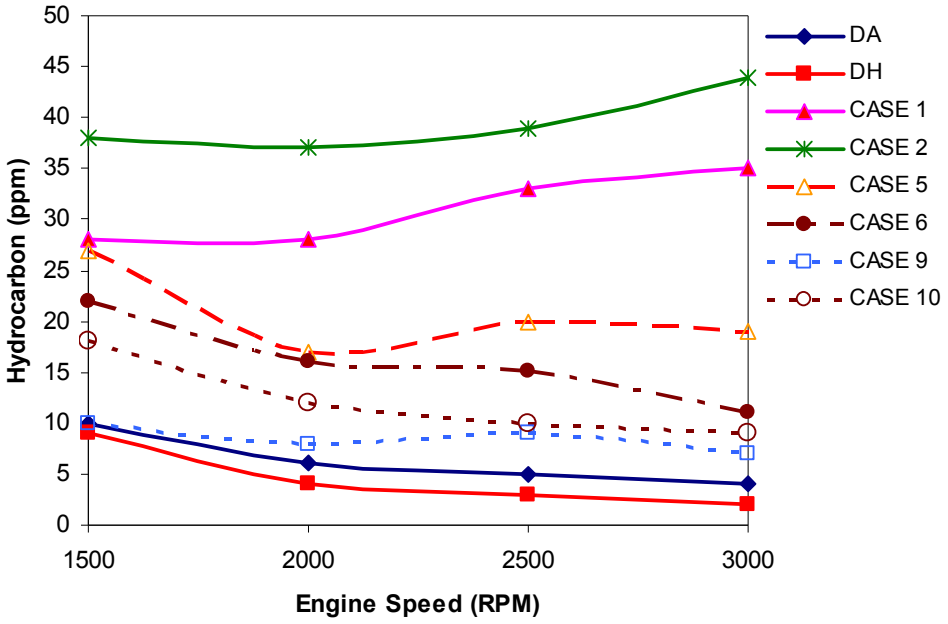

Figure 4.12 Variation of hydrocarbon emission with engine speed

4.2.2.6 Exhaust Gas Temperature

Figure 4.13 illustrates the variation of exhaust gas temperature (EGT) with engine speeds at 1 kW load. It shows that EGT increases as the speed increases for all operations and cases. It also indicates that DH operation produces the highest EGT as compared to DHW and DA operations. Higher EGT for DH operation is due to higher flame speed of hydrogen contributes towards faster combustion rate resulting in high combustion temperature in the cylinder charge.

CASE 3 to CASE 10 shows decrease in EGT ranging between 6 Kelvin to 23 Kelvin as compared to DA operation. Lower EGT in CASE 3 to CASE 10 is due to evaporative cooling effect of water droplet in combustion charge especially during premixed and mixing-controlled combustion phase absorbs the surrounding heat which lower the combustion temperature resulting in lower EGT.

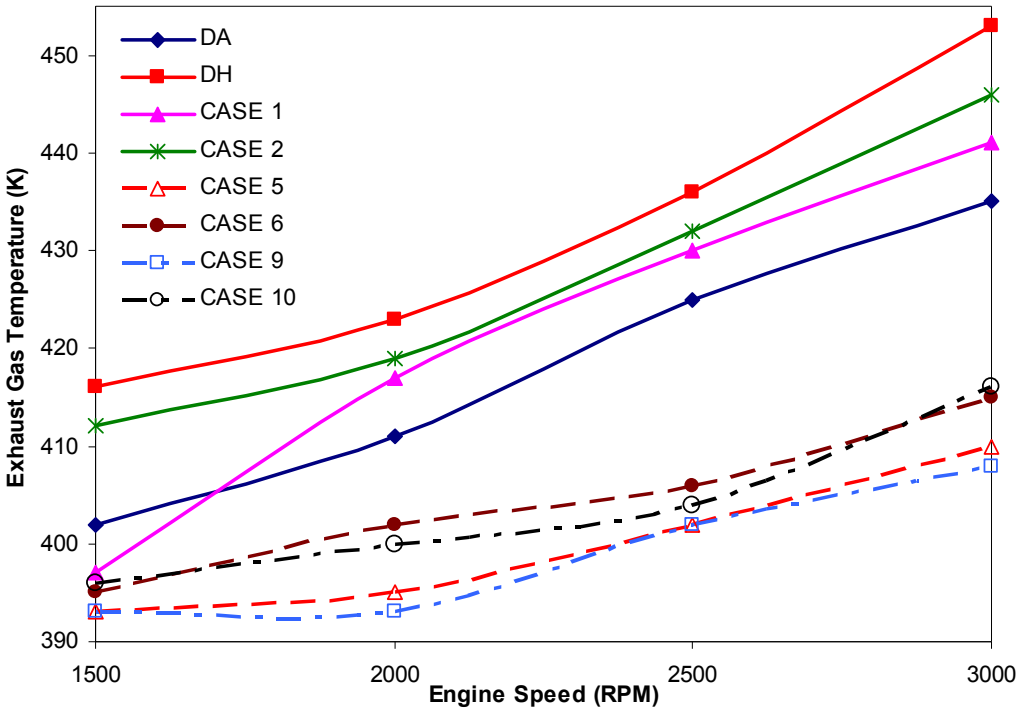

Figure 4.13 Variation of exhaust gas temperature with engine speed at 1 kW load

CASE 1 and 2 shows increase in EGT ranging between 5 Kelvin to 11 Kelvin throughout the speed range. Higher EGT in CASE 1 and 2 can be best interpreted that earlier water injection timing provides more time for water droplet to autodissociate during mixing-controlled and late combustion phases that forms hydrogen and oxygen molecules. The oxygen formed helps in hydrogen combustion and hence increases the cylinder charge temperature. Increase in cylinder charge temperature especially during late combustion phase contributes towards the increase in EGT.

Early water injection timing especially in CASE 1 promotes more homogeneous mixture of water droplet and cylinder charge resulting in higher oxygen concentration that helps combustion of hydrogen gaseous fuel which happens in slower rate due to cooling effect of water. Homogeneous water mixture enhances water droplet entrainment inside the combustion zones during mixing-controlled and late combustion phases. Dissociation of water causes lower cylinder charge temperature and consequently reassociation process takes place to release heat especially during exhaust stroke increases EGT in early water injection (Ganesan, 2004). Lower speed range especially at 1500RPM provides more time for water droplet to evaporate and cools its surroundings during late combustion phase and exhaust stroke resulting in lower EGT.

Figures G.26 to G.30 in Appendix G demonstrates the variation of EGT with engine speeds at 2 kW load. It also shows that EGT increases as engine speed increase especially in CASE 7 since higher speed reduces engine cyclic variation time for instance, 0.04s for engine speed of 3000RPM. In fact, convection and radiation heat transfer coefficients are independent of engine speed. Thus, rate of heat transfer during combustion and power stroke is therefore constant. Due to less cyclic variation time at higher speed, less heat transfer per cycle occurs. Whereas at higher speed ranges, more cycles occurs per unit time meaning that more heat transfer per unit time. Furthermore, more friction to the wall generates extra heat per unit time (Pulkrabek, 2004). These parameters contribute towards higher EGT at higher speed range.

Figure 4.14 portrays the variation of exhaust gas temperature with engine speed at 3 kW load for different cases. The exhaust gas temperature increases with increase in engine speeds. It can be seen that DH operation shows the highest EGT as compared to that of DA for all speeds. It can also be observed that EGT in DHW operation will always be lower than that of DH operation at all speeds. CASE 3 and CASE 4 shows

higher EGT for lower speed range within DHW operation as compared to DA operation.

At 3 kW load, it is found that EGT for DA and DH operations increase in the range of 55 Kelvin to 65 Kelvin as compared to 1 kW load operation. The increase in EGT for DH operation is due to the increase in peak cylinder temperature and peak pressure, which is due to instantaneous combustion that takes place in hydrogen combustion.

In general, CASE 1 until CASE 4 shows increase of EGT as compared to DA operation. Another possible reason is due to water droplet premixed with the intake air and progressively entrained inside the combustion zones during mixing-controlled and late combustion phases. The cooling effect of water causes lower cylinder charge temperature and consequently reassociation process takes place to release the heat and thus, increasing EGT.

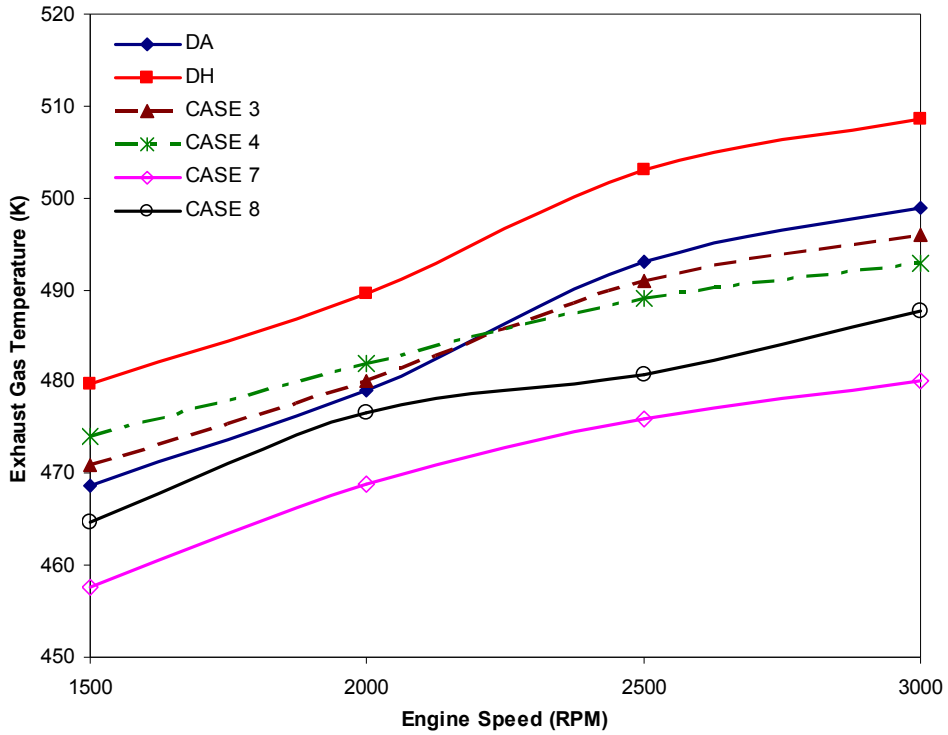

Figure 4.14 Variation of exhaust gas temperature with engine speed at 3 kW load

CASE 5 until CASE 10 shows lower EGT as compared to DA and DH operations. It can be concluded that late injection timing of water lower the heat release rate of the cylinder charge and consequently decreasing the local charge temperature which contributes towards lower EGT. Another possible reason is due to less time provided for better mixing of water droplet and cylinder charge causes less homogeneous mixture. The swirling and squishing water droplet is accumulated within centerline of the cylinder and piston bowl (combustion chamber) due to heavier droplet and higher inertia as compared to fine diesel fuel droplet. Flame front from local side regions propagates to the centerline while compressing and heating the accumulated water droplet during mixing-controlled and late combustion phases. Some water droplet left unburned and pushed out as exhaust gas (Heywood, 1988). This is happened during the conduct of experiment where liquid water was found trapped inside exhaust gas filter.

4.3 Numerical Investigation

The results of numerical investigation from computational simulation of the developed combustion mathematical models for nine (9) combustion products are presented, analyzed and conclusions arrived at in this section. The effect of equivalence ratio and combustion temperature on emission characteristics of HFCI engine with and without water addition will also be discussed and compared.

4.3.1 Effect of Equivalence Ratio on Emissions

The discussion in this section focuses on the effect of equivalence ratio on emission characteristics of HFCI combustion with and without water addition. Nine different types of emissions in terms of mole fraction have shown changes with the increment of

equivalence ratios. In this research, the range of equivalence ratio is limited from 0.20 until 1.60 since this is known as the working equivalence ratios for experimental work.

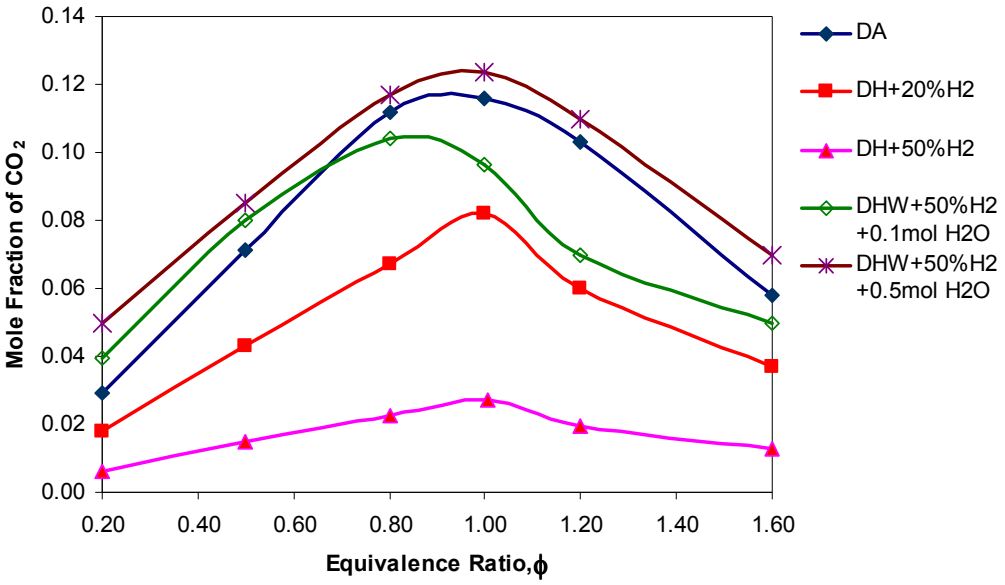

Figure 4.15 Mole fractions of CO_2 with equivalence ratio

The variation of mole fractions of CO_2 with equivalence ratio is shown in Figure 4.15. As the equivalence ratio increases from 0.2 to 1.0, mole fraction of CO_2 also increases and the highest value occurs at equivalence ratio of 1.0. For instance, the highest value of CO_2 is indicated as 0.124 in DHW operation at equivalence ratio of 1.0 or stoichiometric. It shows that during stoichiometric combustion, fuel burns completely and the only products are carbon dioxide and water (Pulkrabek, 2004). However, when the equivalence ratio is greater than unity, mole fractions of CO_2 shows the decreasing in value. Figure 4.15 also shows mole fraction of CO_2 decreases as the percentage of hydrogen substitution increases, it also decreases when amount of water injected decreases as compared to that of diesel alone.

For higher content of water injected, it causes mole fractions of CO_2 to increase. For rich combustion (ϕ=1.2), mole fractions of CO_2 is reduced in the range of 50% to 90% for different amount of H_2 substitution as compared to diesel alone. As for

equivalence ratio equals to 1.6 (ϕ=1.6), mole fractions of CO_2 decreased by 13% as 1mol of water injected and increased by 20% as 5 mol of water injected. Combustion of hydrogen produces mainly water due to the absence of carbon atoms and does not form CO_2 composition.

It can be concluded that mole fraction of CO_2 decreases with the increment of hydrogen substitution and increases as more water is injected into the cylinder. Similar results were obtained for lean combustion (ϕ=0.8), mole fraction of CO_2 for lean combustion is reduced in the range of 40% to 90% with different amount of H_2 substitution and approximately 10% with increment in water injected as compared to diesel alone.

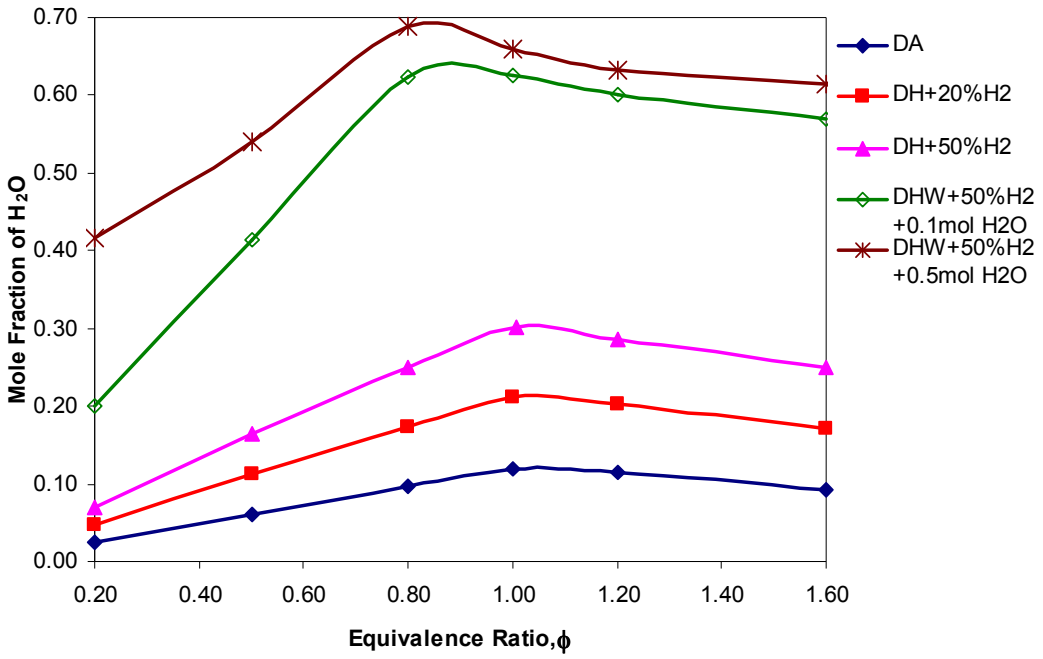

Figure 4.16 Mole fractions of H_2O with equivalence ratio

The relationship between H_2O emissions and equivalence ratio is depicted in Figure 4.16. It is indicated that the highest emissions throughout percentage of hydrogen substitution and amount of water injected occurred when equivalence ratio is near to unity (stoichiometric combustion). It can be concluded that the increase in

amount of water injected and hydrogen substitution greatly increases the H_2O emissions. Consequently, the existence of H_2O in combustion products catalyzes the process of dissociation that reduces the emissions temperature.

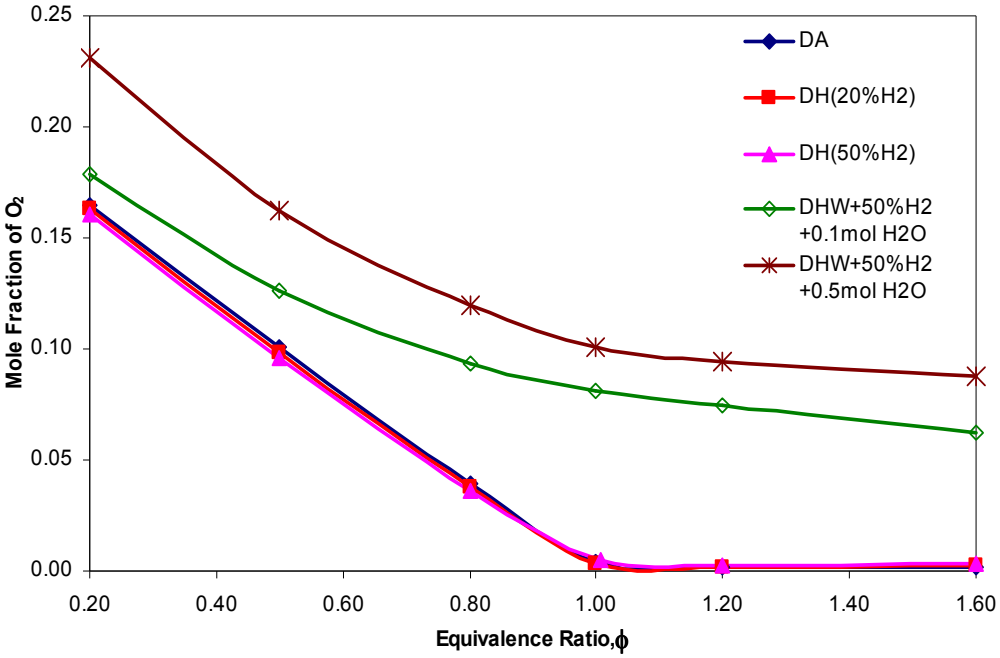

Figure 4.17 Mole fractions of O_2 with equivalence ratio

The variation of O_2 emissions with equivalence ratios is indicated in Figure 4.17. It shows insignificant changes of these emissions ranging in between 5% to 10% as the percentage of hydrogen substitution increases as compared to that of diesel alone. Equilibrium concentrations of those emissions are rather flat and peak in the lean region falling rapidly in the rich region. Similar trends are also observed when water is injected into the cylinder, it also shows that increased amount of water injected increases O_2 concentration. Generally, with the increase in percentage of hydrogen substitution and water injection amount, mole fractions or concentration of O_2 emissions slightly reduced.

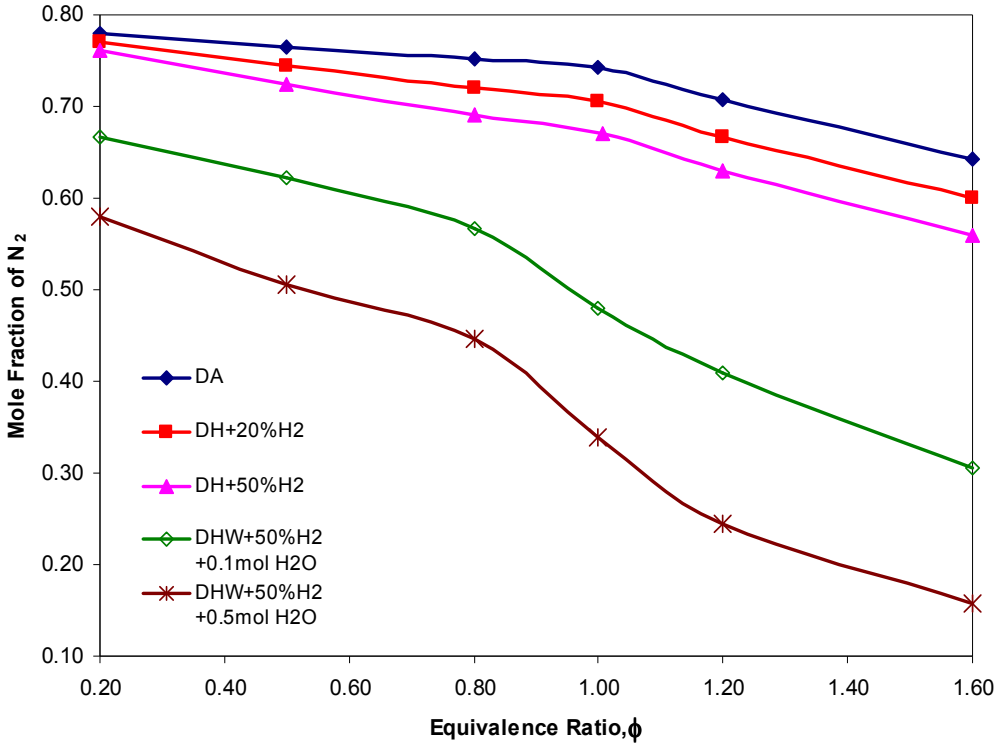

Figure 4.18 Mole fractions of N_2 with equivalence ratio

Figure 4.18 shows the variation of mole fractions of N_2 with equivalence ratio, as the percentage of hydrogen substitution and water injection increases, N_2 emissions decreases. It can be noted that as equivalence ratio increases, mole fractions of N_2 and atom N decreases especially during rich combustion. As the percentage of hydrogen substitution increases, mole fraction of N_2 decreases in the range of 2% to 20%. It is noticed that as the amount of water injected increases, N_2 concentration decreases in the range of 20% to 70% as compared to that of DA operation.

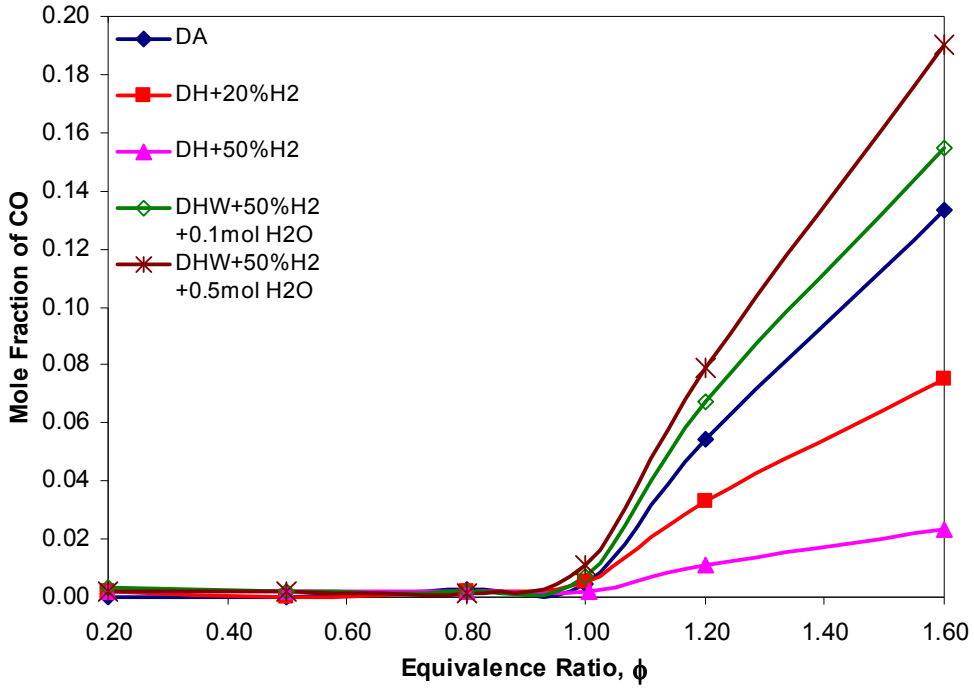

Figure 4.19 Mole fractions of CO with equivalence ratio

Figure 4.19 shows that mole fraction of CO decreases when the percentage of hydrogen substitution increases and amount of water injection decreases. CO is the minor species in the lean combustion and as the mixture gets richer the mole fractions of CO increases due to incomplete combustion of carbon. For example, during rich combustion (ϕ=1.2) mole fractions of CO is reduced in the range of 30% to 90% for different amount of hydrogen substitution as compared to diesel alone. It shows increase in values in the range of 20% to 40% as water is added instead. It is concluded that for lean combustion, there are no significant changes in mole fractions of CO concentration at all equivalence ratios either for DH or DHW operations.

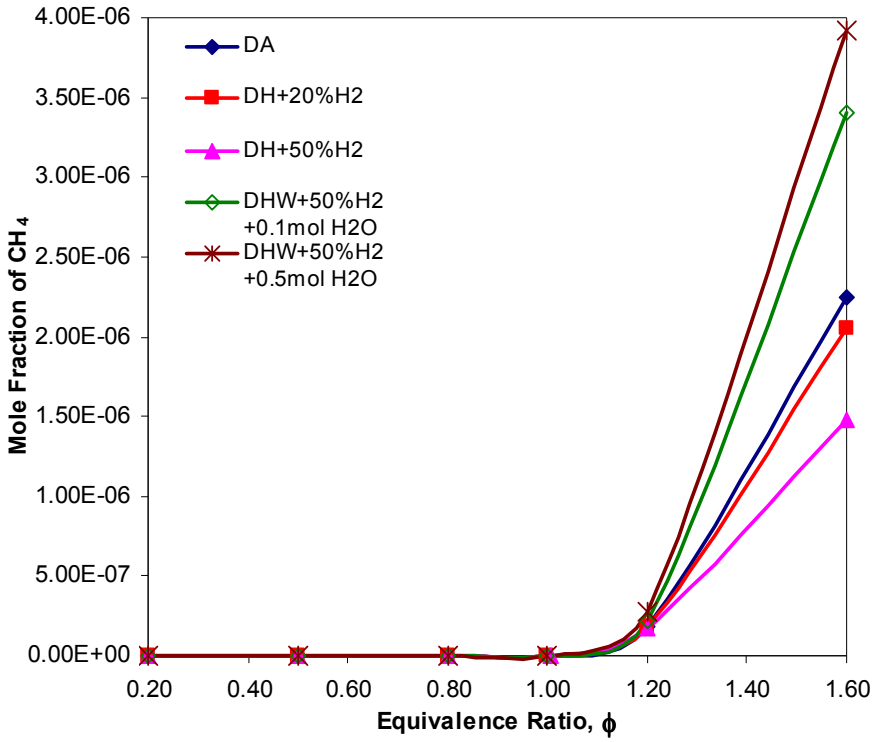

Figure 4.20 Mole fractions of CH_4 with equivalence ratio

Figure 4.20 shows the variation of CH_4 concentration with equivalence ratio. Hydrocarbon emissions such as CH_4 is produced from the presence of unburned fuel in the exhaust of an engine. Hydrocarbon emissions are the greatest during engine start-up and warm-up, due to decreased fuel vaporization and oxidation (Heywood, 1988). As the equivalence ratio increases greater than unity, the emissions of hydrocarbon also increases for DA, DH and DHW operations. This is due to insufficient air to react with the diesel fuel that remains in the exhaust. The molecule structure of the remaining diesel fuel will be altered by chemical reactions within the hot cylinder engine and hence increases the hydrocarbon emissions (Chen et al. 1988).

Hence it is concluded that the increase in hydrogen substitution greatly decreases hydrocarbon and solid carbon material in the exhaust emissions. On the other hand, increase in water addition increases CH_4 concentration. This is due to slower fuel

mixing in the cylinder charge contributes towards richer mixture region and thus increases CH_4 emission.

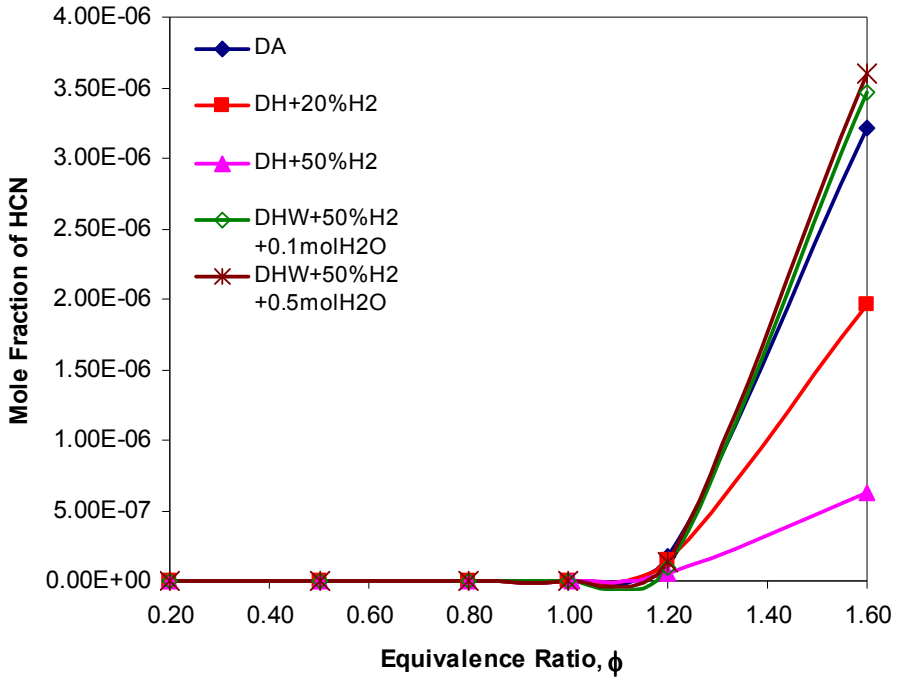

Figure 4.21 Mole fractions of HCN with equivalence ratio

Figure 4.21 shows the variation of HCN emission with equivalence ratio. HCN concentration is classified as hydrocarbon emissions in exhaust gas since it contains carbon and hydrogen bonds. It shows the similar trend with Figure 4.20. It is noticed that as the equivalence ratio increases greater than unity, the emissions of hydrocarbon also increases. Hence it can be concluded that increase in water addition or decrease in hydrogen substitutions, increases HCN concentration.

The variation of NO concentration with equivalvence ratio is indicated in Figure 4.22. It shows that during rich combustion there are insignificant changes of NO emission as amounts of hydrogen substitution increases as compared to that of DA operations. For instance, increase in water addition decreases NO emission greatly. Equilibrium concentrations of NO emission are rather flat in rich region and peak in the lean region falling rapidly in the rich region for DA, DH and DHW operations.

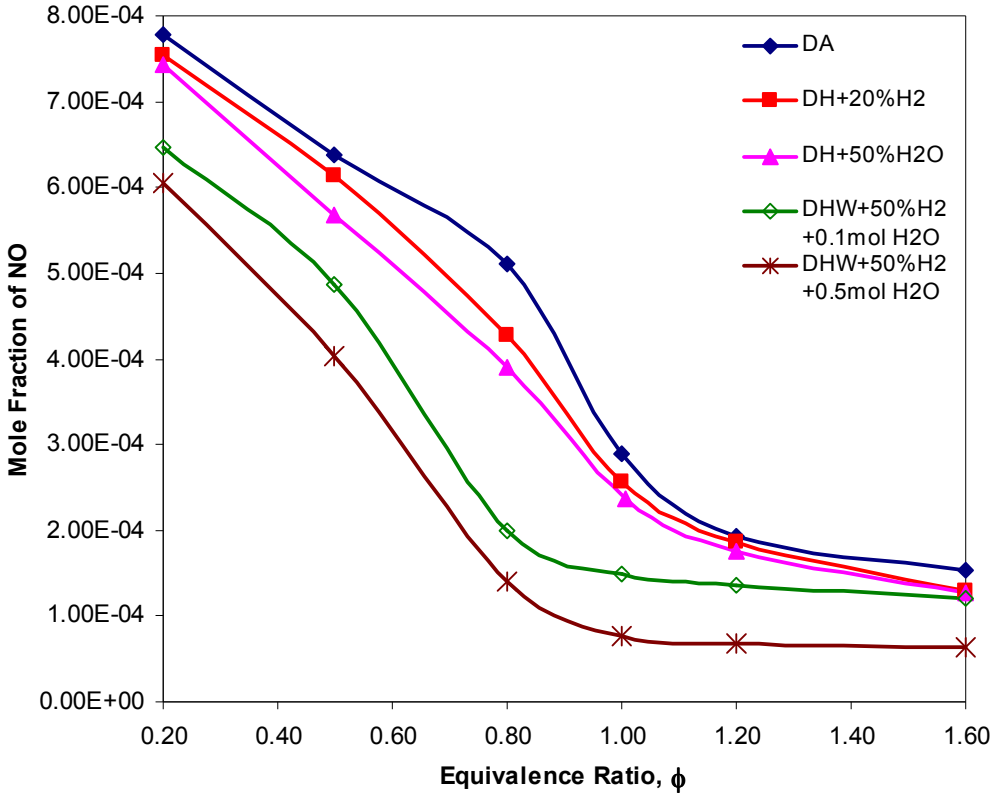

Figure 4.22 Mole fractions of NO with equivalence ratio

The reduction of NO emission can be achieved as the reaction rate of the extended Zeldovich mechanism is reduced. Somehow, the reaction rate for the mechanism depends on the concentration of N_2 and O_2 emissions. It is concluded that increase in percentage of hydrogen substitution and water addition, mole fractions or concentration of these emissions reduced and thus reduces NO emissions. As shown, nitric oxides emissions are maximized when mixtures are slightly lean. The increased temperatures favor nitric oxide formation and burned gas temperatures are maximized with mixtures that are rich. On the other hand, there is little excess of oxygen in rich mixtures to dissociate and attach to nitrogen atoms to form nitric oxide. The interplay between these two effects results in maximum nitric oxides occurring in lean mixtures, where there is an excess of oxygen atoms to react with the nitrogen atoms to form nitric oxide (Nader et al. 1998).

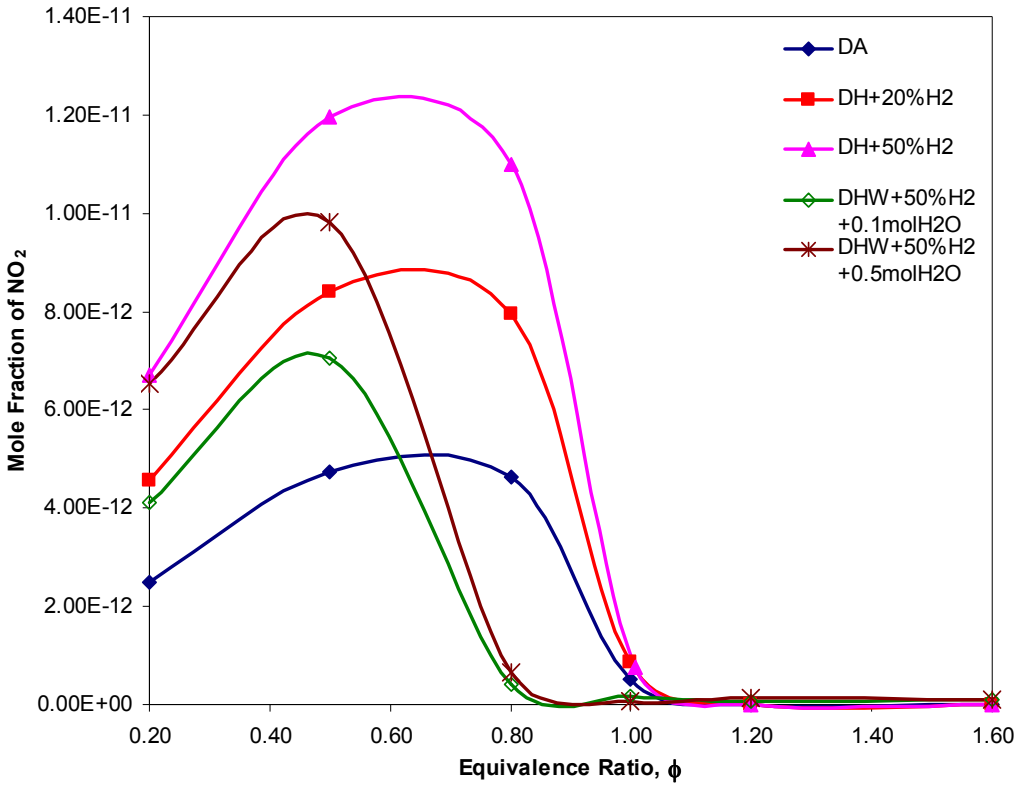

Figure 4.23 Mole fractions of NO_2 with equivalence ratio

Figure 4.23 shows the variation of NO_2 concentration with equivalence ratio. It indicated that NO_2 emission increases as the amount of hydrogen and water injected increases during lean combustion, further increase in equivalence ratio reduces the concentration of NO_2. Increase in NO_2 concentration during lean combustion in DH operation is due to increase in thermal NO_x. Higher combustion temperature with the existence of higher amount of hydrogen substitution increases formation of NO and NO_2 emissions. This means that cooling effect of water in combustion especially during premixed and mixing-controlled combustions reduces the combustion temperature and hence reduces concentration of NO_2. In fact, NO_2 contributes approximately 10% of NO_x in the combustion engine, meaning that its variation does not reflect extremely on the total amount of NO_x emitted by an engine (Heywood, 1988).

4.3.2 Effect of Temperature on Emissions

This section discusses the effect of combustion temperature on emission characteristics of HFCI combustion with and without water addition. Nine (9) types of emissions have shown changes with the increase in combustion temperature. In this study, the range of combustion temperature is limited from 1500K to 3500K.

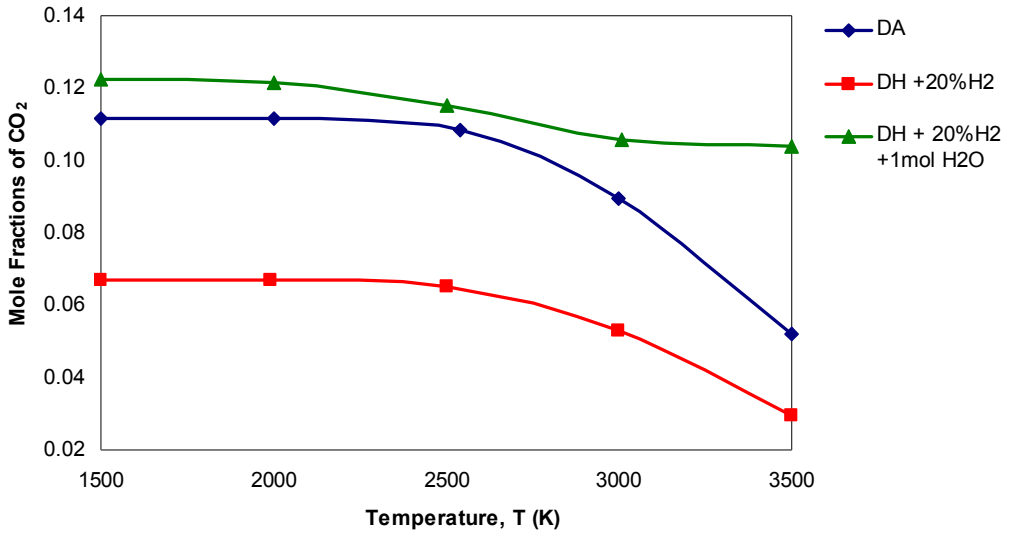

Figure 4.24 Mole fractions of CO_2 with temperature

The variation of mole fractions of CO_2 with combustion temperature is shown in Figure 4.24. It shows the maximum CO_2 concentration is reached in DHW operations whereas its lowest concentration occurred during DH operation. CO_2 is one of the major species present at low combustion temperature (Schafer, 1995). As the combustion temperature increases, mole fractions of CO_2 decreases as a result from dissociation process of CO_2 to form CO and O_2 species in significant amount (Glassman, 2008). It is concluded that lower combustion temperature during DHW operation increases CO_2 concentration and increased temperature in DH operation decreases CO_2 emission.

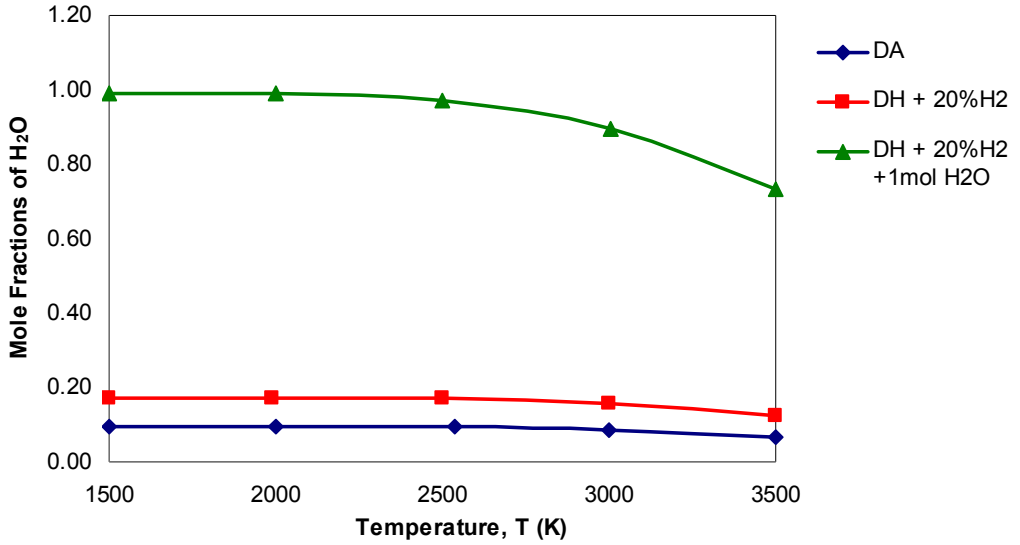

Figure 4.25 Mole fractions of H_2O with temperature

Figure 4.25 shows that increase in combustion temperature decreases H_2O concentration. There were no changes of H_2O emission for all equivalence ratios until the combustion temperature reaches 3000K then it starts to decrease. The highest emission occurs when equivalence ratio equals to unity (stoichiometric combustion). The existence of H_2O at high temperature catalyzing the process of dissociation which forms additional H_2 will be one of the reasons in the increase of H_2 emission as discussed earlier. Hence it can be concluded that the addition of water will definitely increase mole fractions of H_2O since water prolongs the combustion duration and consequently, non-reacted water during mixing-controlled combustion will be released as combustion products.

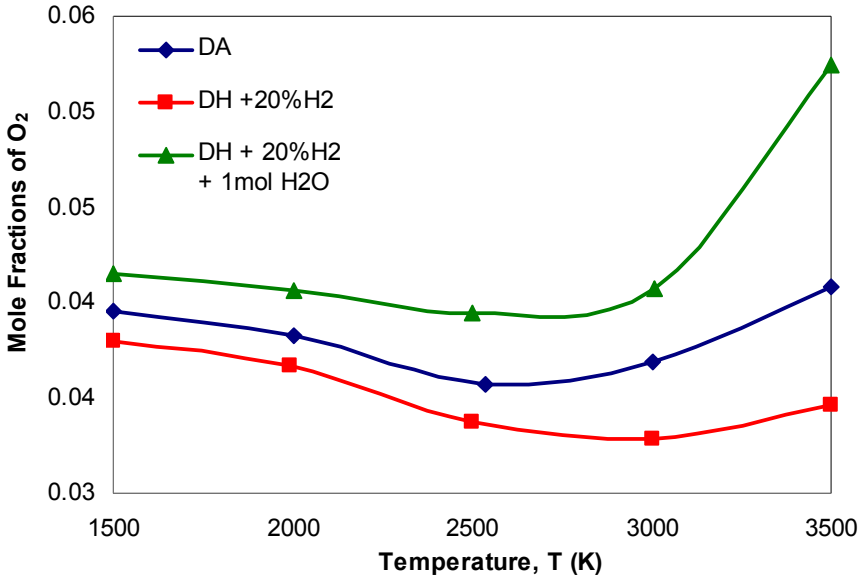

Figure 4.26 Mole fractions of O_2 with temperature

The variation of O_2 emission with combustion temperature is shown in Figure 4.26. In low temperature region, mole fraction of O_2 decreases as combustion temperature increases. As temperature reached 3000K, mole fraction of O_2 increases while the highest amount of O_2 occurs when the combustion temperature reached 3500K. It is observed that during low temperature combustion in DA and DH operations, there were insignificant changes of O_2 emission at all combustion temperatures. The reason that, there is a greater amount of dissociation on the lean side is because the dissociation of one mole of CO_2 results in one mole of CO but only half mole of O_2. Thus lean mixtures can accommodate more O_2 from dissociation than that of the rich mixtures (Chung, 2004). Higher temperature dissociates H_2O and CO_2 greatly and this is shown when temperature is greater than 3000K.

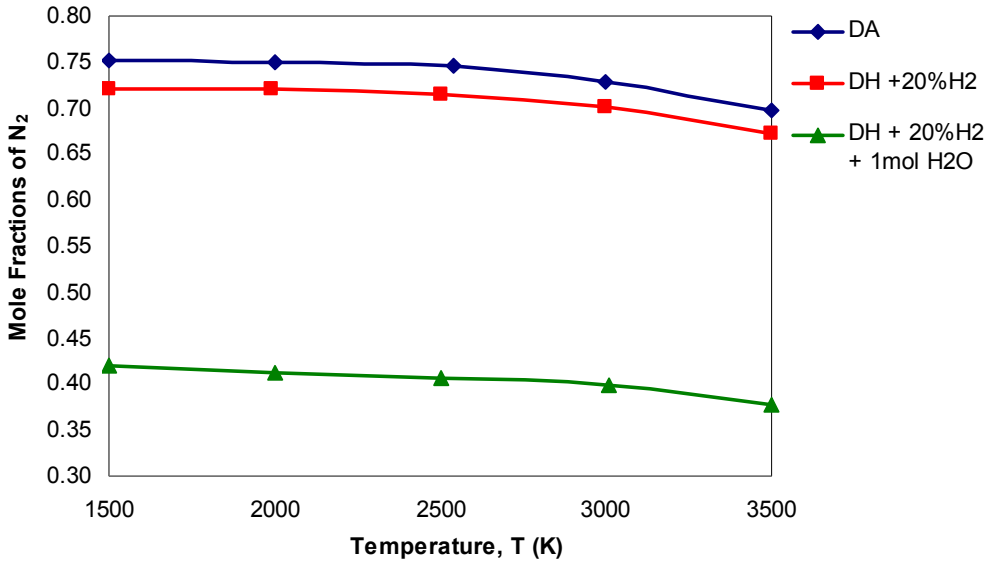

Figure 4.27 Mole fractions of N_2 with temperature

Figure 4.27 shows the variation of mole fractions of N_2 with combustion temperature. It can be noted that as combustion temperature increases, mole fractions of N_2 decreases as the same trends shown for DA, DH and DHW operations . The highest emission of N_2 is shown during low temperature combustions especially for DA operation. Increased combustion temperature increases rate of NO_x formation and consequently lowered N_2 concentration. This means that water addition reduces N_2 emission since autodissociation of water produces excess oxygen and then attached to N_2 to form oxides of nitrogen.

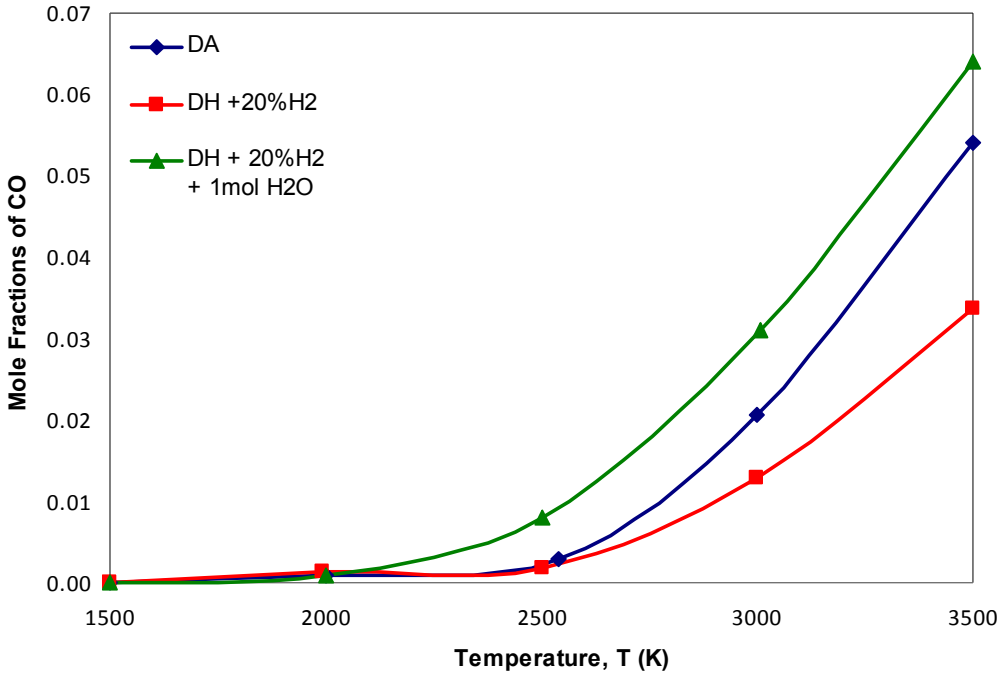

Figure 4.28 Mole fractions of CO with temperature

As shown in Figure 4.28, increase in combustion temperature increases CO emission for all DA, DH and DHW operations. Mole fractions of CO showed a remarkable high value when temperatures greater than 2500K. CO is the minor species in the lean combustion and as the mixture gets richer mole fractions of CO increases due to incomplete combustion of carbon. It is concluded that as the combustion temperature increases CO_2 dissociates to form CO and hence, mole fraction of CO increases as temperature increases (William, 1985).

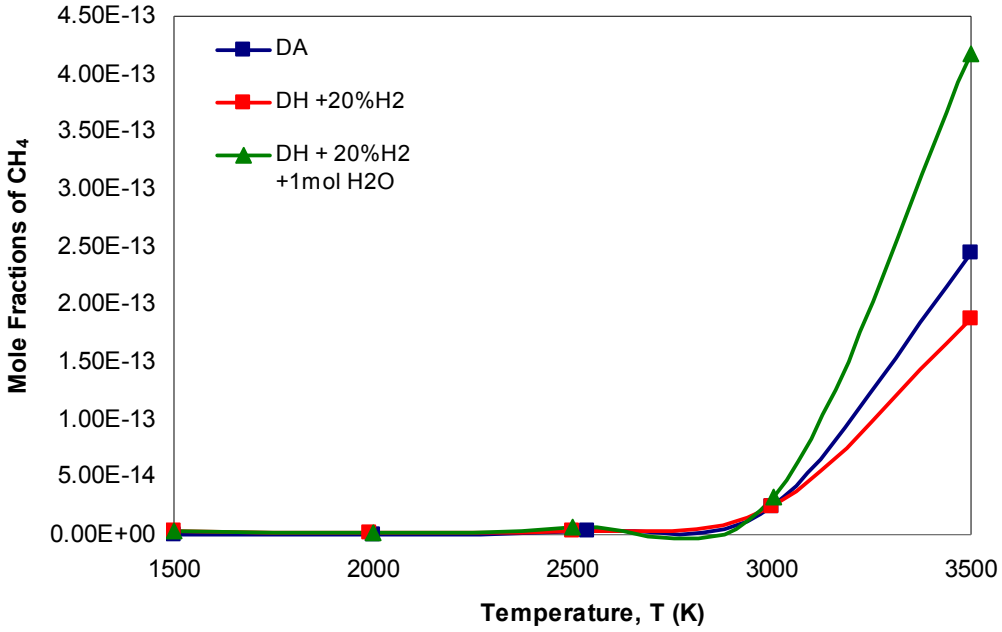

Figure 4.29 Mole fractions of CH_4 with temperature

Figure 4.29 shows CH_4 emission versus combustion temperature. With combustion temperature increases, mole fractions of CH_4 will decrease with respect to the increase in temperature especially after 3000K. It can be seen that insignificant amount of CH_4 concentration during low temperature combustion regardless of any operation.

CH_4 emission is classified as gaseous fuel, during lean mixture these fuels were burnt due to the presence of excess air in the mixture (Pulkrabek, 2004). For rich mixture, late combustion of CH_4 emission occurs when only at high temperature. It is concluded that higher concentration of CH_4 is seen in DHW operation due to prolonged combustion duration and cooling effect of water suppressed the reaction of diesel fuel and resulted in higher CH_4 emission.

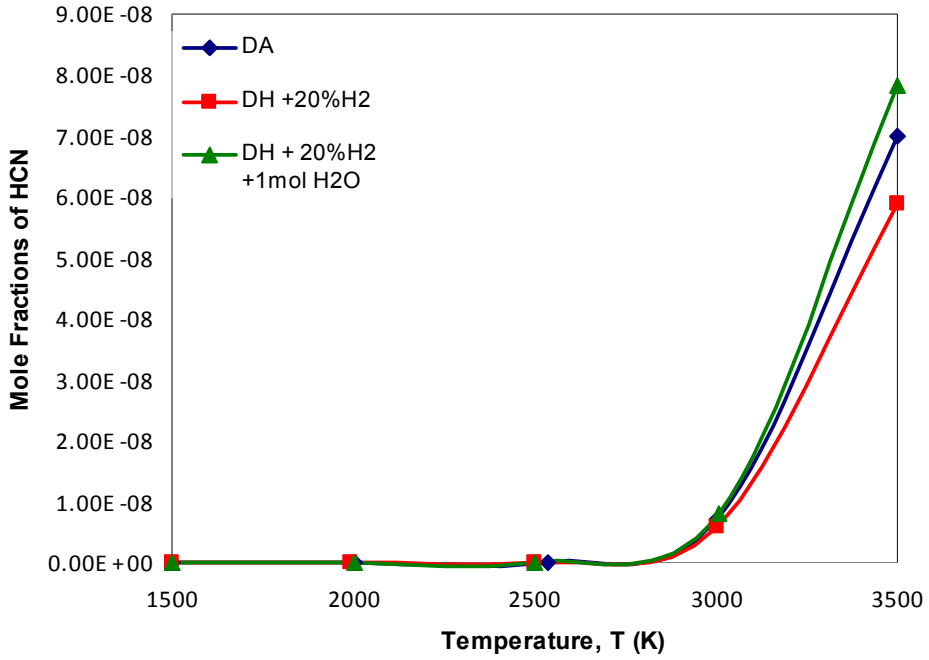

Figure 4.30 Mole fractions of HCN with temperature

Figure 4.30 shows hydrocarbon emission of HCN versus combustion temperature. When combustion temperature increases, mole fractions of HCN will also increase specifically when temperatures are greater than 3000K. It can also be seen that there were insignificant changes of this emission with respect to combustion temperature before 3000K.

It is concluded that as water is added in diesel combustion, the emission of HCN increases when temperature is greater than 3000K. This is due to quenching of combustion reaction during mixing-controlled and late combustion phase which causes insufficient time for air to react with the diesel fuel. The molecules structure of the remaining diesel fuel will be altered by chemical reactions within the hot cylinder engine and hence increases the hydrocarbon emission (Heywood, 1988).

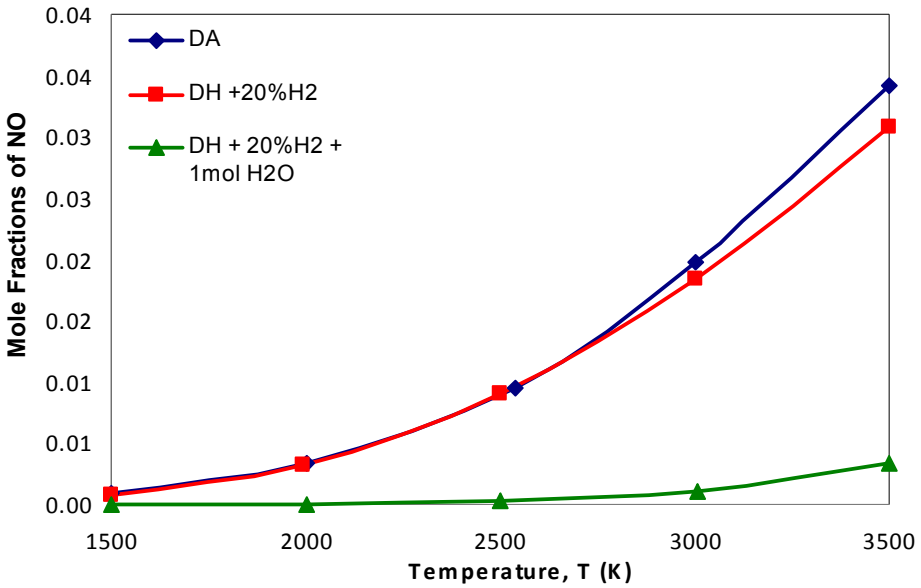

Figure 4.31 Mole fractions of NO with temperature

Figure 4.31 shows the variation of NO emission with combustion temperature. The increase of NO emission occurs as the reaction of the extended Zeldovich mechanism is increased. With combustion temperature increases, mole fractions or concentration of NO emission increases rapidly when temperatures are greater than 2500K. As shown, mole fractions of NO for both DA and DH operations are maximized since increased temperatures favors NO formation.

Generally, the formation of NO is highly dependent on in-cylinder temperatures, oxygen concentration and residence time for the reaction to take place (Andrea, 2004). It is proven that during lean combustion, the formation of NO increases with increasing temperature since excess air during combustion catalyzes the formation of NO. Hence it can be concluded that suppressed combustion temperature due to evaporative cooling of water contributes towards lower NO emission in DHW operation.

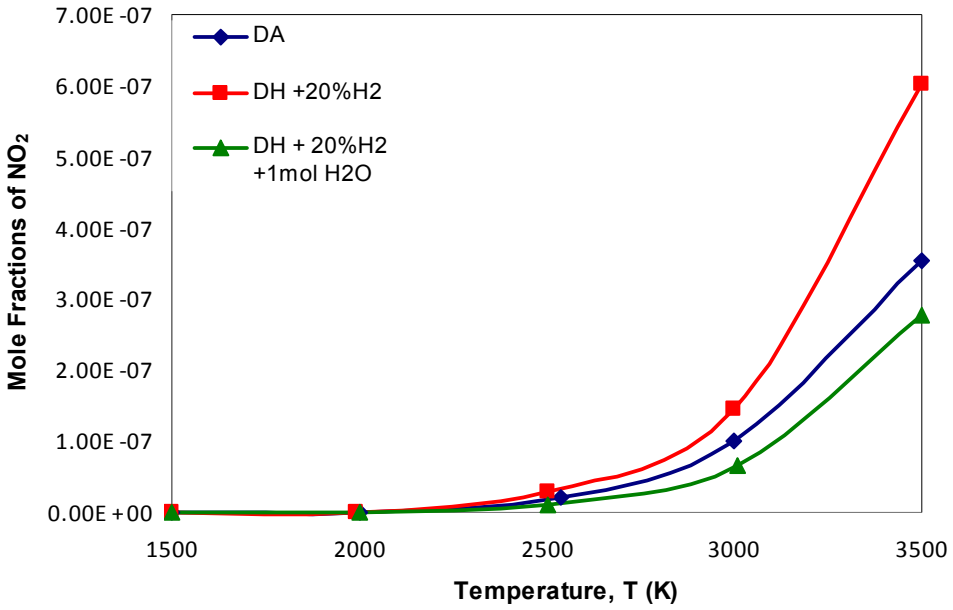

Figure 4.32 Mole fractions of NO_2 with temperature

Figure 4.32 shows the variation of NO_2 emission with combustion temperature. Mole fractions of NO_2 emission increased as combustion temperature increases. It can be seen that mole fraction of NO_2 increases rapidly when combustion temperature is greater than 2500K. Increase of NO_2 emission in DH operation is correlated to the faster burning rate of hydrogen (Naber, 1998). In DHW operation, similar trend is observed with NO concentration which concludes that lowered combustion temperature due to water addition resulting in lower NO and NO_2 emissions.

4.4 Experimental Validation

This section discusses individual experimental validation for each DA, DH and DHW operations in emission characteristics of HFCI engine. Experimental emissions characteristics are validated with numerical results with regard to changes in equivalence ratio.

4.4.1 Oxides of Nitrogen

Figure 4.33, 4.34 and 4.35 illustrates the comparison between simulated and experimental NO_x emission for DA, DH and DHW operations, respectively with equivalence ratio. Similar trend between simulation and experimental is shown for DA operation. As the value of equivalence ratio is increasing, NO_x concentration is decreasing for all type of operations. Despite huge differences in values are shown between simulated and experimental results but all graphs shows almost the same trends especially for DH and DHW operations.

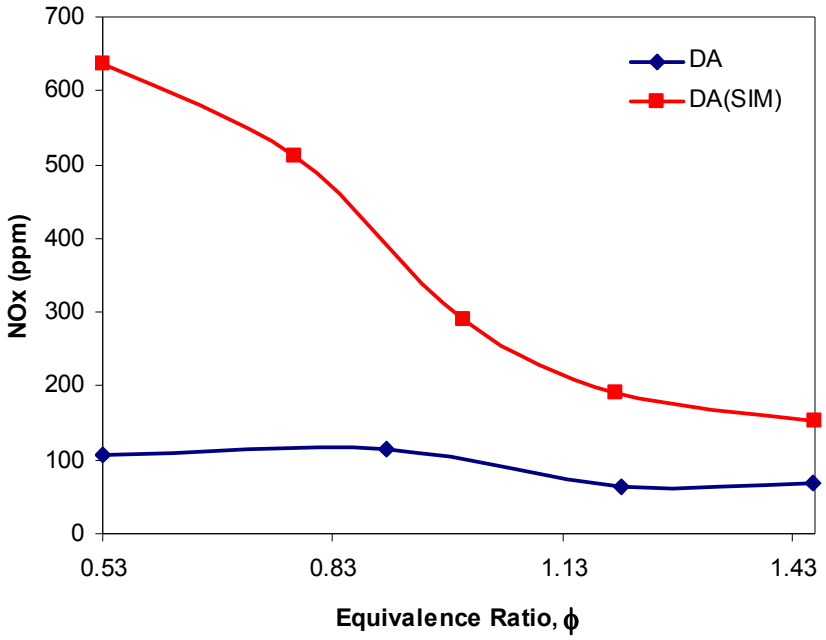

Figure 4.33 Simulated and experimental values of NO_x emission in DA operation

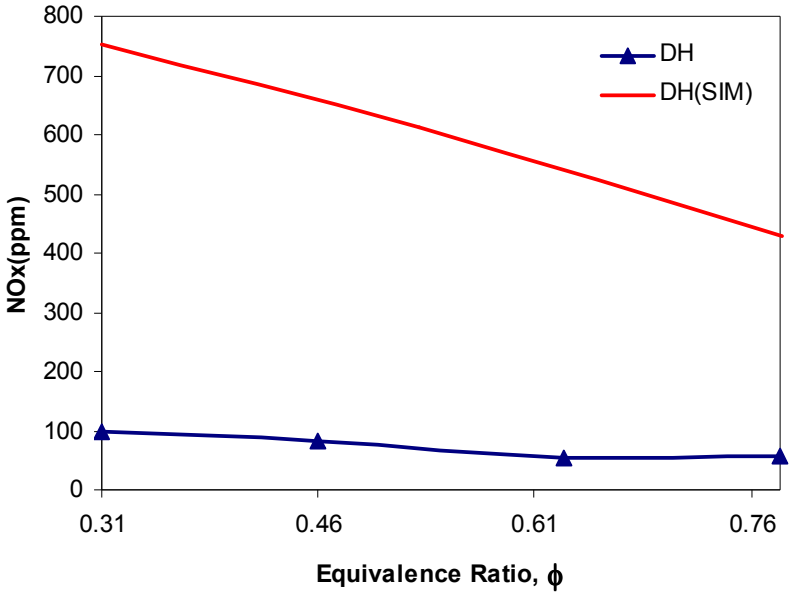

Figure 4.34 Simulated and experimental values of NO_x emission in DH operation

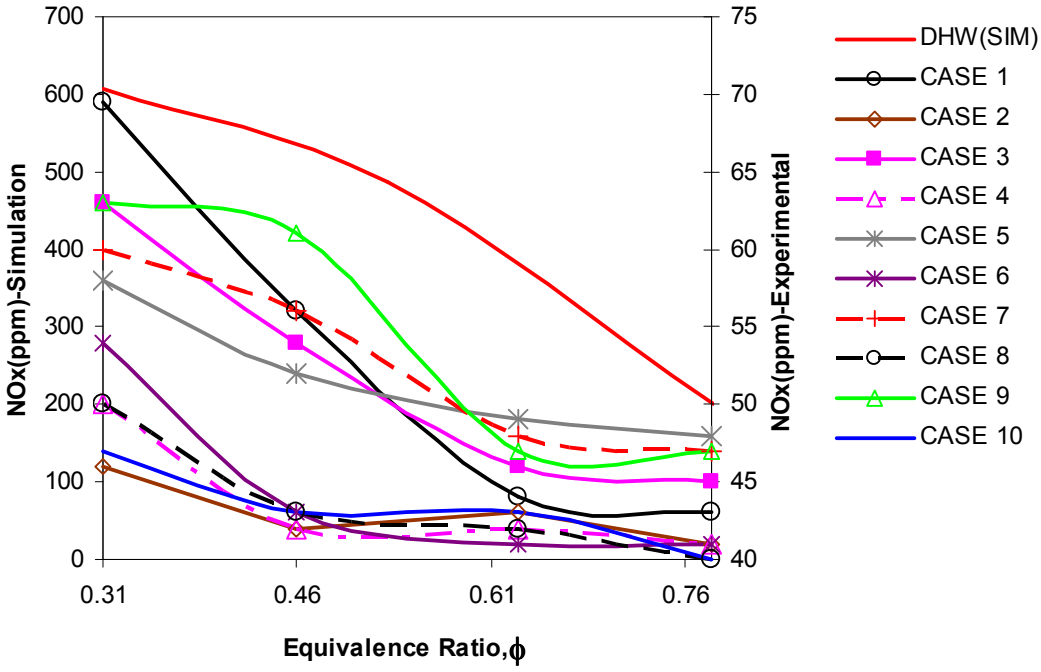

Figure 4.35 Simulated and experimental values of NO_x emission in DHW operation

4.4.2 Carbon Monoxide

Figure 4.36, 4.37 and 4.38 indicates the comparison between simulated and experimental CO emission for DA, DH and DHW operations, respectively with equivalence ratio. It is concluded that the simulated results are in good agreement with experimental results. This proves that the developed mathematical model gives reasonably good results and it is applicable in this investigation.

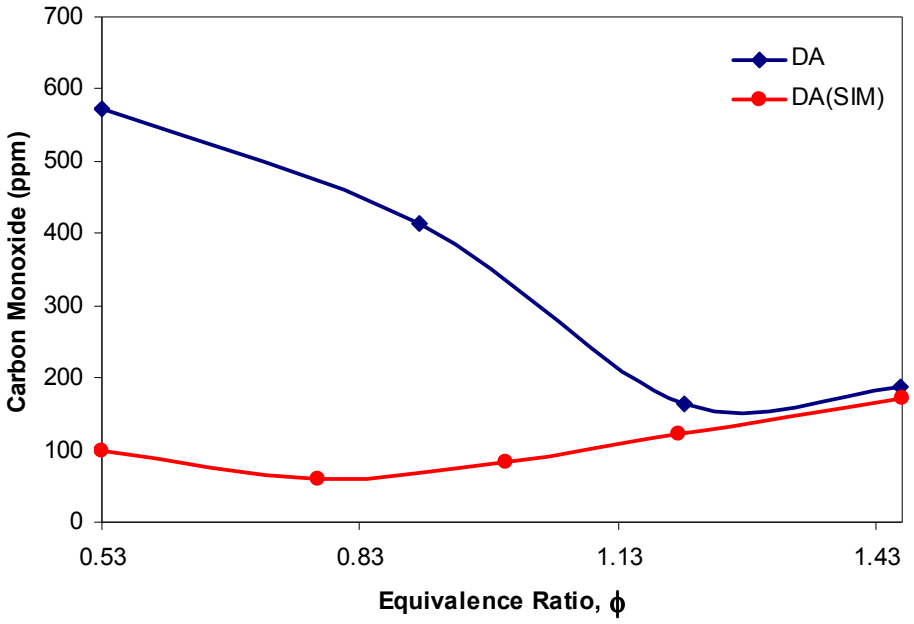

Figure 4.36 Simulated and experimental values of CO emission in DA operation

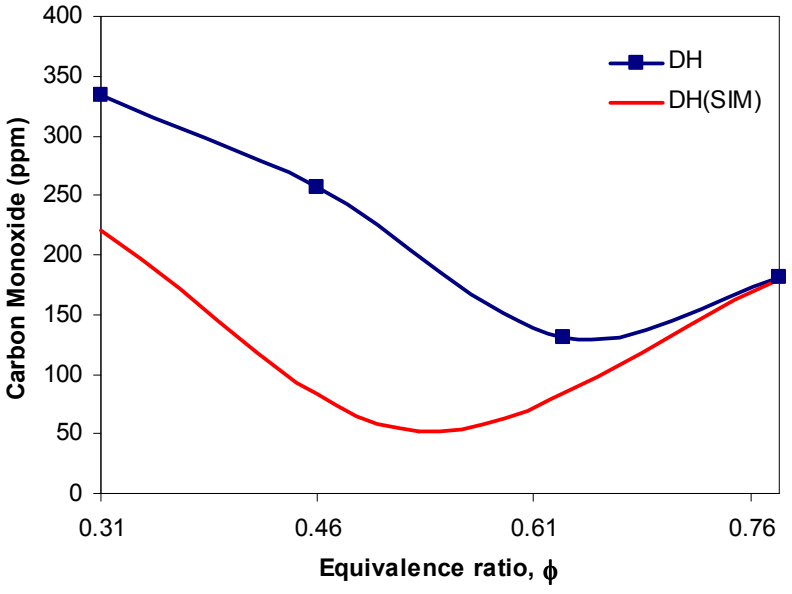

Figure 4.37 Simulated and experimental values of CO emission in DH operation

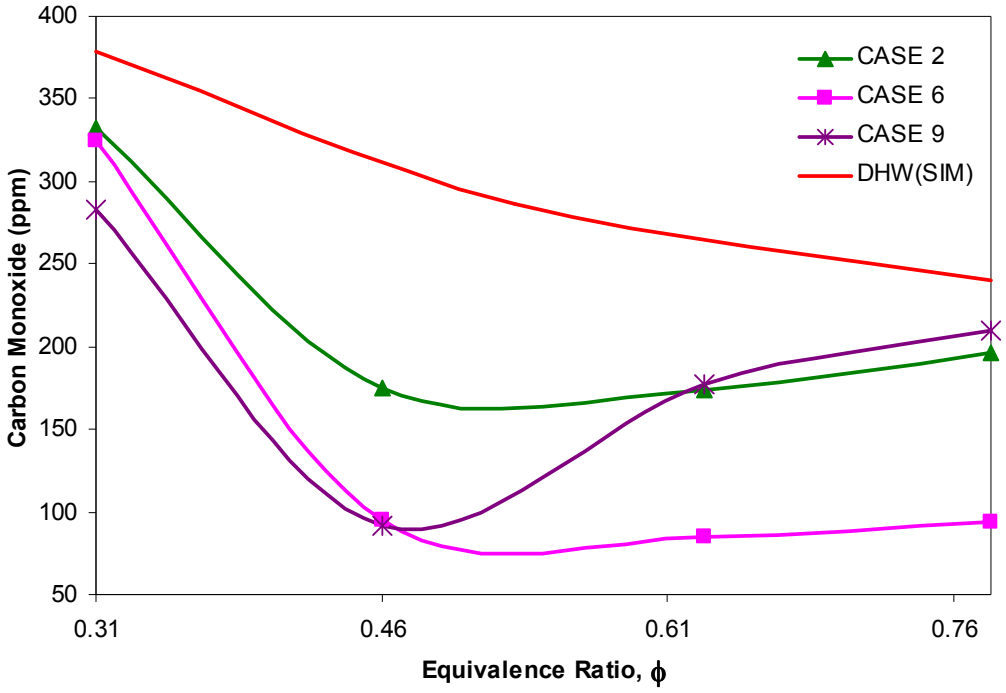

Figure 4.38 Simulated and experimental values of CO emission in DHW operation

4.4.3 Carbon Dioxide

Figure 4.39, 4.40 and 4.41 shows the comparison between simulated and experimental CO_2 emission for DA, DH and DHW operations, respectively with equivalence ratio. The simulated result shows the similar pattern with experimental for DA operations. For DH operations, as the equivalence ratio increases CO_2 concentration increases for simulated results and decreases for experimental results. This is due to a few idealizations were made during numerical solution, such as usage of theoretical air, constant specific heat of the cylinder charge, dissociation of CO_2 and hydrocarbon oxidation. The same phenomenon is shown in DHW operations as no significant changes in CO_2 emissions for experimental results as compared to simulated results with respect to equivalence ratios.

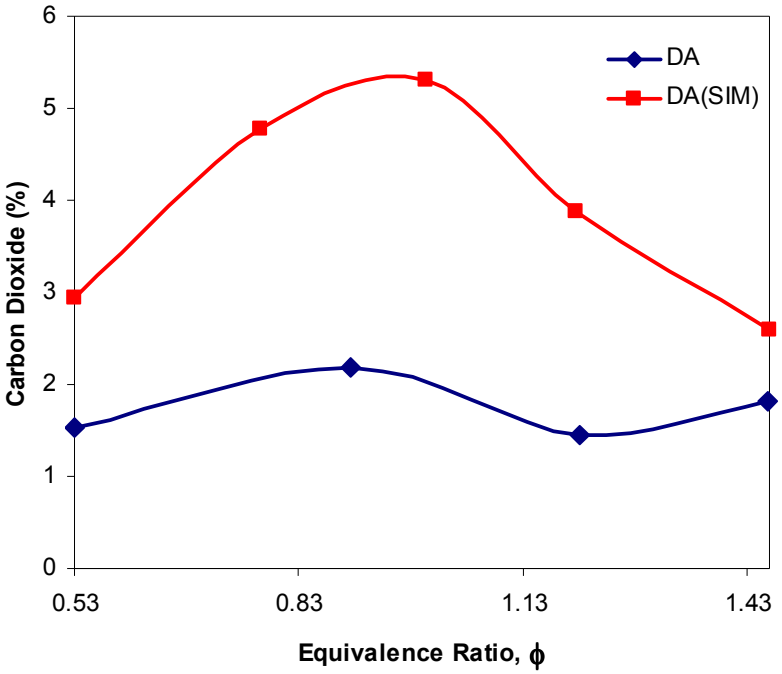

Figure 4.39 Simulated and experimental values of CO_2 emission in DA operation

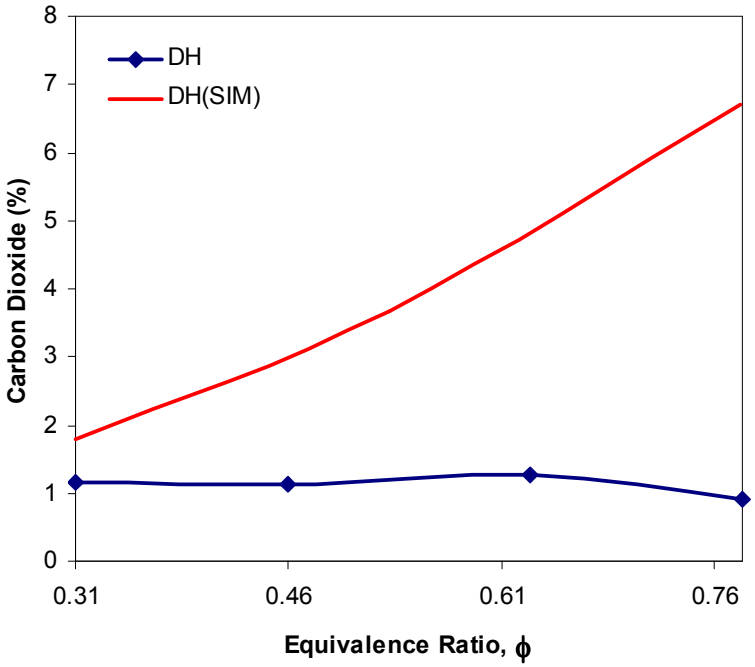

Figure 4.40 Simulated and experimental values of CO_2 emission in DH operation

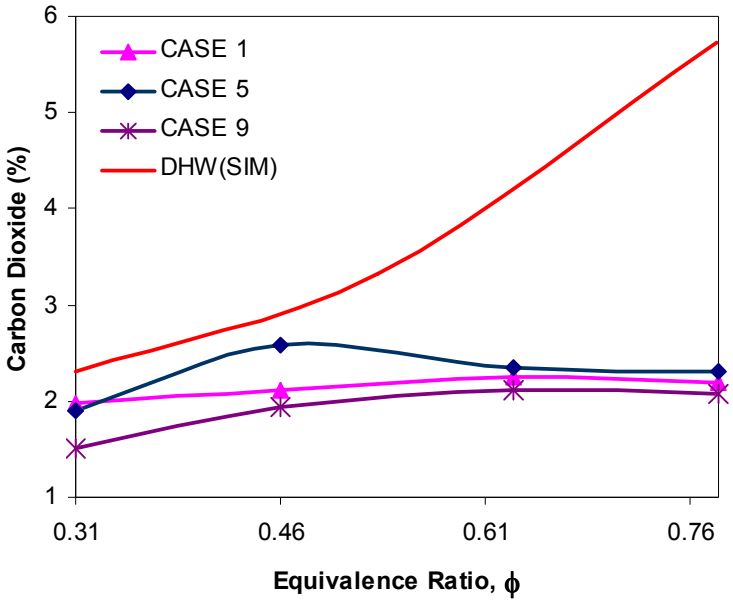

Figure 4.41 Simulated and experimental values of CO_2 emission in DHW operation

4.4.4 Hydrocarbon

Figure 4.42, 4.43 and 4.44 depicts the comparison between simulated and experimental HC emission for DA, DH and DHW operations, respectively with equivalence ratio. The experimental results for DA operation shows volatility with respect to equivalence ratio but its average values shows in good agreement with simulated values. For DHW operations, CASE 5 and CASE 9 showed a good agreement with simulated results. The increasing behavior of HC concentration with respect to equivalence ratio was observed in CASE 1. This proves that early water injection provides more time for combustion deterioration that causes increase in HC emissions especially in higher range of equivalence ratios.

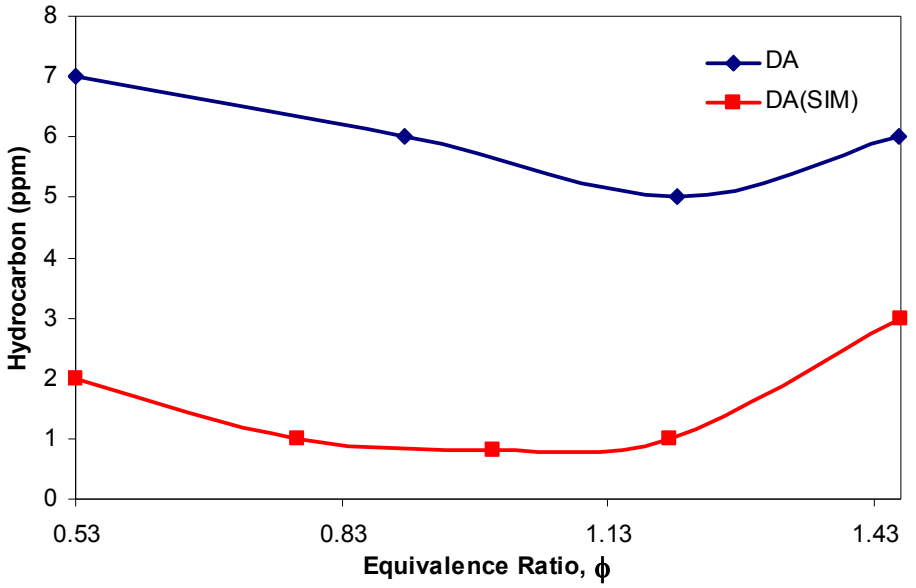

Figure 4.42 Simulated and experimental values of HC emission in DA operation

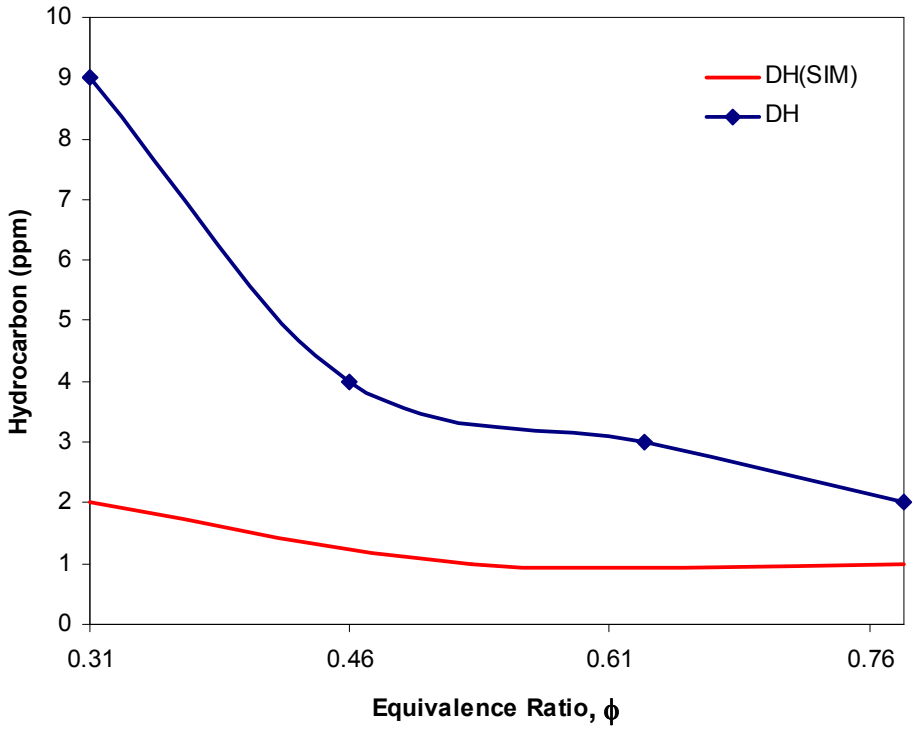

Figure 4.43 Simulated and experimental values of HC emission in DH operation

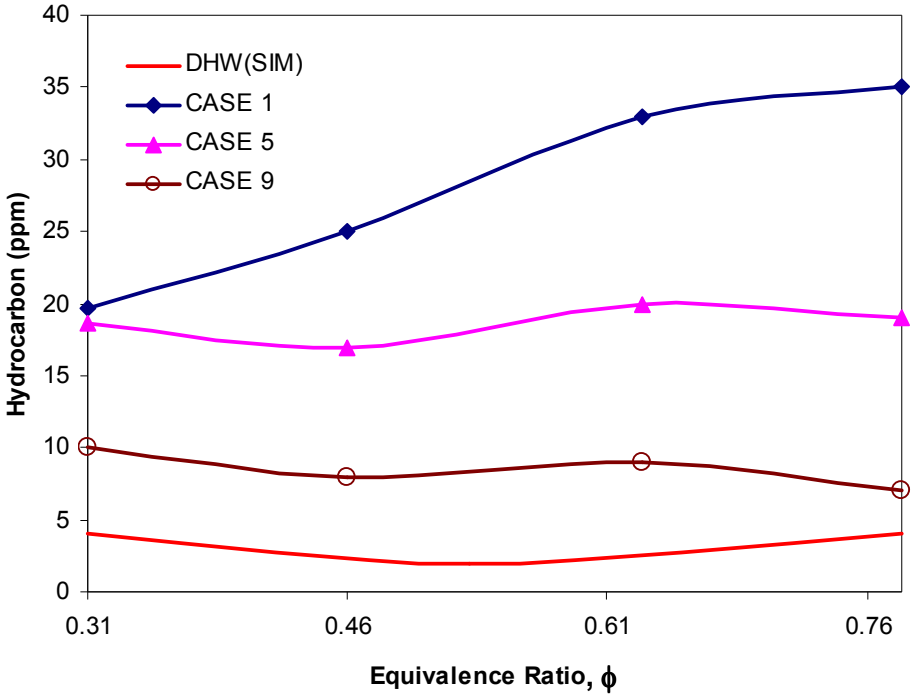

Figure 4.44 Simulated and experimental values of HC emission in DHW operation

Chapter 5

CONCLUSIONS AND SUGGESTIONS FOR FUTURE WORK

5.1 Conclusions

Water injection system with optimum injection timing is among the best method for better performance and emissions control in HFCI engine. In the present study, an attempt was made to determine the optimum water injection timing of HFCI engine. Conclusions drawn from this research are:

a) Compression ignition (CI) engine was successfully modified and converted to HFCI engine equipped with timed port hydrogen gaseous fuel and timed manifold water injection systems. Timed port injection hydrogen gaseous fuel and timed manifold water injection systems have been successfully developed and installed. It provides efficient control, precise detection and fast response on crank angle input signals. In addition, the detection technique of the developed system is able to distinguish between compression and power strokes.

b) The effects of water injection in HFCI on performance and emission were successfully investigated. These results were analyzed and compared with experimental results obtained without water injection system.

c) Mathematical model for predicting emission characteristics of diesel combustion under HFCI conditions with and without water addition has been successfully developed. It is then used to validate experimental emission characteristics of

HFCI engine. Experimental emission characteristics have been validated and it is in good agreement with numerical simulation.

d) Experimental and numerical investigations have been carried out to determine the optimum water injection timing for power augmentation and emission control of HFCI engine. The optimum water injection timings are described as below:

- Water injection timing of 20°ATDC and duration of 20°CA has shown better performance due to increase in gross indicated work, indicated thermal efficiency and it also showed the lowest indicated specific energy consumption especially at 2000RPM.
- Water injection timing of 20°BTDC and duration of 40°CA have shown the highest heat release rate and the longest ignition delay.
- Water injection timing of 20°BTDC and duration of 20°CA has shown the lowest SO_2 emission.
- Water injection timing of 0°CA and duration of 40°CA indicated the lowest in CO_2 emission.
- Water injection timing of 0°CA and duration of 20°CA have shown the lowest in CO emission for higher speed.
- Water injection timing of 20°ATDC and duration of 20°CA indicated the lowest HC emission and EGT throughout all engine speeds.
- All water injection timings indicated lower NO_x concentration for entire speed range.

In this study, it can be concluded that water injection timing of 20°ATDC and duration of 20°CA is the optimum timing for power augmentation and better control of emissions. Generally, water injection system with optimum injection timing appears to be promising method to enhance the performance and emissions quality of HFCI engine effectively. Heading towards this vision, the present study has provided useful findings for helping other researchers and industries to further understand this technology.

5.2 Suggestions for future work

Timed manifold water injection system is proven as one of affordable techniques for emissions control and power augmentation in HFCI engine. It is believed that there are rooms for improvement in order to maximize power output and for better emission control of the engine as described below:

a) This technique could be improved in the near future by widening the range of SOI from 20°BTDC to 180°ATDC and injection durations from 5°CA, 10°CA, 15°CA to 50°CA. In this case, more analysis can be carried out to determine the optimum injection timing of water to improve the performance and emission characteristics. Apart from that, this technique could also be enhanced by adding a few approaches such as addition of exhaust gas recirculation (EGR) along with water injection. It is believed to further decrease NO_x and CO emissions.

b) Direct water injection system is one of the effective method in increasing performance and better emission control, since this method provides capability to control water to diesel ratio in the combustion chamber. This technique will definitely optimize the power performance and emissions characteristics to the maximum possible. In developing this method, high pressure water injector need to be installed in the cylinder head and the same injection control by using ECU will be applied.

c) Emulsification of water and diesel at appropriate mixing ratio may help to improve fuel atomization and mixing characteristics which leads to better fuel droplet micro-explosion. This is believed to further improve emissions characteristics of CI engine and at the same time it could gradually increase the performance.

d) Timed port Hydroxy (HHO) injection system is one of the ways in improving performance and emissions of HFCI engine. HHO is produced from the electrolysis of pure water and its injection into the combustion chamber is believed to further improve engine performance and emissions as compared to pure water injection. Based on chemical kinetics mechanism, HHO requires less energy for ignition as compared to pure water itself. It is perhaps due to lower diffusive energy between HHO molecules.

e) CFD analysis needs to be carried out to research the characteristics of the inflow cylinder charge to further improve water injection in HFCI engine. Better understanding of inflow cylinder charge drives towards an improved water

injection system. Optimum size of water droplet can also be identified from this analysis which will optimize the injection pressure for finest water mist.

f) Steam and heated water injection is one of the promising methods to improve performance and emissions of HFCI engine. Heated water and steam contains higher energy in the form of heat as compared to solid water. In this case, less amount of combustion heat will be absorbed to vaporize solid water during combustion process. It is believed that this method will improve peak pressure and temperature of the cylinder charge in HFCI engine.

g) Water-ethanol blends injection system is seen to be a potential method for improving performance and emissions of HFCI engine. The existence of water in ethanol blends improves the energy balance, enhances miscibility and phase stability of ethanol. This blend is considered as oxygenated additive to combustion process, which will enhance combustion efficiency and contributes towards better engine performance.

h) Sophisticated mathematical model based on real-air as reactant can be developed by analyzing mole fraction of each component of gases in real-air prior to running the experiment. This might helps in reducing percentage of difference between simulated and experimental results.

i) Extensive study on the effect of water injection on combustion of fuels, enthalpy analysis, emission pollutant formation, adiabatic pressure and flame temperature analysis, thermodynamics effects during compression stroke,

stiochiometric analysis, volumetric efficiency and emissions elemental analyses can be performed in order to make this study a holistic one.

References

Alahmer A., Yamin J., Sakhrieh A., Hamdan M.A., (2010). Engine performance using emulsified diesel fuel, Energy Conversion and Management, 51, pp. 1708-1713.

Andrea T.D., Henshaw P.F., Ting D.S.K., (2004). The addition of hydrogen to a gasoline-fueled SI engine, Int. J. Hydrogen Energy, 29, pp.1541-1552.

Brenda J., Micheal C.M., Anshuman K., (2005). Hydrogen: the energy source for the 21st century, J. Technovation, 25, pp. 569-585.

Boretti A., Osman A., Aris I., (2011). Direct injection of hydrogen, oxygen and water in a novel two stroke engine, Int. J. Hydrogen Energy, 36, pp.10100-10106.

Caton J.A., (2001). An investigation of cause of backfire and its control due to creviced volumes in hydrogen fueled engine, Trans. ASME, 23, pp. 204–210.

Cengel, Y.A., Boles, M.A., (2002). Thermodynamics An Engineering Approach. 4th Edition in SI Units, McGraw-Hill Inc., New York.

Chadwell C.J., Dingle P.J., (2008) Effects of diesel and water co-injection with real control time on diesel engine performance and emissions. SAE Paper 2008-01-1190.

Chen D.Z., Weng Z.M., Li X.H., (1988). Theoretical performance evaluation of hydrogen flames, Int. J. Hydrogen Energy, 13, pp.701-709.

Chung K.L., (2006). Combustion Physics, 1st Edition, Cambridge University Press, Cambridge, New York.

Conklin J.C., Szybist J.P., (2010). A highly efficient six-stroke internal combustion engine cycle with water injection for in-cylinder exhaust heat recovery, Energy, 35(4), pp.1658-1664.

Das L.M., (1982). Fuel induction techniques for a hydrogen operated engine, Int. J. of Hydrogen Energy, 15(11), pp.833-842.

DeBoer P.C.T., (1976). Performance and emissions of hydrogen-fuelled internal combustion engines, Int. J. of Hydrogen Energy,1, pp.153-172.

Deboln B., Bohrenkamper G., (1998). Retrofitting, life extension and rehabilitation of heavy duty gas turbines, 7th annual POWER-GEN Asia Conference Proceedings.

Ferguson C.R., Kirkpatrick A.T., (2001) Internal Combustion Engines: Applied Thermo- sciences, John Wiley & Sons, New York.

Gadallah A.H., Elshenawy E.A., Elzahaby A.M., (2009). Effect of in-cylinder water injection strategies on performance and emissions of a hydrogen fuelled direct injection engine. SAE Paper 2009-01-1925.

Ganesan V., (2004). Internal Combustion Engine, 2nd Edition, McGraw-Hill Inc., Singapore.

Glassman I., Yetter R.A., (2008). Combustion, 4th Edition, Elsevier Inc., London.

Gomes A.J.M., Mikalsen R., Roskilly A.P., (2009). An experimental study of a direct injection compression ignition hydrogen engine, Int. J. Hydrogen Energy, 34, pp.6516-6522.

Gopal G., Srinivasa P., Murthy B.S., (1982). Use of Hydrogen in dual-fuel engines, Int. J. of Hydrogen Energy, 7 (3), pp: 267-272.

Heywood J.B., (1988). Internal Combustion Engine Fundamentals. International. Edition, McGraw-Hill Inc., New York.

Hountalas D.T., Kouremenos D.A., Binder K.B., Schwarz V., Mavropoulos G.C., (2003). Effect of injection pressure on the performance and exhaust emissions of a heavy duty DI diesel engine, SAE Paper 2003-01-0340.

Hountalas D.T., Kouremenos D.A., Mavropoulos G.C., Binder K.B,. Schwarz V., (2004). Multi-zone combustion modeling as a tool for DI diesel engine development-application for the effect of injection pressure, SAE Paper 2004-01-0115.

Hountalas D.T., Kouremenos D.A., Pariotis E.G., Schwarz V., Binder K.B., (2002). Using a phenomenological multi-zone model to investigate the effect of injection rate shaping on performance and pollutants of a DI heavy duty diesel engine, SAE Paper 2002-01-0074.

Hountalas D.T., Mavropoulos G.C., Zannis T.C., Mamalis S.D., (2006). Use of water emulsion and intake water injection as NO_x reduction techniques for heavy duty diesel engines, SAE paper no. 2006-01-1414.

Hountalas D.T., Mavropoulos G.C., Zannis T.C., Schwarz V., (2005). Possibilities to achieve future emission limits for HDHI diesel engines using internal measures, SAE Paper 2005-01-0377.

Ikegami M., Miwa K., Shioji M., (1982), A study of hydrogen fuelled compression ignition engines, Int. J. of Hydrogen Energy, 7(4), pp. 341-353.

JANAF Thermochemical Tables (1971), National Bureau of Standards Publication NSRDS-NSBS37, Washington D.C.

Javidi M., (2007). Iterative methods to nonlinear equations. Applied Mathematics Computation, 193, pp.360-365.

Jingding L., DuTianshen L., (1985). Backfire in hydrogen fueled engine and its control, Proceedings of the International Symposium on Hydrogen Systems, Beijing, China, 7-11th May 1985. Beijing: China Academic Publishers, Oxford Pergamon Press, pp.115-125.

Joseph M.N., James W.H., Thomas D.D., (1996). Hydrogen fuel for surface transport, 1st Edition. Society of Automotive Engineers, Warrendale Inc., U.S.A.

Jost K., (1995). Future Saab engine technology. Automotive Engineering, SAE International, 103 (12), pp.113-126.

Kadota T., Yamasaki H., (2001). Recent advances in the combustion of water fuel emulsion. Progress in a pre-combustion chamber diesel engine. Applied Thermal Engineering, 21(15), pp.1565-1582.

Karim G.A., (2003). Combustion in gas fueled compression ignition engines of the dual fuel type, ASME J. Eng. for Gas Turbines and Power, 25, pp. 827-836.

Lakshmanan T., Nagarajan G., (2010). Experimental investigation of timed manifold injection of acetylene in direct injection diesel engine in dual fuel mode, Energy; 35.pp: 3172-3178.

Lata D.B., Misra A., (2010). Theoretical and experimental investigations on the performance of dual fuel diesel engine with hydrogen and LPG as secondary fuels, Int. J. Hydrogen Energy, 35, pp. 11918-11931.

Larbi N., Bessrour J., (2010). Measurement and simulation of pollutant emissions from marine diesel combustion engine and their reduction by water injection. Advances in Engineering Software, 41, pp. 898-906.

Li H., Karim G.A., Sohrabi A., (2003). Knock and combustion characteristics of CH_4, CO, H_2 and their binary mixtures, SAE Paper No. 013088.

Lilik K., G, Zhang H., Herreross J.M., Haworth D.C., Boehman A.L., (2010). Hydrogen assisted diesel combustion, Int. J. Hydrogen Energy, 35, pp.4382-4398.

Lin C., Chen L., (2002). Engine performance and emission characteristics of three-phase diesel emulsions prepared by an ultrasonic emulsification method, Fuel, 81(16), pp.2035-2044.

Liu X., Liu F., Schock H.J., (2008). Backfire prediction in manifold injection hydrogen internal combustion engine, Int. J. Hydrogen Energy, 33, pp.3847- 3855.

Ma J., Su Y., Zhou Y., Zhang Z., (2003). Simulation and prediction on the performance of a vehicle's hydrogen engine, Int. J. Hydrogen Energy, 28, pp.77-83.

Mathur H.B Das L.M., Patro T.N., (1992). Effect of charge diluents on the emission characteristics of a hydrogen fueled diesel engine, Int. J. Hydrogen Energy; 17(8), pp.635-642.

Mathur H.B., Das L.M., Patro T.N., (1993). Hydrogen-fuelled diesel engine:Performance improvement through charge dilution techniques, Int. J. Hydrogen Energy; 18(5), pp. 421-431.

Masood M., Ishrat M.M., (2008). Computer simulations of hydrogen–diesel dual fuel exhaust gas emissions with experimental verification, Fuel, 87, pp. 1372–1378.

Masood M., Ishrat M.M., Reddy A.S., (2007) Computational combustion and emission analysis of hydrogen-diesel blends with experimental verification, Int. J. Hydrogen Energy, 32, pp.2539-2547.

Masjuki H.H., Kalam M.A., Maleque M.A., Kubo A., Nonaka T., (2001). Performance, emissions and wear characteristics of an indirect injection diesel engine using coconut oil blended fuel, Proceeding of Institution of Mechanical Engineers, 215 (Part D), pp.393-401.

Matekunas F.A., (1983). Modes and measures of cyclic combustion variability, SAE Paper 830337.

Miyamoto T., Hasegawa H., Yagenji T., Seo T., Mikami M., Kabashima H., Hashimoto T., (2011). Effects of hydrogen addition to intake mixture on cyclic variation of diesel engine, SAE paper 2011-01-1964.

Momani S.,Abuasada S., Odibat Z., (2006). Variation iteration method for solving nonlinear boundary value problems. Applied Mathematics Computation, 83, pp.1351-1358.

Moran M.J., Shapiro H.N., (2004). Fundamentals of engineering thermodynamics. 5th Edition. John Wiley & Sons. New Jersey.

Mullins, P., (1999). Ro-Ro vessels will have water injection, Diesel & Gas Turbines Publications, 11, pp.28-32.

Nabi M.N., Hustad J.E., (2010). Influence of biodiesel addition to Fisher-Tropsch fuel on diesel engine performance and exhaust emissions. Energy & Fuels, 24(5), pp. 2868-2874.

Nader J.D., Siebers D.L., (1998). Hydrogen combustion under diesel engine conditions, Int. J. Hydrogen Energy, 23, pp.363-371.

Nagar T., Kawahamd M., (1990). Study into reduction of NO_x emissions in medium-speed diesel engines, Technical paper ISME, KOHI.

Nande A.M., Wallner T., Naber J., (2008). Influence of water injection on performance and emissions of a direct-injection hydrogen research engine, SAE Paper 2008-01-2377.

Nienhuys H.K., Van Santen R.A., Bakker H.J., (2000). Orientation relaxation of liquid water molecules as an activated process, Journal of Chemistry and Physics, 112, pp. 8487-8494

Nunney M.J., (1982). Engine Technology. 2nd Edition, Butterworth & Co (Publishers) Ltd., Norwich.

Odaka M., Koike N., Tsukamoto Y., Kazuysawa, Yoshida K., (1991). Effects of EGR with a supplemental manifold water injection to control exhaust emissions for heavy-duty diesel powered vehicles. SAE Paper 910739.

Olikara C., Borman G.L, (1975). A computer program for calculating properties of equilibrium combustion products with some applications to I.C. Engines. SAE Paper 750468.

Overend, E., (1999). Hydrogen Combustion Engines, The University of Edinburgh, School of Mechanical Engineering, Final-year report, September 1999.

Papagiannakis R.G., Hountalas D.T., (2004). Combustion and exhaust emission characteristics of a dual fuel compression ignition engines operated with pilot diesel fuel and natural gas, Energy Conversion and Management, 45, pp. 2971-2987.

Perini F., Paltrinieri F., Mattarelli E., (2010). A quasi-dimensional combustion model for performance and emissions of SI engines running on hydrogen-methane blends, Int. J. Hydrogen Energy, 35, pp. 4687-4701.

Prabhukumar G.P., Swaminathan S., Nagalingam B., Gopalakrishnan K.V., (1987). Water induction studies in a hydrogen-diesel dual-fuel engine, Int. J. Hydrogen Energy,12 (3), pp. 177-186.

Pulkrabek W.W., (2004). Engineering Fundamentals of the Internal Combustion Engine. Pearson Prentice-Hall, New Jersey.

Rakopoulos C.D., Hountalas D.T., Tzanos E.I., Taklis G.N,, (1994). A fast algorithm for calculating the composition of diesel combustion products using 11 species chemical equilibrium scheme. Advanced Engineering Software,19, pp.109-119.

Rashidi M., (1998). Calculation of equilibrium composition in combustion products. Applied Thermal Engineering, 18, pp.103-109.

Roy M.K., Kawahara N., Tomita E., Fujitani T., (2011). High-pressure hydrogen jet and combustion characteristics in a direct-injection hydrogen engine, SAE Paper 2011-01-2003.

Roy M.M., Tomita E., Kawahara N., Harada Y., Sakane A., 2009. Performance and emission comparison of a supercharged dual-fuel engine fueled by producer gases with varying hydrogen content, Int. J. Hydrogen Energy, 34, pp. 7811-7822.

Sahin Z., Durgun O., Bayram C, (2008). Experimental investigation of gasoline fumigation in a single cylinder direct injection (DI) diesel engine, Energy, 33, pp.1298-1310.

Saravanan N., Nagarajan G., (2008). An experimental investigation of hydrogen-enriched air induction in a diesel engine system. Int. J. Hydrogen Energy, 33, pp. 1769-1775.

Saravanan N., Nagarajan G., Dhanasekaran C., Kalaiselvan K.M., (2007). Experimental investigation of hydrogen port fuel injection in DI diesel engine. Int. J. Hydrogen Energy, 32, pp.4071-4080.

Saravanan N., Nagarajan G., Sanjay G., Dhanasekaran C., Kalaiselvan K.M., (2008). Combustion analysis on a DI diesel engine with hydrogen in dual fuel mode. Fuel, 87, pp.3591-3599.

Saravanan N., Nagarajan G., (2010). Performance and emissions studies on port injection of hydrogen with varied flow rates with diesel as an ignition source, Applied Energy, 87, pp. 2218-2229.

Saravanan N., Nagarajan G., (2009). Performance and emission study in manifold hydrogen injection with diesel as an ignition source for different start of injection, Renewable Energy, 34, pp.328-334.

Saravanan N., Nagarajan G., Narayanasamy S., (2008). An experimental investigation on DI diesel engine with hydrogen fuel, Renewable Energy, 33, pp. 415-421.

Saravanan N., Nagarajan G., Kalaiselvan K.M., Dhanasekaran C., (2008). An experimental investigation on hydrogen as a dual fuel for diesel engine system with exhaust gas recirculation technique, Renewable energy, 33, pp.422-427.

Saravanan N., Nagarajan G., (2008). An experimental investigation on performance and emissions study with port injection using diesel as an ignition source for different EGR flow rates, Int. J. Hydrogen Energy; 33, pp. 4456-4462.

Saravanan, N., Nagarajan, G., (2010). Performance and emission studies on port injection of hydrogen with varied flow rates with diesel as an ignition source, Applied Energy, 87, pp. 2218-2229.

Schafer F., Basshuysen R.V., (1995). Reduce emissions and fuel consumption in automobile engines, 1st Edition. Springer-Verlag Wien, New York.

Senthil Kumar M, Ramesh A, Nagalingam B., (2003). Use of hydrogen to enhance the performance of a vegetable oil fuelled compression ignition engine. Int. J. Hydrogen Energy, 28, pp.1143-1154.

Singhyadav V, Soni S.L, Sharma D., (2011). Performance and emission studies of direct injection CI engine in dual fuel mode (hydrogen-diesel) with EGR, Int. J. Hydrogen Energy; doi 10.1016/j.ijhydene.2011.04.163.

Stanglmaier R.H, Dingle P.J, Stewart D., (2008). Cycle-controlled water injection for steady-state and transient emissions reduction from a heavy-duty diesel engine. J. Eng. Gas Turbines and Power, 130 (3), Paper No. 032801, pp.1-7.

Stephen R.T., (2000). An Introduction to Combustion: Concepts and Applications. McGraw-Hill, New York.

Stull D.R., Prophet H., (1971). JANAF Thermo-chemical Tables, National Bureau of Standards Publication NSRDS- NBS37, Washington D.C.

Subramaniam K.A., (2011). A comparison of water-diesel emulsion and timed injection of water into the intake manifold of a diesel engine for simultaneous control of NO and smoke emissions. Energy Conversion and Management, 52, pp. 849-857.

Szwaja S, Grab-Rogalinski K., (2009). Hydrogen combustion in a compression ignition diesel, Int. J. Hydrogen Energy, 34, pp.4413-4421.

Tauzia X, Maiboom A, Shah S.R., (2010). Experimental study of inlet manifold water injection on combustion and emissions of an automotive direct injection diesel engine, Energy, 35, pp.3628-3639.

Tesfa B., Mishra R., Gu F, Ball A.D., (2011). Water injection effects on the performance and emission characteristics of a CI engine operating with biodiesel. Renewable Energy, 37, pp.333-344.

Verhelst S, Sierens R., (2006). A critical review of experimental research on hydrogen fueled SI engines, SAE Paper 2006-01-0430.

Verhelst S, Sierens R., (2001). Hydrogen engine-specific properties, Int. J. Hydrogen Energy, 26, pp. 987-990.

Verhelst S., Sierens R., (2007). A quasi-dimensional model for the power cycle of a hydrogen-fuelled internal combustion engine, Int. J. Hydrogen Energy, 32, pp.3545 – 3554.

Wallner T., Matthias N.S, Scarcelli R., (2011). Influence of injection strategy in a high-efficiency hydrogen direct injection engine, SAE Paper 2011-01-2001.

Wallner T., Nande A.M, Naber J.D., (2008). Evaluation of injector location and nozzle design in a direct-injection hydrogen research engine, SAE Paper 2008-01-2267.

Wang Y., Zhang X., Li C., Wu J., (2010). Experimental and modeling study of performance and emissions of SI engine fueled by natural gas-hydrogen mixtures, Int. J. Hydrogen Energy,35, pp.2680-2683.

Westbrook, C.K., Adamczyk A.A, Lavoie G.A., (1981). A number study of laminar wall quenching, Combustion and Flame, 40, pp.81-91.

Williams F.A., (1985). Combustion Theory: The Fundamental Theory of Chemically Reacting Flow Systems, 2nd Edition. The Benjamin/Cummings Publishing Company, Inc., California, USA.

Wimmer A., Wallner T, Ringler J, Gerbig F., (2005). H_2-direct injection-A highly promising combustion concept. SAE Paper 2005-01-0108.

Xing-hua L, Fu-shui L, Lei Z, Bai-gang S, Harold J.S., (2008). Backfire prediction in a manifold injection hydrogen internal combustion engine," Int. J. Hydrogen Energy, 33, pp.3847-3855.

Appendix A: Coefficients of Equilibrium Constant Method

The values of equilibrium constants K_1 to K_{14} for combustion equations are calculated by using Equation (1) until Equation (14) as described below:

a) $CO_2 \Leftrightarrow CO + \frac{1}{2}O_2$ yields $K_1 = \left(\frac{y_{10} y_6^{0.5}}{y_3}\right)(P)^{0.5}$ (1)

b) $CO \Leftrightarrow C + \frac{1}{2}O_2$ yields $K_2 = \left(\frac{y_{11} y_6^{0.5}}{y_{10}}\right)(P)^{0.5}$ (2)

c) $CH_4 \Leftrightarrow C + 2H_2$ yields $K_3 = \left(\frac{y_{11} y_1^2}{y_{12}}\right)(P)^2$ (3)

d) $HCN \Leftrightarrow C + \frac{1}{2}H_2 + \frac{1}{2}N_2$ yields $K_4 = \left(\frac{y_{11} y_1^{0.5} y_4^{0.5}}{y_{17}}\right)(P)$ (4)

e) $H_2O \Leftrightarrow H_2 + \frac{1}{2}O_2$ yields $K_5 = \left(\frac{y_1 y_6^{0.5}}{y_2}\right)(P)^{0.5}$ (5)

f) $H_2O \Leftrightarrow OH + \frac{1}{2}H_2$ yields $K_6 = \left(\frac{y_9 y_1^{0.5}}{y_2}\right)(P)^{0.5}$ (6)

g) $\frac{1}{2}H_2 \Leftrightarrow H$ yields $K_7 = \left(\frac{y_8}{y_1^{0.5}}\right)(P)^{0.5}$ (7)

h) $\frac{3}{2}O_2 \Leftrightarrow O$ yields $K_8 = \left(\frac{y_5}{y_6^{0.5}}\right)(P)^{0.5}$ (8)

i) $\frac{3}{2}O_2 \Leftrightarrow O_3$ yields $K_9 = \left(\frac{y_7}{y_6^{1.5}}\right)(P)^{-0.5}$ (9)

j) $\frac{1}{2}N_2 \Leftrightarrow N$ yields $K_{10} = \left(\frac{y_{18}}{y_4^{0.5}}\right)(P)^{0.5}$ (10)

k) $\frac{1}{2}N_2 + \frac{1}{2}O_2 \Leftrightarrow NO$ yields $K_{11} = \left(\frac{y_{13}}{y_4^{0.5}y_6^{0.5}}\right)(P)^{0}$ (11)

l) $NO_2 \Leftrightarrow NO + \frac{1}{2}O_2$ yields $K_{12} = \left(\frac{y_{13}y_6^{0.5}}{y_{14}}\right)(P)^{0.5}$ (12)

m) $NH_3 \Leftrightarrow \frac{1}{2}N_2 + \frac{3}{2}H_2$ yields $K_{13} = \left(\frac{y_4^{0.5}y_1^{1.5}}{y_{15}}\right)(P)$ (13)

n) $2HNO_3 + NO \Leftrightarrow 3NO_2 + H_2O$ yields $K_{14} = \left(\frac{y_{14}^3 y_2}{y_{13}y_{16}^2}\right)(P)$ (14)

Equilibrium Constant	Chemical reaction equations	A_1	A_2	A_3	A_4	A_5	A_6	A_7	A_8	A_9	A_{10}	A_{11}	A_{12}
K_1	$CO_2 \leftrightarrow CO + 0.5\ O_2$	-4.7060	4.5548	-1.9275	0.6914	-0.2143	0.0568	-0.0118	0.6918	0.7740	-0.1600	0.0297	-0.0053
K_2	$CO \leftrightarrow C + 0.5\ O_2$	-23.3871	13.5989	-5.6463	2.0147	-0.6290	0.1745	-0.0436	-7.0178	2.4494	-0.4831	0.0876	-0.0146
K_3	$CH_4 \leftrightarrow C + 2\ H_2$	-12.3506	13.1975	-5.5245	1.9729	-0.6151	0.1704	-0.0425	3.4195	2.3113	-0.4651	0.0856	-0.0144
K_4	$HCN \leftrightarrow C + 0.5\ H_2 + 0.5\ N_2$	-12.6282	9.5942	-4.0164	1.4348	-0.4479	0.1243	-0.0310	-1.1652	1.6762	-0.3401	0.0622	-0.0104
K_5	$H_2O \leftrightarrow H_2 + 0.5\ O_2$	-5.1798	4.0998	-1.6966	0.6008	-0.1828	0.0461	-0.0081	-0.2380	0.7418	-0.1478	0.0290	-0.0066
K_6	$H_2O \leftrightarrow OH + 0.5\ H_2$	-5.6771	4.7100	-1.9572	0.6958	-0.2168	0.0510	-0.0143	-0.0217	0.8372	-0.1692	0.0317	-0.0055
K_7	$0.5\ H_2 \leftrightarrow H$	-4.2669	3.6898	-1.5150	0.5328	-0.1618	0.0418	-0.0086	0.2000	0.6740	-0.1360	0.0268	-0.0063
K_8	$0.5\ O_2 \leftrightarrow O$	-4.8419	4.1600	-1.7225	0.6135	-0.1940	0.0570	-0.0163	0.1700	0.7458	-0.1456	0.0235	-0.0021
K_9	$1.5\ O_2 \leftrightarrow O_3$	-8.23556	2.3730	-0.9800	0.3462	-0.1077	0.0299	-0.0075	-5.3797	0.4183	-0.0869	0.0158	-0.0026
K_{10}	$0.5\ N_2 \leftrightarrow N$	-12.1749	7.8225	-3.2406	1.1510	-0.3568	0.0984	-0.0249	-2.7519	1.4098	-0.2776	0.0501	-0.0068
K_{11}	$0.5\ N_2 + 0.5\ O_2 \leftrightarrow NO$	-2.2991	1.4798	-0.6119	0.2102	-0.0593	0.0126	-0.0015	-0.5281	0.2562	-0.0520	0.0080	-0.0003
K_{12}	$NO_2 \leftrightarrow NO + 0.5\ O_2$	2.0772	0.9404	-0.3968	0.1434	-0.0450	0.0125	-0.0031	3.1992	0.1675	-0.0320	0.0059	-0.0010
K_{13}	$NH_3 \leftrightarrow 0.5\ N_2 + 1.5\ H_2$	4.3247	0.9087	-0.3926	0.1381	-0.0427	0.0119	-0.0030	5.3672	0.1264	-0.0338	0.0062	-0.0010
K_{14}	$2HNO_3 + NO \leftrightarrow 3\ NO_2 + H_2O$	7.6818	0.5958	-0.2475	0.1101	-0.0781	0.0699	-0.0526	8.4100	0.1200	-0.0600	0.0533	-0.0400

Appendix B: Photographic Views of Experimental Apparatus

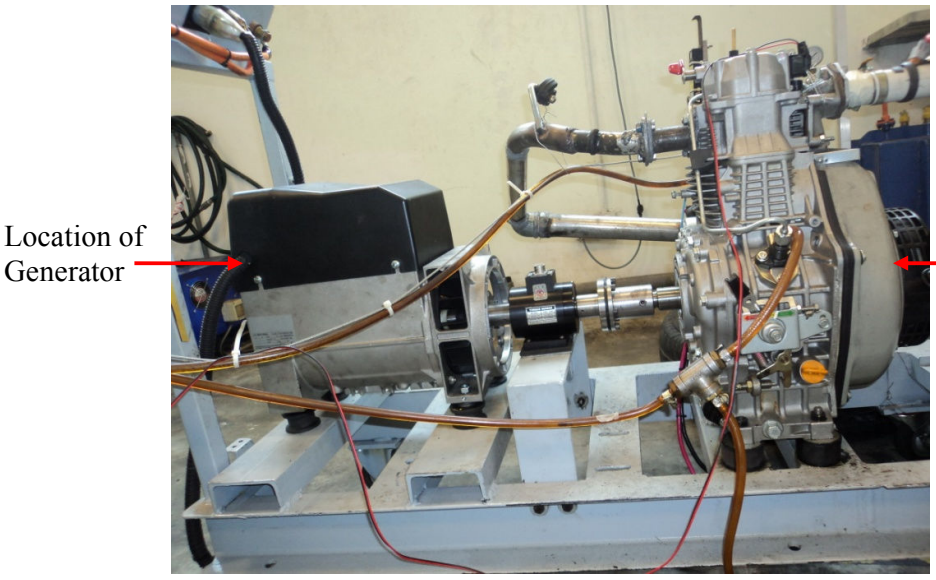

(a) Engine setup

(b) Photographic View of Load Controller

Figure B.1 Photographic view of engine setup

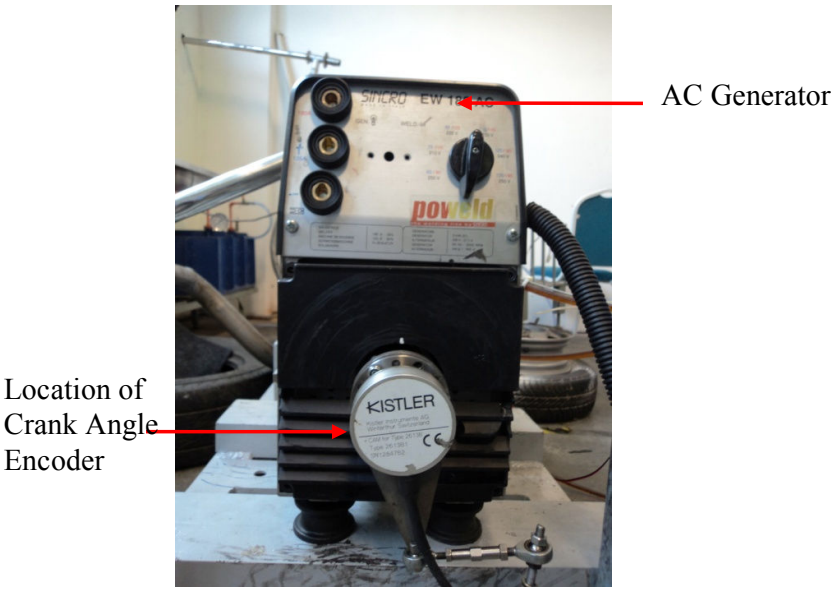

Figure B.2 Alternate current synchronous generator

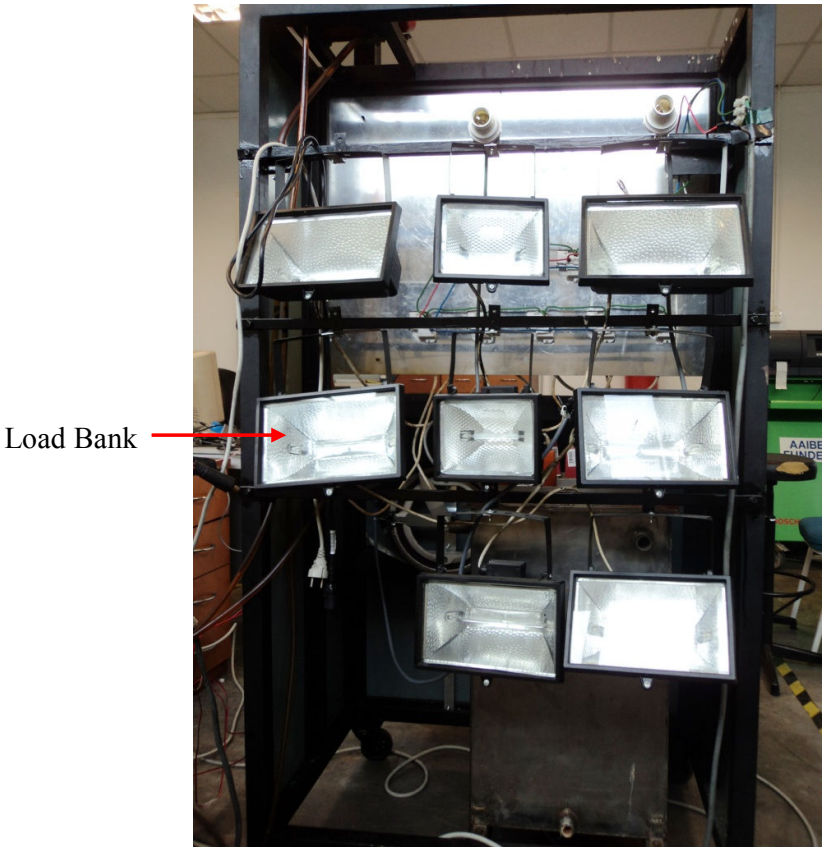

Figure B.3 Photographic view of load bank

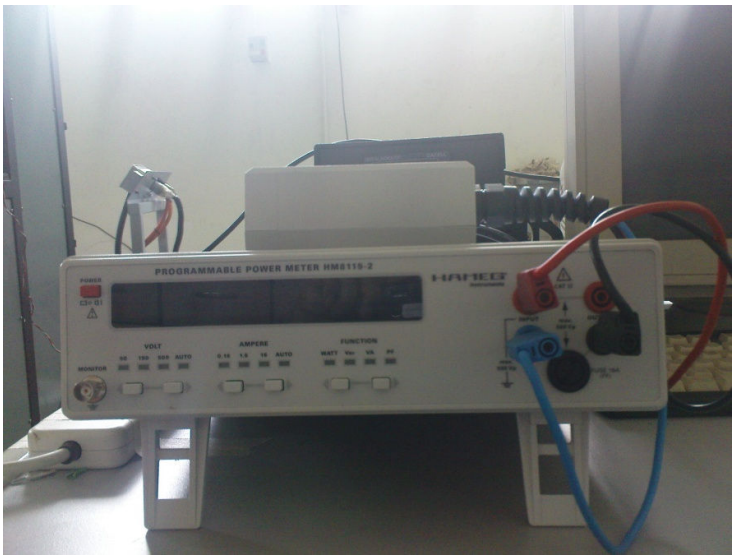

Figure B.4 HAMEG power meter

Figure B.5 FLUKE 922 airflow meter

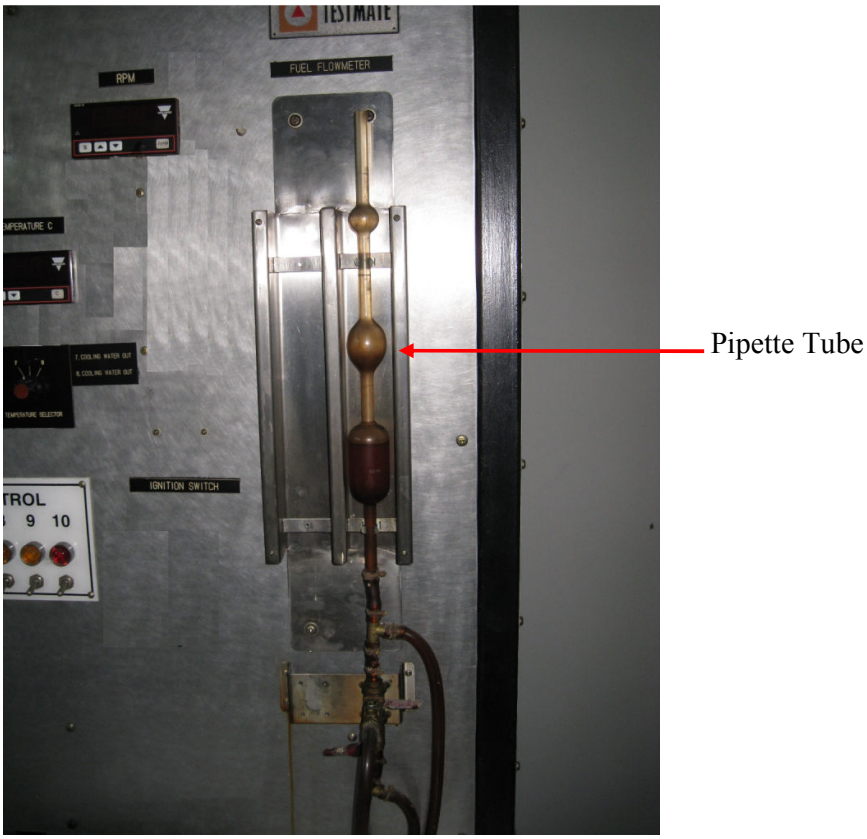

Figure B.6 Pipette tube for diesel fuel flow rate measurement

(a) KISTLER pressure transducer

(b) KISTLER crank angle encoder

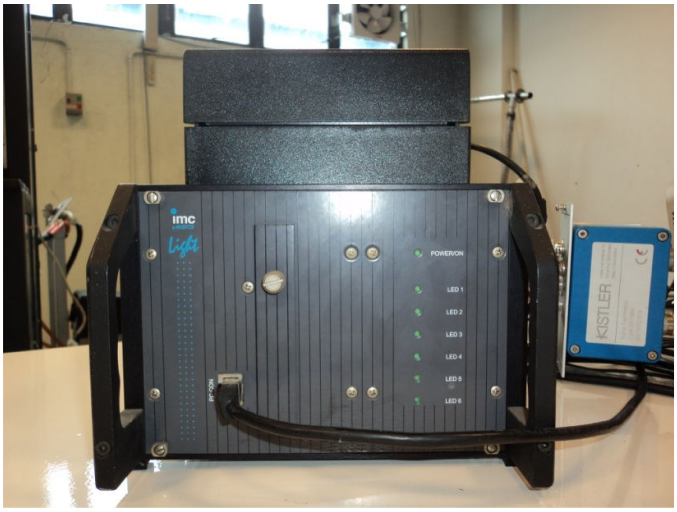

(c) μ-MUSYCS data acquisition system

Figure B.7 KISTLER pressure transducer, crank angle encoder and μ-MUSYCS

(a) BACHARACH 300NSX

(b) AUTOCHECK 974/5

Figurer B.8 Photographic view of gas analyzers

Figure B.9 OMEGA digital mass flow meter

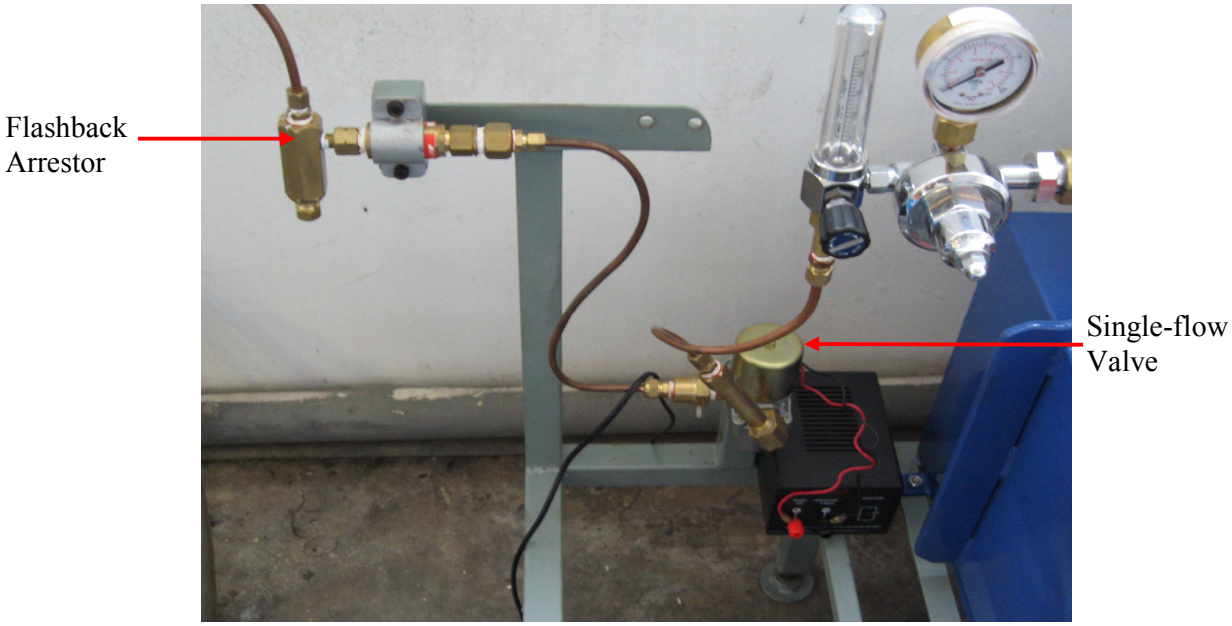

Figure B.10 Single-flow valve and flashback arrestor

Figure B.11 NAMUR electronic injector

(a) Cooling mist Vari-Cool water injection system

(b) DENSO electronic injector for water injection

Figure B.12 Cooling mist Vari-Cool and DENSO electronic injector for water injection

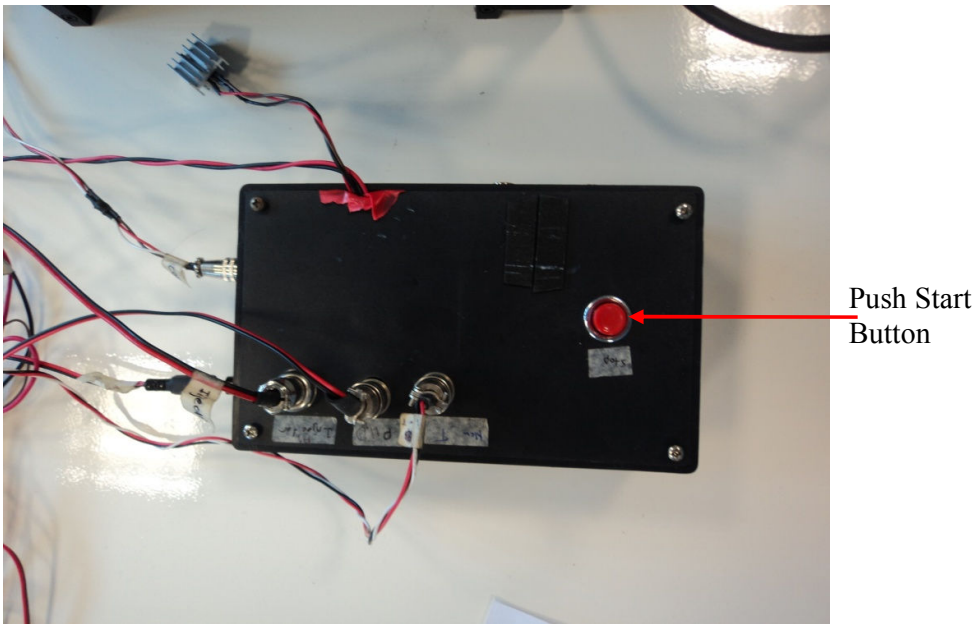

(a) Top view of the developed ECU

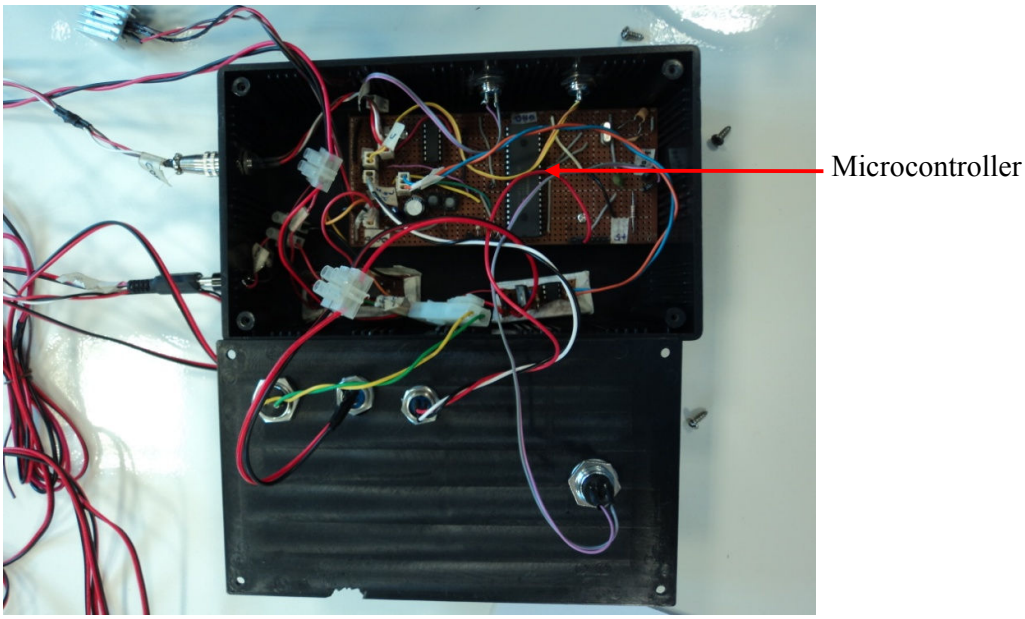

(b) Internal view of the developed ECU

Figure B.13 Photographic view of the developed ECU

Appendix C: Mikroelectronika C Language Compiler for ECU development

```
unsigned int angle=0,start=0,end=1; // to record the angle
unsigned char state=0;

void Display_angle(unsigned int angle)
{
unsigned char digit[3];
unsigned int number;
number = angle;
digit[0]=number/100;
number=number%100;
digit[1]=number/10;
digit[2]=number%10;
digit[1]+=0x30;
digit[2]+=0x30;
digit[1]+=0x30;
Usart_write(digit[1]);
Usart_write(digit[2]);
Usart_write(digit[1]);
}

void read_user_input(void)
{
unsigned char k,receive[8];

for(k=0;k<8;k++)
{
 while(!Usart_data_ready());
  receive[k]=Usart_read();
  receive[k]-=0x30;
 }

start=receive[3]*100+receive[2]*10+receive[5];
end=receive[7]*100+receive[8]*10+receive[9];
}

void Display_user_input(void)
{
char txt[7],i;
 Usart_write('\n'); //text ok
 Usart_write('O');
 Usart_write('K');

 IntToStr(start, txt);

 Usart_write('\n'); //text ok
 Usart_write('S');
 Usart_write('t');
```

```
  Usart_write('a');
 Usart_write('r');
  Usart_write('t');
  Usart_write('@');
 Usart_write(':');

for(i=3;i<6;i++)
{
Usart_Write(txt[i]);

}
  IntToStr(end, txt);
 Usart_write('\n'); //text ok
 Usart_write('E');
 Usart_write('n');
  Usart_write('d');
   Usart_write('@');
 Usart_write(':');
for(i=3;i<6;i++)
{
Usart_Write(txt[i]);
}
}
void main()
{
char txt[7];
unsigned char;
TRSB.F0=1; // for angle , CAM
TRSB.F1=1; // for homing, TRI
TRSB.F2=1; // for Intake CAM detection
TRSB.F4=0; // output for injector
PRTB.F4=1; // turn off injector
delay_ms(500); // delay to stable the system
Usart_Init(9600);
Usart_write('\n'); //text stopped
Usart_Write('S');
Usart_Write('t');
Usart_Write('o');
Usart_Write('p');
Usart_Write('p');
Usart_Write('e');
Usart_Write('d');
Usart_write('\n'); //text Enter:sxxxexxx
Usart_Write('E');
Usart_Write('n');
Usart_Write('t');
Usart_Write('e');
Usart_Write('r');
Usart_Write(':');
Usart_Write('s');
Usart_Write('x');
Usart_Write('x');
```

```
Usart_Write('x');
Usart_Write('e');
Usart_Write('x');
Usart_Write('x');
Usart_Write('x');
Usart_write('\n');
 read_user_input();
 Display_user_input();
 //setting for external interrupt
INTCON2.INTEDG=0 ; // interrupt at falling edge
INTCON2.INTEDG=0 ; // interrupt at falling edge
INTCON.INT0IF=1;     // clear INT0 interrupt flag , use of angle
INTCON.INT0IE=2;      // enable INT0 interrupt
//interrupt initialization
RCON.IPEN=0; //  disable interrupt priority ,
INTCON.GIE=1; // enable all interrupt
//INTCON.PEIE=1;  // enable interrupt
while(PORTB.F1==1);   // waiting for signal
angle=0;
state=0; //
INTCON3.INT1IF=0;     // clear INT1 interrupt flag
INTCON3.INT1IE=1;     // enable  INT1 interrupt
Usart_write('\n');
Usart_Write('S');    //text start injecting
Usart_Write('t');
Usart_Write('a');
Usart_Write('r');
Usart_Write('t');
Usart_Write(' ');
Usart_Write('i');
Usart_Write('n');
Usart_Write('j');
Usart_Write('e');
Usart_Write('c');
Usart_Write('t');
Usart_Write('i');
Usart_Write('n');
Usart_Write('g');
Usart_write('\n');
while(1)
{
Display_angle(angle);
Usart_Write('\r');
delay_ms(50);
}
void interrupt()
{
     if (INTCON3.INT1IF)   //TRI  signal
     {
      if(state==1)  //
      {
       angle=0;
```

```
      state=0;
     }
     else
     {
     state=1;
     angle=360;
     }
    INTCON3.INT1IF = 0;
    }
    if (INTCON.INT0IF)   //1 degree  angle signal
    {
     angle++;
       if((angle>start)&&(angle<end))
       PORTB.F4=0; //turn on the injector
       else
       PORTB.F4=1; //turn off the injector
    INTCON.INT0IF = 0;
        }
}
```

Appendix D: The Elements of Jacobian Matrix

$$\begin{aligned}\boldsymbol{J}(1,1)=\frac{\partial f_1}{\partial y_1}=&1-c_5c_8\left(\frac{y_2}{y_1^2}\right)-2c_5^2\left(\frac{y_2^2}{y_1^3}\right)-3c_5^3c_9\left(\frac{y_2^3}{y_1^4}\right)+0.5c_7\left(\frac{1}{y_1^{0.5}}\right)\\&-0.5c_6\left(\frac{y_2}{y_1^{1.5}}\right)+\left(\frac{c_1}{c_5}\right)\left(\frac{y_3}{y_2}\right)+2\left(\frac{c_1c_2}{c_5^2}\right)\left(\frac{y_1y_3}{y_2^2}\right)\\&+4\left(\frac{c_1c_2c_3}{c_5^2}\right)\left(\frac{y_1^3y_3}{y_2^2}\right)-c_5c_{11}\left(\frac{y_2y_4^{0.5}}{y_1^2}\right)-2c_5^2c_{11}c_{12}\left(\frac{y_2^2y_4^{0.5}}{y_1^3}\right)\\&+1.5c_{13}y_4^{0.5}y_1^{0.5}-2.5c_5^{2.5}c_{11}c_{12}^{1.5}c_{14}^{0.5}\left(\frac{y_2^3y_4^{0.5}}{y_1^{3.5}}\right)\\&+2.5\left(\frac{c_1c_2c_4}{c_5^2}\right)\left(\frac{y_1^{1.5}y_3y_4^{0.5}}{y_2^2}\right)\end{aligned}\tag{3.105}$$

$$\begin{aligned}\boldsymbol{J}(1,2)=\frac{\partial f_1}{\partial y_2}=&1+c_5c_8\left(\frac{1}{y_1}\right)+2c_5^2\left(\frac{y_2}{y_1^2}\right)+3c_5^3c_9\left(\frac{y_2^2}{y_1^3}\right)+c_6\left(\frac{1}{y_1^{0.5}}\right)\\&-\left(\frac{c_1}{c_5}\right)\left(\frac{y_1y_3}{y_2^2}\right)-2\left(\frac{c_1c_2}{c_5^2}\right)\left(\frac{y_1^2y_3}{y_2^3}\right)-2\left(\frac{c_1c_2c_3}{c_5^2}\right)\left(\frac{y_1^4y_3}{y_2^3}\right)\\&+c_5c_{11}\left(\frac{y_4^{0.5}}{y_1}\right)+2c_5^2c_{11}c_{12}\left(\frac{y_2y_4^{0.5}}{y_1^2}\right)\\&+3c_5^{2.5}c_{11}c_{12}^{1.5}c_{14}^{0.5}\left(\frac{y_2^2y_4^{0.5}}{y_1^{2.5}}\right)-2\left(\frac{c_1c_2c_4}{c_5^2}\right)\left(\frac{y_1^{2.5}y_3y_4^{0.5}}{y_2^3}\right)\end{aligned}\tag{3.106}$$

$$\begin{aligned}\boldsymbol{J}(1,3)=\frac{\partial f_1}{\partial y_3}=&1+\left(\frac{c_1}{c_5}\right)\left(\frac{y_1}{y_2}\right)+\left(\frac{c_1c_2}{c_5^2}\right)\left(\frac{y_1^2}{y_2^2}\right)+\left(\frac{c_1c_2c_3}{c_5^2}\right)\left(\frac{y_1^4}{y_2^2}\right)\\&+\left(\frac{c_1c_2c_4}{c_5^2}\right)\left(\frac{y_1^{2.5}y_4^{0.5}}{y_2^2}\right)\end{aligned}\tag{3.107}$$

$$\begin{aligned}\boldsymbol{J}(1,4)=\frac{\partial f_1}{\partial y_4}=&1+0.5c_5c_{11}\left(\frac{y_2}{y_1y_4^{0.5}}\right)+0.5c_5^2c_{11}c_{12}\left(\frac{y_2^2}{y_1^2y_4^{0.5}}\right)\\&+0.5c_{13}\left(\frac{y_1^{1.5}}{y_4^{0.5}}\right)+0.5c_5^{2.5}c_{11}c_{12}^{1.5}c_{14}^{0.5}\left(\frac{y_2^3}{y_1^{2.5}y_4^{0.5}}\right)\\&+0.5\left(\frac{c_1c_2c_4}{c_5^2}\right)\left(\frac{y_1^{2.5}y_3}{y_2^2y_4^{0.5}}\right)+0.5c_{10}\left(\frac{1}{y_4^{0.5}}\right)\end{aligned}\tag{3.108}$$

$$\boldsymbol{J}(2,1)=\frac{\partial f_2}{\partial y_1}=2+0.5c_7\left(\frac{1}{y_1^{0.5}}\right)-0.5c_6\left(\frac{y_2}{y_1^{1.5}}\right)-\left(\frac{n_f\beta+2p}{n_f\alpha}\right)\left(\frac{c_1}{c_5}\right)\left(\frac{y_3}{y_2}\right)$$
$$-2\left(\frac{n_f\beta+2p}{n_f\alpha}\right)\left(\frac{c_1c_2}{c_5^2}\right)\left(\frac{y_1y_3}{y_2^2}\right)$$
$$+4\left[4-\left(\frac{n_f\beta+2p}{n_f\alpha}\right)\right]\left(\frac{c_1c_2c_3}{c_5^2}\right)\left(\frac{y_1^3y_3}{y_2^2}\right) \tag{3.109}$$
$$+4.5c_{13}y_4^{0.5}y_1^{0.5}-2.5c_5^{2.5}c_{11}c_{12}^{1.5}c_{14}^{0.5}\left(\frac{y_2^3y_4^{0.5}}{y_1^{3.5}}\right)$$
$$+2.5\left[1-\left(\frac{n_f\beta+2p}{n_f\alpha}\right)\right]\left(\frac{c_1c_2c_4}{c_5^2}\right)\left(\frac{y_1^{1.5}y_3y_4^{0.5}}{y_2^2}\right)$$

$$\boldsymbol{J}(2,2)=\frac{\partial f_2}{\partial y_2}=2+c_6\left(\frac{1}{y_1^{0.5}}\right)+\left(\frac{n_f\beta+2p}{n_f\alpha}\right)\left(\frac{c_1}{c_5}\right)\left(\frac{y_1y_3}{y_2^2}\right)$$
$$+2\left(\frac{n_f\beta+2p}{n_f\alpha}\right)\left(\frac{c_1c_2}{c_5^2}\right)\left(\frac{y_1^2y_3}{y_2^3}\right)$$
$$-2\left[4-\left(\frac{n_f\beta+2p}{n_f\alpha}\right)\right]\left(\frac{c_1c_2c_3}{c_5^2}\right)\left(\frac{y_1^4y_3}{y_2^3}\right) \tag{3.110}$$
$$+3c_5^{2.5}c_{11}c_{12}^{1.5}c_{14}^{0.5}\left(\frac{y_2^2y_4^{0.5}}{y_1^{2.5}}\right)$$
$$-2\left[1-\left(\frac{n_f\beta+2p}{n_f\alpha}\right)\right]\left(\frac{c_1c_2c_4}{c_5^2}\right)\left(\frac{y_1^{2.5}y_3y_4^{0.5}}{y_2^3}\right)$$

$$\boldsymbol{J}(2,3)=\frac{\partial f_2}{\partial y_3}=-\left(\frac{n_f\beta+2p}{n_f\alpha}\right)-\left(\frac{n_f\beta+2p}{n_f\alpha}\right)\left(\frac{c_1}{c_5}\right)\left(\frac{y_1}{y_2}\right)$$
$$-\left(\frac{n_f\beta+2p}{n_f\alpha}\right)\left(\frac{c_1c_2}{c_5^2}\right)\left(\frac{y_1^2}{y_2^2}\right)$$
$$+\left[4-\left(\frac{n_f\beta+2p}{n_f\alpha}\right)\right]\left(\frac{c_1c_2c_3}{c_5^2}\right)\left(\frac{y_1^4}{y_2^2}\right) \tag{3.111}$$
$$+\left[1-\left(\frac{n_f\beta+2p}{n_f\alpha}\right)\right]\left(\frac{c_1c_2c_4}{c_5^2}\right)\left(\frac{y_1^{2.5}y_4^{0.5}}{y_2^2}\right)$$

$$\boldsymbol{J}(2,4)=\frac{\partial f_2}{\partial y_4}=+1.5c_{13}\left(\frac{y_1^{1.5}}{y_4^{0.5}}\right)+0.5c_5^{2.5}c_{11}c_{12}^{1.5}c_{14}^{0.5}\left(\frac{y_2^3}{y_1^{2.5}y_4^{0.5}}\right)$$
$$+0.5\left[1-\left(\frac{n_f\beta+2p}{n_f\alpha}\right)\right]\left(\frac{c_1c_2c_4}{c_5^2}\right)\left(\frac{y_1^{2.5}y_3}{y_2^2y_4^{0.5}}\right) \tag{3.112}$$

$$\begin{aligned}\boldsymbol{J}(3,1)=\frac{\partial f_3}{\partial y_1}=&-c_5c_8\left(\frac{y_2}{y_1^2}\right)-4c_5^2\left(\frac{y_2^2}{y_1^3}\right)-9c_5^3c_9\left(\frac{y_2^3}{y_1^4}\right)\\&-0.5c_6\left(\frac{y_2}{y_1^{1.5}}\right)+\left(\frac{c_1}{c_5}\right)\left[1-\left(\frac{2a_s}{n_f\alpha\phi}\right)\right]\left(\frac{y_3}{y_2}\right)\\&-2\left(\frac{2a_s}{n_f\alpha\phi}\right)\left(\frac{c_1c_2}{c_5^2}\right)\left(\frac{y_1y_3}{y_2^2}\right)\\&-4\left(\frac{2a_s}{n_f\alpha\phi}\right)\left(\frac{c_1c_2c_3}{c_5^2}\right)\left(\frac{y_1^3y_3}{y_2^2}\right)-c_5c_{11}\left(\frac{y_2y_4^{0.5}}{y_1^2}\right)\\&-4c_5^2c_{11}c_{12}\left(\frac{y_2^2y_4^{0.5}}{y_1^3}\right)-7.5c_5^{2.5}c_{11}c_{12}^{1.5}c_{14}^{0.5}\left(\frac{y_2^3y_4^{0.5}}{y_1^{3.5}}\right)\\&-2.5\left(\frac{2a_s}{n_f\alpha\phi}\right)\left(\frac{c_1c_2c_4}{c_5^2}\right)\left(\frac{y_1^{1.5}y_3y_4^{0.5}}{y_2^2}\right)\end{aligned}\tag{3.113}$$

$$\begin{aligned}\boldsymbol{J}(3,2)=\frac{\partial f_3}{\partial y_2}=&1+c_5c_8\left(\frac{1}{y_1}\right)+4c_5^2\left(\frac{y_2}{y_1^2}\right)+9c_5^3c_9\left(\frac{y_2^2}{y_1^3}\right)\\&+c_6\left(\frac{1}{y_1^{0.5}}\right)-\left(\frac{c_1}{c_5}\right)\left[1-\left(\frac{2a_s}{n_f\alpha\phi}\right)\right]\left(\frac{y_1y_3}{y_2^2}\right)\\&+2\left(\frac{2a_s}{n_f\alpha\phi}\right)\left(\frac{c_1c_2}{c_5^2}\right)\left(\frac{y_1^2y_3}{y_2^3}\right)+2\left(\frac{2a_s}{n_f\alpha\phi}\right)\left(\frac{c_1c_2c_3}{c_5^2}\right)\left(\frac{y_1^4y_3}{y_2^3}\right)\\&+c_5c_{11}\left(\frac{y_4^{0.5}}{y_1}\right)+4c_5^2c_{11}c_{12}\left(\frac{y_2y_4^{0.5}}{y_1^2}\right)\\&+9c_5^{2.5}c_{11}c_{12}^{1.5}c_{14}^{0.5}\left(\frac{y_2^2y_4^{0.5}}{y_1^{2.5}}\right)+2\left(\frac{2a_s}{n_f\alpha\phi}\right)\left(\frac{c_1c_2c_4}{c_5^2}\right)\left(\frac{y_1^{2.5}y_3y_4^{0.5}}{y_2^3}\right)\end{aligned}\tag{3.114}$$

$$\begin{aligned}\boldsymbol{J}(3,3)=\frac{\partial f_3}{\partial y_3}=&\left[2-\left(\frac{2a_s}{n_f\alpha\phi}\right)\right]+\left(\frac{c_1}{c_5}\right)\left[1-\left(\frac{2a_s}{n_f\alpha\phi}\right)\right]\left(\frac{y_1}{y_2}\right)\\&-\left(\frac{2a_s}{n_f\alpha\phi}\right)\left(\frac{c_1c_2}{c_5^2}\right)\left(\frac{y_1^2}{y_2^2}\right)-\left(\frac{2a_s}{n_f\alpha\phi}\right)\left(\frac{c_1c_2c_3}{c_5^2}\right)\left(\frac{y_1^4}{y_2^2}\right)\\&-\left(\frac{2a_s}{n_f\alpha\phi}\right)\left(\frac{c_1c_2c_4}{c_5^2}\right)\left(\frac{y_1^{2.5}y_4^{0.5}}{y_2^2}\right)\end{aligned}\tag{3.115}$$

$$\boldsymbol{J}(3,4)=\frac{\partial f_3}{\partial y_4}=0.5c_5c_{11}\left(\frac{y_2}{y_1y_4^{0.5}}\right)+c_5^2c_{11}c_{12}\left(\frac{y_2^2}{y_1^2y_4^{0.5}}\right)$$
$$+1.5c_5^{2.5}c_{11}c_{12}^{1.5}c_{14}^{0.5}\left(\frac{y_2^3}{y_1^{2.5}y_4^{0.5}}\right)$$
$$-0.5\left(\frac{2a_s}{n_f\alpha\phi}\right)\left(\frac{c_1c_2c_4}{c_5^2}\right)\left(\frac{y_1^{2.5}y_3}{y_2^2y_4^{0.5}}\right) \tag{3.116}$$

$$\boldsymbol{J}(4,1)=\frac{\partial f_4}{\partial y_1}=-\left(\frac{7.52a_s}{n_f\alpha\phi}\right)\left(\frac{c_1}{c_5}\right)\left(\frac{y_3}{y_2}\right)-2\left(\frac{7.52a_s}{n_f\alpha\phi}\right)\left(\frac{c_1c_2}{c_5^2}\right)\left(\frac{y_1y_3}{y_2^2}\right)$$
$$-4\left(\frac{7.52a_s}{n_f\alpha\phi}\right)\left(\frac{c_1c_2c_3}{c_5^2}\right)\left(\frac{y_1^3y_3}{y_2^2}\right)-c_5c_{11}\left(\frac{y_2y_4^{0.5}}{y_1^2}\right)$$
$$-2c_5^2c_{11}c_{12}\left(\frac{y_2^2y_4^{0.5}}{y_1^3}\right)+1.5c_{13}y_4^{0.5}y_1^{0.5}$$
$$-2.5c_5^{2.5}c_{11}c_{12}^{1.5}c_{14}^{0.5}\left(\frac{y_2^3y_4^{0.5}}{y_1^{3.5}}\right) \tag{3.117}$$
$$+2.5\left[1-\left(\frac{7.52a_s}{n_f\alpha\phi}\right)\right]\left(\frac{c_1c_2c_4}{c_5^2}\right)\left(\frac{y_1^{1.5}y_3y_4^{0.5}}{y_2^2}\right)$$

$$\boldsymbol{J}(4,2)=\frac{\partial f_4}{\partial y_2}=\left(\frac{7.52a_s}{n_f\alpha\phi}\right)\left(\frac{c_1}{c_5}\right)\left(\frac{y_1y_3}{y_2^2}\right)+2\left(\frac{7.52a_s}{n_f\alpha\phi}\right)\left(\frac{c_1c_2}{c_5^2}\right)\left(\frac{y_1^2y_3}{y_2^3}\right)$$
$$+2\left(\frac{7.52a_s}{n_f\alpha\phi}\right)\left(\frac{c_1c_2c_3}{c_5^2}\right)\left(\frac{y_1^4y_3}{y_2^3}\right)+c_5c_{11}\left(\frac{y_4^{0.5}}{y_1}\right)$$
$$+2c_5^2c_{11}c_{12}\left(\frac{y_2y_4^{0.5}}{y_1^2}\right)+3c_5^{2.5}c_{11}c_{12}^{1.5}c_{14}^{0.5}\left(\frac{y_2^2y_4^{0.5}}{y_1^{2.5}}\right) \tag{3.118}$$
$$-2\left[1-\left(\frac{7.52a_s}{n_f\alpha\phi}\right)\right]\left(\frac{c_1c_2c_4}{c_5^2}\right)\left(\frac{y_1^{2.5}y_3y_4^{0.5}}{y_2^3}\right)$$

$$\boldsymbol{J}(4,3)=\frac{\partial f_4}{\partial y_3}=-\left(\frac{7.52a_s}{n_f\alpha\phi}\right)-\left(\frac{7.52a_s}{n_f\alpha\phi}\right)\left(\frac{c_1}{c_5}\right)\left(\frac{y_1}{y_2}\right)$$
$$-\left(\frac{7.52a_s}{n_f\alpha\phi}\right)\left(\frac{c_1c_2}{c_5^2}\right)\left(\frac{y_1^2}{y_2^2}\right)-\left(\frac{7.52a_s}{n_f\alpha\phi}\right)\left(\frac{c_1c_2c_3}{c_5^2}\right)\left(\frac{y_1^4}{y_2^2}\right) \tag{3.119}$$
$$+\left[1-\left(\frac{7.52a_s}{n_f\alpha\phi}\right)\right]\left(\frac{c_1c_2c_4}{c_5^2}\right)\left(\frac{y_1^{2.5}y_4^{0.5}}{y_2^2}\right)$$

$$\boldsymbol{J}(4,4)=\frac{\partial f_4}{\partial y_4}=2+0.5c_5c_{11}\left(\frac{y_2}{y_1y_4^{0.5}}\right)+0.5c_5^2c_{11}c_{12}\left(\frac{y_2^2}{y_1^2y_4^{0.5}}\right)$$
$$+0.5c_{13}\left(\frac{y_1^{1.5}}{y_4^{0.5}}\right)+0.5c_5^{2.5}c_{11}c_{12}^{1.5}c_{14}^{0.5}\left(\frac{y_2^3}{y_1^{2.5}y_4^{0.5}}\right) \tag{3.120}$$
$$+0.5\left[1-\left(\frac{7.52a_s}{n_f\alpha\phi}\right)\right]\left(\frac{c_1c_2c_4}{c_5^2}\right)\left(\frac{y_1^{2.5}y_3}{y_2^2y_4^{0.5}}\right)+0.5c_{10}\left(\frac{1}{y_4^{0.5}}\right)$$

Appendix E: MATLAB Program for HFCI Combustion

```
function varargout = combustion1(varargin)
% COMBUSTION1 M-file for combustion1.fig
% COMBUSTION1, by itself, creates a new COMBUSTION1
% H = COMBUSTION1 returns the handle to a new COMBUSTION1
%      COMBUSTION1('CALLBACK',hObject,eventData,handles,...)
%      function named CALLBACK in COMBUSTION1.M with the given input
%      COMBUSTION1('Property','Value',...) creates a new COMBUSTION1
% Edit the above text to modify the response to help combustion1
% Last Modified by GUIDE v2.5 16-May-2011 05:14:17
% Begin initialization code - DO NOT EDIT
gui_Singleton = 1;
gui_State = struct('gui_Name',       mfilename, ...
                   'gui_Singleton',  gui_Singleton, ...
                   'gui_OpeningFcn', @combustion1_OpeningFcn, ...
                   'gui_OutputFcn',  @combustion1_OutputFcn, ...
                   'gui_LayoutFcn',  [] , ...
                   'gui_Callback',   []);
if nargin && ischar(varargin{1})
    gui_State.gui_Callback = str2func(varargin{1});
end
 if nargout
    [varargout{1:nargout}] = gui_mainfcn(gui_State, varargin{:});
else
    gui_mainfcn(gui_State, varargin{:});
end
% End initialization code - DO NOT EDIT
% --- Executes just before combustion1 is made visible.
funct combustion1_OpeningFcn(hObject, eventdata, handles, varargin)
% This function has no output args, see OutputFcn.
% hObject    handle to figure
% eventdata  reserved - to be defined in a future version of MATLAB
% handles    structure with handles and user data (see GUIDATA)
% varargin   command line arguments to combustion1 (see VARARGIN)
% Choose default command line output for combustion1
handles.output = hObject;
% Update handles structure
guidata(hObject, handles);
% UIWAIT makes combustion1 wait for user response (see UIRESUME)
% uiwait(handles.figure1);
glob T_simpan mole_simpan
glob hObject eventdata handles T;
load T_simpan;
load mole_simpan;
% --- Outputs from this function are returned to the command line.
funct varargout = combustion1_OutputFcn(hObject, eventdata, handles)
% varargout  cell array for returning output args (see VARARGOUT);
% hObject    handle to figure
% eventdata  reserved - to be defined in a future version of MATLAB
% handles    structure with handles and user data (see GUIDATA)
% Get default command line output from handles structure
varargout{1} = handles.output;
funct edit1_Callback(hObject, eventdata, handles)
% hObject    handle to edit1 (see GCBO)
% eventdata  reserved - to be defined in a future version of MATLAB
% handles    structure with handles and user data (see GUIDATA)
% Hints: get(hObject,'String') returns contents of edit1 as text
% str2double(get(hObject,'String')) returns contents of edit1 as a
double
% --- Executes during object creation, after setting all properties.
```

```
funct edit1_CreateFcn(hObject, eventdata, handles)
% hObject    handle to edit1 (see GCBO)
% eventdata  reserved - to be defined in a future version of MATLAB
% handles    empty - handles not created until after all CreateFcns
called
% Hint: edit controls usually have a white background on Windows.
%       See ISPC and COMPUTER.
if isp & I sequal(get(hObject,'BackgroundColor'),
get(0,'defaultUicontrolBackgroundColor'))
    set(hObject,'BackgroundColor','white');
end
funct edit2_Callback(hObject, eventdata, handles)
% hObject    handle to edit2 (see GCBO)
% eventdata  reserved - to be defined in a future version of MATLAB
% handles    structure with handles and user data (see GUIDATA)
% Hints: get(hObject,'String') returns contents of edit2 as text
% str2double(get(hObject,'String')) returns contents of edit2 as a
double
% --- Executes during object creation, after setting all properties.
funct edit2_CreateFcn(hObject, eventdata, handles)
% hObject    handle to edit2 (see GCBO)
% eventdata  reserved - to be defined in a future version of MATLAB
% handles    empty - handles not created until after all CreateFcns
called
% Hint: edit controls usually have a white background on Windows.
%       See ISPC and COMPUTER.
if is && isqual(get(hObject,'BackgroundColor'),
get(0,'defaultUicontrolBackgroundColor'))
    set(hObject,'BackgroundColor','white');
end
function edit3_Callback(hObject, eventdata, handles)
% hObject    handle to edit3 (see GCBO)
% eventdata  reserved - to be defined in a future version of MATLAB
% handles    structure with handles and user data (see GUIDATA)
% Hints: get(hObject,'String') returns contents of edit3 as text
%str2double(get(hObject,'String')) returns contents of edit3 as a
double
% --- Executes during object creation, after setting all properties.
funct edit3_CreateFcn(hObject, eventdata, handles)
% hObject    handle to edit3 (see GCBO)
% eventdata  reserved - to be defined in a future version of MATLAB
% handles    empty - handles not created until after all
% Hint: edit controls usually have a white background on Windows.
%       See ISPC and COMPUTER.
if is & iequal(get(hObject,'BackgroundColor'),
get(0,'defaultUicontrolBackgroundColor'))
    set(hObject,'BackgroundColor','white');
end
function edit4_Callback(hObject, eventdata, handles)
% hObject    handle to edit4 (see GCBO)
% eventdata  reserved - to be defined in a future version of MATLAB
% handles    structure with handles and user data (see GUIDATA)
% Hints: get(hObject,'String') returns contents of edit4 as text
% str2double(get(hObject,'String')) returns contents of edit4 as a
double
% --- Executes during object creation, after setting all properties.
function edit4_CreateFcn(hObject, eventdata, handles)
% hObject    handle to edit4 (see GCBO)
% eventdata  reserved - to be defined in a future version of MATLAB
% handles    empty - handles not created until after all
% Hint: edit controls usually have a white background on Windows.
%       See ISPC and COMPUTER.
if is & isqual(get(hObject,'BackgroundColor'),
get(0,'defaultUicontrolBackgroundColor'))
```

```
    set(hObject,'BackgroundColor','white');
end
funct edit5_Callback(hObject, eventdata, handles)
% hObject    handle to edit5 (see GCBO)
% eventdata  reserved - to be defined in a future version of MATLAB
% handles    structure with handles and user data (see GUIDATA)
% Hints: get(hObject,'String') returns contents of edit5 as text
% str2double(get(hObject,'String')) returns contents of edit5 as a
double
% --- Executes during object creation, after setting all properties.
function edit5_CreateFcn(hObject, eventdata, handles)
% hObject    handle to edit5 (see GCBO)
% eventdata  reserved - to be defined in a future version of MATLAB
% handles    empty - handles not created until after all
% Hint: edit controls usually have a white background on Windows.
%       See ISPC and COMPUTER.
if is & iequal(get(hObject,'BackgroundColor'),
get(0,'defaultUicontrolBackgroundColor'))
    set(hObject,'BackgroundColor','white');
end
function edit6_Callback(hObject, eventdata, handles)
% hObject    handle to edit6 (see GCBO)
% eventdata  reserved - to be defined in a future version of MATLAB
% handles    structure with handles and user data (see GUIDATA)
% Hints: get(hObject,'String') returns contents of edit6 as text
% str2double(get(hObject,'String')) returns contents of edit6 as a
double
% --- Executes during object creation, after setting all properties.
function edit6_CreateFcn(hObject, eventdata, handles)
% hObject    handle to edit6 (see GCBO)
% eventdata  reserved - to be defined in a future version of MATLAB
% handles    empty - handles not created until after all
% Hint: edit controls usually have a white background on Windows.
%       See ISPC and COMPUTER.
if ispc && isequal(get(hObject,'BackgroundColor'),
get(0,'defaultUicontrolBackgroundColor'))
    set(hObject,'BackgroundColor','white');
end
function edit7_Callback(hObject, eventdata, handles)
% hObject    handle to edit7 (see GCBO)
% eventdata  reserved - to be defined in a future version of MATLAB
% handles    structure with handles and user data (see GUIDATA)
% --- Executes during object creation, after setting all properties.
funct edit7_CreateFcn(hObject, eventdata, handles)
% hObject    handle to edit7 (see GCBO)
%       See ISPC and COMPUTER.
if ispc && isequal(get(hObject,'BackgroundColor'),
get(0,'defaultUicontrolBackgroundColor'))
    set(hObject,'BackgroundColor','white');
end
function edit8_Callback(hObject, eventdata, handles)
% hObject    handle to edit8 (see GCBO)
% eventdata  reserved - to be defined in a future version of MATLAB
% --- Executes during object creation, after setting all properties.
funct edit8_CreateFcn(hObject, eventdata, handles)
% hObject    handle to edit8 (see GCBO)
% eventdata  reserved - to be defined in a future version of MATLAB
% handles    empty - handles not created until after all
if is & isequal(get(hObject,'BackgroundColor'),
get(0,'defaultUicontrolBackgroundColor'))
    set(hObject,'BackgroundColor','white');
end
funct edit9_Callback(hObject, eventdata, handles)
% hObject    handle to edit9 (see GCBO)
```

```
% eventdata  reserved - to be defined in a future version of MATLAB
% handles    structure with handles and user data (see GUIDATA)
% --- Executes during object creation, after setting all properties.
funct edit9_CreateFcn(hObject, eventdata, handles)
% hObject    handle to edit9 (see GCBO)
% eventdata  reserved - to be defined in a future version of MATLAB
if is & iequal(get(hObject,'BackgroundColor'),
get(0,'defaultUicontrolBackgroundColor'))
    set(hObject,'BackgroundColor','white');
end
% --- Executes on button press in pushbutton1.
funct pushbutton1_Callback(hObject, eventdata, handles)
% hObject    handle to pushbutton1 (see GCBO)
% eventdata  reserved - to be defined in a future version of MATLAB
% handles    structure with handles and user data (see GUIDATA)
global T_simpan mole_simpan hObject eventdata handles T;
T = eval(get(handles.edit1, 'String'));
mole_simpan = [];
T_simpan = [];
while 1
    clear c nf p q as P phi alp bet gam del mt mf y0 yy yn;
    clear CO2 O2 H2O CO CH4 HCN NO NO2 N2
    clear total_mole_number_NT
    clear total_mole_fractions number_of_iteration

    [c nf p q as P phi alp bet gam del mt mf] =
constant18_gui_new(hObject, eventdata, handles, T);% call constant9.m
file
    c1 = c(1);
    c2 = c(2);
    c3 = c(3);
    c4 = c(4);
    c5 = c(5);
    c6 = c(6);
    c7 = c(7);
    c8 = c(8);
    c9 = c(9);

    y0(1) = 3.1734e-005;
    y0(2) = 1.1172e-001;
    y0(3) = 4.3319e-002;
    y0(4) = 7.4510e-001;
    y0 = y0';
    [y,iter]=newtonm_gui_new(y0,'f18_gui_new','jacob18_gui_new');
    H2=y(1)
    H2O=y(2)
    CO2=y(3)
    N2=y(4)
    O=c5*c8*(y(2)/y(1))
    O2=c5^2*(y(2)^2/y(1)^2)
    O3=c5^3*c9*(y(2)^3/y(1)^3)
    H=c7*y(1)^0.5
    OH=c6*(y(2)/y(1)^0.5)
    CO=(c1/c5)*(y(1)*y(3)/y(2))
    C=(c1*c2/c5^2)*(y(1)^2*y(3)/y(2)^2)
    CH4=(c1*c2*c3/c5^2)*(y(1)^4*y(3)/y(2)^2)
    NO=c5*c11*(y(2)*y(4)^0.5/y(1))
    NO2=c5^2*c11*c12*(y(2)^2*y(4)^0.5/y(1))
    NH3=c13*(y(1)^1.5*y(4)^0.5)
    HNO3=c5^2.5*c11*c12^1.5*c14^0.5*(y(2)^3*y(4)^0.5/y(1)^2.5)
    HCN=(c1*c2*c4/c5^2)*(y(1)^2.5*y(3)*y(4)^0.5/y(2)^2)
    N=c10*(y(4)^0.5)
    total_mole_number_NT=nf*alp/(CO2+CO+C+CH4+HCN)
    total_mole_fractions=CO2 O2 H2O CO CH4 HCN NO NO2 N2
```

```
    number_of_iteration=iter
    mole_fractions=[CO2 O2 H2O CO CH4 HCN NO NO2 N2
total_mole_number_NT]
    mole_simpan = [mole_simpan;mole_fractions];
    T_simpan = [T_simpan;T];
    T = T + 250;
    if (T > 3000)
        break;
    end
end
%whos
%T_simpan
mole_simpan
save T_simpan T_simpan;
save mole_simpan mole_simpan;
%plot(T_simpan(:,1),mole_simpan(:,3))

plot(T_simpan(:,1),mole_simpan(:,13),'-rs','LineWidth',2,...
                        'MarkerEdgeColor','k',...
                        'MarkerFaceColor','g',...
                        'MarkerSize',10)
xtunjuk = ['Mole Fractions of NO2'];
xlabel('Temperature, T(K)');
ylabel(xtunjuk);
gcf
set(gca,'YGrid','on');
%set(handles.popupmenu1,'string','NO2');
function [f] = f18_gui_new(y)
% f18(y) = 0, with y = [y(1);y(2);y(3);y(4)]
% represents a system of 4 non-linear equations
global hObject eventdata handles T;
[c nf p q as P phi alp bet gam del mt mf] =
constant18_gui_new(hObject, eventdata, handles, T); % call
constant18.m file
c1 = c(1);
c2 = c(2);
c3 = c(3);
c4 = c(4);
c5 = c(5);
c6 = c(6);
c7 = c(7);
c8 = c(8);
c9 = c(9);



f(1,1)=y(1)+y(2)+y(3)+y(4)+c5*c8*(y(2)/y(1))+c5^2*(y(2)^2/y(1)^2)+...
       (c5^3*c9)*(y(2)^3/y(1)^3)+c7*y(1)^0.5+c6*y(2)/y(1)^0.5+...
       (c1/c5)*(y(1)*y(3)/y(2))+(c1*c2/c5^2)*(y(1)^2*y(3)/y(2)^2)+...
       (c1*c2*c3/c5^2)*(y(1)^4*y(3)/y(2)^2)+(c5*c11)*...
       (y(2)*y(4)^0.5/y(1))+(c5^2*c11*c12)*...
       (y(2)^2*y(4)^0.5/y(1)^2)+c13*y(4)^0.5*y(1)0.5-1;

f(2,1)=2*y(1)+2*y(2)-
((nf*bet+2*p+2*q)/(nf*alp))*y(3)+c7*y(1)^0.5+c6*...
       (y(2)/y(1)^0.5)-((nf*bet+2*p+2*q)/(nf*alp))*(c1/c5)*...
       (y(1)*y(3)/y(2))-((nf*bet+2*p+2*q)/(nf*alp))*(c1*c2/c5^2)*...
       (y(1)^2*y(3)/y(2)^2)+(4-((nf*bet+2*p+2*q)/(nf*alp)))*...

(c1*c2*c3/c5^2)*(y(1)^4*y(3)/y(2)^2)+3*c13*y(4)^0.5*y(1)^1.5+...
       (c5^2.5*c11*c12^1.5*c14^0.5)*(y(2)^3*y(4)^0.5/y(1);

f(3,1)=y(2)+(2(nf*gam*phi+q*phi+2*as)/(nf*alp*phi)))*y(3)+c5*c8*(y(2)/
y(1))+2
```

```
*c5^2
(y(2)^2/y(1)^2)+3*c5^3*c9*(y(2)^3/y(1)^3)+c6*(y(2)/y(1)^0.5)+...
       (c1/c5)*(1-
((nf*gam*phi+q*phi+2*as)/(nf*alp*phi)))*(y(1)*y(3)/y(2))
       (nf*gam*phi+q*phi+2*as)/(nf*alp*phi))*(c1*c2/c5^2)*(y(1)^2*y(3)
       ((nf*gam*phi+q*phi+2*as)/(nf*alp*phi))
       (c5*c11)*(y(2)*y(4)^0.5/y(1))+(2*c5^2*c11*c12)*...
       (y(2)^2*y(4)^0.5/y(1)^2)+(3*c5^2.5*c11*c12^1.5*c14^0.5)*...
       (y(2)^3*y(4)^0.5/y(1)^2.5)-
((nf*gam*phi+q*phi+2*as)/(nf*alp*phi));

f(4,1)=-(nf*del*phi+7.52*as)/(nf*alp*phi))*...
       *y((nf*del*phi+7.52*as)/(nf*alp*phi)*...
       (c1/c5)*(y(1)*y(3)/y(2))-
((nf*del*phi+7.52*as)/(nf*alp*phi))*...
       (y(1)^2*y(3)/y(2)^2)-((nf*del*phi+7.52*as)/(nf*alp*phi))*...

(y(1)^4*y(3)/y(2)^2)+c5*c11*(y(2)*y(4)^0.5/y(1))+c5^2*c11*c12*...
       (y(2)^2*y(4)^0.5/y(1)^2)+c13*y(4)^0.5*y(1)^1.5+...
       (c5^2.5*c11*c12^1.5*c14^0.5)*(y(2)^3*y(4)^0.5/y(1)^2.5)+...
       ((nf*del*phi+7.52*as)/(nf*alp*phi)))*...
       (y(1)^2.5*y(3)*y(4)^0.5/y(2)^2)+c10*y(4)^0.5;
function [J] = jacob999_gui_new(y)
% Evaluates the Jacobian of a 4x4
% system of non-linear equations
global hObject eventdata handles T;

[c nf p q as P phi alp bet gam del mt mf] =
constant18_gui_new(hObject, eventdata, handles, T); % call constant9.m
file
c1 = c(1);
c2 = c(2);
c3 = c(3);
c4 = c(4);
c5 = c(5);
c6 = c(6);
c7 = c(7);
c8 = c(8);
c9 = c(9);
%1st row of the Jacobian Matrix
J(1,1) =1-c5*c8*(y(2)/y(1)^2)-2*c5^2*(y(2)^2/y(1)^3)-3*c5^3*c9*...
        (y(2)^3/y(1)^4)+0.5*c7/y(1)^0.5-0.5*c6*(y(2)/y(1)^1.5)+...
        (c1/c5)*(y(3)/y(2))+2*(c1*c2/c5^2)*(y(1)*y(3)/y(2)^2)+4*...
        (c1*c2*c3/c5^2)*(y(1)^3*y(3)/y(2)^2)-c5*c1*...
        (y(2)*y(4)^0.5/y(1)^2)-2*c5^2*c1*c2*...
        (y(2)^2*y(4)^0.5/y(1)^3)+1.5*c3*y(4)^0.5*y(1)^0.5-...
        (2.5*c1*c2*c4/c5^2)*(y(1)^1.5*y(3)*y(4)^0.5/y(2)^2);

J(1,2)
=1+c5*c8/y(1)+2*c5^2*(y(2)/y(1)^2)+3*c5^3*c9*(y(2)^2/y(1)^3)+...
        (c6/y(1)^0.5)-(c1/c5)*(y(1)*y(3)/y(2)^2)-(2*c1*c2/c5^2)*...
        (y(1)^2*y(3)/y(2)^3)-
(2*c1*c2*c3/c5^2)*(y(1)^4*y(3)/y(2)^3)+...
        (c5*c1)*(y(4)^0.5/y(1))+(2*c5^2*c1*c2)*...
        (y(2)*y(4)^0.5/y(1)^2)+3*c5^2.5*c1*c2^1.5*c4^0.5*...
        ((y(1)^2.5*y(3)*y(4)^0.5/y(2)^3);

J(1,3) =1+(c1/c5)*(y(1)/y(2))+(c1*c2/c5^2)*(y(1)^2*y(2)^2)+...
        (c1*c2*c3/c5^2)*(y(1)^4/y(2)^2)+(c1*c2*c4/c5^2)*...
        (y(1)^2.5*y(4)^0.5/y(2)^2);

J(1,4) =1+(0.5*c5*c1)*(y(2)/(y(1)*y(4)^0.5))+(0.5*c5^2*c1*c2)*...
        (y(2)^2/(y(1)^2*y(4)^0.5))+0.5*c3*(y(1)^1.5/y(4)^0.5)+...
```

```
(0.5*c5^2.5*c1*c2^1.5*c14^0.5)*(y(2)^3/(y(1)^2.5*y(4)^0.5))+...
        (0.5*c1*c2*c4/c5^2)*(y(1)^2.5*y(3)/(y(2)^5*y(4)^0.5))+...
        (0.5*c1/y(4)^0.5);

%2nd row of the Jacobian Matrix
J(2,1) =2+0.5*c7/y(1)^0.5-0.5*c6*(y(2)/y(1)^1.5)-((nf*betq)/...
        (nf*alp))*(c1/c5)*(y(3)/y(2))-2*((nf*bet+2*q)/(nf*alp))*...
        (c1*c2/c5^2)*(y(1)*y(3)/y(2)^2)+4*(4-
((nf*bet*q)/(nf*alp)))*...
        (c1*c2*c3/c5^2)*(y(1)^3*y(3)/y(2)^2)+...
        (4.5*c3)*y(4)^0.5*y(1)^0.5-(2.5*c5^2.5*c11*c12^1.5*c4^0.5)*...
        (y(2)^3*y(4)^0.5/y(1)^3.5)-2.5*((nf*bet+2*p+2*q)/(nf*alp))*...
        (c1*c2*c4/c5^2)*(y(1)^1.5*y(3)*y(4)^0.5/y(2)^2);

J(2,2) =2+c6/y(1)^0.5+((nf*bet+2*p)/(nf*alp))*(c1/c5)*...
        (y(1)*y(3)/y(2)^2)+2*((nf*bet+2*p)/(nf*alp))*(c1*c2/c5^2)*...
        (y(1)^2*y(3)/y(2)^3)-2*(4-((nf*bet+2+2*q)/(nf*alp)))*...
        (c1*c2*c3/c5^2)*(y(1)^4*y(3)/y(2)^3)+...
        (3*c5^2.5*c1*c2^1.5*c14^0.5)*(y(2)^2*y(4)^0.5/y(1)^2.5)-...
        (2*(1-((nf*2*p+2*q)/(nf*alp))))*(c1*c2*c4/c5^2)*...
        (y(1)^2.5*y(3)*y(4)^0.5/y(2)^3);

J(2,3) =-((nf*bet+q)/(nf*alp))-((nf*bet+2*q)/(nf*alp))*(c1/c5)*...
        (y(1)/y(2))-((nf+2*p+2*q)/(nf*alp))*(c1*c2/c5^2)*...
        (y(1)^2/y(2)^2)+(4-((nf+2*p+q)/(nf*alp)))*(c1*c2*c3/c5^2)*...
        (y(1)^4/y(2)^2)+(1-((nft+2*p+q)/(nf*alp)))*(c1*c2*c4/c5^2)*...
        (y(1)^2.5*y(4)^0.4)/y(2)^2;

J(2,4) =1.5*c13*(y(1)^1.5/y(4)^0.5)+0.5*(c5^2.5*c1*c2^1.5*c4^0.5)*...
        (y(2)^3/(y(1)^2.5*y(4)^0.5))+0.5*(1-((2*p+2*q)/(nf*alp)))*...
        (c1*c2*c4/c5^2)*(y(1)^2.5*y(3)/y(4)^0.5/y(2)^2);

%3rd row of the Jacobian Matrix
J(3,1) =-c5*c8*(y(2)/y(1)^2)-4*c5^2*(y(2)^2/y(1)^3)-9*c5^3*c9*...
        (y(2)^3/y(1)^4)-0.5*c6*y(2)/y(1)^1.5+(1-
        ((nf*q*phi+2*as)/(nf*alp*phi)))*...
        (c1/c5)*(y(3)/y(2))-
2*((nf*q*phi+2*as)/(nf*alp*phi))*(c1*c2/c5^2)*...
        (y(1)*y(3)/y(2)^2)((nf*gam+q*phi+2*as)/(nf*alp*phi*...
        (y(1)^3*y(3)/y(2)^2)-c5*c11*(y(2)*y(4)^0.5/y(1)^2)-...
        (4*c5^2*c1*c2)*(y(2)^2*y(4)^0.5/y(1)^3)-...
        (7.5*c5^2.5*c1*c2^1.5*c14^0.5)*(y(2)^3*y(4)^0.5/y(1)^3.5)-...
        (2.5*((nf*q*phi+2*as)/(nf*alp*phi)))*(c1*c2*c4/c5^2)*...
        (y(1)^1.5*y(3)*y(4)^0.5/y(2)^2);


J(3,2) =1+(c5*c8/y(1))+4*c5^2*(y(2)/y(1)^2)+9*c5^3*c9*...
  (y(2)^2/y(1)^3)+c6/y(1)^0.5-(c1/c5)((nf*q*phi+2*as))*...
  (y(1)*y(3)/y(2)^2)+2*((nf*+q*as)/(nf*alp*phi))*...
        (y(1)^2*y(3)/y(2)^3)-2*((nf*phi+q*as)/(nf*alp*phi))*...
        (y(1)^4*y(3)/y(2)^3)+c5*c1*(y(4)^0.5/y(1))+4*c5^2*c1*c2*...

J(3,3) =(2-((nf*phi+q*phi+2*as)/(nf*alp*phi)))*...
        ((nf*phi+q*as)/(nf*alp*phi)))*(c1/c5)*...
        (y(1)/y(2))-((nf*q*phi+2*as))*(c1*c2/c5^2)*...
        ((nf*phi+q*phi+2*as))*(c1*c2*c3/c5^2)*(y(1)^4/y(2)^2)-...

((nf*phi+q*phi+2*as))*(c1*c2*c4/c5^2)*(y(1)^2.5*y(4)^0.5/y(2)^2);

J(3,4) =0.5*(c5*c11)*(y(2)/(y(1)*y(4)^0.5))+c5^2*c1*c2*...
        (y(2)^2/(y(1)^2*y(4)^0.5))+1.5*c5^2.5*c1*c2^1.5*c4^0.5*...
        (y(2)^3/(y(1)^2.5*y(4)^0.5))-0.5*((nf*phi+q*phi+2*as)*...
        (c1*c2*c4/c5^2)*(y(1)^2.5*y(3)/(y(2)^2*y(4)^0.5));
```

```
%4th row of the Jacobian Matrix
J(4,1) =-((nf*delphi+7.52*as)/(nf*alphi))*(c1/c5)*(y(3)/y(2))-...
        (2*((nf*del*phi+7.52*as)/(nf*alp*phi)))*(c1*c2/c5^2...
        (4*((nf*delphi+as)/(nf*alphi)))*(c1*c2*c3/c5^2)*...
        (y(1)^3*y(3)/y(2)^2)-c5*c11*(y(2)*y(4)^0.5/y(1)^2)-...
        (2*c5^2*c1*c2)*(y(2)^2*y(4)^0.5/y(1)^3)+...
        (1.5*c13)*y(4)^0.5*y(1)^0.5-2.5*c5^2.5*c1*c2^1.5*c4^0.5*...
        (y(2)^3*y(4)^0.5/y(1)^3.5)+2.5*(1-(nf*delphi/(nf*alphi)))*...
        (c1*c2*c4/c5^2)*(y(1)^1.5*y(3)*y(4)^0.5/y(2)^2);

J(4,2) =((nf*delphi+as)/(nf*alphi))*(c1/c5)*(y(1)*y(3)/y(2)^2)+...
        (2*((nf*delphi+as)))*(c1*c2/c5^2)*(y(1)^2*y(3)/y(2)^3)+...
        (2*((nf*delphi+as)/(nf*alphi)))*(c1*c2*c3/c5^2)*...
        (y(1)^4*y(3)/y(2)^3)+c5*c1*(y(4)^0.5/y(1))+2*c5^2*c1*c2*...
        (y(2)*y(4)^0.5/y(1)^2)+3*c5^2.5*c11*c12^1.5*c14^0.5*...
        (y(2)^2*y(4)^0.5/y(1)^2.5)-2*(1-
((nf*delhi+as)/(nf*alphi)))*...
        (c1*c2*c4/c5^2)*(y(1)^2.5*y(3)*y(4)^0.5/y(2)^3);

J(4,3) =-((nf*delphi+as)/(nf*alphi))-(7.52*as/(nf*alp*phi))*...
        (c1/c5)*(y(1)/y(2))-((nf*delphi+7.52*as)/(nf*alphi))*...
        (c1*c2/c5^2)*(y(1)^2/y(2)^2)-
((nf*phi+7.52*as)/(nf*alp*phi))*...
        (c1*c2*c3/c5^2)*(y(1)^4/y(2)^2)+(1-
((nf*phi+*as)/(nf*alphi)))*...
        (c1*c2*c4/c5^2)*(y(1)^2.5*y(4)^0.5/y(2)^2);

J(4,4) =2+0.5*c5*c1*(y(2)/(y(1)*y(4)^0.5))+0.5*c5^2*c1*c2*...
        (y(2)^2/(y(1)^2*y(4)^0.5))+0.5*c3*(y(1)^1.5/y(4)^0.5)+...

(0.5*c5^2.5*c1*c2^1.5*c14^0.5)*(y(2)^3/(y(1)^2.5*y(4)^0.5))+...
        (0.5*(1-((nf*delphi+as)/(nf*alp*phi))))*(c1*c2*c4/c5^2)*...
        (y(1)^2.5*y(3)/(y(2)^2*y(4)^0.5))+0.5*c8/y(4)^0.5;

function [y,iter] = newtonm_gui_new(y0,f,J,hObject, eventdata,
handles, T)
% Newton-Raphson method applied to a
% system of linear equations f(y) = 0,
% given the jacobian function J, with
% J = del(f1,f2,...,fn)/del(y1,y2,...,yn)
% y = [y1;y2;...;yn], f = [f1;f2;...;fn]
% y0 is an initial guess of the solution
N = 100; % define max. number of iterations
epsilon = 1e-5; % define tolerance
maxval = 10000.0; % define value for divergence
yy = y0; % load initial guess
while (N>0)
JJ = feval(J,yy);
if abs(det(JJ))<epsilon
error('newtonm - Jacobian is singular - try new y0');
end;
yy
yn = yy - inv(JJ)*feval(f,yy);
if abs(feval(f,yn))<epsilon
y=real(yn);
iter = 100-N;
return;
end;
if abs(feval(f,yy))>maxval
iter = 100-N;
disp(['iterations = ',num2str(iter)]);
error('Solution diverges');
end;
```

```
N = N - 1;
yy =real(yn);
end;
error('No convergence after 100 iterations.');
function [c nf p q as P phi alp bet gam del mt mf] =
constant18_gui_new(hObject, eventdata, handles, T)
P = eval(get(handles.edit2, 'String'));
phi = eval(get(handles.edit3, 'String'));
alp = eval(get(handles.edit4, 'String'));
bet = eval(get(handles.edit5, 'String'));
mt = eval(get(handles.edit8, 'String'));
mf = eval(get(handles.edit9, 'String'));
pw= eval (get(handles.edit10, 'String'));
mt = mt*1E-6;
mf = mf*1E-6;
mh2=mt-mf;              %mh2=mass of hydrogen fuel
nf=mf/(12*alp+bet);     %nf=mole of diesel
p=mh2/2;                %p=mole of hydrogen gas
pw1=pw/18;                    %pw1=mole of water
as=nf*alp+(nf*bet+2*p)/4-nf*gam/2;
format short e;
if (T>=1600 && T<=4000)
    K1=10^(-4.7060+4.5548*(T-1600)*(1E-3)-1.9275*(T-1600)*(T-2000)*...
       (1E-6)+0.6914*(T-1600)*(T-2000)*(T-2400)*(1E-9)-0.2143*...
       (T-1600)*(T-2000)*(T-2400)*(T-2800)*(1E-12)+0.0568*(T-1600)*...
       (T-2000)*(T-2400)*(T-2800)*(T-3200)*(1E-15)-0.0118*(T-1600)*...
       (T-2000)*(T-2400)*(T-2800)*(T-3200)*(T-3600)*(1E-18));

    K2=10^(-23.3871+13.5989*(T-1600)*(1E-3)-5.6463*(T-1600)*...
       (T-2000)*(1E-6)+2.0147*(T-1600)*(T-2000)*(T-2400)*...
       (1E-9)-0.6290*(T-1600)*(T-2000)*(T-2400)*(T-2800)*...
       (1E-12)+0.1745*(T-1600)*(T-2000)*(T-2400)*(T-2800)*(T-3200)*...
       (1E-15)-0.0436*(T-1600)*(T-2000)*(T-2400)*(T-2800)*(T-3200)*...
       (T-3600)*(1E-18));

    K3=10^(-12.3506+13.1975*(T-1600)*(1E-3)-5.5245*(T-1600)*...
       (T-2000)*(1E-6)+1.9729*(T-1600)*(T-2000)*(T-2400)*...
       (1E-9)-0.6151*(T-1600)*(T-2000)*(T-2400)*(T-2800)*...
       (1E-12)+0.1704*(T-1600)*(T-2000)*(T-2400)*(T-2800)*...
       (T-3200)*(1E-15)-0.0425*(T-1600)*(T-2000)*(T-2400)*...
       (T-2800)*(T-3200)*(T-3600)*(1E-18));

    K4=10^(-12.6282+9.5942*(T-1600)*(1E-3)-4.0164*(T-1600)*...
       (T-2000)*(1E-6)+1.4348*(T-1600)*(T-2000)*(T-2400)*...
       (1E-9)-0.4479*(T-1600)*(T-2000)*(T-2400)*(T-2800)*...
       (1E-12)+0.1243*(T-1600)*(T-2000)*(T-2400)*(T-2800)*...
       (T-3200)*(1E-15)-0.0310*(T-1600)*(T-2000)*(T-2400)*...
       (T-2800)*(T-3200)*(T-3600)*(1E-18));

    K5=10^(-5.1798+4.0998*(T-1600)*(1E-3)-1.6966*(T-1600)*(T-2000)*...
       (1E-6)+0.6008*(T-1600)*(T-2000)*(T-2400)*(1E-9)-0.1828*...
       (T-1600)*(T-2000)*(T-2400)*(T-2800)*(1E-12)+0.0461*(T-1600)*...
       (T-2000)*(T-2400)*(T-2800)*(T-3200)*(1E-15)-0.0081*(T-1600)*...
       (T-2000)*(T-2400)*(T-2800)*(T-3200)*(T-3600)*(1E-18));

    K6=10^(-5.6771+4.7100*(T-1600)*(1E-3)-1.9572*(T-1600)*(T-2000)*...
       (1E-6)+0.6958*(T-1600)*(T-2000)*(T-2400)*(1E-9)-0.2168*...
       (T-1600)*(T-2000)*(T-2400)*(T-2800)*(1E-12)+0.0510*(T-1600)*...
       (T-2000)*(T-2400)*(T-2800)*(T-3200)*(1E-15)-0.0143*(T-1600)*...
       (T-2000)*(T-2400)*(T-2800)*(T-3200)*(T-3600)*(1E-18));

    K7=10^(-4.2669+3.6898*(T-1600)*(1E-3)-1.5150*(T-1600)*(T-2000)*...
       (1E-6)+0.5328*(T-1600)*(T-2000)*(T-2400)*(1E-9)-0.1618*...
       (T-1600)*(T-2000)*(T-2400)*(T-2800)*(1E-12)+0.0418*(T-1600)*...
```

```
        (T-2000)*(T-2400)*(T-2800)*(T-3200)*(1E-15)-0.0086*(T-1600)*...
        (T-2000)*(T-2400)*(T-2800)*(T-3200)*(T-3600)*(1E-18));

    K8=10^(-4.8419+4.1600*(T-1600)*(1E-3)-1.7225*(T-1600)*(T-2000)*...
        (1E-6)+0.6135*(T-1600)*(T-2000)*(T-2400)*(1E-9)-0.1940*...
        (T-1600)*(T-2000)*(T-2400)*(T-2800)*(1E-12)+0.0570*(T-1600)*...
        (T-2000)*(T-2400)*(T-2800)*(T-3200)*(1E-15)-0.0163*(T-1600)*...
        (T-2000)*(T-2400)*(T-2800)*(T-3200)*(T-3600)*(1E-18));

    K9=10^(-8.23556+2.3730*(T-1600)*(1E-3)-0.9800*(T-1600)*(T-
2000)*...
        (1E-6)+0.3462*(T-1600)*(T-2000)*(T-2400)*(1E-9)-0.1077*...
        (T-1600)*(T-2000)*(T-2400)*(T-2800)*(1E-12)+0.0299*(T-1600)*...
        (T-2000)*(T-2400)*(T-2800)*(T-3200)*(1E-15)-0.0075*(T-1600)*...
        (T-2000)*(T-2400)*(T-2800)*(T-3200)*(T-3600)*(1E-18));

     elseif (T>4000 && T<=6000)
    K1=10^(0.6918+0.7740*(T-4000)*(1E-3)-0.1600*(T-4000)*(T-4500)*...
        (1E-6)+0.0297*(T-4000)*(T-4500)*(T-5000)*(1E-9)-0.0053*...
        (T-4000)*(T-4500)*(T-5000)*(T-5500)*(1E-12));

    K2=10^(-7.0178+2.4494*(T-4000)*(1E-3)-0.4831*(T-4000)*(T-4500)*...
        (1E-6)+0.0876*(T-4000)*(T-4500)*(T-5000)*(1E-9)-0.0146*...
        (T-4000)*(T-4500)*(T-5000)*(T-5500)*(1E-12));

    K3=10^(3.4197+2.3113*(T-4000)*(1E-3)-0.4651*(T-4000)*(T-4500)*...
        (1E-6)+0.0856*(T-4000)*(T-4500)*(T-5000)*(1E-9)-0.0144*...
        (T-4000)*(T-4500)*(T-5000)*(T-5500)*(1E-12));

    K4=10^(-1.1652+1.6762*(T-4000)*(1E-3)-0.3401*(T-4000)*(T-4500)*...
        (1E-6)+0.0622*(T-4000)*(T-4500)*(T-5000)*(1E-9)-0.0104*...
        (T-4000)*(T-4500)*(T-5000)*(T-5500)*(1E-12));

    K5=10^(-0.2380+0.7418*(T-4000)*(1E-3)-0.1478*(T-4000)*(T-4500)*...
        (1E-6)+0.0290*(T-4000)*(T-4500)*(T-5000)*(1E-9)-0.0066*...
        (T-4000)*(T-4500)*(T-5000)*(T-5500)*(1E-12));


    K6=10^(-0.0217+0.8372*(T-4000)*(1E-3)-0.1692*(T-4000)*(T-4500)*...
        (1E-6)+0.0317*(T-4000)*(T-4500)*(T-5000)*(1E-9)-0.0055*...
        (T-4000)*(T-4500)*(T-5000)*(T-5500)*(1E-12));

    K7=10^(0.2000+0.6740*(T-4000)*(1E-3)-0.1360*(T-4000)*(T-4500)*...
        (1E-6)+0.0268*(T-4000)*(T-4500)*(T-5000)*(1E-9)-0.0063*...
        (T-4000)*(T-4500)*(T-5000)*(T-5500)*(1E-12));

    K8=10^(0.1700+0.7458*(T-4000)*(1E-3)-0.1456*(T-4000)*(T-4500)*...
        (1E-6)+0.0235*(T-4000)*(T-4500)*(T-5000)*(1E-9)-0.0021*...
        (T-4000)*(T-4500)*(T-5000)*(T-5500)*(1E-12));

    K9=10^(-5.3797+0.4183*(T-4000)*(1E-3)-0.0869*(T-4000)*(T-4500)*...
        (1E-6)+0.0158*(T-4000)*(T-4500)*(T-5000)*(1E-9)-0.0026*...
        (T-4000)*(T-4500)*(T-5000)*(T-5500)*(1E-12));

    end

K = [K1;K2;K3;K4;K5;K6;K7;K8;K9];

%define constants

c1=K1/P^0.5; c2=K2/P^0.5; c3=P^2/K3; c4=P/K4; c5=K5/P^0.5;
c6=K6/P^0.5;
c7=K7/P^0.5;c8=K8/P^0.5; c9=K9*P^0.5;
```

```
c=[c1;c2;c3;c4;c5;c6;c7;c8;c9];
 % --- Executes on selection change in popupmenu1.
function popupmenu1(hObject, eventdata, handles)
% hObject
% eventdata  reserved - to be defined in a future version of MATLAB
% handles    structure with handles and user data (see GUIDATA)
function popupmenu1_CreateFcn(hObject, eventdata, handles)
% hObject    handle to popupmenu1 (see GCBO)
% eventdata  reserved - to be defined in a future version of MATLAB
% handles    empty - handles not created
% Hint: popupmenu controls usually have a white background on Windows.
%       See ISPC and COMPUTER.
if ispc && isequal(get(hObject,'BackgroundColor'),
get(0,'defaultUicontrolBackgroundColor'))
    set(hObject,'BackgroundColor','white');
end
% --- Executes on button press in pushbutton2.
function pushbutton2_Callback(hObject, eventdata, handles)
% hObject    handle to pushbutton2 (see GCBO)
% eventdata  reserved - to be defined in a future version of MATLAB
global T_simpan mole_simpan;
popup1_string = get(handles.popupmenu1, 'String');
popup1_value = get(handles.popupmenu1, 'Value');
xgas = char(popup1_string(popup1_value,:))
%plot(T_simpan(:,1),mole_simpan(:,popup1_value));
plot(T_simpan(:,1),mole_simpan(:,popup1_value),'-rs','LineWidth',2,...
                      'MarkerEdgeColor','k',...
                      'MarkerFaceColor','g',...
                      'MarkerSize',10)
xtunjuk = ['Mole Fractions of ' xgas];
xlabel('Temperature, T(K)');
ylabel(xtunjuk);
gcf
set(gca,'YGrid','on');
```

Appendix F: Performance Characteristics of HFCI Engine

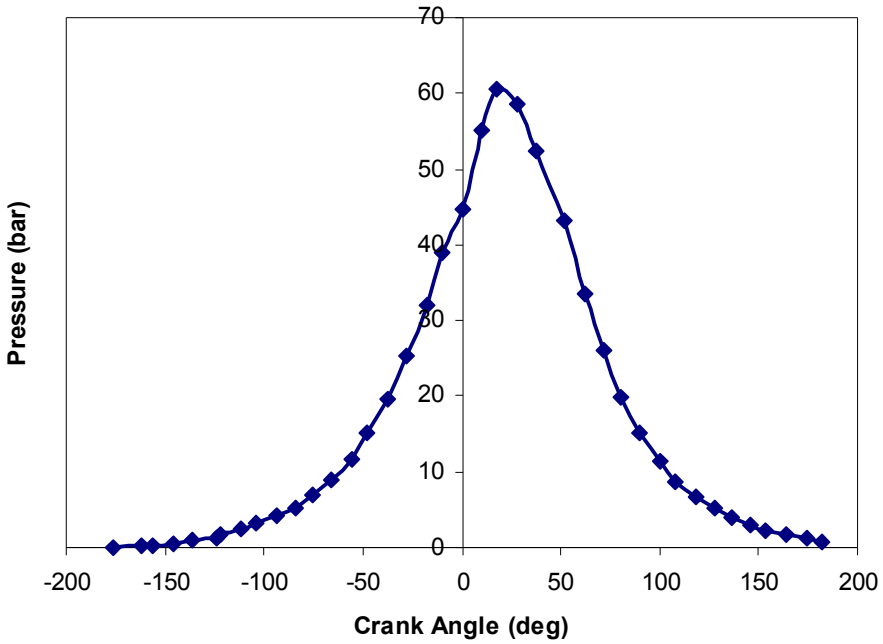

Figure F.1 In-cylinder pressure of diesel alone at 1500 RPM and 4 kW load

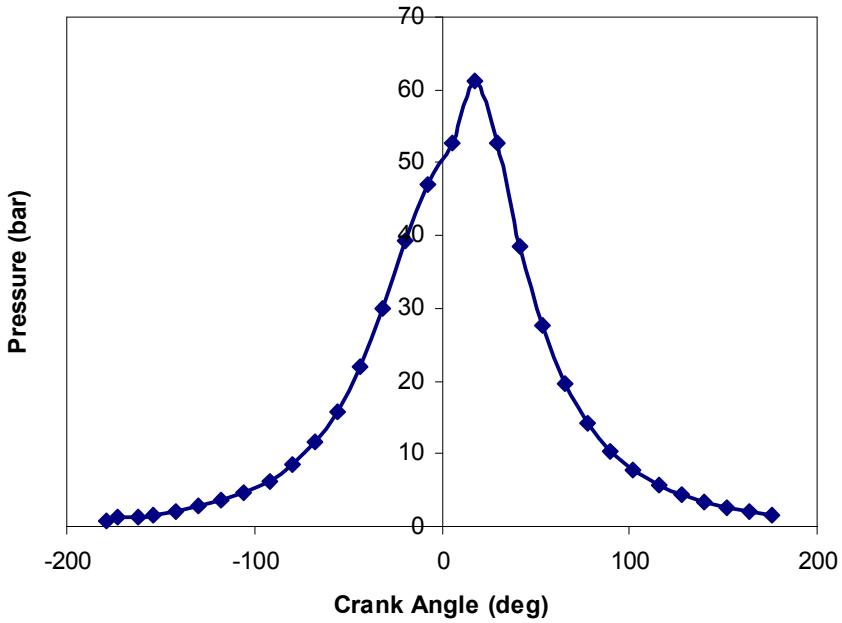

Figure F.2 In-cylinder pressure of diesel alone at 2000 RPM and 3 kW load

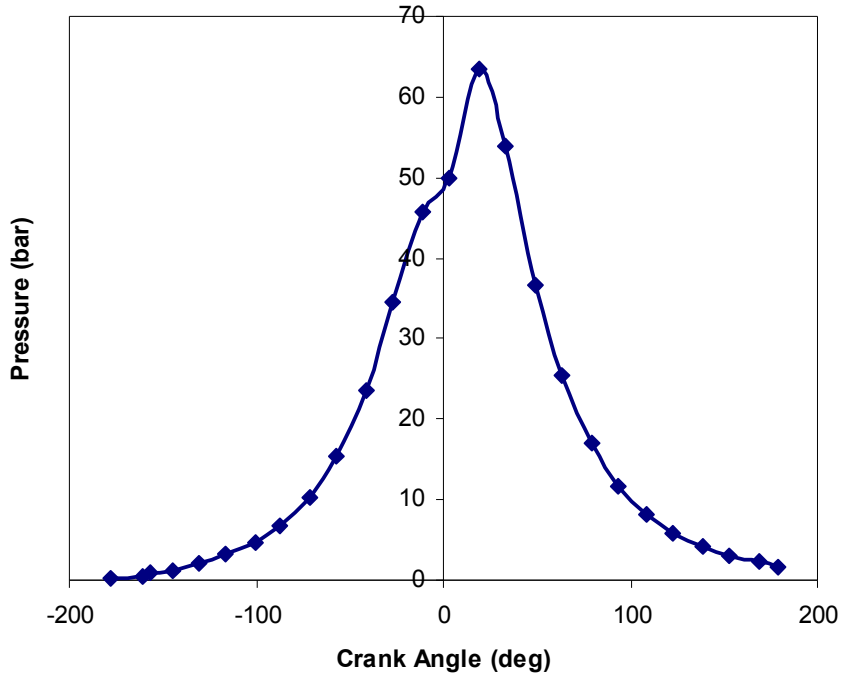

Figure F.3 In-cylinder pressure of diesel alone at 2500 RPM and 2 kW load

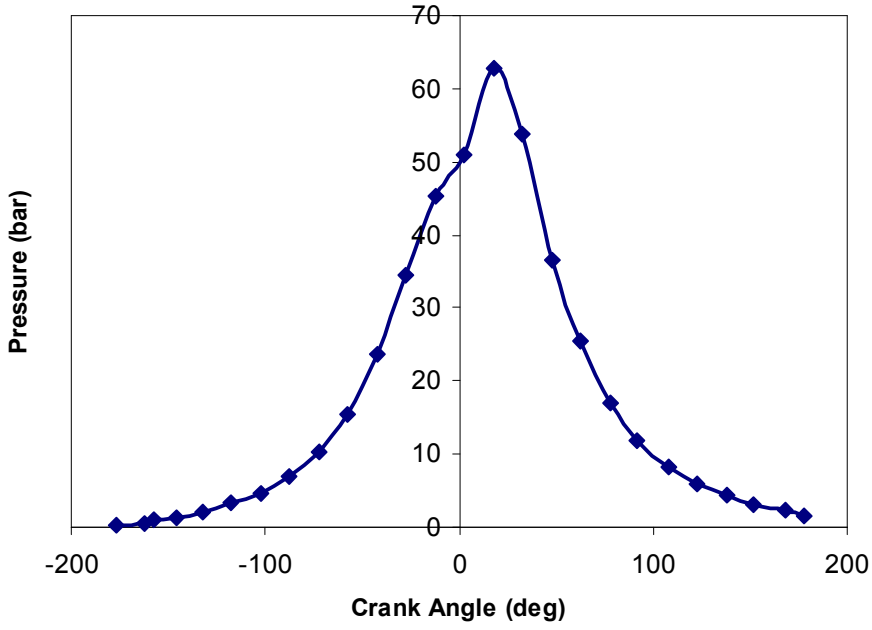

Figure F.4 In-cylinder pressure of diesel alone at 3000 RPM and 1 kW load

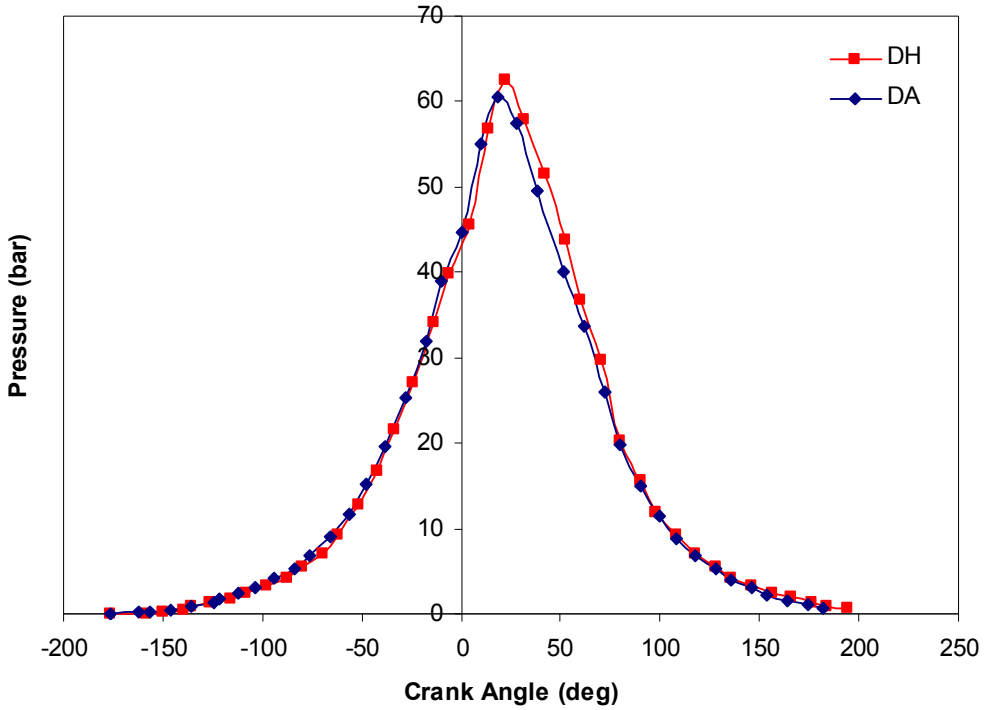

Figure F.5 Comparison of in-cylinder pressure between DA and DH operations at 1500 RPM and 5 kW load

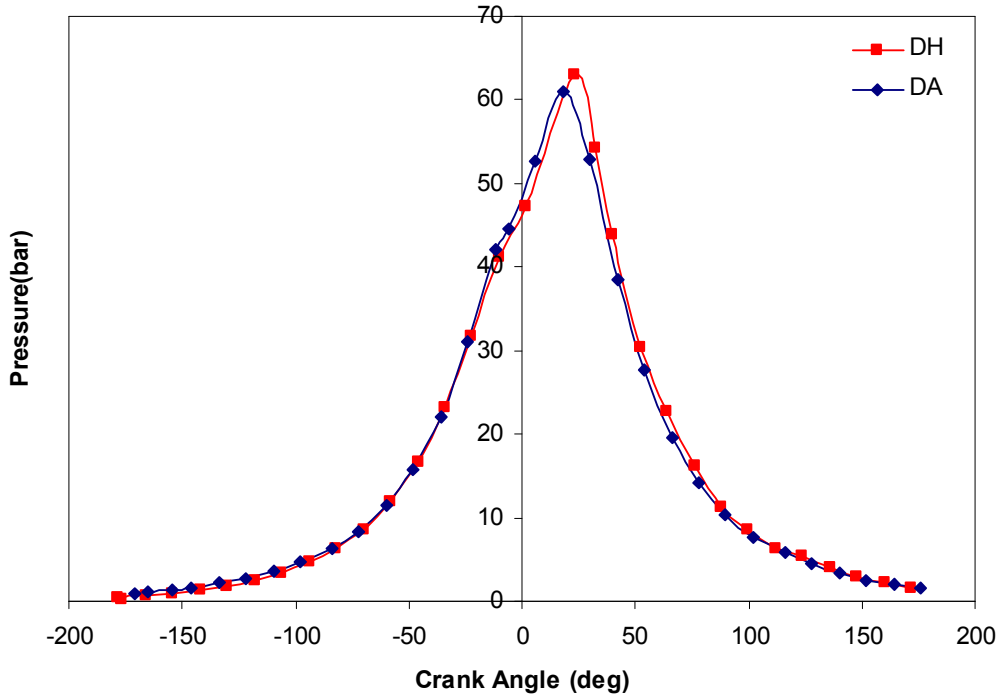

Figure F.6 Comparison of in-cylinder pressure between DA and DH operations at 2000 RPM and 3 kW load

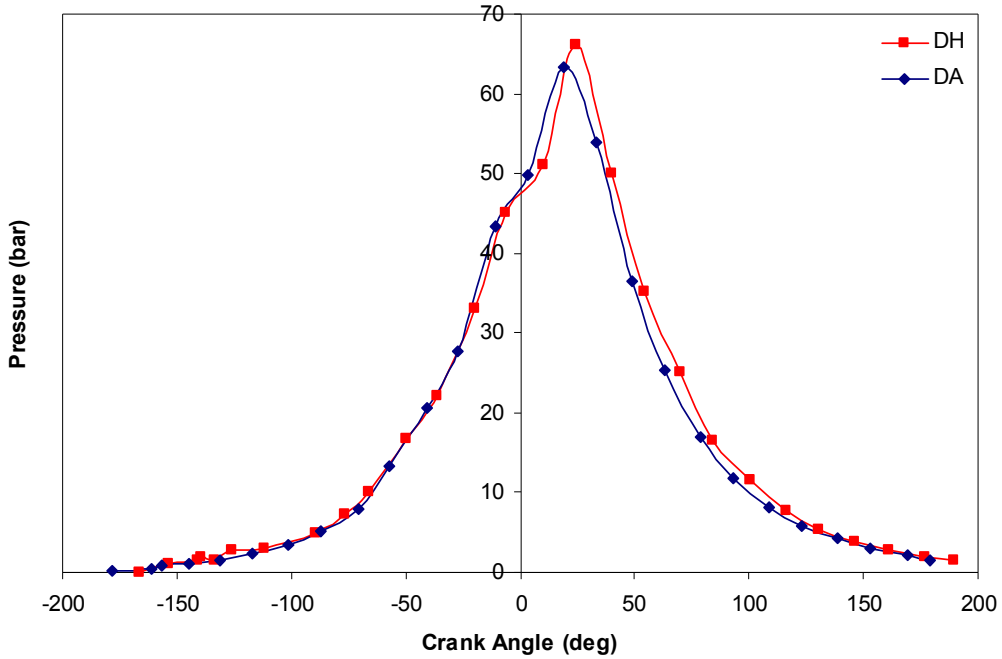

Figure F.7 Comparison of in-cylinder pressure between DA and DH operations at 2500 RPM and 2 kW load

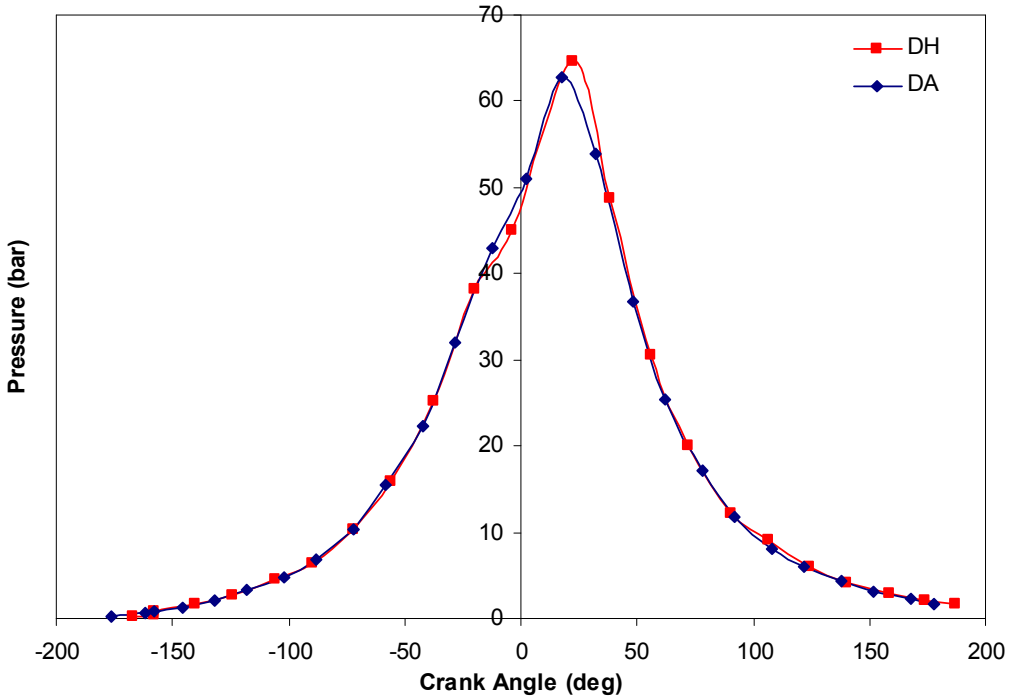

Figure F.8 Comparison of in-cylinder pressure between DA and DH operations at 3000 RPM and 1 kW load

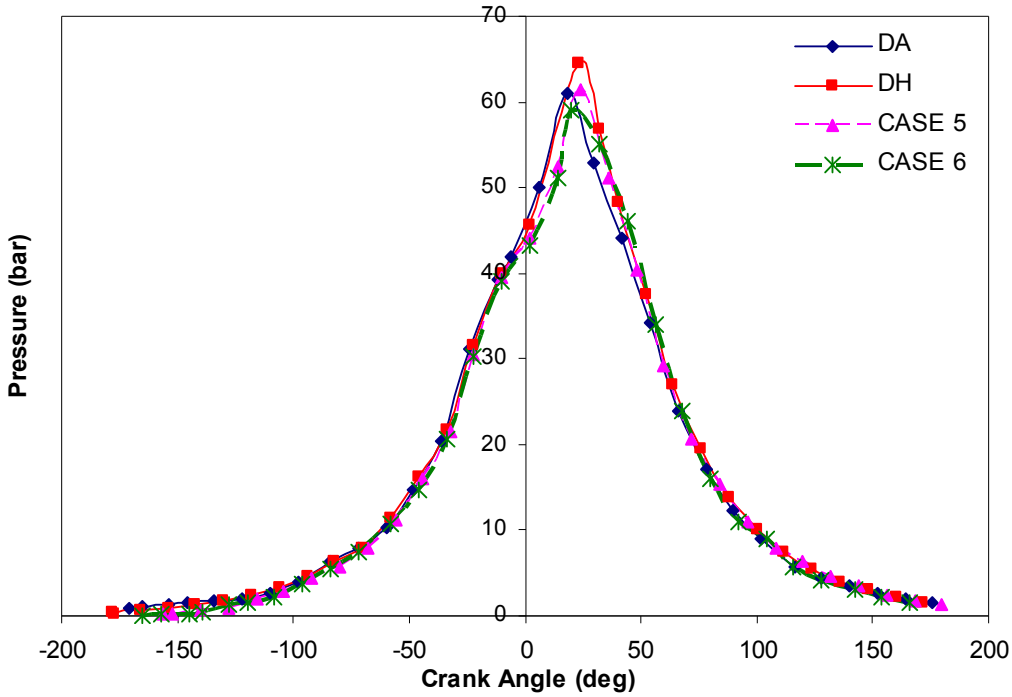

Figure F.9 Comparison of in-cylinder pressure between DA, DH and DHW operations at 2000 RPM and 3 kW load

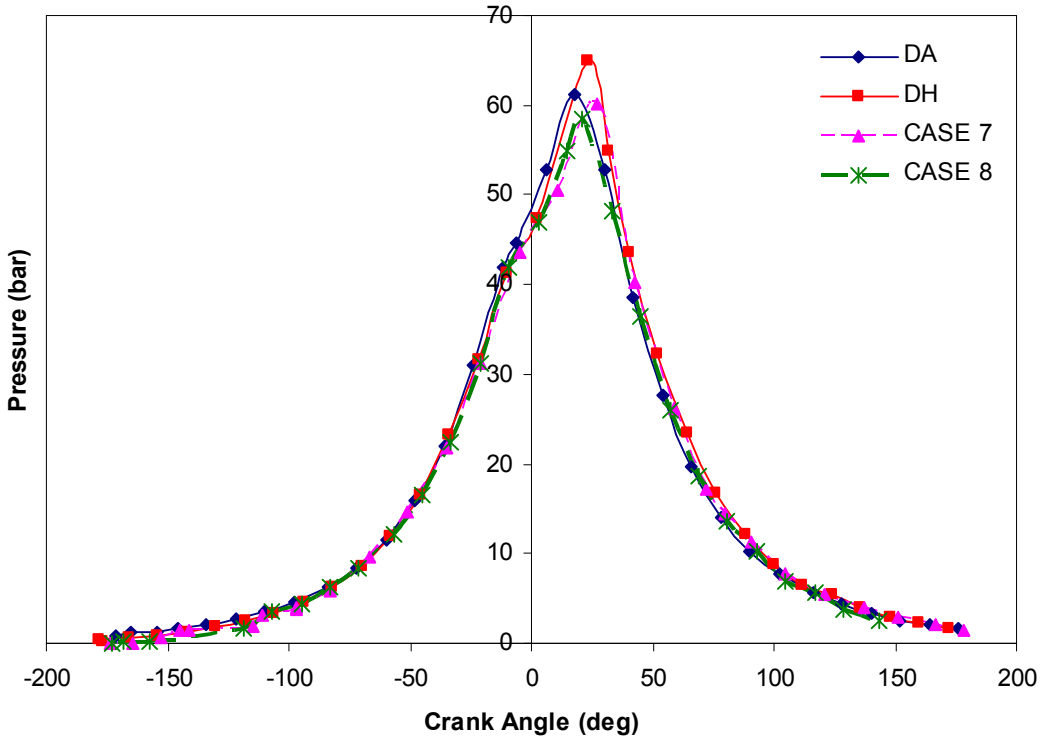

Figure F.10 Comparison of in-cylinder pressure between DA, DH and DHW operations at 2500 RPM and 2 kW load

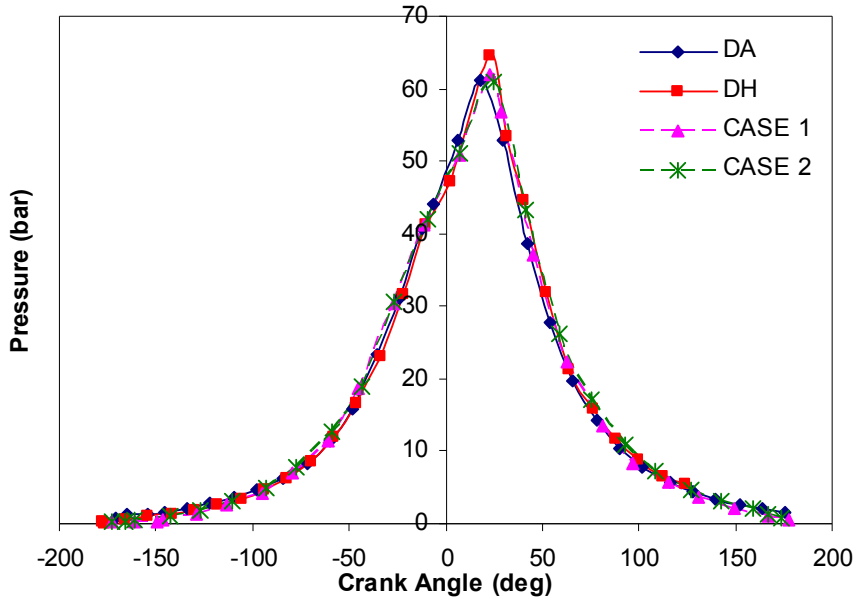

Figure F.11 Comparison of in-cylinder pressure between DA, DH and DHW operations at 2500 RPM and 2 kW load

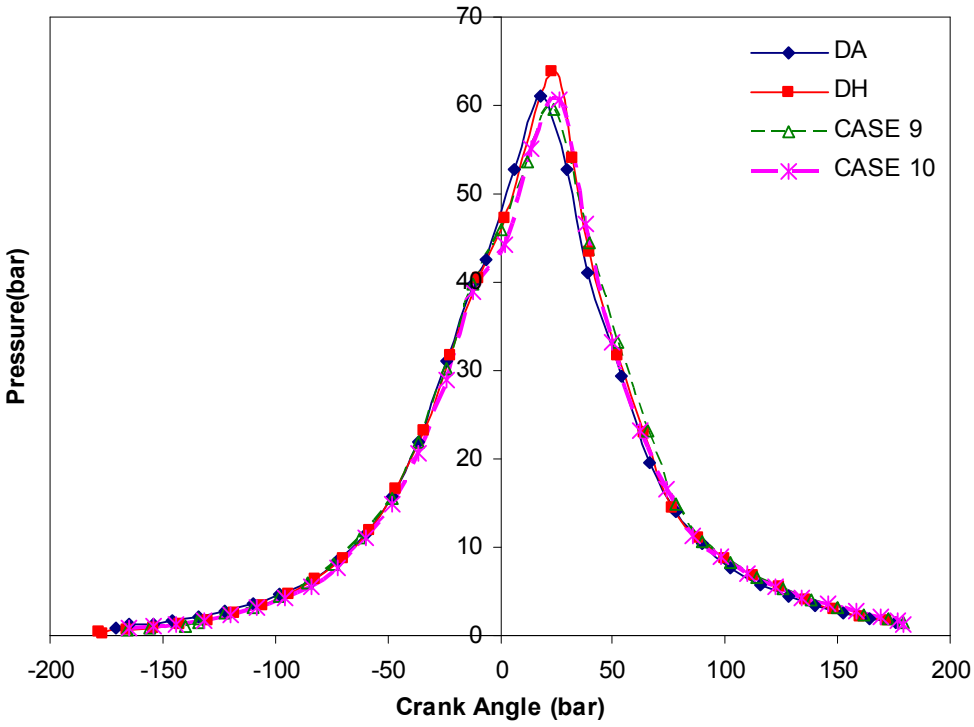

Figure F.12 Comparison of in-cylinder pressure between DA, DH and DHW operations at 2500 RPM and 2 kW load

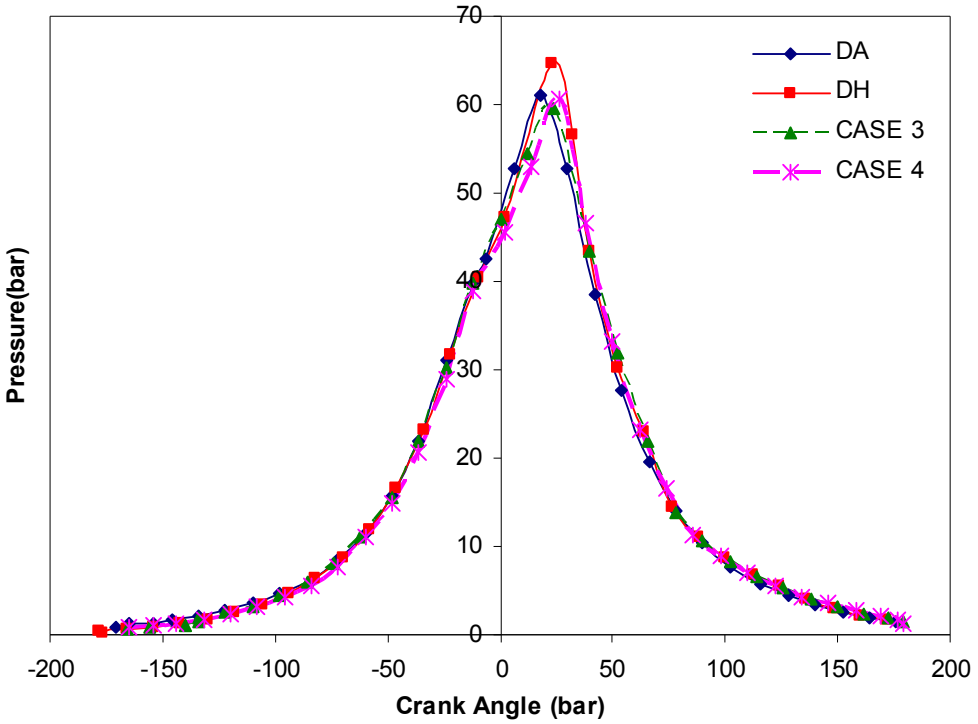

Figure F.13 Comparison of in-cylinder pressure between DA, DH and DHW operations at 2000 RPM and 3 kW load

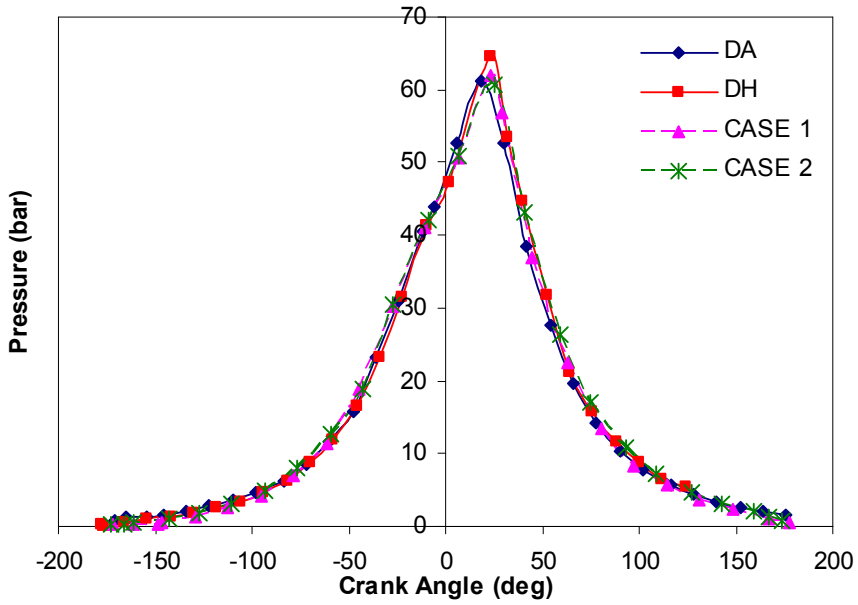

Figure F.13 Comparison of in-cylinder pressure between DA, DH and DHW operations at 3000 RPM and 1 kW load

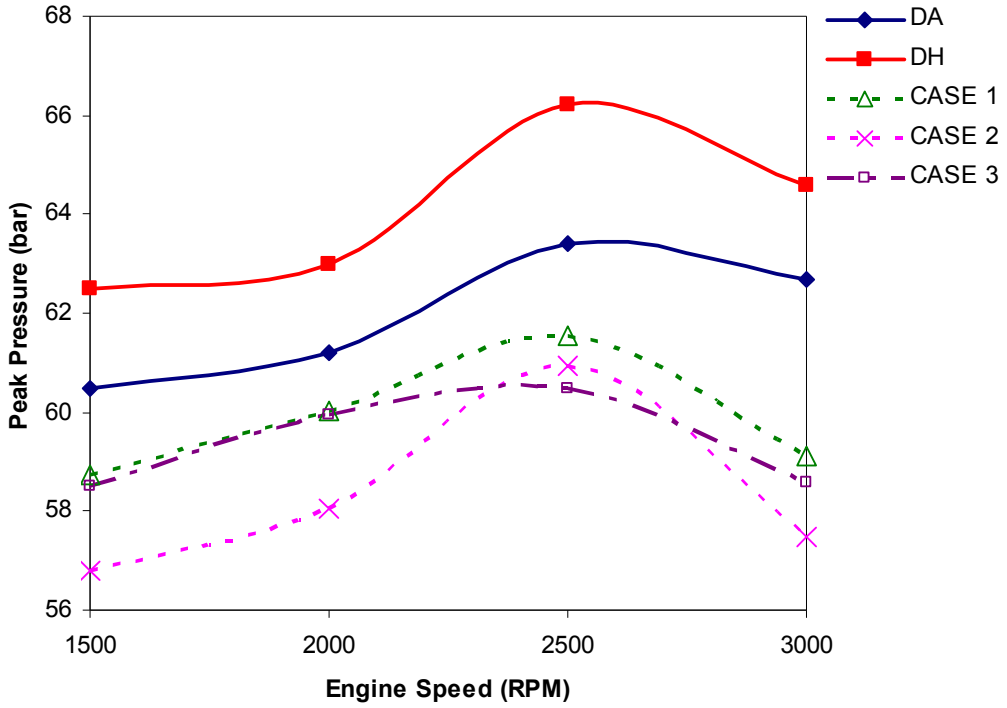

Figure F.14 Comparison of peak pressure between DA, DH and DHW operations

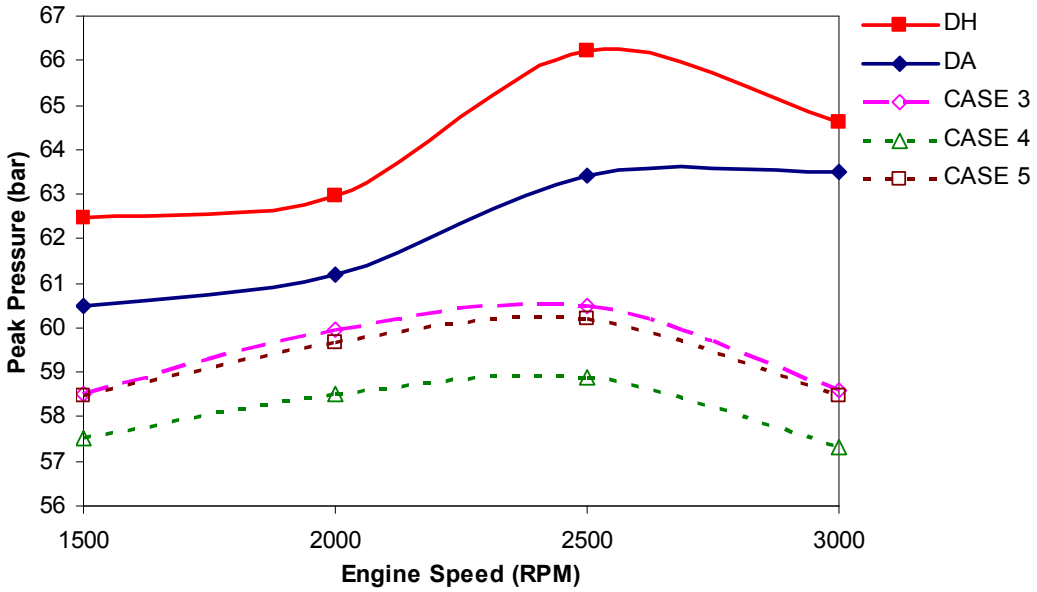

Figure F.15 Comparison of peak pressure between DA, DH and DHW operations

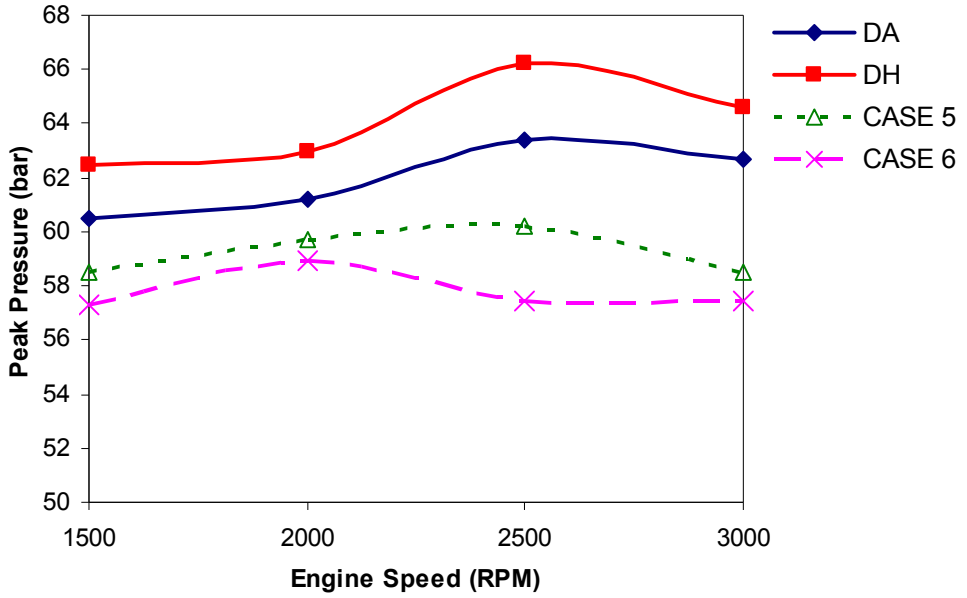

Figure F.16 Comparison of peak pressure between DA, DH and DHW operations

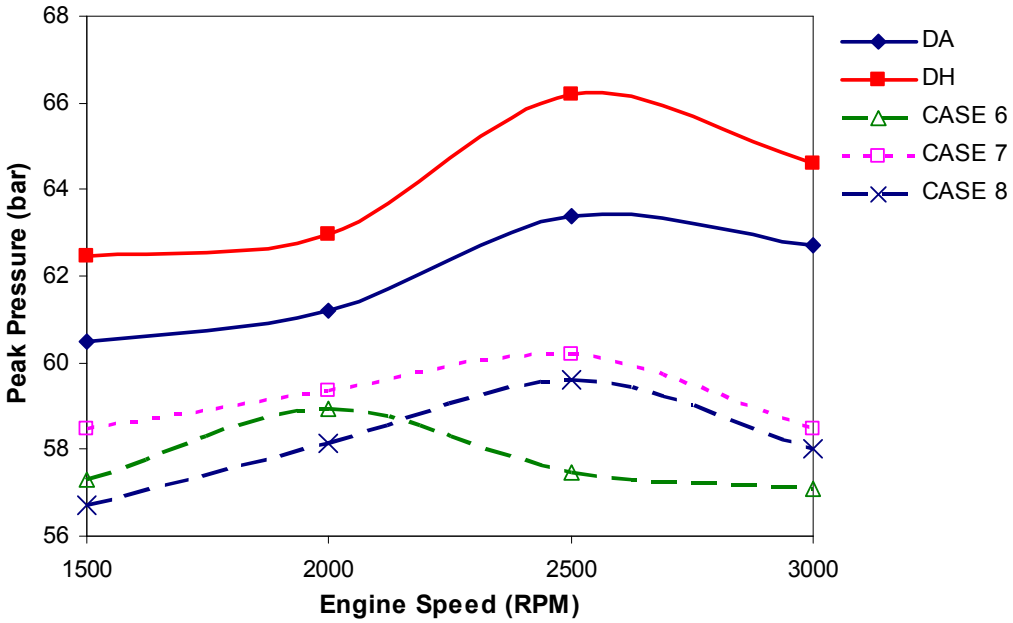

Figure F.17 Comparison of peak pressure between DA, DH and DHW operations

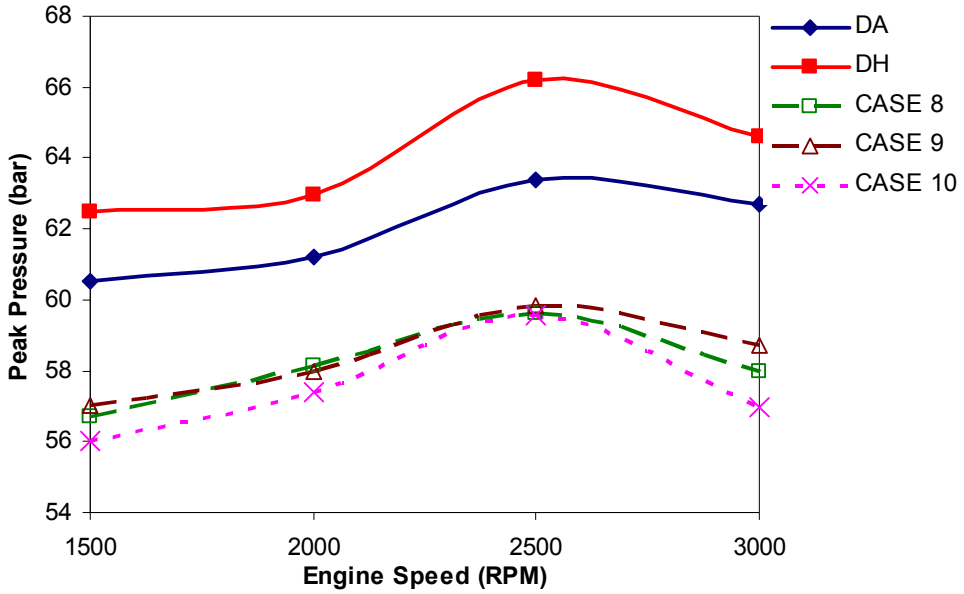

Figure F.18 Comparison of peak pressure between DA, DH and DHW operations

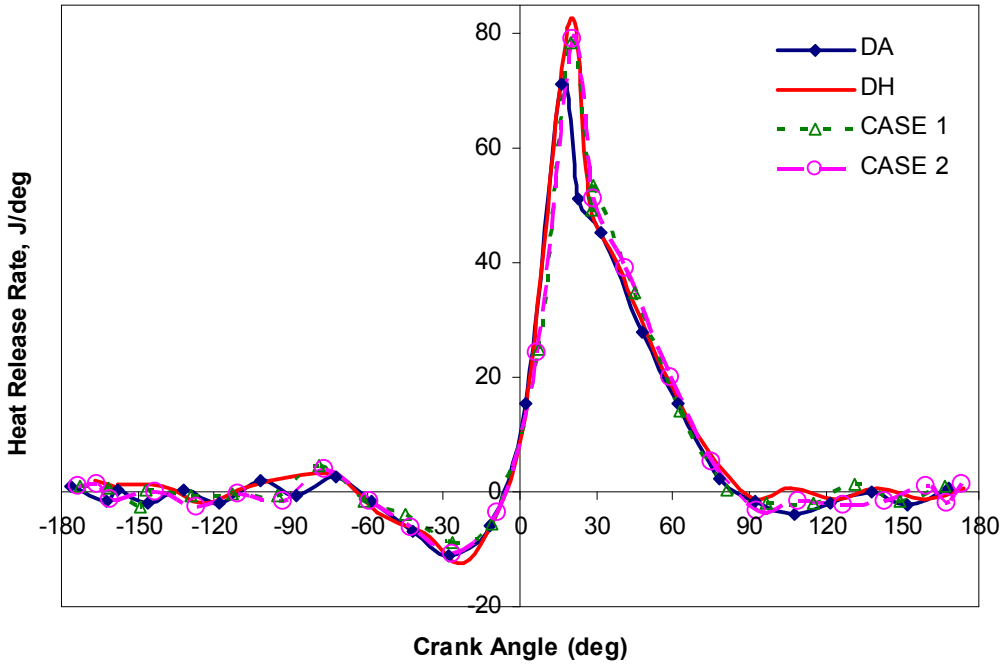

Figure F.19 Heat release rate for DA, DH and DHW operations at 1500 RPM

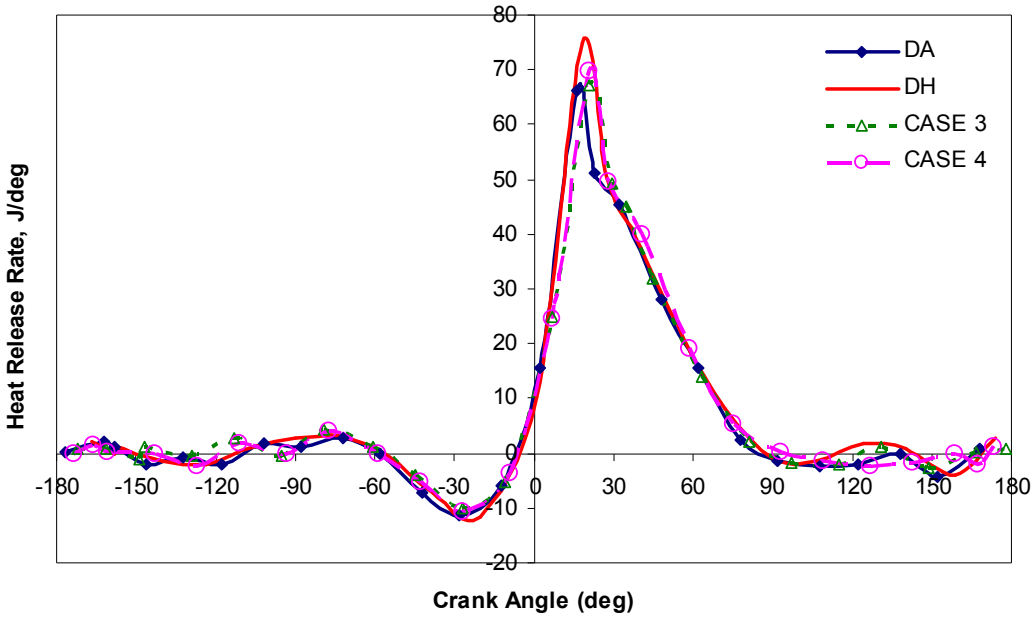

Figure F.20 Heat release rate for DA, DH and DHW operations at 2000 RPM

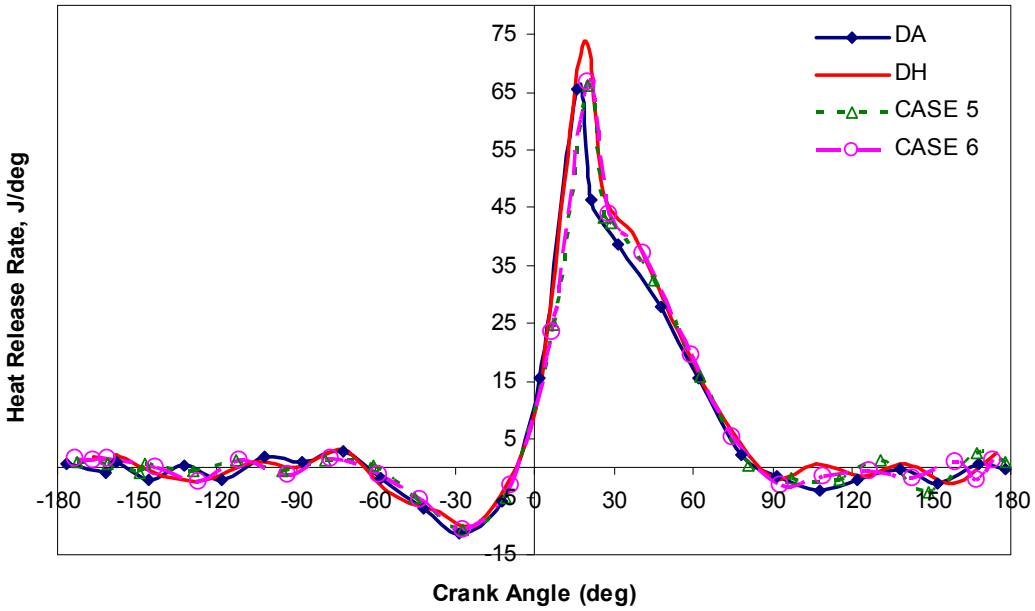

Figure F.21 Heat release rate for DA, DH and DHW operations at 2500 RPM

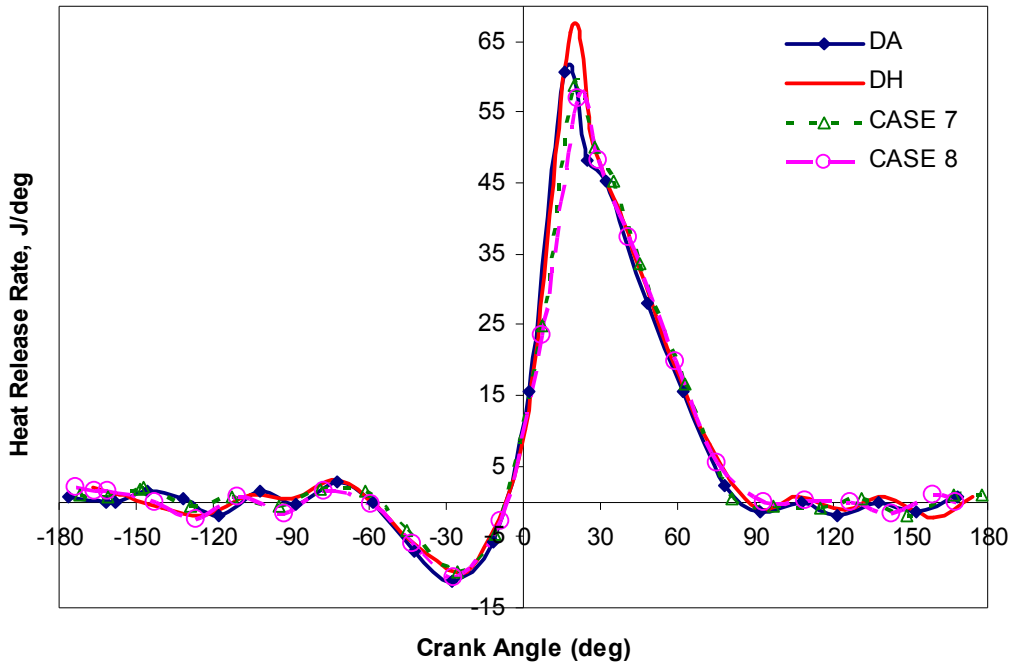

Figure F.22 Heat release rate for DA, DH and DHW operations at 3000 RPM

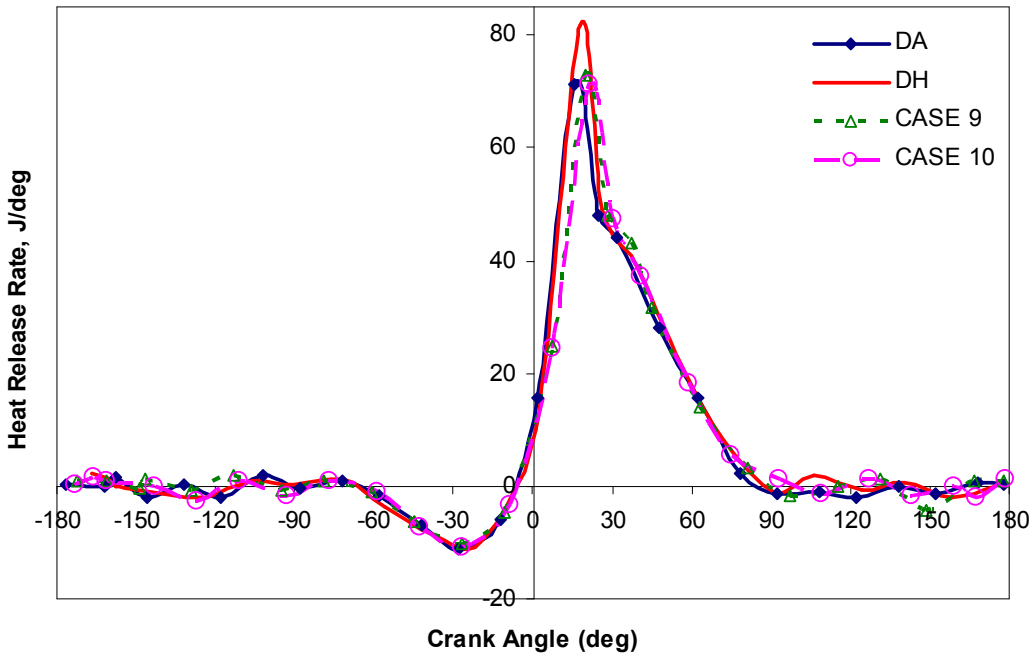

Figure F.23 Heat release rate for DA, DH and DHW operations at 1500 RPM

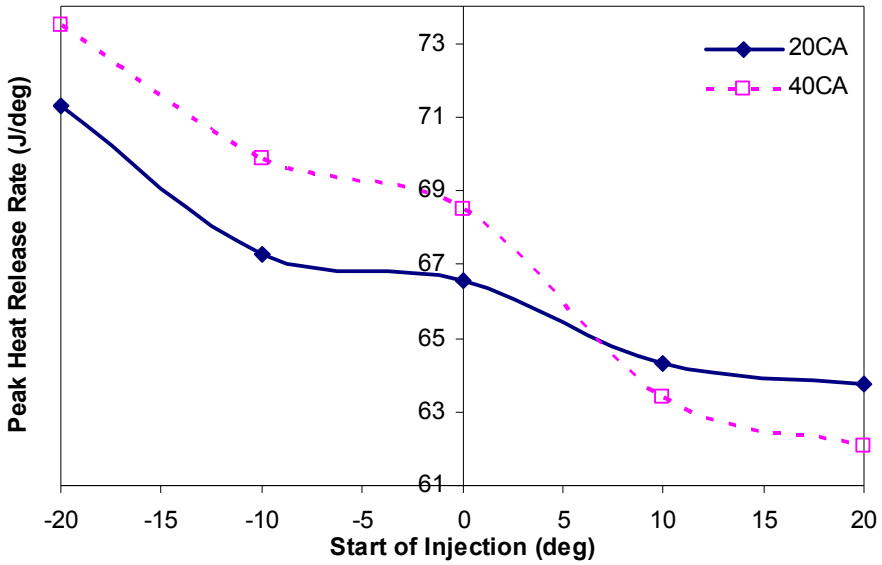

Figure F.24 Peak heat release rate at variable SOI and duration at 2000 RPM

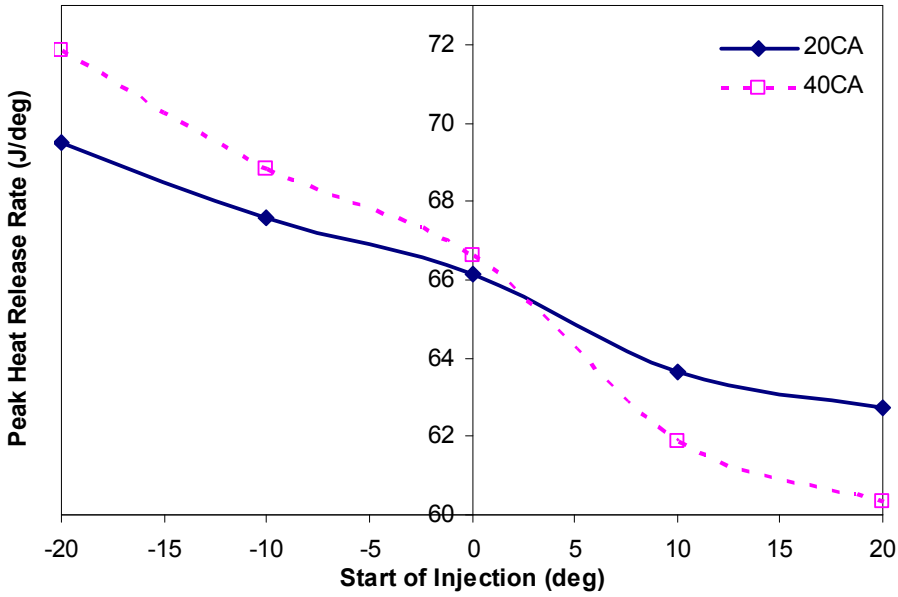

Figure F.25 Peak heat release rate at variable SOI and duration at 2500 RPM

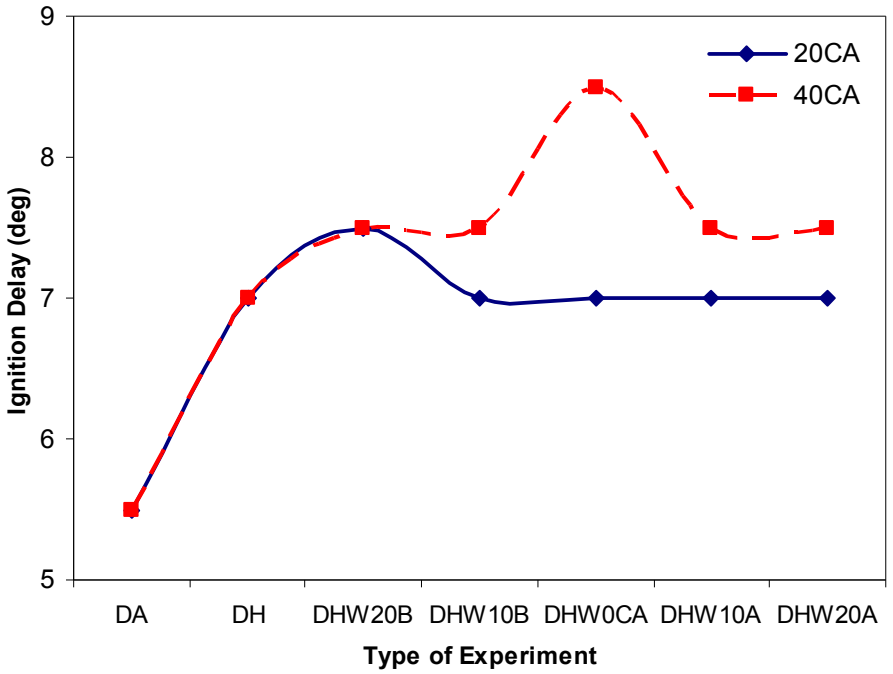

Figure F.26 Variation of ignition delay with different type of experiment at 2500 RPM

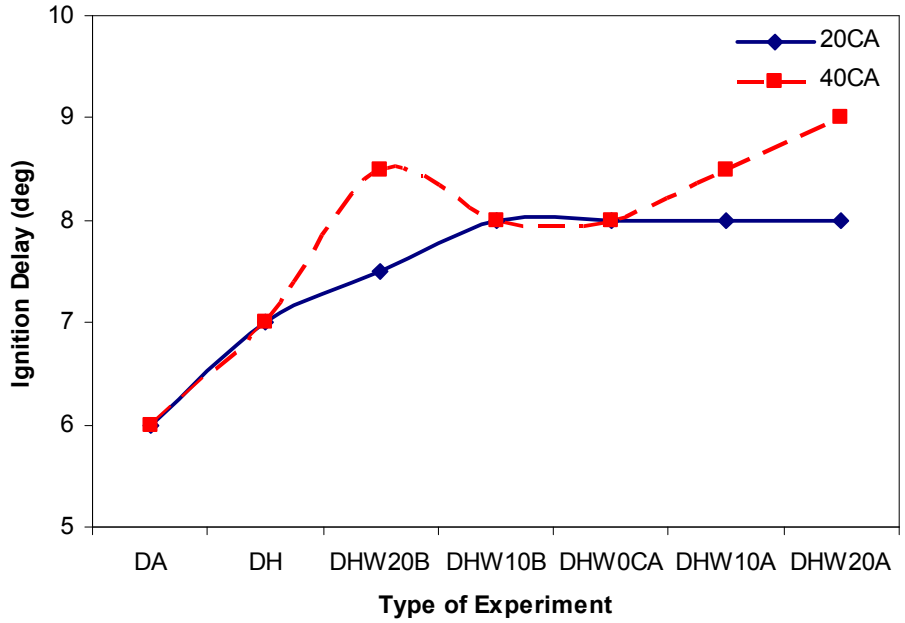

Figure F.27 Variation of ignition delay with different type of experiment at 3000 RPM

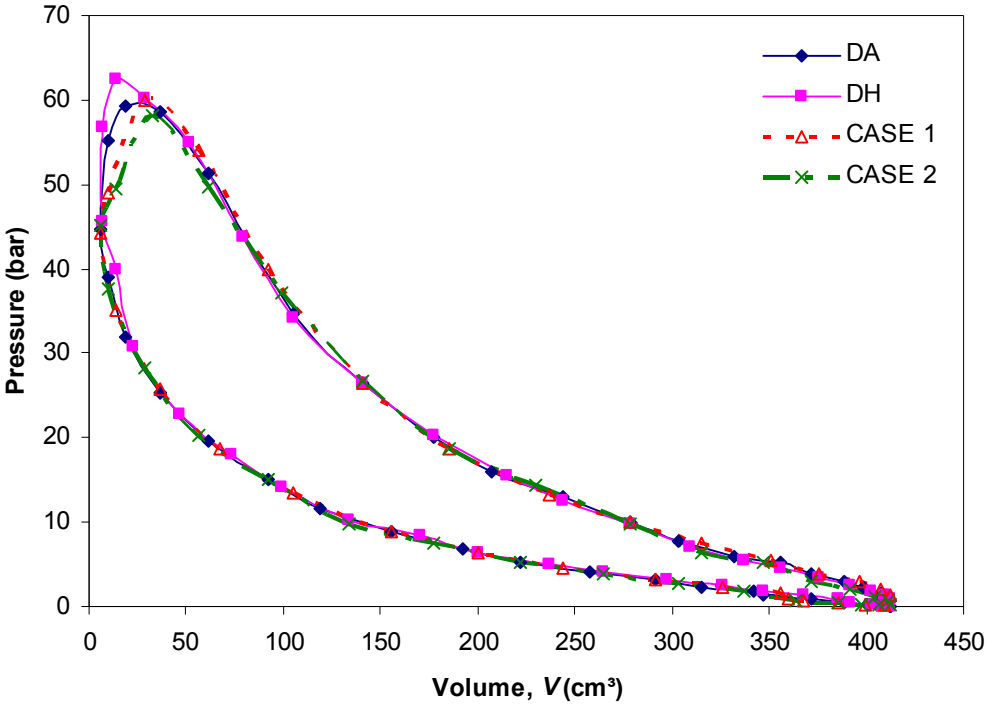

Figure F.28 P-*V* diagram for DA, DH and DHW operations at 1500 RPM and 5kW load

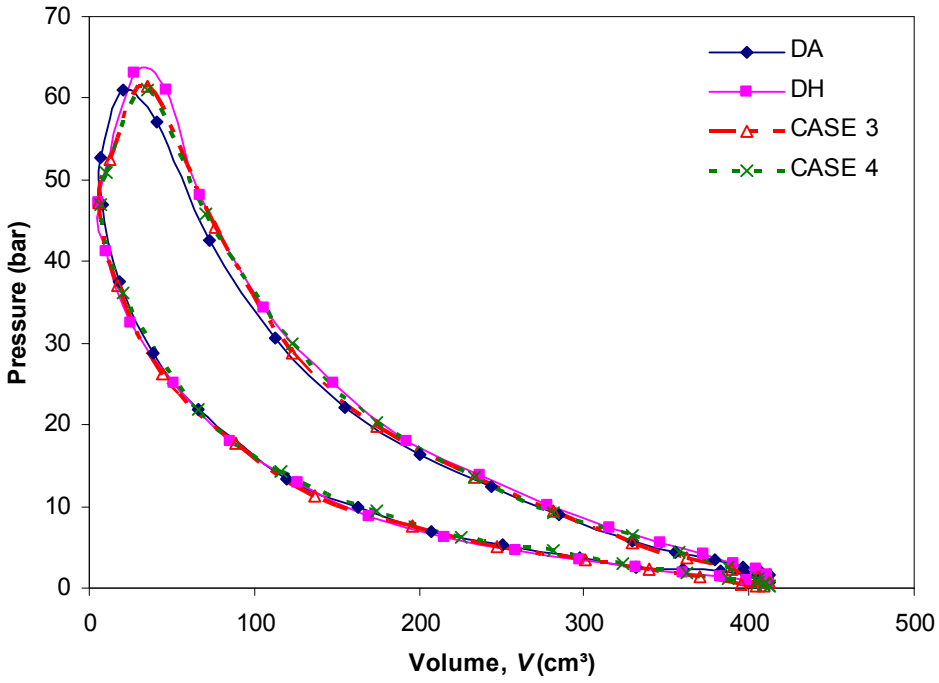

Figure F.29 P-*V* diagram for DA, DH and DHW operations at 2000 RPM and 3kW load

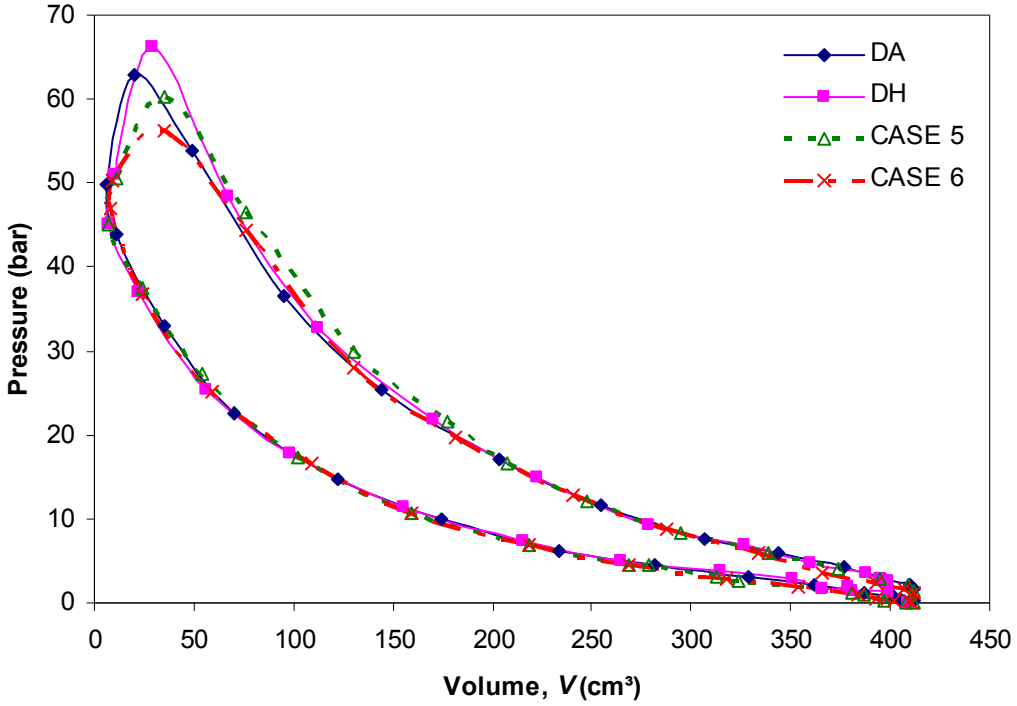

Figure F.30 P-*V* diagram for DA, DH and DHW operations at 2000 RPM and 3kW load

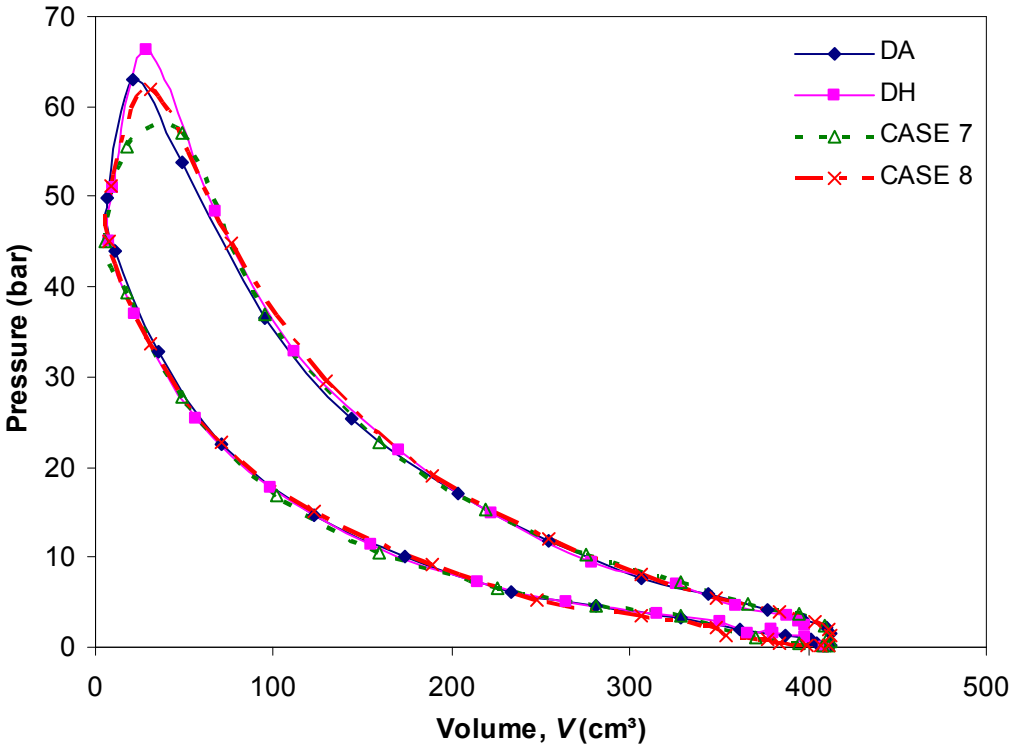

Figure F.31 P-*V* diagram for DA, DH and DHW operations at 2500 RPM and 2kW load

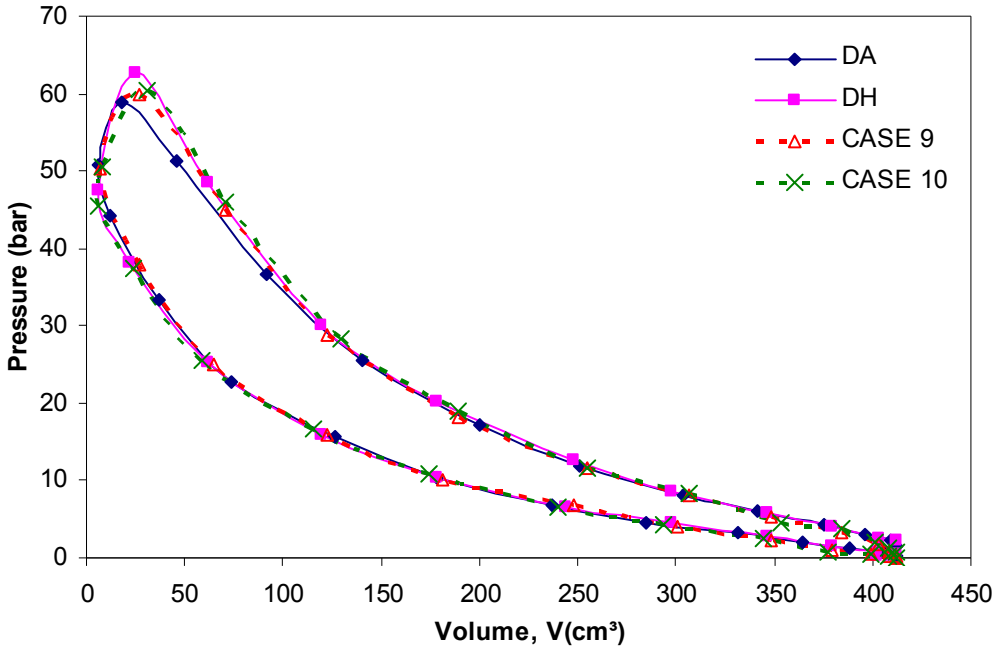

Figure F.31 P-*V* diagram for DA, DH and DHW operations at 3000 RPM and 1kW load

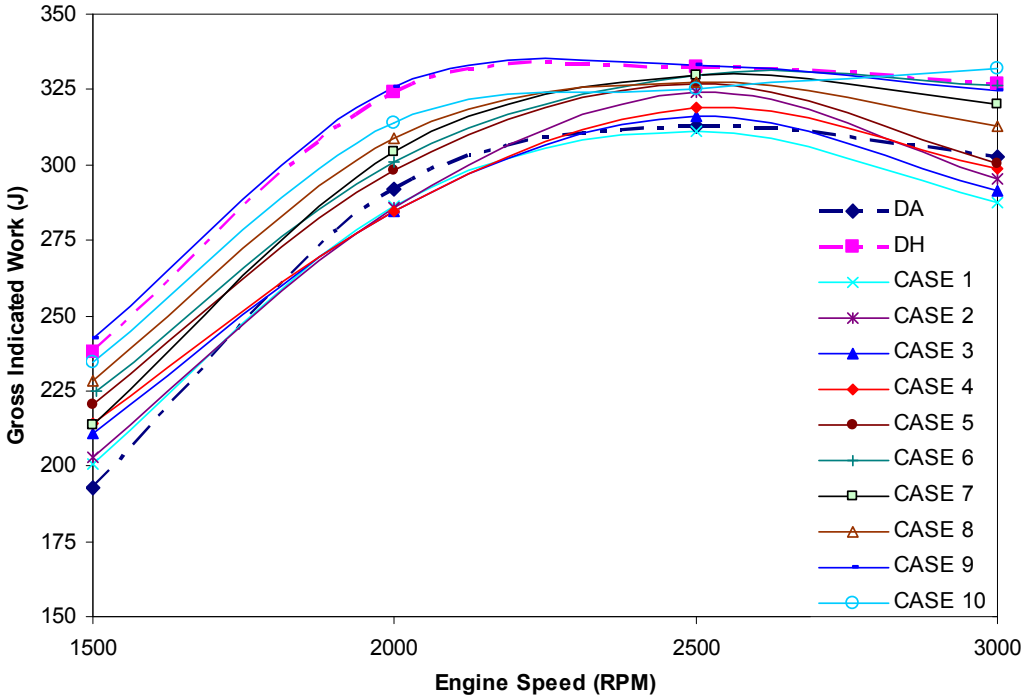

Figure F.32 Variation of gross indicated work with engine speeds

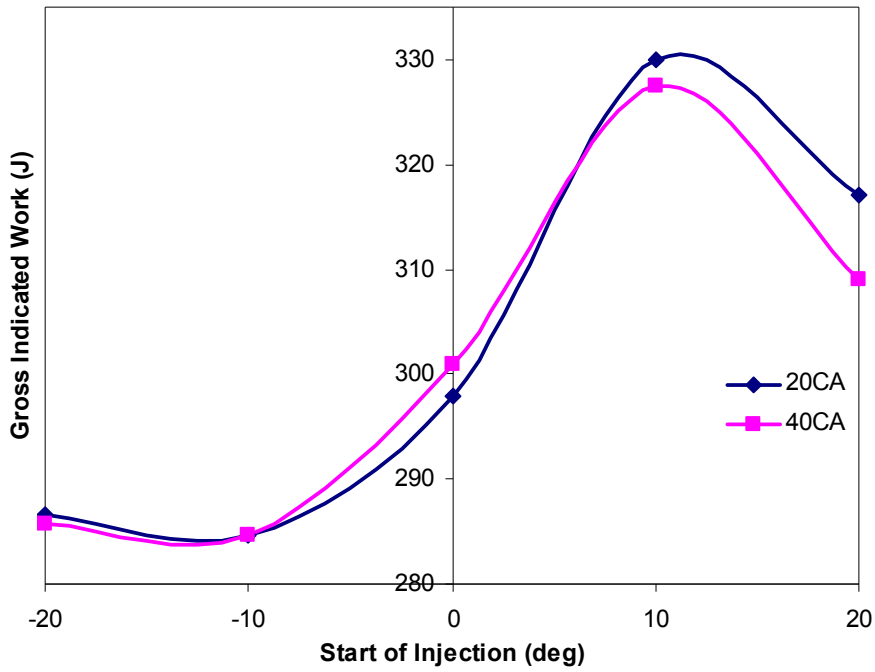

Figure F.33 Variation of gross indicated work with injection timing at 2000 RPM

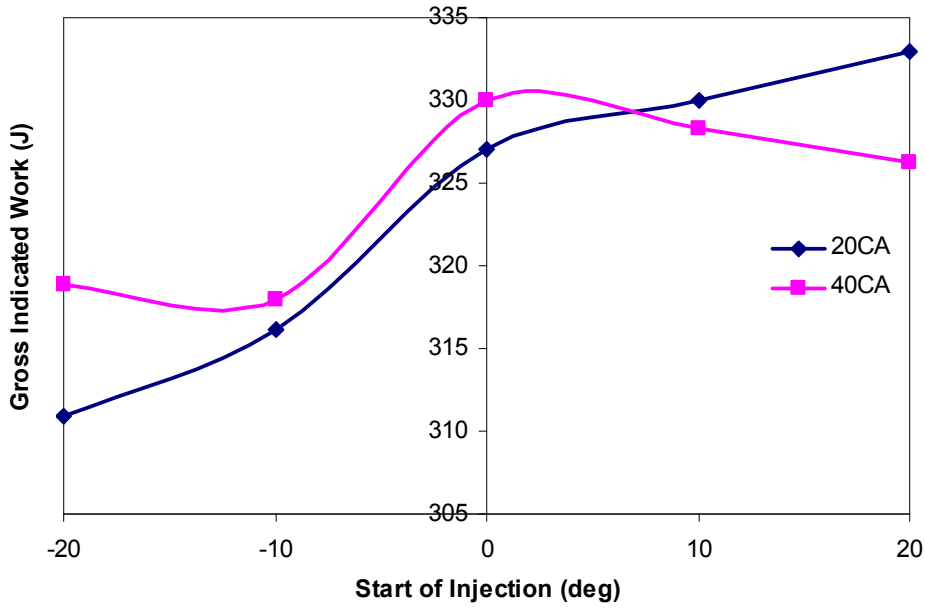

Figure F.34 Variation of gross indicated work with injection timing at 2500 RPM

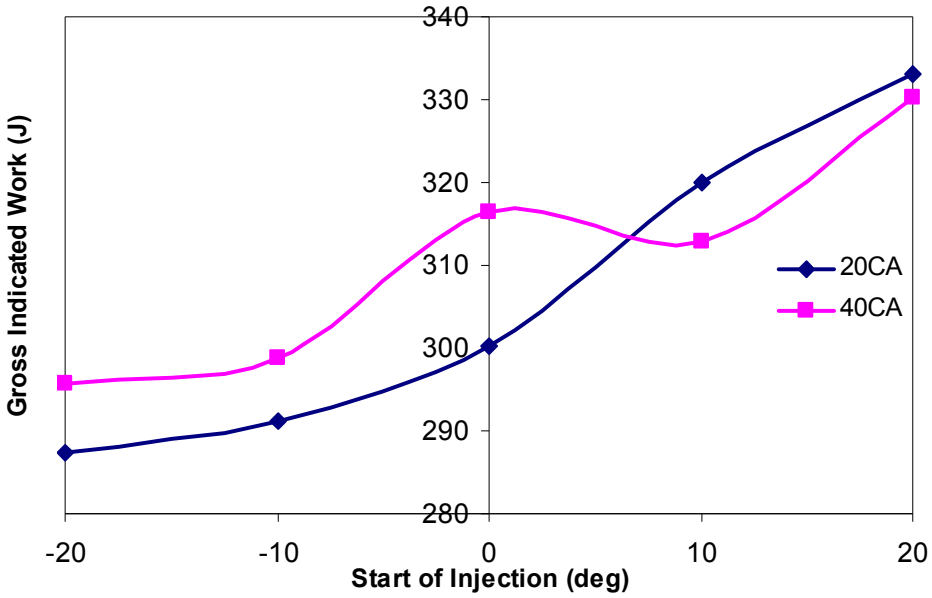

Figure F.35 Variation of gross indicated work with injection timing at 3000 RPM

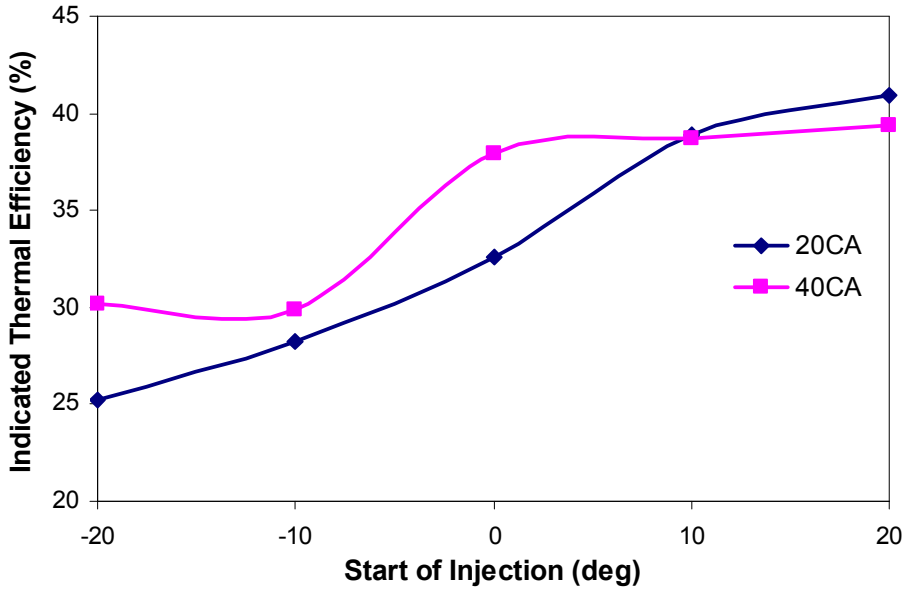

Figure F.36 Variation of ITE with injection timing at 1500 RPM and 5 kW load

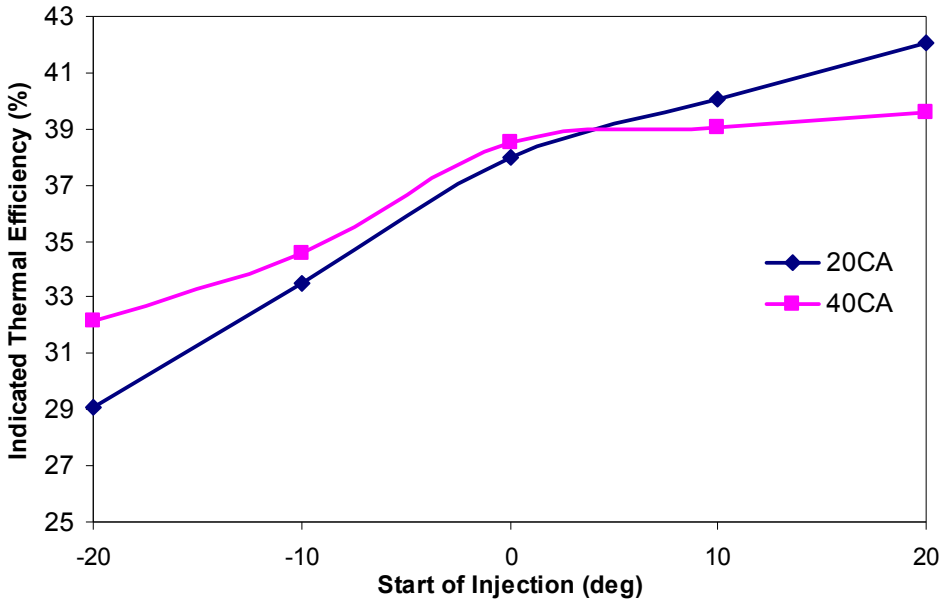

Figure F.37 Variation of ITE with injection timing at 2000 RPM and 3 kW load

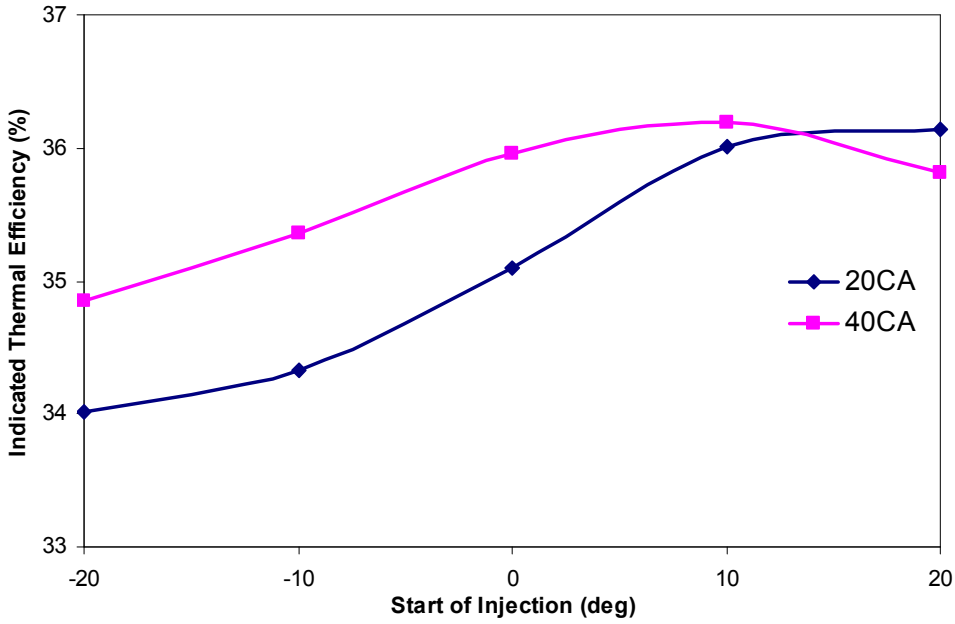

Figure F.38 Variation of ITE with injection timing at 2500 RPM and 1 kW load

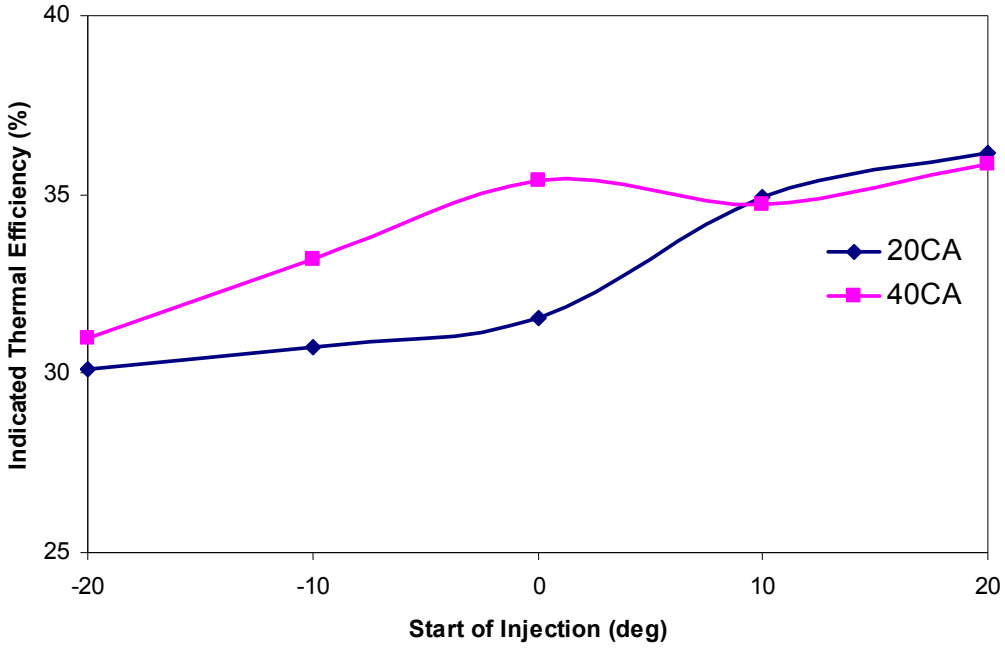

Figure F.39 Variation of ITE with injection timing at 3000 RPM and 1 kW load

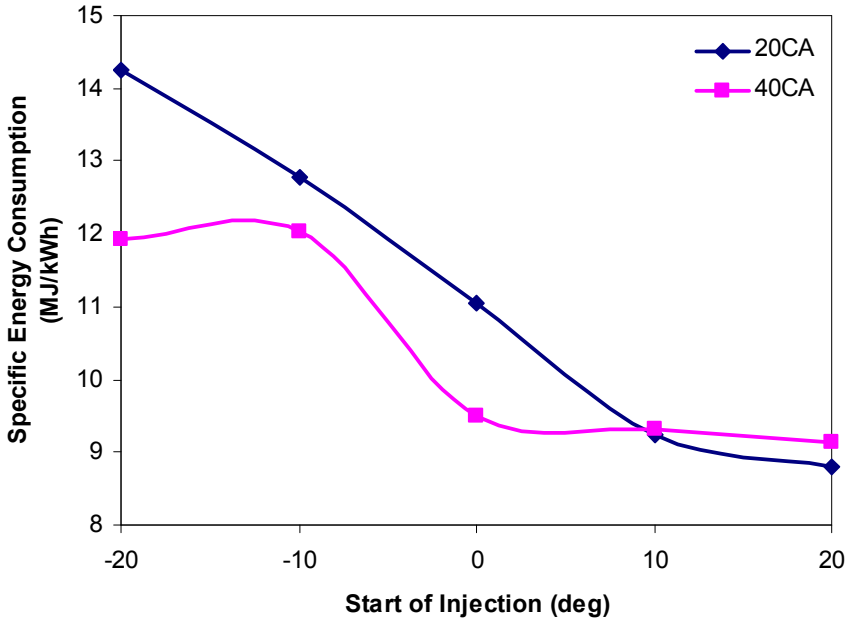

Figure F.40 Variation of ISEC with injection timing at 1500 RPM

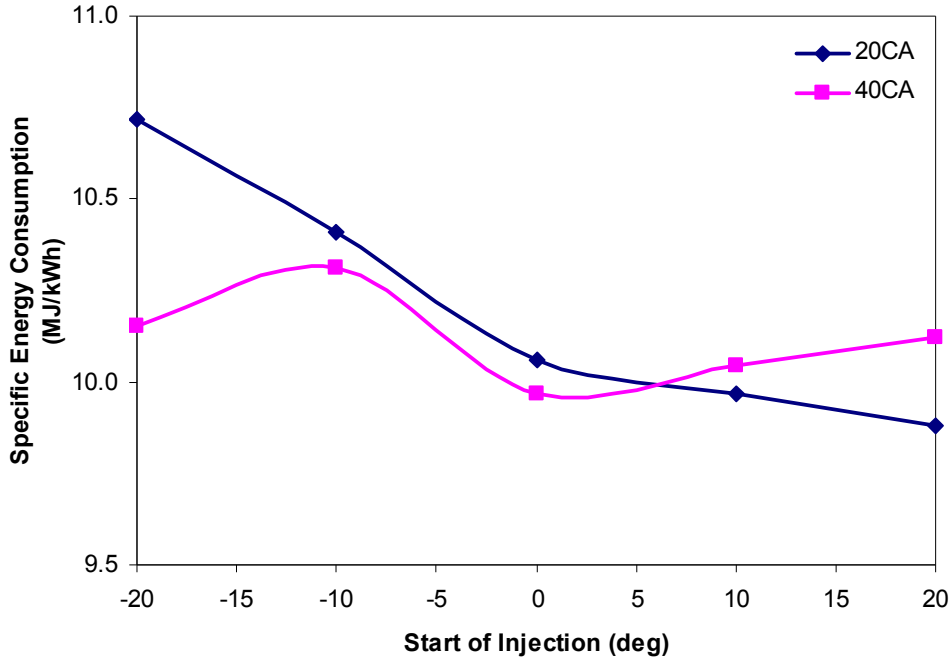

Figure F.41 Variation of ISEC with injection timing at 2500 RPM

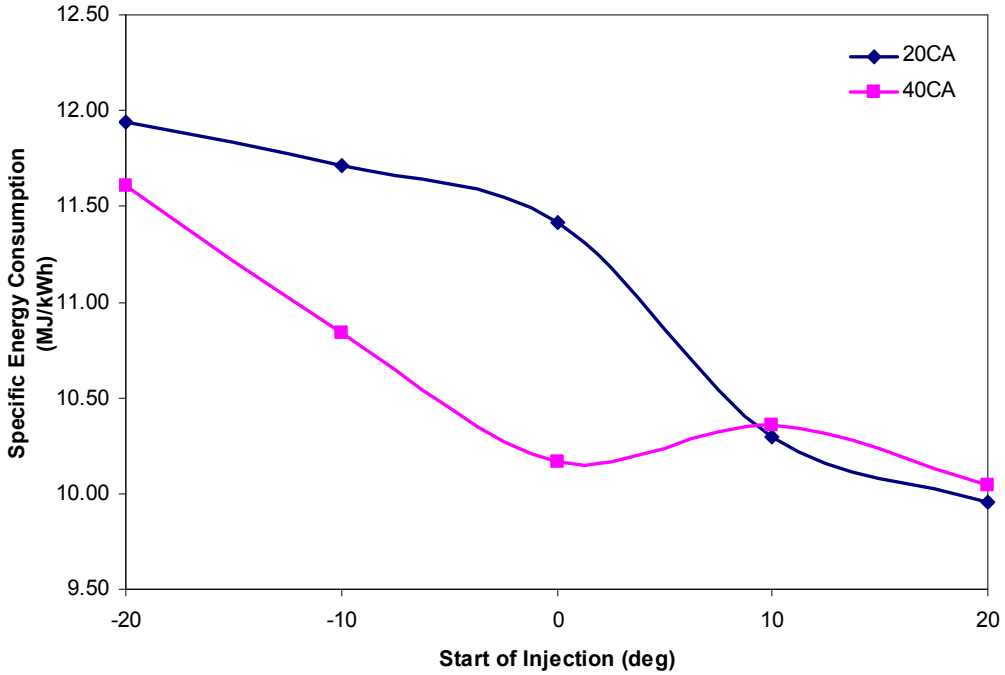

Figure F.41 Variation of ISEC with injection timing at 3000 RPM

Appendix G: Emissions Characteristics of HFCI Engine

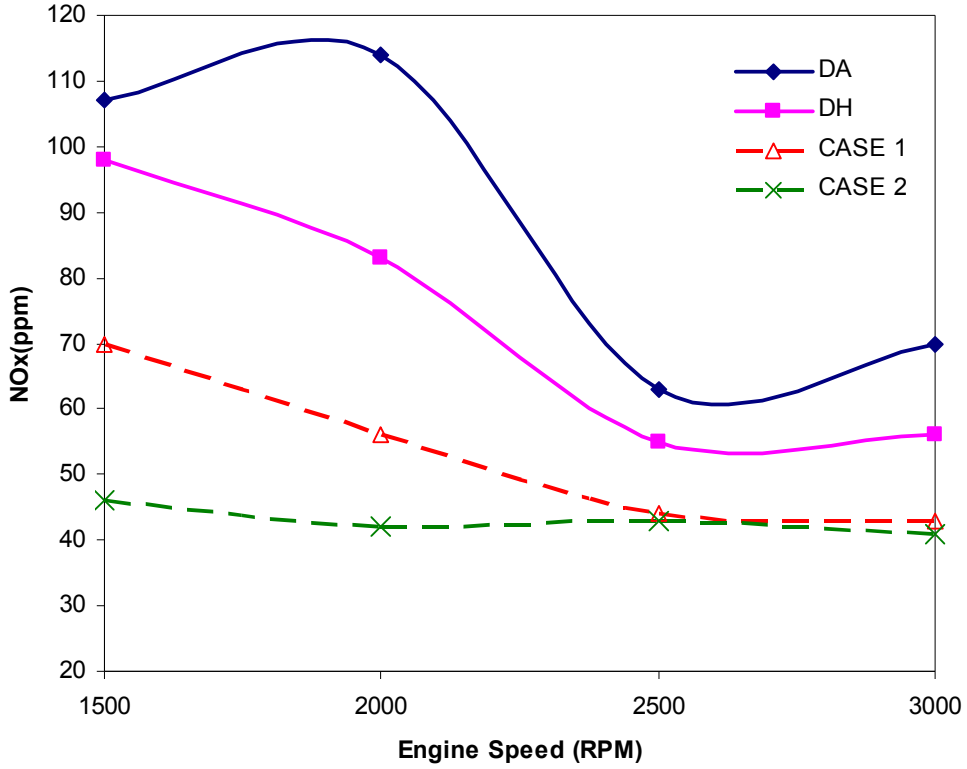

Figure G.1 Variation of NO_x emission with engine speed for CASE 1 and CASE 2

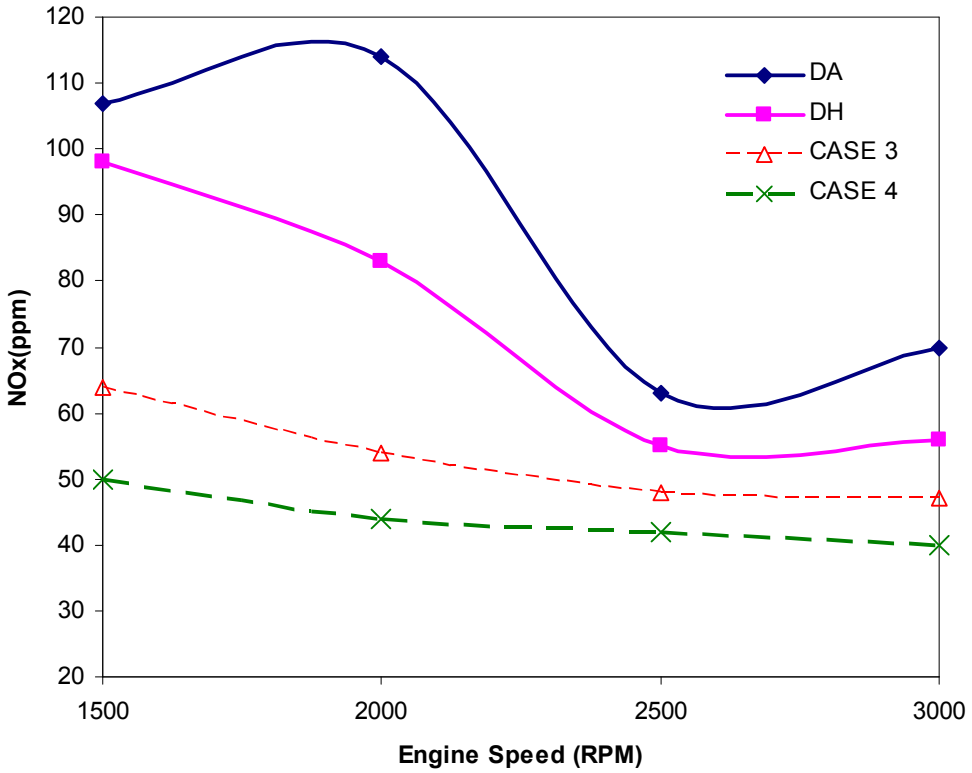

Figure G.2 Variation of NO_x emission with engine speed for CASE 3 and CASE 4

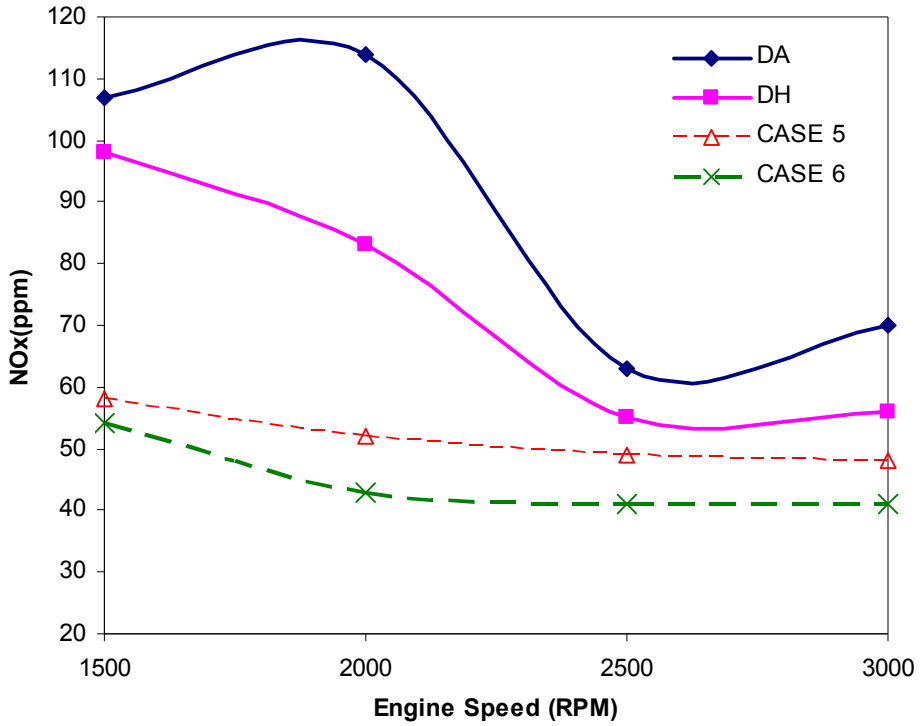

Figure G.3 Variation of NO_x emission with engine speed for CASE 5 and CASE 6

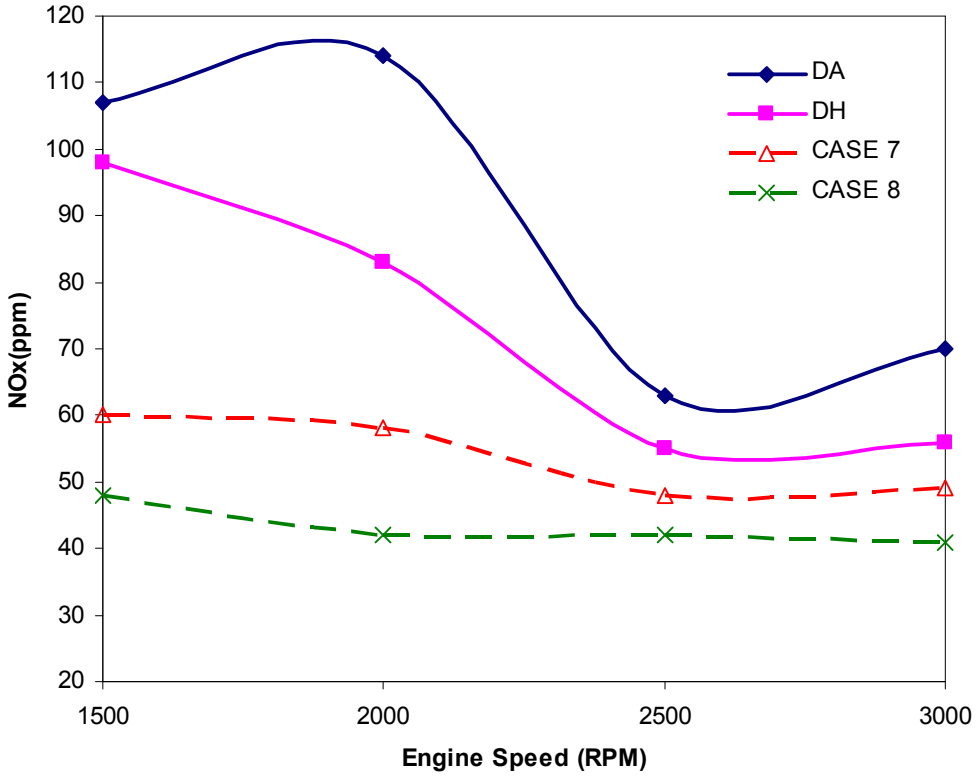

Figure G.4 Variation of NO_x emission with engine speed for CASE 7 and CASE 8

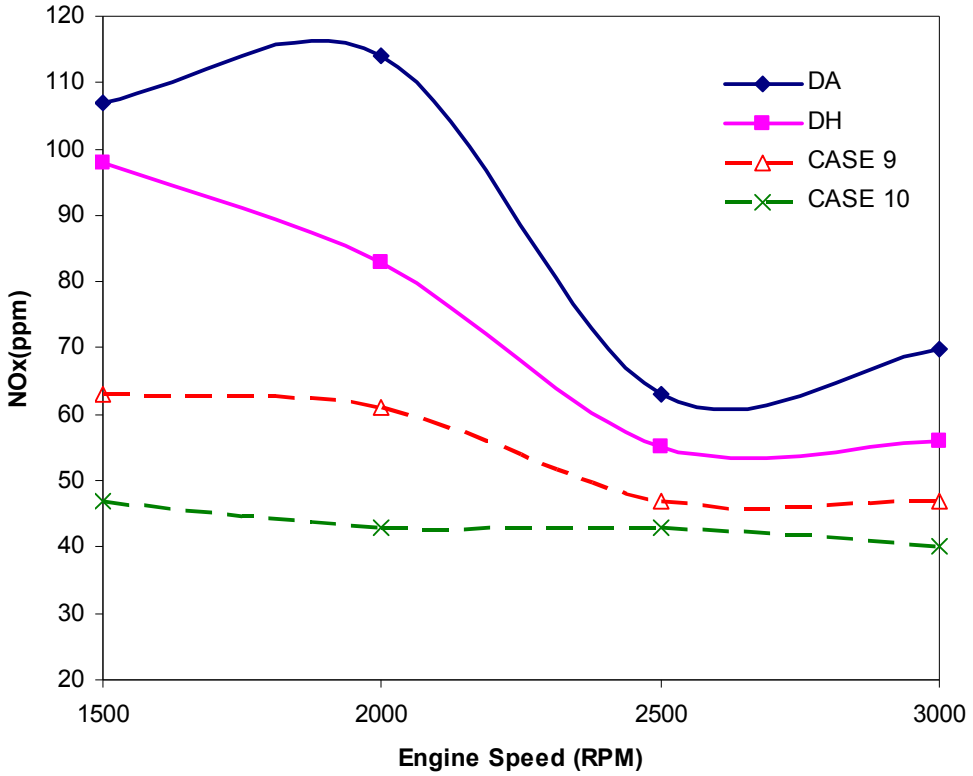

Figure G.5 Variation of NO_x emission with engine speed for CASE 9 and CASE 10

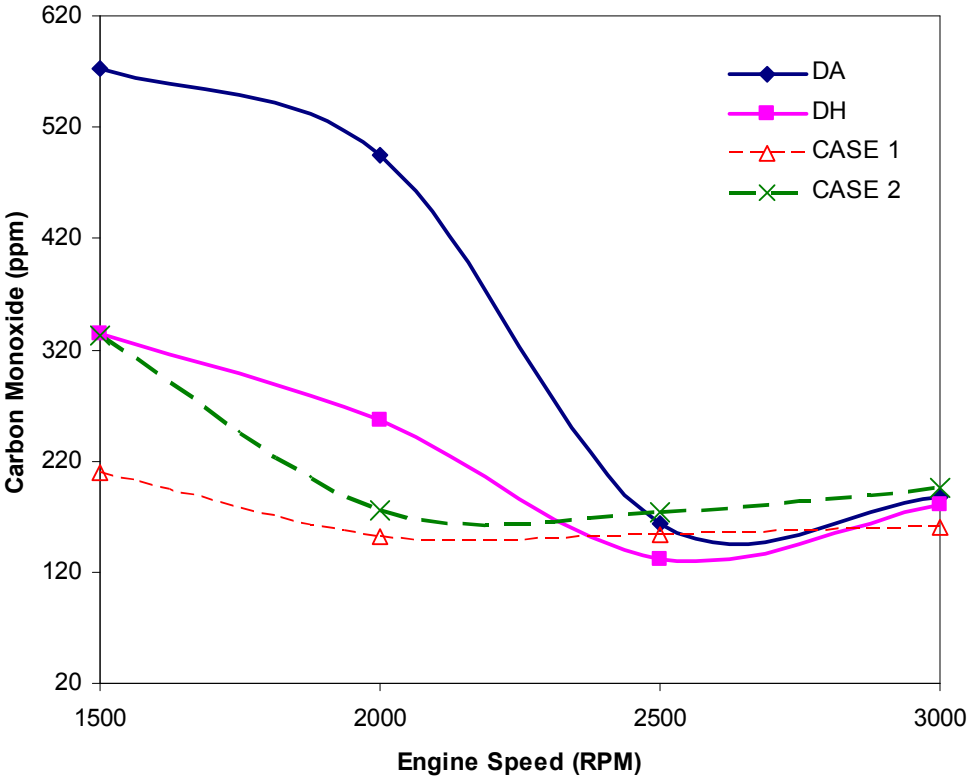

Figure G.6 Variation of CO emission with engine speed for CASE 1 and CASE 2

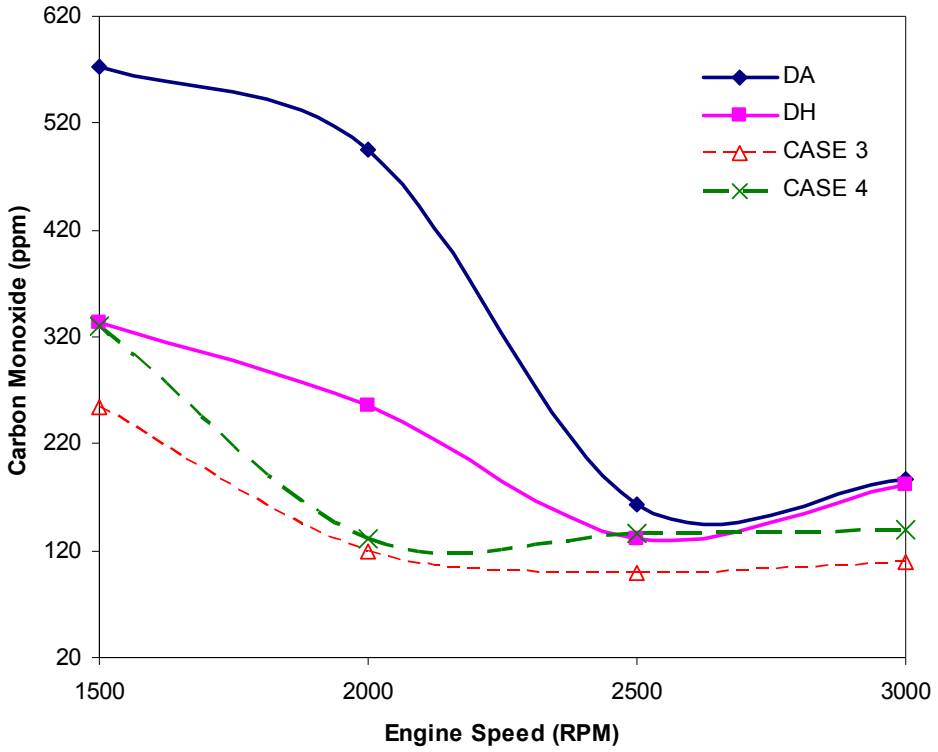

Figure G.7 Variation of CO emission with engine speed for CASE 3 and CASE 4

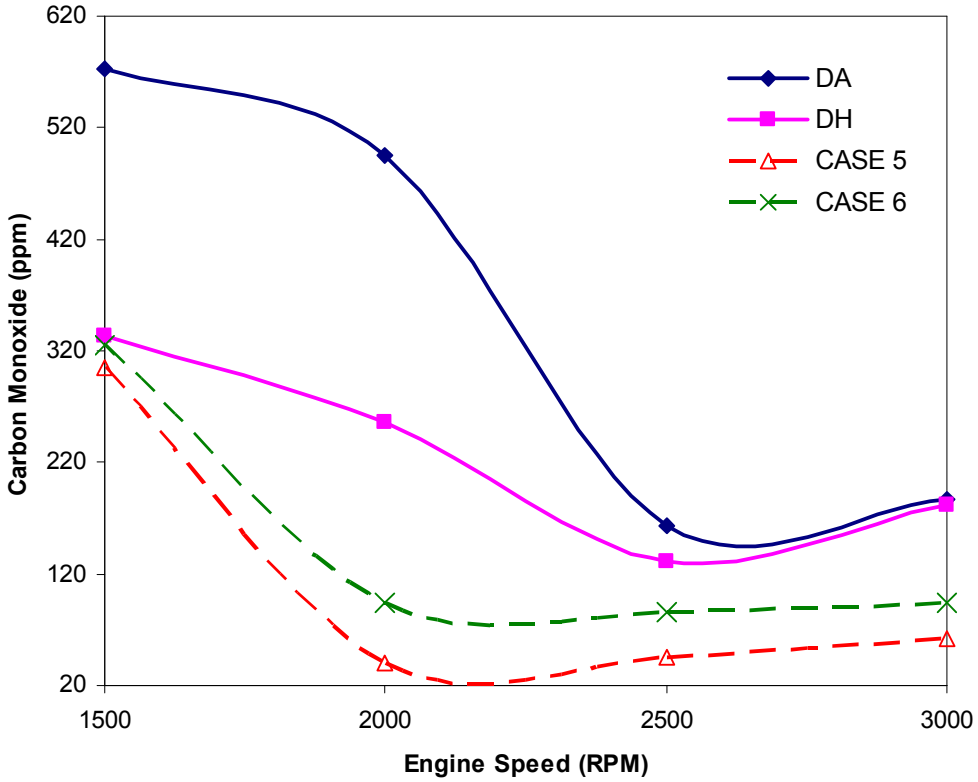

Figure G.8 Variation of CO emission with engine speed for CASE 5 and CASE 6

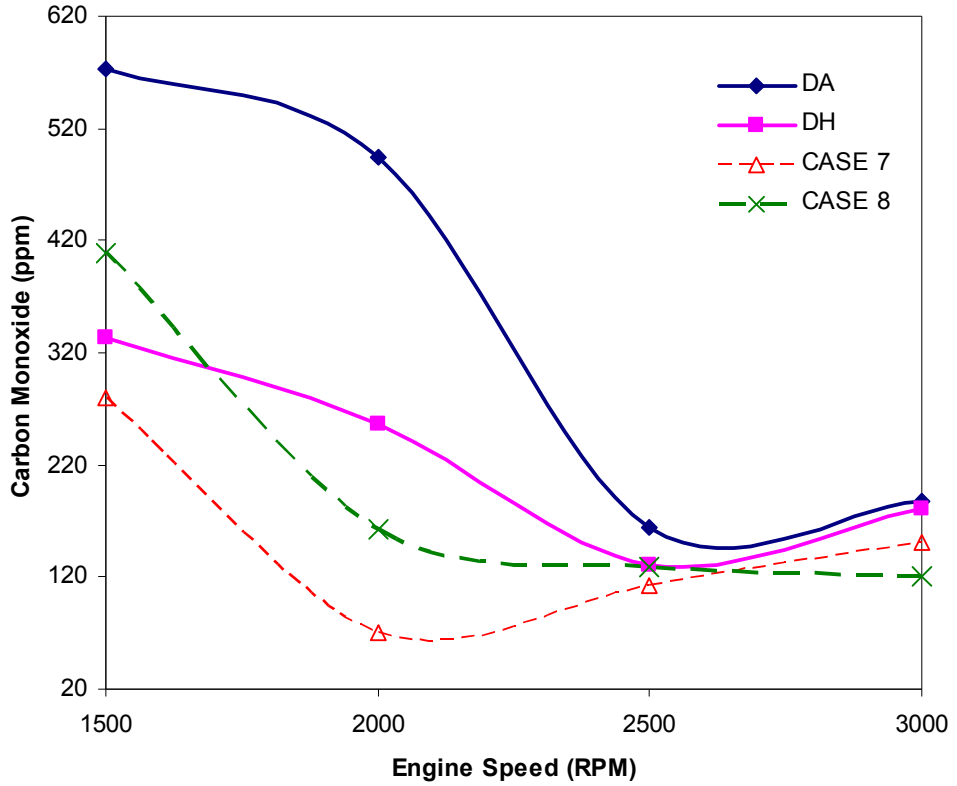

Figure G.9 Variation of CO emission with engine speed for CASE 7 and CASE 8

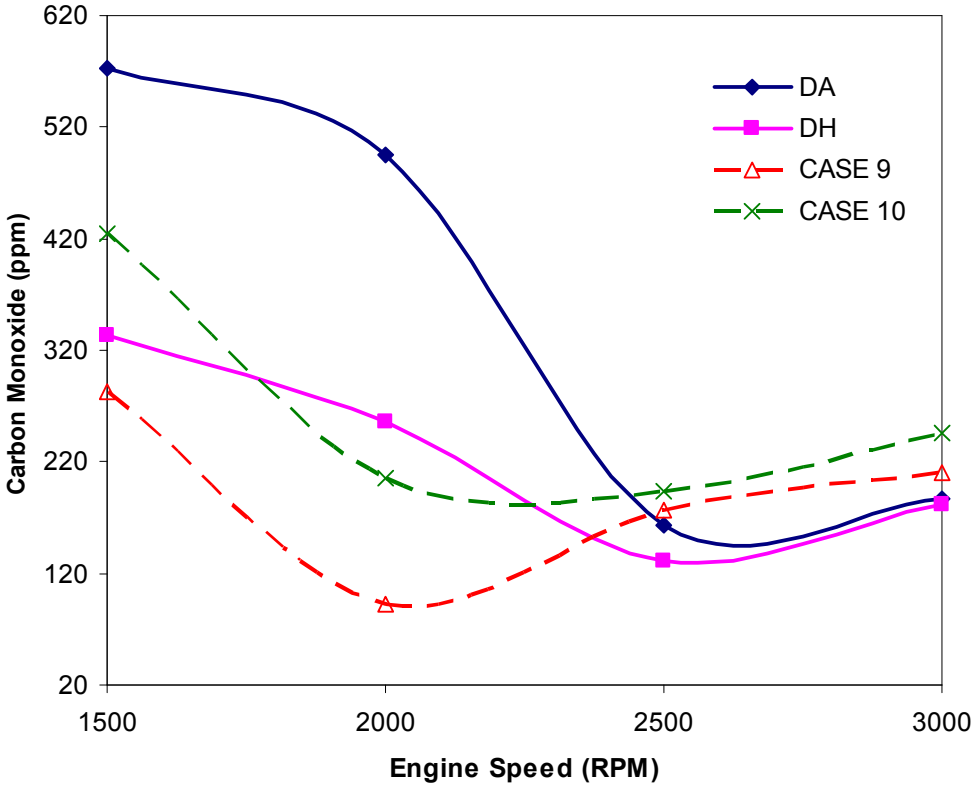

Figure G.10 Variation of CO emission with engine speed for CASE 9 and CASE 10

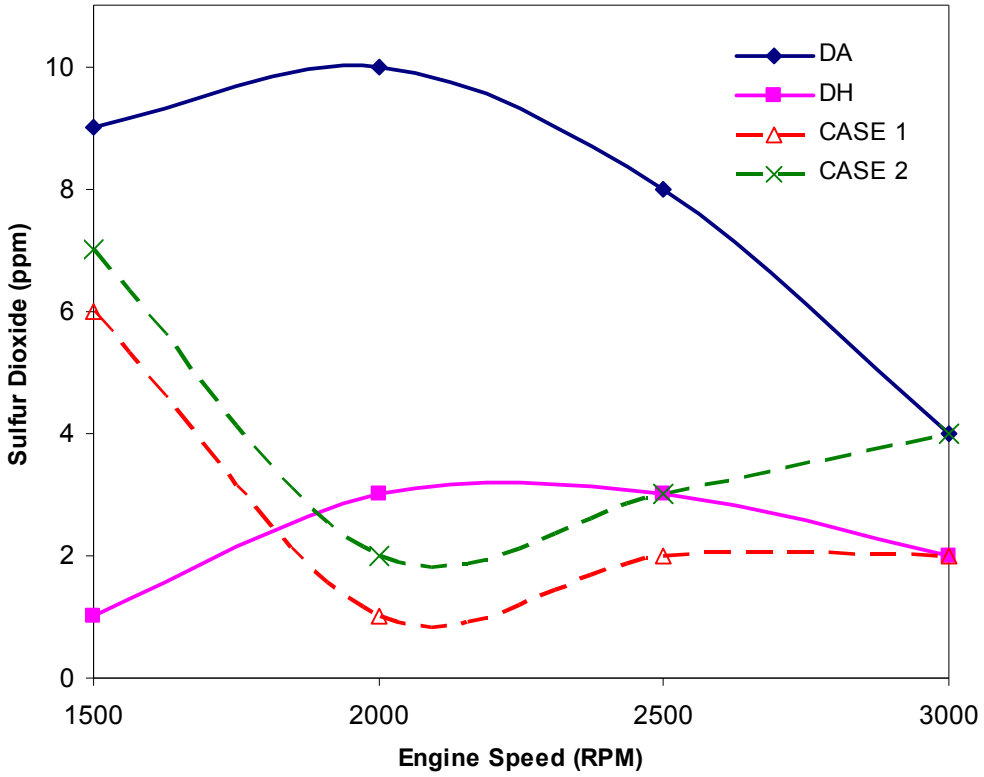

Figure G.11 Variation of SO_2 emission with engine speed for CASE 1 and CASE 2

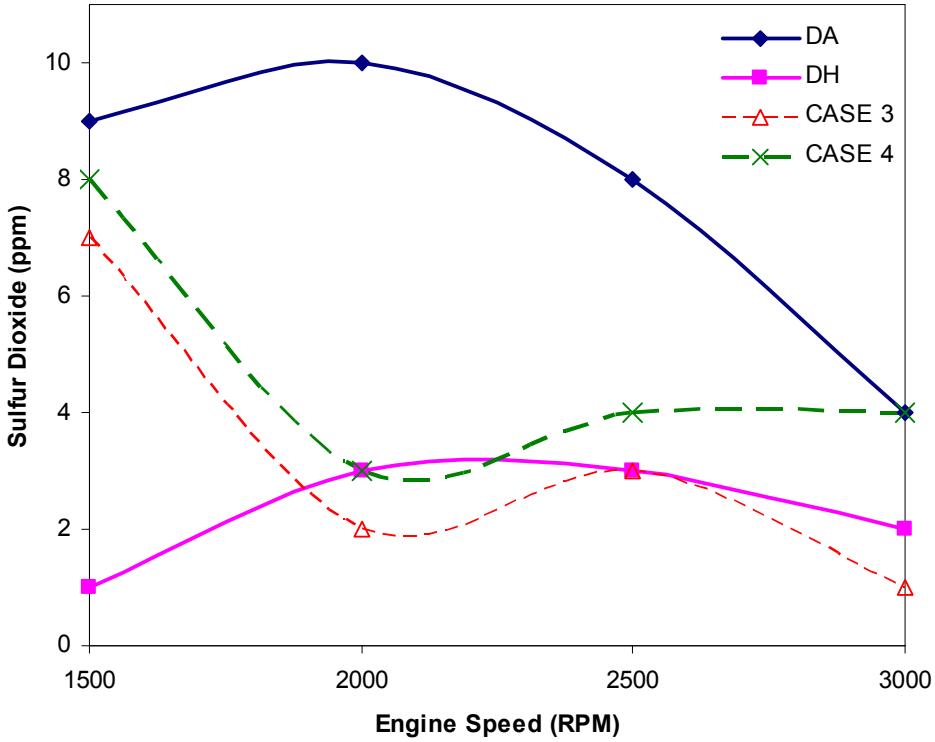

Figure G.12 Variation of SO_2 emission with engine speed for CASE 3 and CASE 4

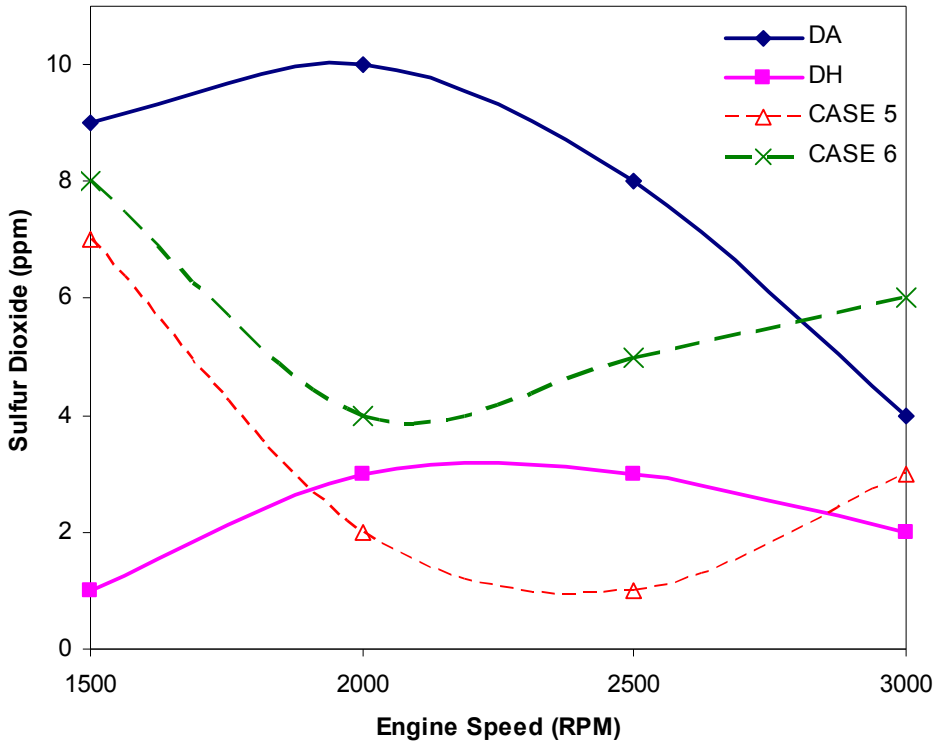

Figure G.13 Variation of SO_2 emission with engine speed for CASE 5 and CASE 6

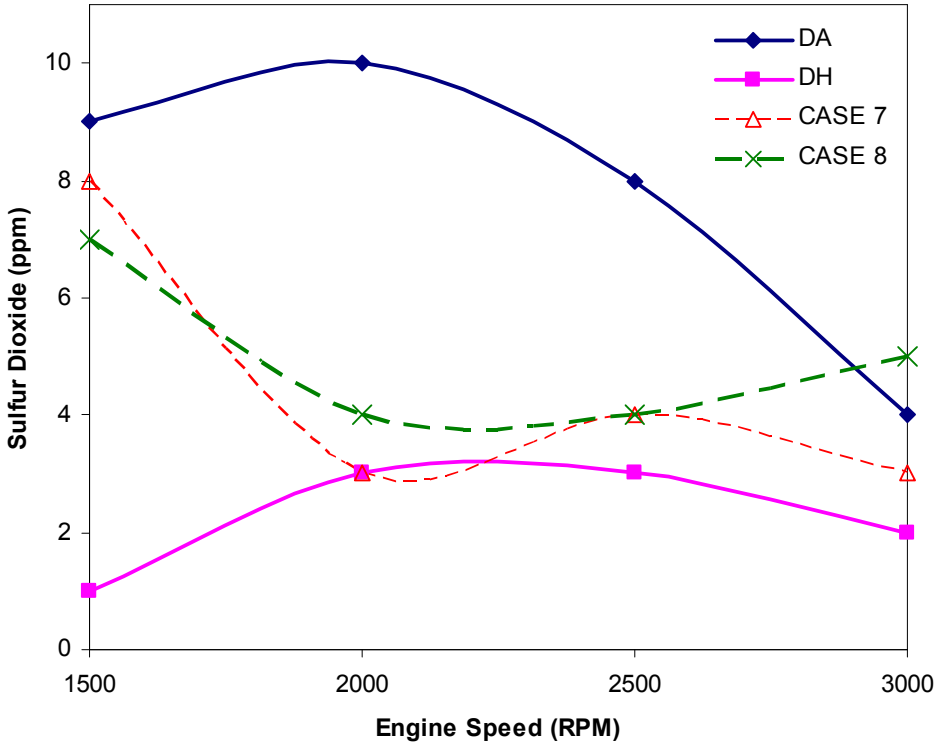

Figure G.14 Variation of SO_2 emission with engine speed for CASE 7 and CASE 8

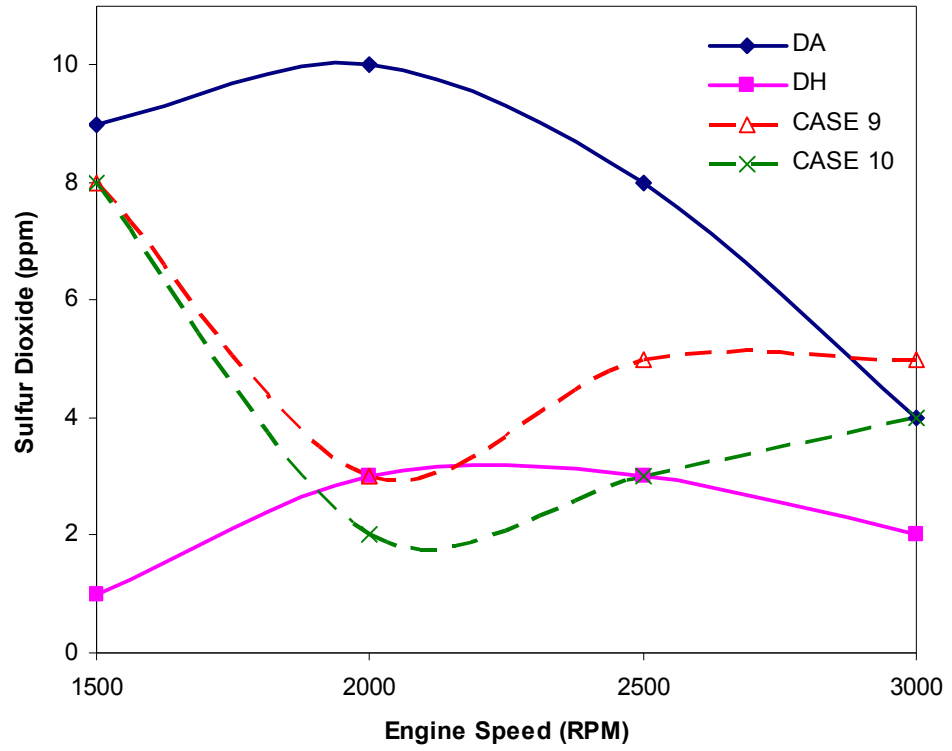

Figure G.15 Variation of SO_2 emission with engine speed for CASE 9 and CASE 10

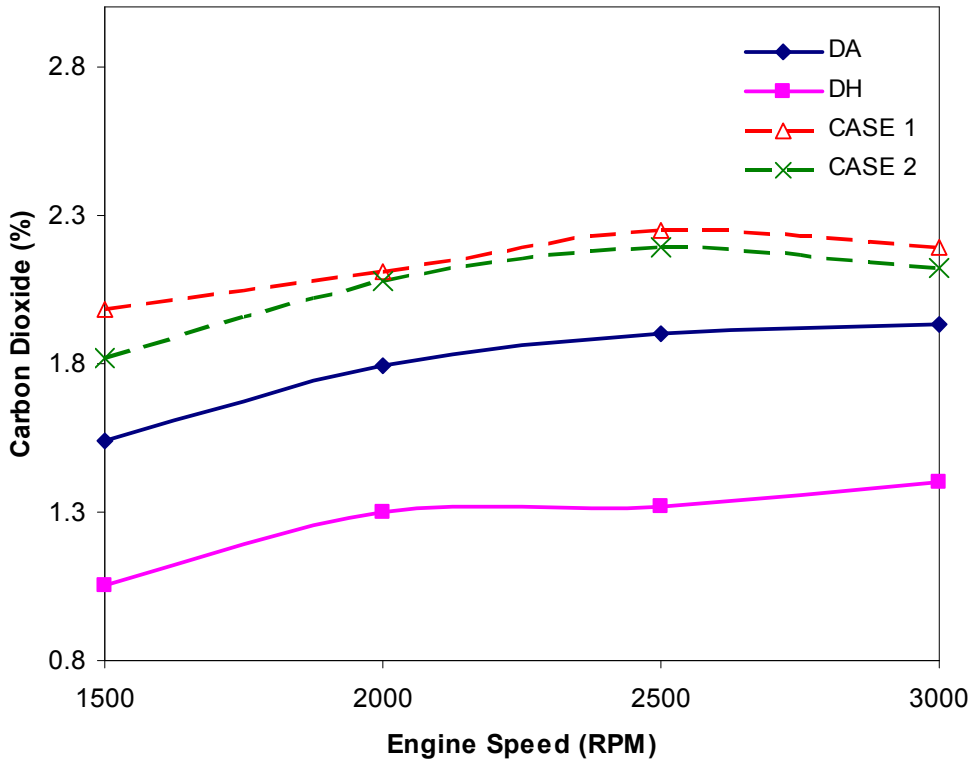

Figure G.16 Variation of CO_2 emission with engine speed for CASE 1 and CASE 2

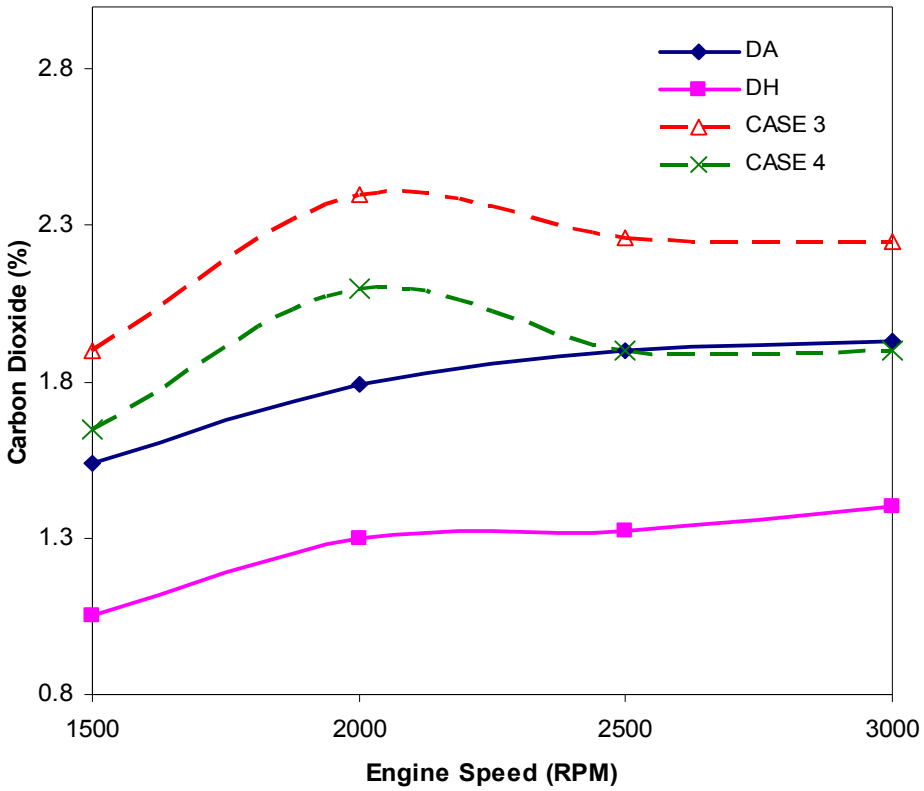

Figure G.17 Variation of CO_2 emission with engine speed for CASE 3 and CASE 4

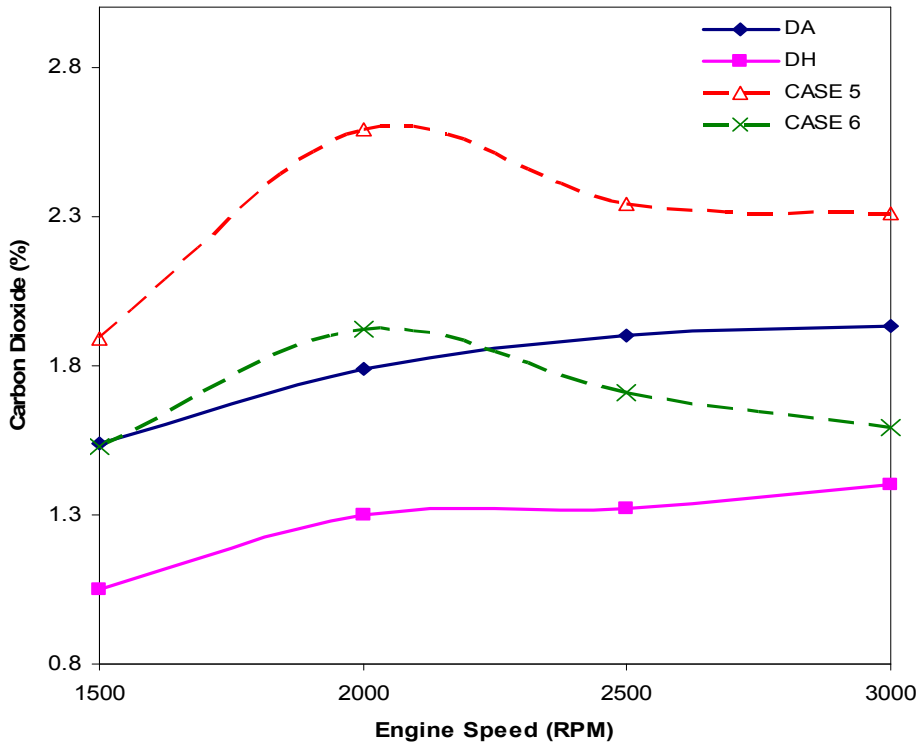

Figure G.18 Variation of CO_2 emission with engine speed for CASE 5 and CASE 6

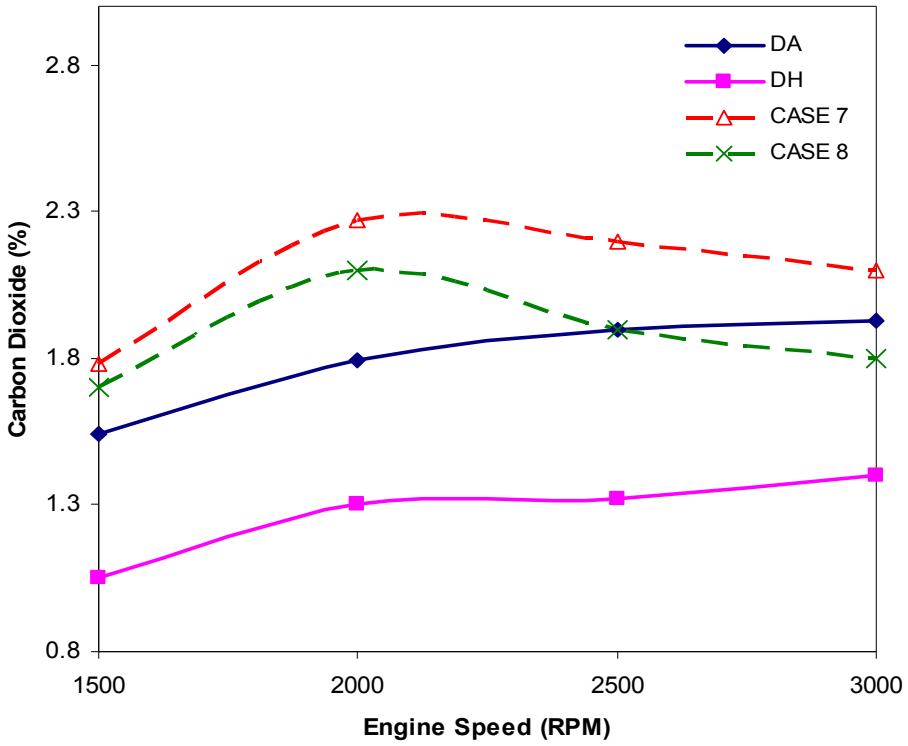

Figure G.19 Variation of CO_2 emission with engine speed for CASE 7 and CASE 8

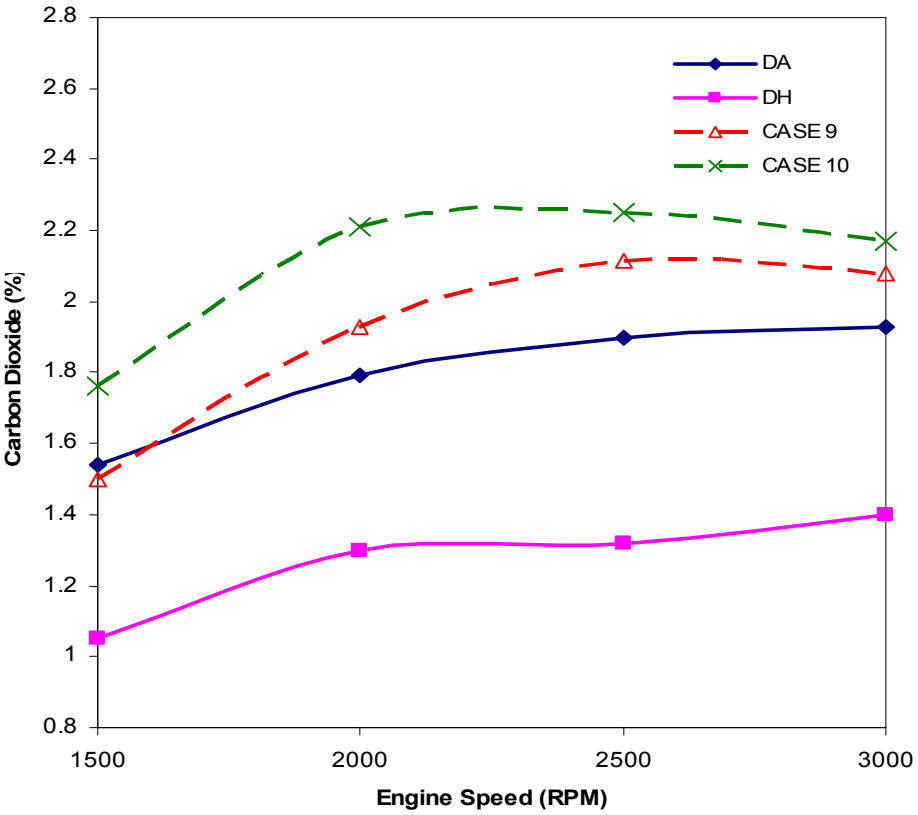

Figure G.20 Variation of CO_2 emission with engine speed for CASE 9 and CASE 10

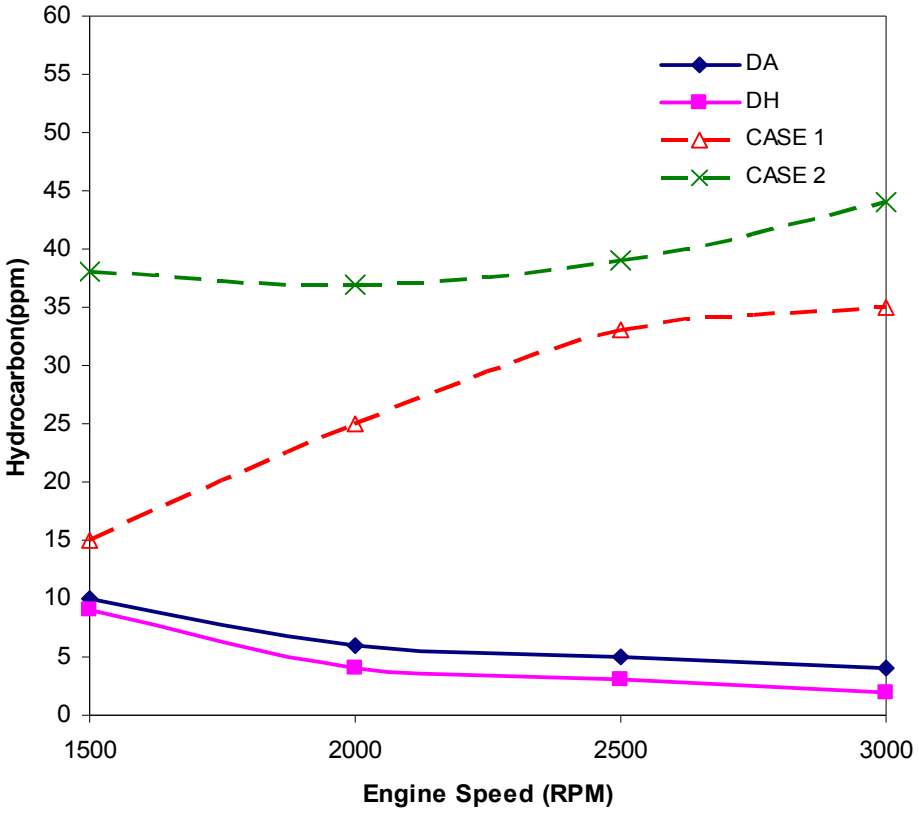

Figure G.21 Variation of HC emission with engine speed for CASE 1 and CASE 2

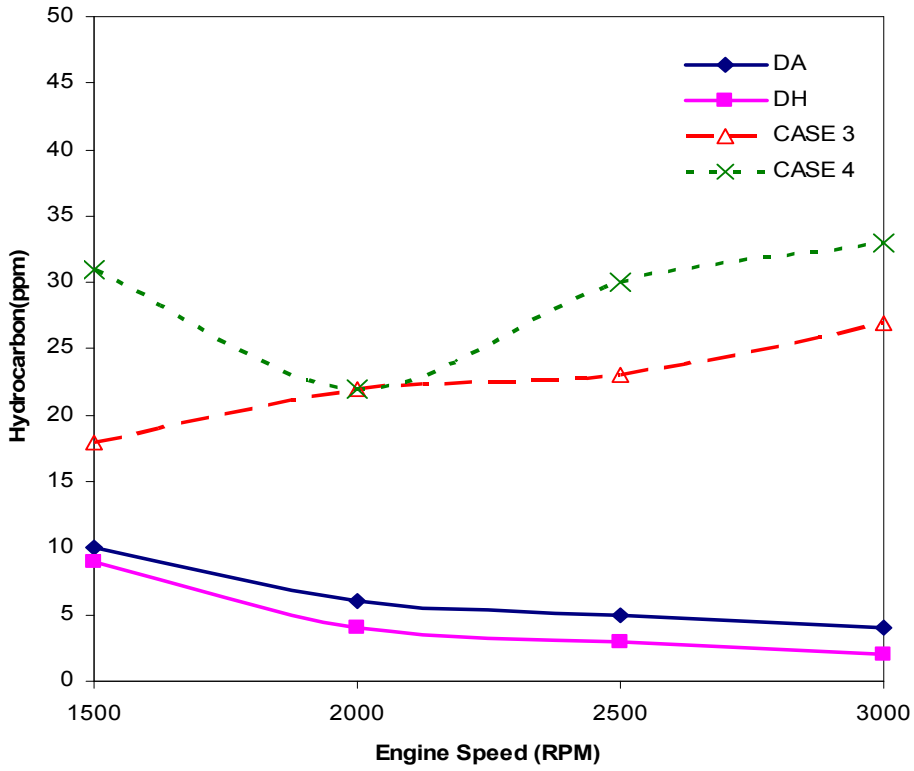

Figure G.22 Variation of HC emission with engine speed for CASE 3 and CASE 4

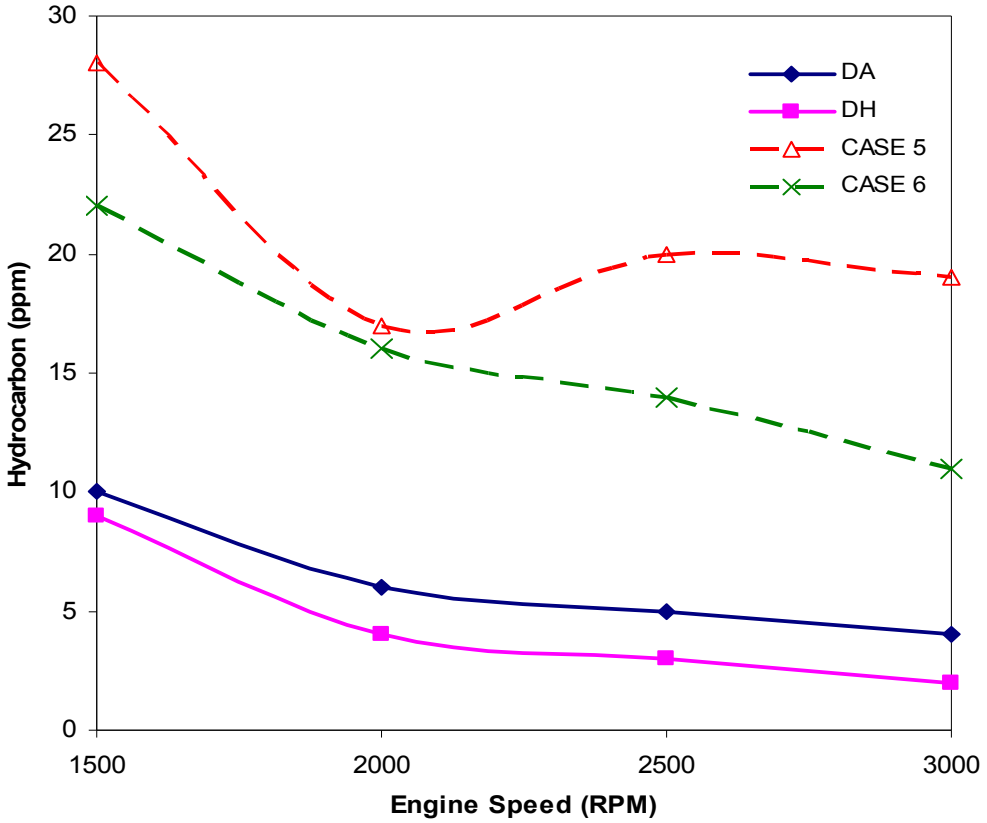

Figure G.23 Variation of HC emission with engine speed for CASE 5 and CASE 6

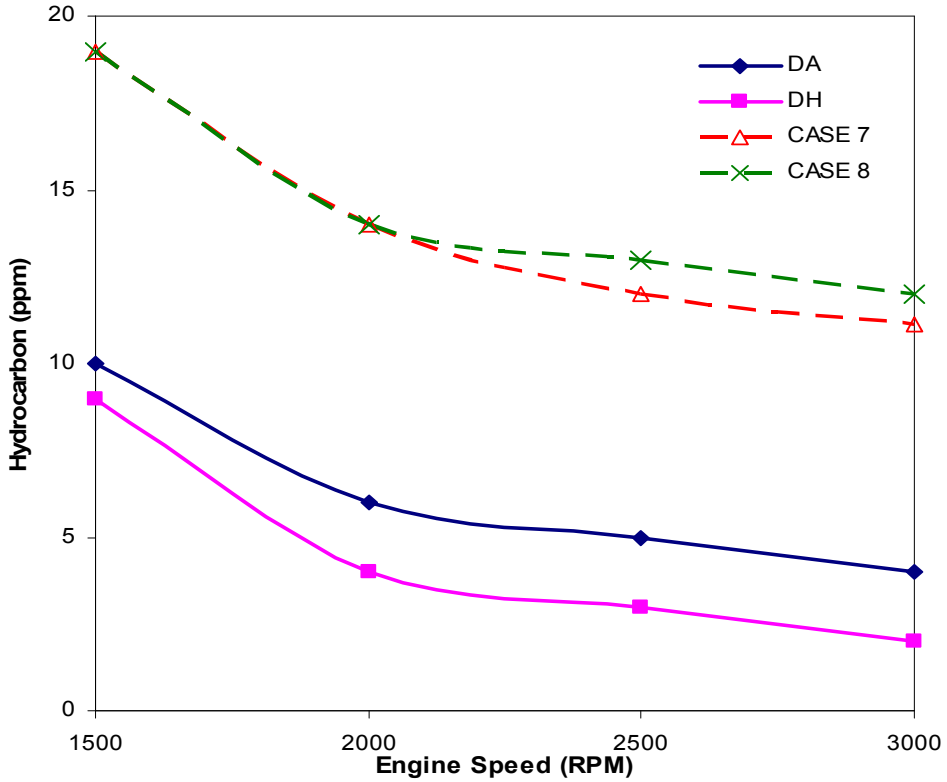

Figure G.24 Variation of HC emission with engine speed for CASE 7 and CASE 8

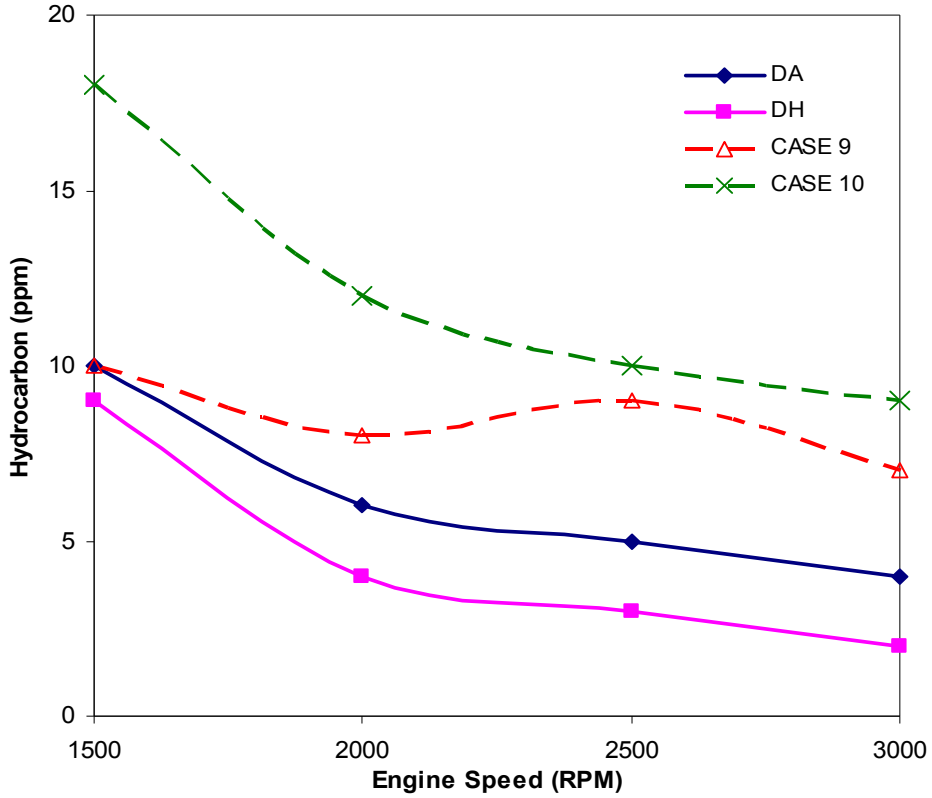

Figure G.25 Variation of HC emission with engine speed for CASE 9 and CASE 10

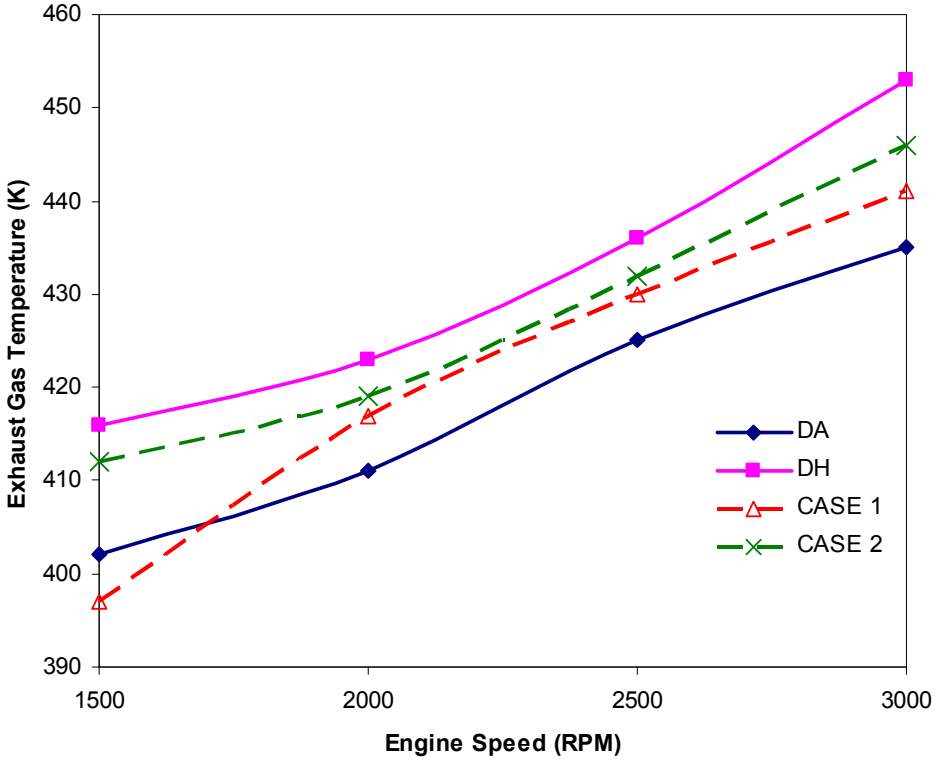

Figure G.26 Variation of EGT with engine speed for CASE 1 and CASE 2

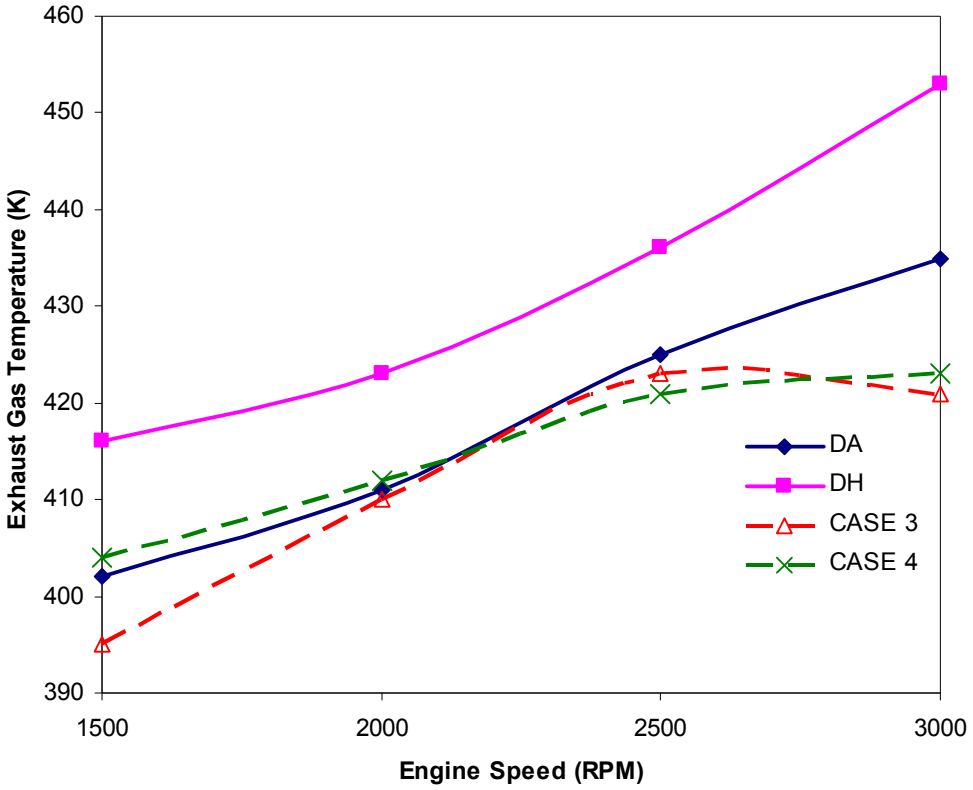

Figure G.27 Variation of EGT with engine speed for CASE 3 and CASE 4

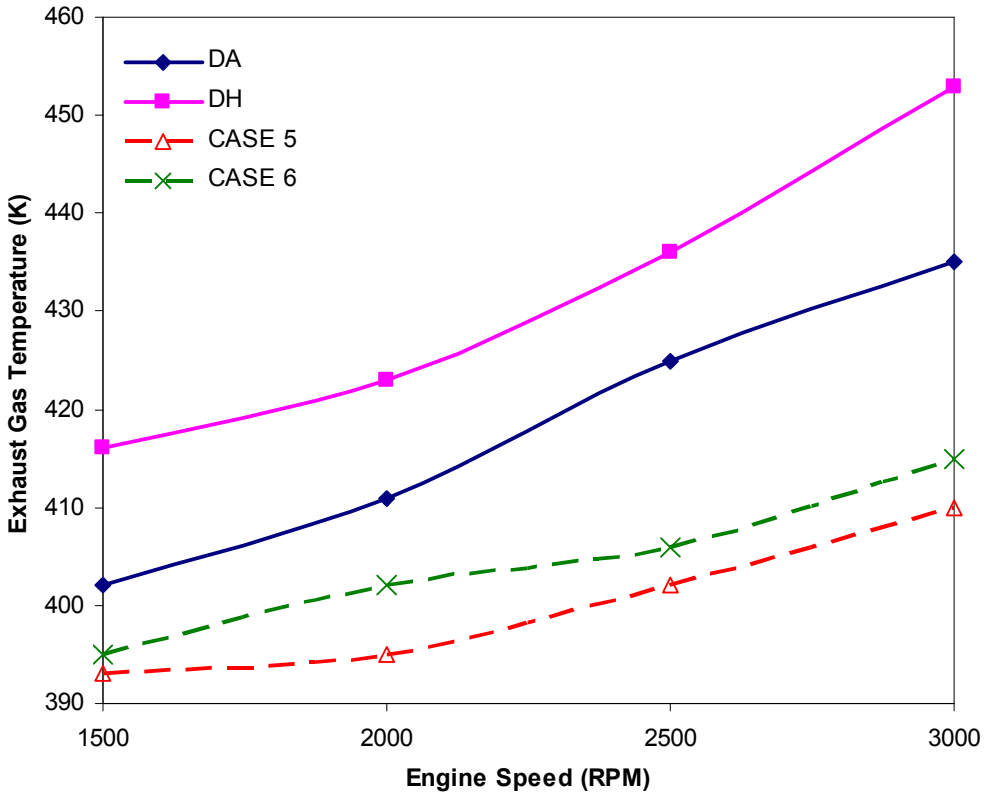

Figure G.28 Variation of EGT with engine speed for CASE 5 and CASE 6

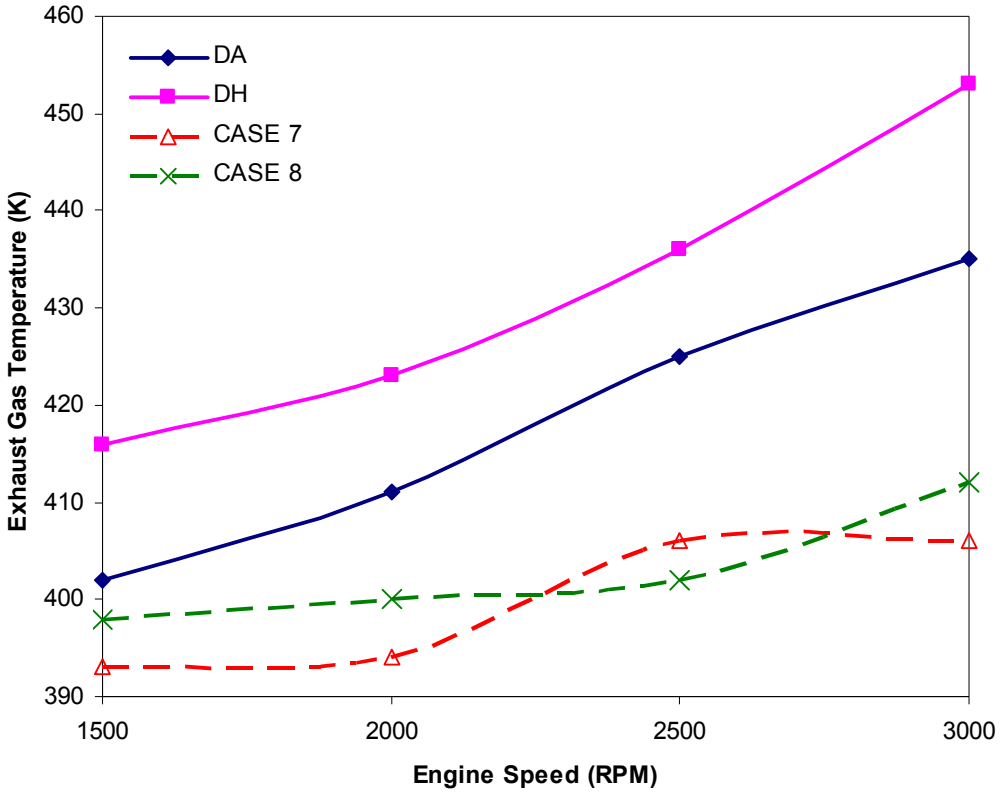

Figure G.29 Variation of EGT with engine speed for CASE 7 and CASE 8

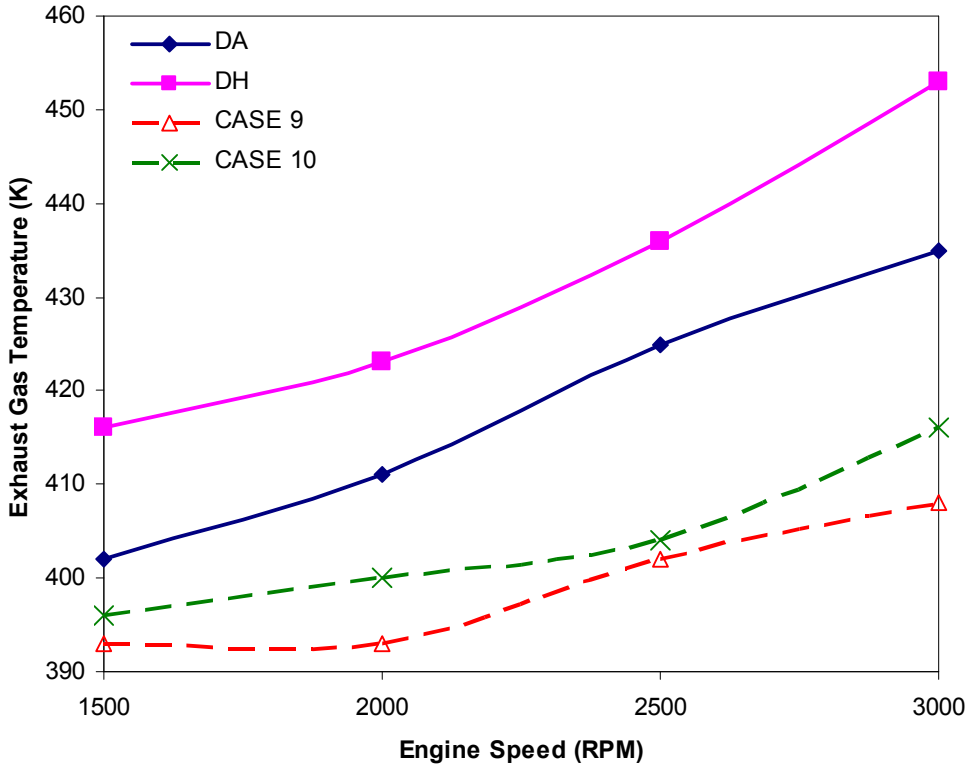

Figure G.30 Variation of EGT with engine speed for CASE 9 and CASE 10

Appendix H: Details of Publications

Journal Publications:

(a) Published Journal:

1. **R.Adnan,** H.H.Masjuki, T.M.I. Mahlia, (2012), Performance and emissions analysis of hydrogen-fuelled compression ignition engine with variable water injection timing, Energy, 43(1), pp. 416-426. (ISI Journal, Q.1).

2. **R.Adnan,** H.H.Masjuki, T.M.I. Mahlia, (2011), Mathematical modeling on the effect of equivalence ratio in emission characteristics of compression ignition engine with hydrogen substitution, Applied Mathematics and Computation, 217(13), pp. 6144-6158. (ISI Journal, Q.1).

3. **R.Adnan,** H.H.Masjuki, T.M.I. Mahlia, (2010), Experimental investigation on in-cylinder pressure and emission of diesel engine with port injection hydrogen system, International Journal of Mechanical and Materials Engineering (IJMME), 5 (2), 136-141. (Scopus Journal).

4. **R.Adnan,** H.H.Masjuki, T.M.I. Mahlia, (2010), Computational simulation on emission of hydrogen fuelled compression ignition engine with variable combustion temperature, International Journal of Mechanical and Materials Engineering (IJMME), 5(2), 251-259. (Scopus Journal).

(b) Under Review:

1. **R.Adnan,** H.H.Masjuki, T.M.I. Mahlia, Experimental study of water injection technique on hydrogen-fuelled diesel engine, Energy Conversion and Management. (ISI Journal, Q.1).

2. **R.Adnan,** H.H.Masjuki, T.M.I. Mahlia, Combustion analysis of hydrogen-fuelled diesel engine with timed manifold water injection at variable start of injection, Renewable Energy. (ISI Journal, Q.2).

Conferences:

1. **R.Adnan**, H.H. Masjuki, T.M.I. Mahlia, An experimental investigation of unmodified DI diesel engine with hydrogen addition, 3rd International Conference on Energy and Environment (ICEE2009), 7-8th Dec 2009, Malacca. (Scopus).

2. **R.Adnan**, H.H.Masjuki, T.M.I.Mahlia, Combustion modeling : Effects of temperature on emissions of hydrogen-diesel dual fuel system, *IEEE Xplore*-International Conference for Technical Postgraduates (TechPos2009),14-15th Dec 2009, Kuala Lumpur.

3. **R.Adnan,** H.H. Masjuki, T.M.I. Mahlia, Computational simulation and prediction on the performance and emissions of dual fuel diesel engine operated with pilot diesel fuel and hydrogen gas, International Conference on Construction and Building Technology (ICCBT 2008), 16-20th June 2008, Kuala Lumpur.

4. **R.Adnan**, H.H.Masjuki, T.M.I. Mahlia, Performance analysis of hydrogen fuelled Diesel engine, International Seminar on Advances in Renewable Energy Technology (ISARET 2009), 18-19th April 2009, Kuala Lumpur, Malaysia